frontiers | Research Topics

Recent advances in volatile organic compounds, heavy metals, microplastics, and solid wastes in ecosystems

Edited by
Zhenming Zhang, Yaoguang Guo, Ji Qi, Zhiyang Zhang and Peng Cheng

Published in
Frontiers in Environmental Science

ISSN 1664-8714
ISBN 978-2-8325-7211-5
DOI 10.3389/978-2-8325-7211-5

Generative AI statement
Any alternative text (Alt text) provided alongside figures in the articles in this ebook has been generated by Frontiers with the support of artificial intelligence and reasonable efforts have been made to ensure accuracy, including review by the authors wherever possible. If you identify any issues, please contact us.

About Frontiers

Frontiers is more than just an open access publisher of scholarly articles: it is a pioneering approach to the world of academia, radically improving the way scholarly research is managed. The grand vision of Frontiers is a world where all people have an equal opportunity to seek, share and generate knowledge. Frontiers provides immediate and permanent online open access to all its publications, but this alone is not enough to realize our grand goals.

Frontiers journal series

The Frontiers journal series is a multi-tier and interdisciplinary set of open-access, online journals, promising a paradigm shift from the current review, selection and dissemination processes in academic publishing. All Frontiers journals are driven by researchers for researchers; therefore, they constitute a service to the scholarly community. At the same time, the *Frontiers journal series* operates on a revolutionary invention, the tiered publishing system, initially addressing specific communities of scholars, and gradually climbing up to broader public understanding, thus serving the interests of the lay society, too.

Dedication to quality

Each Frontiers article is a landmark of the highest quality, thanks to genuinely collaborative interactions between authors and review editors, who include some of the world's best academicians. Research must be certified by peers before entering a stream of knowledge that may eventually reach the public - and shape society; therefore, Frontiers only applies the most rigorous and unbiased reviews. Frontiers revolutionizes research publishing by freely delivering the most outstanding research, evaluated with no bias from both the academic and social point of view. By applying the most advanced information technologies, Frontiers is catapulting scholarly publishing into a new generation.

What are Frontiers Research Topics?

Frontiers Research Topics are very popular trademarks of the *Frontiers journals series*: they are collections of at least ten articles, all centered on a particular subject. With their unique mix of varied contributions from Original Research to Review Articles, Frontiers Research Topics unify the most influential researchers, the latest key findings and historical advances in a hot research area.

Find out more on how to host your own Frontiers Research Topic or contribute to one as an author by contacting the Frontiers editorial office: frontiersin.org/about/contact

Recent advances in volatile organic compounds, heavy metals, microplastics, and solid wastes in ecosystems

Topic editors

Zhenming Zhang — Guizhou University, China

Yaoguang Guo — Shanghai Polytechnic University, China

Ji Qi — Chung-Ang University, Republic of Korea

Zhiyang Zhang — Yantai Institute of Coastal Zone Research, Chinese Academy of Sciences (CAS), China

Peng Cheng — UMR6296 Institut de Chimie de Clermont-Ferrand (ICCF), France

Citation

Zhang, Z., Guo, Y., Qi, J., Zhang, Z., Cheng, P., eds. (2025). *Recent advances in volatile organic compounds, heavy metals, microplastics, and solid wastes in ecosystems*. Lausanne: Frontiers Media SA. doi: 10.3389/978-2-8325-7211-5

Table of contents

frontiers | Frontiers in Environmental Science

TYPE Editorial
PUBLISHED 17 November 2025
DOI 10.3389/fenvs.2025.1740845

OPEN ACCESS

EDITED AND REVIEWED BY
Oladele Ogunseitan,
University of California, Irvine, United States

*CORRESPONDENCE
Yifan Sui,
suiyifan24@mails.ucas.ac.cn

RECEIVED 06 November 2025
ACCEPTED 06 November 2025
PUBLISHED 17 November 2025

CITATION
Guo Y, Sui Y and Zhang Z (2025) Editorial: Recent advances in volatile organic compounds, heavy metals, microplastics, and solid wastes in ecosystems.
Front. Environ. Sci. 13:1740845.
doi: 10.3389/fenvs.2025.1740845

Editorial: Recent advances in volatile organic compounds, heavy metals, microplastics, and solid wastes in ecosystems

Yaoguang Guo[1], Yifan Sui [2]* and Zhenming Zhang[3]

[1]School of Resources and Environmental Engineering, Shanghai Polytechnic University, Shanghai, China, [2]Yantai Institute of Coastal Zone Research, Chinese Academy of Sciences, Yantai, China, [3]College of Resources and Environmental Engineering, Guizhou University, Guiyang, China

KEYWORDS

volatile organic compounds, heavy metals, solid waste management and resourcerecovery, micro-nano-bubble, bibliometric analysis

Editorial on the Research Topic
Recent advances in volatile organic compounds, heavy metals, microplastics, and solid wastes in ecosystems

Introduction

The accelerating pace of industrialization and urbanization has led to widespread pollution of air, water, and soil. Key pollutants, including volatile organic compounds (VOCs), heavy metals, microplastics, and solid wastes, pose significant risks to ecosystems and human health. Despite their chemical differences, these pollutants share traits like persistence, bioaccumulation, and complex transformation, threatening both natural and human-made environments (Zhou et al., 2023; Lou et al., 2024; Xu et al., 2024; Zhang et al., 2024; Boisseaux et al., 2025; Hu et al., 2025; Jomova et al., 2025; Peng et al., 2025; Xiao et al., 2025; Yan et al., 2025). To address these challenges, *Frontiers in Environmental Science* presents a Research Topic entitled "Recent Advances in Volatile Organic Compounds, Heavy Metals, Microplastics, and Solid Wastes in Ecosystems." This Research Topic consists of nine peer-reviewed papers, including original research articles and bibliometric analyses, which collectively investigate the distribution patterns, transformation mechanisms, ecological impacts, and sustainable remediation strategies of pollutants across various environmental interfaces.

Key elements in this Research Topic

VOCs are a crucial class of air pollutants and precursors of ground-level ozone and secondary organic aerosols. Zhu et al. conducted a bibliometric analysis of 2,493 studies on photocatalytic oxidation of VOCs between 1998 and 2023, revealing China as the most active contributor. The research focus has transitioned from TiO_2-based ultraviolet

photocatalytic systems to visible-light-responsive and hybrid nanostructured catalysts, with increased emphasis on charge carrier separation, adsorption regulation, and optimization of reaction kinetics. These advancements reflect a paradigm shift from empirical catalyst development toward mechanism-driven design strategies.

Complementary insights emerge from the study by Chen et al., who investigated the photodegradation processes of the representative pharmaceutical contaminant clofibric acid in urban, suburban and rural water bodies. They demonstrated that the composition of dissolved organic matter (DOM) regulates the balance between direct and indirect photolysis. However, the resulting by-products demonstrated higher eco-toxicity compared to the parent compound. Collectively, these findings underscore both the potential and complexity of photocatalytic and photochemical pathways for the control of VOCs and organic contaminants, necessitating further investigation into reaction intermediates and the environmental safety of degradation processes.

Heavy metals continue to represent one of the most persistent threats to terrestrial and aquatic ecosystems due to their inherent toxicity, environmental mobility, and resistance to degradation. Jiang et al. examined soil heavy-metal variations in Guizhou's karst region, finding lower concentrations of Hg, Cd, and Pb in natural forest soils compared with cultivated lands. Vegetation cover effectively reduced atmospheric deposition, whereas fertilizer application enhanced Cd accumulation, highlighting the link between land-use change and heavy metal enrichment. Similarly, Qian et al. evaluated five key metals (Cd, As, Pb, Hg, Cu) in Gastrodia elata cultivation areas in Yunnan. Although elevated levels of Hg, Cd, and Cu were observed, health risk indices indicated no immediate threat to human health. Collectively, these studies demonstrate how ecological functions, agricultural practices, and geological backgrounds jointly govern the behavior of heavy metals. At broader scales, Jia et al. conducted a knowledge-map analysis of heavy-metal source apportionment (1994–2022), revealing global research hotspots in positive matrix factorization (PMF) modeling, health-risk assessment, and sediment-based tracing. Meanwhile, Lu et al. investigated the distribution of pollutants and microbial responses in the Qaidam Basin, revealing that gradients of heavy metals and organic pollutants are closely associated with microbial community restructuring. Their findings indicate that microbial adaptation mechanisms play crucial roles in pollutant cycling within extreme saline environments. Future research should integrate cross-media transport models with microbial ecology to improve the quantification of heavy metal bioavailability and long-term ecological feedbacks.

Beyond chemical pollutants, solid waste management and resource recovery have become pivotal to environmental sustainability. Liu et al. developed a phosphogypsum-based ecological concrete using electrolytic manganese slag as a cementitious binder and clay ceramics as aggregate. The optimized mixture exhibited higher compressive strength and improved water retention, while simultaneously supporting grass growth and immobilizing heavy metals such as As, Cu, and Pb. This study presents a practical pathway for transforming hazardous industrial by-products into functional green construction materials. Similarly, Dai et al. utilized rosa roxburghii residue to synthesize FeOOH-modified biochar, achieving a maximum adsorption capacity of 5.7 mg g^{-1} for Sb(V) at pH 2. The process not only enabled efficient removal of toxic antimony but also facilitated the valorization of agricultural waste. These studies mark a shift from traditional end-of-pipe treatment toward a circular economy approach that unites pollutant control with material reuse and ecosystem restoration, advancing the "waste-to-resource" concept essential for low-carbon, sustainable development.

Among the innovative approaches highlighted in this Research Topic, Chen et al. provided a comprehensive review of micro-nano-bubble (MNB) technologies and their expanding role in environmental remediation. MNBs exhibit exceptional physicochemical properties, including high interfacial potential, large specific surface area, and prolonged stability, which enhance oxygen transfer and promote the *in situ* generation of reactive oxygen species. When integrated with photocatalytic or biochar-based systems, MNBs produce synergistic effects that accelerate pollutant transformation and increase overall treatment efficiency. This study demonstrates how advanced interfacial engineering and cross-disciplinary innovation can transform pollution control by integrating physical, chemical, and biological mechanisms to support sustainable ecosystem restoration.

Conclusion

This Research Topic brings together interdisciplinary studies on the behavior and control of VOCs, heavy metals, and solid wastes in various ecosystems. The papers provide insights into pollutant distribution, transformation, and ecological effects, linking air, water, and soil processes. Covering both fundamental mechanisms and applied remediation, they highlight advances in catalytic oxidation, microbial adaptation, biochar adsorption, and resource recycling. Future research should integrate multi-pollutant models, assess long-term ecological risks, and develop low-carbon technologies. Together, these studies support evidence-based environmental policies and promote the goal of resilient, sustainable ecosystems.

Author contributions

YG: Writing – review and editing, Writing – original draft. YS: Writing – original draft, Writing – review and editing. ZZ: Writing – original draft, Writing – review and editing.

Funding

The authors declare that financial support was received for the research and/or publication of this article. The present work was financially supported by Natural Science Foundation of China (52270129), Oriental Talent Youth Program, Shanghai Shuguang Program (23SG52), Guizhou Provincial Key Technology R&D

Program (QKHZC (2024)153), and Guizhou Provincial Science and Technology Projects (QKHZC (2023)YB138 and QKHZC (2023) YB141). YG also thanks the financial support of Science and Technology Development Fund of Pudong New Area (PKJ2022-C07).

Acknowledgements

We thank all the authors, and reviewers who collaborated with this Research Topic.

Conflict of interest

The authors declare that the research was conducted in the absence of any commercial or financial relationships that could be construed as a potential conflict of interest.

Generative AI statement

The authors declare that no Generative AI was used in the creation of this manuscript.

Any alternative text (alt text) provided alongside figures in this article has been generated by Frontiers with the support of artificial intelligence and reasonable efforts have been made to ensure accuracy, including review by the authors wherever possible. If you identify any issues, please contact us.

Publisher's note

References

Boisseaux, P., Delignette-Muller, M. L., and Galloway, T. (2025). A quantitative environmental risk assessment for microplastics in sewage sludge applied to land. *Environ. Sci. Technol.* doi:10.1021/acs.est.5c08026

Hu, W., Zhang, Z., and Mu, G. (2025). Microplastics indirectly affect soil respiration of different-aged forest by altering microbial communities and carbon metabolism. *J. Hazard. Mater.* 494, 138532. doi:10.1016/j.jhazmat.2025.138532

Jomova, K., Alomar, S. Y., Nepovimova, E., Kuca, K., and Valko, M. (2025). Heavy metals: toxicity and human health effects. *Archives Toxicol.* 99 (1), 153–209. doi:10.1007/s00204-024-03903-2

Lou, X.-Y., Liang, J., Liu, S., Wang, J., and Chen, H. (2024). From grave to cradle: treatment, resource recycling, and valorization of phosphogypsum wastes. *Environ. Sci. Technol.* 11 (9), 908–919. doi:10.1021/acs.estlett.4c00530

Peng, J., Feng, Y., Xiao, A., Li, B., Ding, D., Wang, G., et al. (2025). A review of emission characteristics and risk assessments of volatile organic compounds in petrochemical industry areas. *Environ. Pollut.* 367, 125576. doi:10.1016/j.envpol.2024.125576

Xiao, J., Zhang, Z., Liu, P., Guo, X., Yang, X., Zhang, F., et al. (2025). Microplastic-derived carbon emissions: from granular carbon to dissolved organic carbon and carbon dioxide under ultraviolet radiation. *Environ. Sci. Technol.* 59 (32), 17310–17321. doi:10.1021/acs.est.5c06601

Xu, W., Jin, Y., and Zeng, G. (2024). Introduction of heavy metals contamination in the water and soil: a review on source, toxicity and remediation methods. *Green Chem. Lett. Rev.* 17 (1), 2404235. doi:10.1080/17518253.2024.2404235

Yan, Q., Lin, S., Wei, F., Deng, T., Yang, Y., Zhang, Z., et al. (2025). Effects of different eco-stoichiometric ratios of calcium and cadmium on the detoxification mechanisms of Capsicum annuum L. under cadmium stress. *J. Hazard. Mater.* 487, 137059. doi:10.1016/j.jhazmat.2024.137059

Zhang, Y., Fu, P., Ni, W., Zhang, S., Li, S., Deng, W., et al. (2024). A review of solid wastes-based stabilizers for remediating heavy metals co-contaminated soil: applications and challenges. *Sci. Total Environ.* 920, 170667. doi:10.1016/j.scitotenv.2024.170667

Zhou, X., Zhou, X., Wang, C., and Zhou, H. (2023). Environmental and human health impacts of volatile organic compounds: a perspective review. *Chemosphere* 313, 137489. doi:10.1016/j.chemosphere.2022.137489

frontiers | Frontiers in Environmental Science

TYPE Review
PUBLISHED 09 August 2024
DOI 10.3389/fenvs.2024.1443633

OPEN ACCESS

EDITED BY
Zhenming Zhang,
Guizhou University, China

REVIEWED BY
Wenbing Tan,
Chinese Research Academy of Environmental Sciences, China
Xunfeng Chen,
Jiangsu Univerisity, China

*CORRESPONDENCE
Yuan Liu,
liuyuan01@caas.cn

RECEIVED 04 June 2024
ACCEPTED 30 July 2024
PUBLISHED 09 August 2024

CITATION
Jia Z, Cai A, Li R, Wang X and Liu Y (2024) Knowledge map and hotspot analysis in source appointment of heavy metals from 1994 to 2022: a scientometric review.
Front. Environ. Sci. 12:1443633.
doi: 10.3389/fenvs.2024.1443633

Knowledge map and hotspot analysis in source appointment of heavy metals from 1994 to 2022: a scientometric review

Ziyi Jia[1,2], Angzu Cai[3], Rui Li[2], Xia Wang[2] and Yuan Liu[1]*

[1]Institute of Farmland Irrigation of CAAS, Xinxiang, China, [2]College of Energy and Environment Engineering, Hebei University of Engineering, Handan, China, [3]Institute of Environmental Planning and Management, College of Environmental Science and Engineering, Tongji University, Shanghai, China

In recent decades, more and more studies have been conducted on source appointment of heavy metals, since they can accumulate in the food chain and have a negative impact on the ecological environment and human health. However, almost never before had scholars tried to make a comprehensive and methodical review in this field from the scientometric and bibliometric perspective. The purpose of this review is to offer insights into the research topics and trend evaluation in terms of source appointment of heavy metals over time using the visualization and analysis software, CiteSpace. We retrieved a total of 2,533 articles from the Web of Science Core Collection (WoSCC) dated between 1994 and 2022, and analysed the progress, hotspots, and trends in this field by synthesized networks of cooperation analysis, co-citation analysis, keyword co-occurrence and cluster analysis, and keywords burst analysis. The overall development of the topic can be divided into four periods, and the rapid development began from 2010. Environmental Sciences was the leading subject category, and the journal Science of the Total Environment had the highest number of publications (9.51%), which was most cited as well (2,390 times). China published the most articles in this field, in which Chinese Academy of Sciences was the leading institution. Said Muhammad and Xinwei Lu were the top two most productive authors. According to citation frequency, Hakanson L was the movers and shakers. Keyword co-occurrence and cluster analysis results showed that "the health risk assessment," "lake sediments", "trace elements," "positive matrix factorization," "air pollution," "road dust," and "megacity" are likely to be hotspots. The "particulate matter," "China," "sediments" and "road dust" demonstrated the research tendencies of this domain by keyword burst analysis.

KEYWORDS

bibliometric analysis, heavy metals, source appointment, knowledge mapping, citespace

1 Introduction

With the rapid development of industrialization and urbanization in the world, heavy metals pollution in the environment has become common on a global scale, and it interferes with the natural geochemical cycle of the ecosystem. The sources of heavy metals in the environment can be divided into natural sources and man-made sources. The natural source is influenced by geological background and weathering of parent rock. Man-made sources are affected by human activities, including mining, smelting, transportation, the improper discharge and use of industrial wastewater and domestic sewage, and the overuse

of pesticides and fertilizers (De Temmerman et al., 2003; Chary et al., 2008; Cai et al., 2009; Lu et al., 2012). Heavy metals are relatively stable once entering the environment and difficult to be degraded, hence heavy metal pollution has concealment, lag and stability (Jacob et al., 2018). In addition, heavy metals can also enter the human body through a variety of ways, thereby endangering human health (Zhang et al., 2018; Duan et al., 2020; Wang X. et al., 2023; Zhou et al., 2023). The source apportionment of heavy metals can effectively identify the main sources of heavy metals, which makes it possible to control the environmental pollution from the source and to make better prevention and control measures (Dong et al., 2019; Banerjee et al., 2023; Sun et al., 2023; Zhang et al., 2023; Zou et al., 2023). Therefore, source apportionment is very important for effectively alleviating pollution of heavy metals.

In recent years, the field of source apportionment of heavy metals has attracted more and more scholars' attention, and many articles on source apportionment of heavy metals have been published, including review articles (Cheema et al., 2020; Sun et al., 2020; Chu et al., 2023). With the involvement of scholars in various fields, the source analysis techniques have become more diversified. Existing source apportionment can be classified into source identification and source quantification. Source identification defines the types of pollution sources, while source quantification determines their contribution (Xue et al., 2023). So far, there are a tremendous number of methods for the source apportionment of heavy metals. Multivariate statistical analysis is the traditional source apportionment method (Simeonov et al., 2005), which includes Diffusion Model and Receptor Model (Henry et al., 1984). The diffusion model is based on the emission intensity of pollution sources, combined with the geographical location, climate and other factors, to simulate the process of pollutant transmission and transformation, and then quantify the contribution of pollution sources. Diffusion Model includes geostatistics and mixed distribution model method, *etc.* (Xu and Tao, 2004; Lee et al., 2006). The receptor model takes the polluted area as the research object, carries out the qualitative and quantitative analysis for the pollutants in the samples of the studied area, and combines the model algorithm to identify the kind of pollution sources, which is the most widely used model in the field of the source apportionment of heavy metals. The enrichment factors (EFs), factor analysis (FA), cluster analysis (CA), principal component analysis (PCA), absolute principal component analysis (APCS), chemical mass balance (CMB), positive matrix factorization (PMF), empirical orthogonal functions (EOF), multiple linear regression (MLR), UNMIX, and other multivariate data analysis methods are the commonly used receptor models (Watson et al., 2002; Xue et al., 2014; Wang et al., 2015; Huang et al., 2018; Xu et al., 2023a; Khan et al., 2023). In addition to the above, the isotope tracer technique has also been widely used recently (Chen et al., 2022; Shen et al., 2023). The Diffusion Model and Receptor Model both possess advantages, uncertainty and other inevitable disadvantages. Therefore, most researchers often combine multiple models to carry out source apportionment of heavy metals, making the results more accurate and reliable (Liu et al., 2018; Men et al., 2019; Wang Y. et al., 2021). These published literatures focus on how to use source apportionment methods, which indicates that the research progress of source apportionment of heavy metals has been neglected to a certain extent. We think it is necessary to summarize the development of this field and predict the future trend. By conducting a systematic scientometrics review of the field, it is possible to explore the scope of research, quantify research models, clarify knowledge structures, predict emerging trends, and fill gaps in the existing published literature. In addition, mapping and visualizing the structure and dynamics of a research field helps to quickly organize a large number of published articles and efficiently grasp the progress and frontiers of the research field.

Bibliometrics analysis is a discipline that performs qualitative and quantitative analysis of all publications included in a database, based on statistics and computational techniques (Aleixandre-Benavent et al., 2017; Liu et al., 2019). Through bibliometrics, the development process, characteristics and future trends of a certain field can be clearly and succinctly summarized (Batagelj and Cerinšek, 2013; Martínez et al., 2015; Gutiérrez-Salcedo et al., 2018). To date, bibliometrics has been widely used in different studies by scholars in various fields (Ekundayo and Okoh, 2018; Wang et al., 2018). Based on co-occurrence, clustering and emergent analysis of literature information and other bibliometrics methods, the science knowledge map in a certain research field can be visualized in the form of graphs and tables (Fu et al., 2022; Liu M. et al., 2023), by which researchers can get a more intuitive understanding of this research field (Osinska and Bala, 2015).

It is difficult to obtain valuable information directly from a large number of literatures, which requires the assistance of computers. Since the introduction of visualization in bibliometrics, there are many scientific knowledge mapping tools available today. Citation Space (CiteSpace), VOSviewer, CitNetExplorer, SCI2, and Gephi are the commonly used scientometrics softwares (Light et al., 2014; Van Eck and Waltman, 2014; 2017; Donthu et al., 2020; Ding and Yang, 2022). Among them, CiteSpace has some advantages. CiteSpace is a visual analysis software developed by Dr. Chaowei Chen on the basis of bibliometrics and data visualization, and the analysis is based on the premise of cited literature information (Chen, 2004), and carried out from multiple dimensions when figuring out the development of a certain field. And it is capable of conducting time domain analysis and burst detection to more accurately show the dynamic change of information in the research field (Meerow et al., 2016; Yang et al., 2017; Chen and Song, 2019). Compared to other software, it can be run without a complex java environment, and updated easily. In addition, its results are presented visually. When the citation data is large or involves a long period of time, CiteSpace provides some network pruning algorithms, such as MST or Pathfinder, to highlight the main body by reducing unnecessary weak branches.

CiteSpace has been successfully used in many cases. For example, using CiteSpace software, a bibliometrics analysis was conducted on the development of PAHs bioremediation in water environment from 1990 to 2022, and the basic characteristics, hotspots and prospects of the research field from the perspective of time and space were discussed (Xia et al., 2023). Nearly 25 years of data in China's climate resilient infrastructure were analyzed by Yijun Liu et al. using CiteSpace to provide guidance for urban planning and construction (Liu Y. et al., 2023). Based on CiteSpace, a comprehensive understanding of sediment and nutrient interception in river DAMS was obtained (Shi and Qin, 2023). This software is also gradually applied in the source apportionment of heavy metals (Wang J. et al., 2021), the relevant literature is however very scarce, and up to now, no scholars have conducted a

complete, intuitive and reliable analysis in the research progress of source apportionment of heavy metals in various environmental media. Review articles in this field generally focused on introducing the source appointment methods, or used summary language to quickly bring readers up to speed on the latest developments in the field. While this kind of landscape fails to present the whole picture of the research field and its dynamics, and the identified emerging trends by which has certain limitations (Wu et al., 2021). Specifically, at present, there is a lack of systematic review of the research field of source apportionment of heavy metals, hindering the sufficient understanding of the characteristics and emerging trends of existing research as well as the development of research. Consequently, it is very necessary to summarize the development process of this research field, point out the shortcomings of the present study, and predict the future development trend.

This review aims to comprehensively get the whole picture of the research field of source apportionment of heavy metals by answering the following questions: 1) What is the change trend of the number of papers published in this field? What is the overall development process of this field? What are the characteristics of the development of this field? Is this field gaining more scholars attention now? 2) In the development process of this field, what are the important subject categories, journals, countries, institutions, scholars, and literatures? How is the cooperation between countries, institutions and scholars? 3) Do the research hotspots in this field change significantly with years? How has it changed? 4) How will this field develop in the future? The visual analysis work using CiteSpace (6.2.R2) in this review was carried out to summarize the overall development process in this field from 1994 to 2022.

2 Data acquisition and methods

2.1 Data collection

Web of Science (WoS) is the worldwide premier scientific index website developed by the Institute for Scientific Information (ISI) and currently operated by Clarivate Analytics (Chi and Glänzel, 2017; Bao et al., 2023). In order to select high-quality articles in the field of source apportionment of heavy metals, this paper selects representative literatures from the Web of Science Core Collection (WoSCC), so that the subsequent visualization results can be more convincing. In this paper, the search scope of WoS was set as "topic" and the search terms were set as "source apportionment" and "heavy metals". A total of 2,553 articles were retrieved, and the earliest literature was published in 1988, so the time span was set as 1988–2022. The literature selection type is "Article" and "Review Article". In addition, in order to ensure the relevance of the data, the contents of the retrieved literature are scanned and checked according to title, abstract and keywords, and the irrelevant and duplicated literatures were removed (Zhang et al., 2021). Accordingly, 2,533 relevant publications, ranged from 1994 to 2022, were obtained and analyzed. Then, the content and the file format were set to "Full Records and Cited References" and "Pure Text" to export WoS information, respectively. All files were exported in batches in sequence and their formats were converted to a download_.txt format that CiteSpace can identify. Finally, the sorted literature records were imported into CiteSpace (6.2.R2) for visual analysis.

2.2 CiteSpace parameters setting

CiteSpace (6.2.R2) was used to visually analyze the annual number of publications, category, journal, country, institution, author, number of co-citations and keywords of the literature data, and the time threshold was selected from 1994 to 2022. The parameters used in the construction of these above graphics varied depending on the presentation effect. For the visual analysis of co-citation of keywords and journals, the top 20 papers cited in each time slice (1 year) were selected, and the node type was selected as Keyword or Cited Journal according to the analysis purpose. In the visual analysis of Country cooperation, the top 50 papers in a 1-year time slice were selected, and the node type was selected as Country. In the visual analysis of institutional cooperation, the time slice was set as 1 year, during which the top 10 papers cited were analysed, and the node type was selected as Institution. For the visual analysis of Author cooperation and co-citation, the top 10 papers cited in each 2 years were selected, and the Author or Cited Author was chosen for the node type. Network Pruning modes employed are Pathfinder and Pruning the merged network. Other parameters are the default ones.

3 Results

3.1 Basic characteristics of published articles

3.1.1 The number of published articles

By analyzing the annual and accumulated number of publication output in a certain field, we can grasp the overall development level and speed, and predict the future trend. In addition, the degree of attention paid by scholars to the topic in different time stages can also be presented (Geng et al., 2023; Song et al., 2023). From 1994 to 2022, the total number of publications was 2,533, with an increasing trend year by year in general, as shown in Figure 1.

According to the change of annual publication number in Figure 1, the research progress can be divided into four stages, with the annual publication number of less than 10, 10–20, 20–200, and more than 200 in the first, second, third, and fourth stage. In the initial stage from 1994 to 2002, only 19 papers were published, accounting for 0.75% of the total number of papers, and scholars lacked enough experience in exploring knowledge and conducting experiments in this field. Most literatures in this period were focusing on the source apportionment of heavy metals in the atmospheric environment, during which a study was conducted on heavy metals in indoor dust in 1998 (Adgate et al., 1998). The first paper on the source apportionment of heavy metals in the soil of industrial zones and in river basins was published in 1997 and in 1999, respectively (Davies, 1997; Vink et al., 1999). In stage 2 (a slowly developing stage) from 2003 to 2009, the number of published papers and associated scholars increased slightly, and totally 81 papers were published during this period, accounting for 3.2% of the total. The period from 2010 to 2017 (a rapidly developing stage) is the third stage, in which increasing scholars paid attention to this field, and the research system was gradually maturing. During this period, a total of 524 papers were published, accounting for 20.69% of the total number of papers. Lastly, the number of literatures publications grew exponentially from 2018 to 2022 in

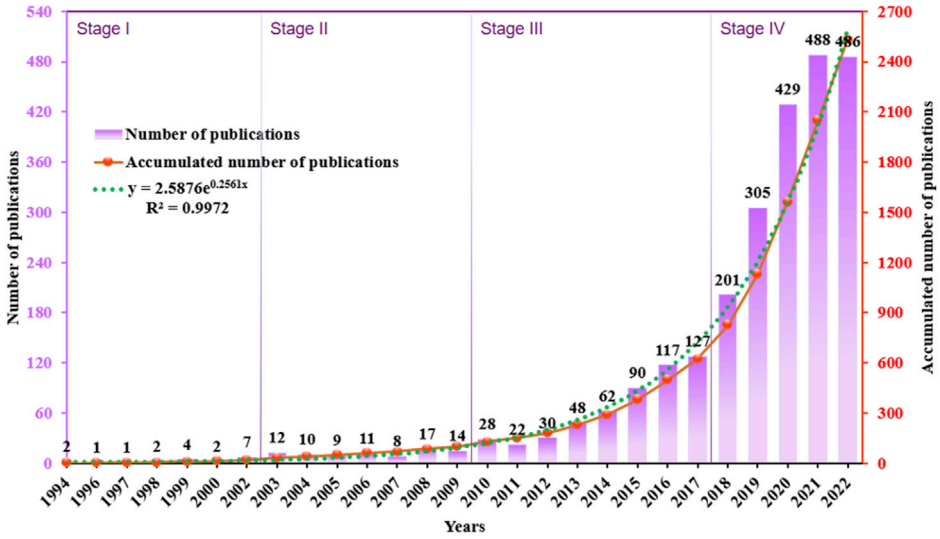

FIGURE 1
Annual and accumulated number of publication output.

TABLE 1 The articles output of the top ten subject categories.

Category	Stage 1 (1994–2002)	Stage 2 (2003–2009)	Stage 3 (2010–2017)	Stage 4 (2018–2022)	Article number
Environmental Sciences	10	61	425	1,591	2087
Environmental Engineering	1	11	44	228	284
Water Resources	4	7	52	191	254
Meteorology Atmospheric Sciences	5	22	70	134	231
Public Environmental Occupational Health	0	4	30	193	227
Toxicology	2	0	27	120	149
Geosciences Multidisciplinary	2	1	21	68	92
Green Sustainable Science Technology	0	0	6	67	73
Marine Freshwater Biology	1	1	22	46	70
Biodiversity Conservation	0	1	14	50	65

the fourth stage, and during which 1909 papers were published, comprising 75.37% of the total.

The research content and methods in this field are becoming more and more diversified, and the research areas involved are also increasingly extensive. According to WoS statistics, only 33 research areas were involved in the first stage, and 53, 92, and 101 areas in the second, the third, and the fourth stage, respectively. This demonstrates that the source apportionment of heavy metals is being paid more and more attention by scholars in various fields. In summary, the study of source apportionment of heavy metals is gradually becoming common, and this trend will continue in the future as the government and the public are progressively concerned about environmental pollution.

3.1.2 Category analysis

The category analysis can reveal the breadth of the types of subject categories involved in the field of source apportionment of heavy metals, and help researchers grasp the scope of categories, so as to judge whether the field tends to be specialized or comprehensive. According to the statistics of WoS database, the top ten subject categories of this field are obtained, which are listed in Table 1.

Changes in the number of publications in each category reflects the development tendency of source apportionment of heavy metals research in each different research area. As shown in Table 1, the categories to which these articles belong are intersected, and most of the literatures are closely related to the category of Environmental

TABLE 2 Top 10 journals in terms of number of articles.

Rank	Journal	Number of publications	Total citations	Total citations per publication	h-index	Impact factor (2021–2022)	Quartile in JCR
1	Science of The Total Environment	241	328,230	1,362.0	205	10.753	Q1
2	Environmental Science and Pollution Research	177	110,000	621.5	82	5.190	Q1
3	Environmental Pollution	130	119,445	918.8	194	9.988	Q1
4	Chemosphere	125	172,919	1,383.4	212	8.943	Q1
5	International Journal of Environmental Research and Public Health	91	123,105	1,352.8	78	4.614	Q2
6	Environmental Geochemistry and Health	81	8,659	106.9	60	4.898	Q2
7	Atmospheric Environment	80	77,550	969.4	211	5.755	Q2
8	Ecotoxicology and Environmental Safety	72	56,014	778.0	110	7.129	Q1
9	Journal of Hazardous Materials	72	187,102	2,598.6	235	14.224	Q1
10	Environmental Monitoring and Assessment	69	32,152	466.0	91	3.307	Q3

Sciences. In addition, the number of publications in stage 4 in the Environmental Sciences, Environmental Engineering and Public Environmental Occupational Health categories increased significantly by more than 158 times comparing stage 1, while the growth trend of publications in other categories was much more moderate. Compared with stage 1, only no more than three published articles were increased in stage 2 in most categories (Water Resources, Public Environmental Occupational Health, Biodiversity Conservation, Green Sustainable Science Technology, Marine Freshwater Biology, and Toxicology and Geosciences Multidisciplinary). From 1994 to 2009 (stage 1 and stage 2), the related papers were mainly published in the categories of Environmental Sciences, Environmental Engineering, and Meteorology Atmospheric Sciences, and most papers only concentrated on atmospheric environment. In contrast, compared with stage 2, the article number of all categories in stage 3 mounted markedly, with six in the category of Green Sustainable Science Technology, more than 20 in the category of Toxicology, Geosciences Multidisciplinary and Marine Freshwater Biology, and the maximum 364 in the category of Environmental Sciences. Excitedly, compared with the third stage, the article number augment in each category in the fourth stage is between 24 and 1,166, showing an obvious increasing trend. The field of source apportionment of heavy metals is developing in the direction of diversification, and has received more and more attention. The range of categories in this field is very extensive, indicating researchers can communicate and collaborate across categories, which is conducive to promote the rapid development of this field.

3.1.3 Journal analysis

Number of publications in a journal can reflect its influence in a certain field, which can help scholars to effectively get an overview of leading journals in this field, lock the key learning scope, and grasp the latest research development status. According to the statistics of WoS database, the 2,533 literatures selected in this study come from 200 journals. Table 2 shows the top 10 journals with the highest number of publications, totally accounting for 44.91% of all literatures. All the 10 journals are related to the category Environmental Sciences. Additionally, both “International Journal of Environmental Research and Public Health” and “Environmental Geochemistry and Health” belong to the category Public Environmental Occupational Health; both “Environmental Geochemistry and Health” and “Journal of Hazardous Materials”, “Atmospheric Environment”, and “are also involved in the category Environmental Engineering; “Environmental Geochemistry and Health”, and “Ecotoxicology and Environmental Safety” are also associated with emerging fields Water Resources, Meteorology Atmospheric Sciences, and Toxicology, respectively.

“Total citations” (TC) refers to the total number of citations of articles in a journal. Generally speaking, the more TC is, the more influence is reflected in the research field. Total citations per publication (TC/P) represents the average number of citations per article in the journal. The influence of a journal may vary in different research fields, so the combination of TC and TC/P can be a relatively good measure of the relative importance of a journal in a specific field (Ji et al., 2014; Huang et al., 2020). The h-index is “high citations”, which means that h articles in a journal are cited at least h times per article. The higher the h-index, the more influential the articles published in the journal (Hirsch, 2005). The impact factor (IF) data (2021–2022) are obtained from Web of Science. IF is generally used to measure the value and position of a journal in science communication. Based on the Web of Science database, Clarivate Analytics ranks journals in each discipline according to the IF numerical ranking, forming the Journal Citation Reports (JCR), the official internationally recognized zoning method of SCI. Both the IF and the Quartile in JCR represent the quality of the journal.

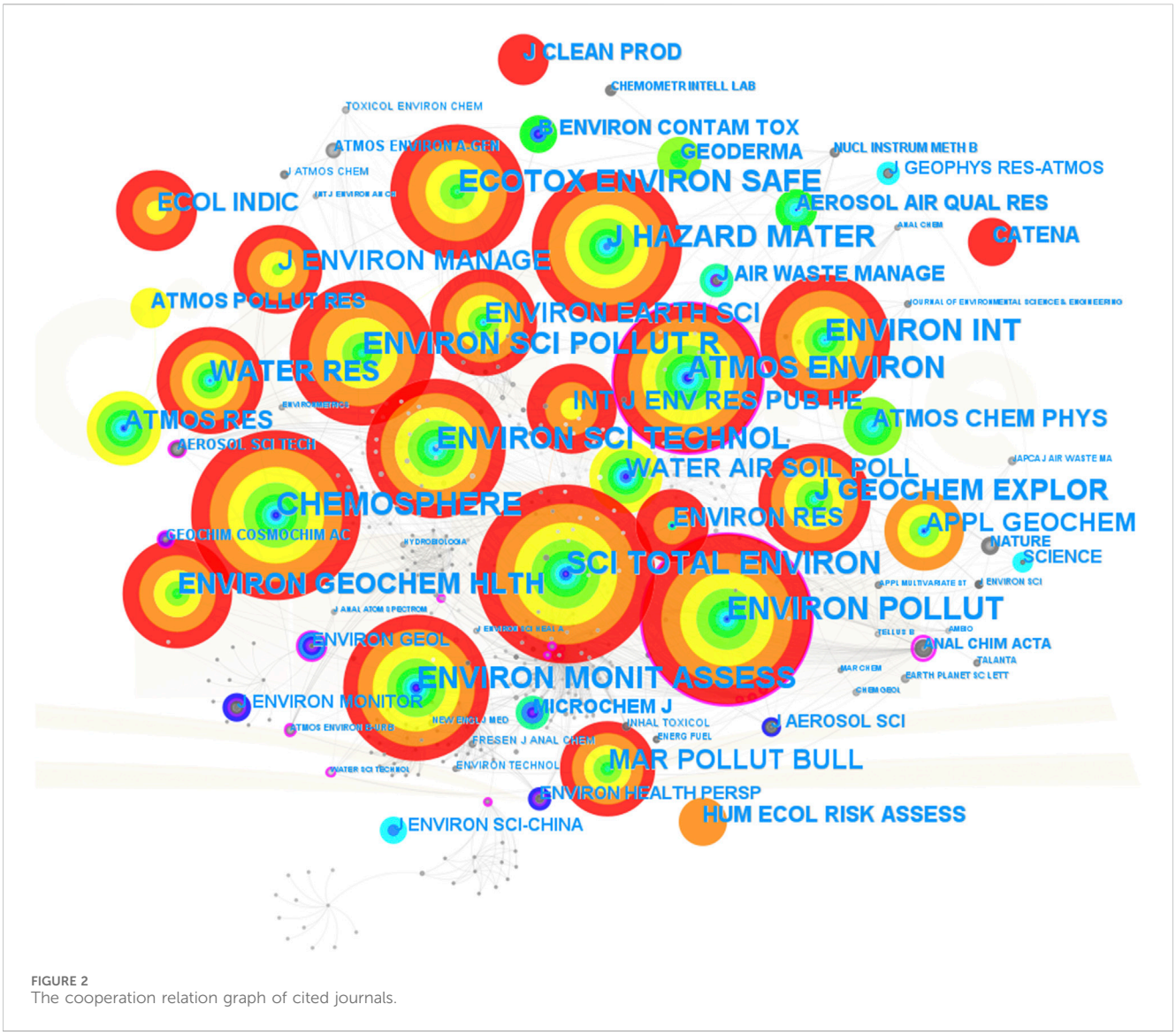

FIGURE 2
The cooperation relation graph of cited journals.

All the values for these above parameters are shown in Table 2. Science of The Total Environment is the top journal in terms of publication quantity, followed by Environmental Science and Pollution Research, Environmental Pollution and Chemosphere. Except for the Q1 journals, there is no significant difference in the number of publications of the remaining journals. The journal with the highest TC/P is Journal of Hazardous Materials (JHM), followed by Chemosphere and Science of The Total Environment. JHM also possesses the topmost h-index, followed by Chemosphere, Atmospheric Environment, and Science of The Total Environment. The journals with high IF are JHM, Science of The Total Environment, and Environmental Pollution, in that order. It can be seen that the three parameters TC/P, h-index and IF of the journals have a certain consistency. However, there is no positive relationship between the number of publications and them. For example, Environmental Science and Pollution Research has the second maximum number of publications, but it does not have a high TC/P, h-index or IF. Therefore, the publication of high-quality literatures is more conducive to improving the influence of journals in the field. And scholars should not blindly pursue the quantity of published papers, but rather improve the quality of published papers, so as to bring leading value to the research field. Collectively, JHM, Science of The Total Environment, Environmental Pollution, Chemosphere, and Atmospheric Environment have both a high number of publications and a high influence in the field of source apportionment of heavy metals. The top ten journals in Table 2 cover publications related to a wide range of research fields, which indicates that the researches on source appointment of heavy metals are intersectional and diverse.

The number of co-citation frequency is positively correlated with the influence of journals. Figure 2 shows the cooperation relation graph of cited journals, containing 466 nodes and 1,665 links. The co-citation frequency of each journal can be intuitively sensed, and the nodes are proportional to the co-citation frequency of the journal (Xu et al., 2023b). In addition, in order to further analyze the co-citation of journals in detail, the top 10 journals in the field of source appointment of heavy metals were counted, as shown in Table 3. Number of co-citation frequency, centrality, and Year are all exported by CiteSpace, in which the

TABLE 3 Top 10 co-citation by journals.

Rank	Cited journals	Number of co-citation Frequency	Centrality	Year	If (2021–2022)	Quartile in JCR
1	Science of The Total Environment	2,390	0.03	1996	10.753	Q1
2	Environmental Pollution	2,123	0.17	1997	9.988	Q1
3	Chemosphere	2,110	0	2002	8.943	Q1
4	Atmospheric Environment	1729	0.12	1994	5.755	Q2
5	Journal of Hazardous Materials	1,660	0	2008	14.224	Q1
6	Environmental Science & Technology	1,619	0.07	1994	11.357	Q1
7	Environmental Science and Pollution Research	1,557	0.03	2002	5.190	Q1
8	Environmental Monitoring and Assessment	1,554	0.03	2002	3.307	Q3
9	Ecotoxicology and Environmental Safety	1,328	0	2005	7.129	Q1
10	Environment International	1,322	0	2002	13.352	Q1

higher the centrality, the greater the influence of the journal, and the "Year" refers to the earliest co-cited year of the journal.

As shown in Table 3, Science of The Total Environment has the highest co-citation frequency (2,390 times), followed by Environmental Pollution (2,123 times), Chemosphere (2,110 times), Atmospheric Environment (1729 times), Journal of Hazardous Materials (1,660 times). However, there is no consistency between the results of co-citation frequency and centrality. The two journals with higher centrality are Environmental Pollution (0.17) and Atmospheric Environment (0.12) in order. The rest have very low centrality, in particular the centrality of Chemosphere and Journal of Hazardous Materials is 0. In other words, the more co-citation do not necessarily mean the higher influence. The same conclusion can be obtained by comparing the number of co-citation frequency and the IF. Therefore, scholars should consider multiple factors such as number of co-citation frequency, centrality, and IF simultaneously when exploring high-impact journals in the field. In general, high impact analysis results of journals are highly consistent with the results of number of publications analysis. Almost all journals in Table 3 have low centrality. And no journal has both high centrality and high IF. This indicates that no journal has a very prominent performance and also plays a very important role in this research field so far, and the journals still need to further improve the quality of their papers and enhance their influence in the future, so as to obtain more citations from scholars. The earliest co-cited year is mainly between 1994 and 2008, indicating that in this initial stage, scholars begun to pay attention to the source apportionment of heavy metals, which provided the necessary foundation for the subsequent exponential growth in this field. Atmospheric Environment, Environmental Science and Technology, Science of the Total Environment and Environmental Pollution are the first batch of co-citations, indicating they are undoubtedly veteran journals in this field.

In summary, both journal number of publications analysis and journal co-citation analysis show that Science of The Total Environment, Environmental Pollution, Chemosphere, Atmospheric Environment and Journal of Hazardous Materials are leading journals in the field of source apportionment of heavy metals. Besides, Environmental Science and Technology is a veteran journal, and deserve scholars' attention. And the above analysis results can provide researchers some insights: If researchers are looking for authoritative journals in a research field in order to grasp the research frontiers, they should take into account the number of co-citation, centrality, impact factor, and Quartile in JCR of the journal synthetically. And they should consult a variety of journals instead of a single one, ensuring the comprehensiveness of the study.

3.2 Research power analysis

3.2.1 The major countries and institutions

The countries cooperation network can directly reflect the number of papers issued by each country and the international cooperation situation, and indirectly reveal the influence of each country in the field of source apportionment of heavy metals. Figure 3 shows the visualization network map of countries cooperation derived by CiteSpace, which contains 104 nodes and 204 links. Each node represents the published papers by one country in this field. The larger the node, the more the published papers. And the number of links is directly proportional to the frequency of cooperation between countries. In addition, in order to show more detailed information, Table 4 shows the top 15 countries in this field, which includes 10 developed countries and five developing countries. The higher the centrality, the greater the influence of the country in the research field. The "Year" refers to the time of the first publication of a country.

As shown in Table 4, it can be seen that the development degree of a country has a certain relationship with its influence in the field of source appointment of heavy metals. The more advanced the development degree of a country is, the greater its influence in this field is, and the more it cooperates with other countries. For example, the countries with a high centrality include Japan (0.25), Spain (0.22), Germany (0.15) and America (0.11), indicating that they have a greater influence and a leading role in this field, and at the same time they are all developed countries. The

FIGURE 3
The cooperation network of countries.

reason for this may be that the higher a country's level of development is, the stronger people's awareness of environmental protection tends to be. In addition, the comprehensive environment-related policies and highly developed research technologies also underpin the research in the developed countries, which always cooperate frequently to jointly promote development. Countries with a large number of publications include China, India, America, Iran and Pakistan. China takes the leading position with 1,389 published papers. However, the centrality of China is only 0.04, indicating that despite the high volume of Chinese publications, it lacks cooperation and communication with other countries, and its influence in this field is still insufficient. Therefore, Chinese scholars need to seek innovation and breakthrough. Similar to China are countries like India, Iran, Pakistan, and so on, whose partnerships and influence will have greater room for progress in the future. The earliest articles were published before the 20th century in Canada, Germany and America. It shows that they started to pay attention to environmental pollution earlier. In conclusion, Japan, Spain, Germany, America and China are the countries that have made major contributions to the field of source apportionment of heavy metals. Researchers should comprehensively consider the development degree, publications and influence of a country when choosing partners. In addition, researchers should select more international scholars who are cooperative to promote research progress.

The analysis of cooperation network of institutions can reveal the contribution degree of each institution in the field of source apportionment of heavy metals, and can also reflect the cooperation situation among institutions. To better understand the recent research situation and analyze the potential development trend in the future, Figure 4 shows the visual network diagram of institutional cooperation exported by CiteSpace, which contains 338 nodes and 475 links. The size of the node is proportional to

TABLE 4 Top 15 contributing countries.

Rank	Country	Development situation	Number of publications	Centrality	Year
1	China	Developing	1,389	0.04	2004
2	India	Developing	201	0	2004
3	United States	Developed	189	0.11	1999
4	Iran	Developing	127	0.04	2014
5	Pakistan	Developing	119	0.04	2006
6	England	Developed	79	0.01	2003
7	Australia	Developed	75	0.1	2002
8	Italy	Developed	72	0	2006
9	Spain	Developed	69	0.22	2002
10	South Korea	Developed	64	0.04	2011
11	Germany	Developed	62	0.15	1999
12	Canada	Developed	58	0.04	1998
13	Japan	Developed	55	0.25	2004
14	Bangladesh	Developing	50	0.03	2008
15	Saudi Arabia	Developed	49	0.07	2012

the institutional number of publications. And the more links, the more inter-institutional cooperation.

As shown in Figure 4, compared to the number of nodes, the number of links is relatively small, indicating that inter-institutional cooperation is lacking. In addition, there are obvious four cooperative groups, and there are no links among these groups, so institutions in this field tend to have fixed partners and form groups, and communication between groups is very poor. This phenomenon may be related to different laws and policies in different countries (Zhang et al., 2017). Such solidified partnerships are not conducive to research breakthroughs. For further precise analysis, Table 5 lists the top 15 institutions in this field by number of publications.

As shown in Table 5, most of the institutions are from China (12/15), and the other three institutions are from Pakistan and India. The top five institutions with the largest number of publications are the Chinese Academy of Sciences, the University of Chinese Academy of Sciences, Beijing Normal University, China University of Geosciences and the Chinese Academy of Environmental Sciences. They are major contributors to the literatures in the field of source apportionment of heavy metals, and have played an important role in the progress of this research. Besides, institutions with a high number of publications are all from China, meaning China takes the important position, which is consistent with the analysis conclusion of the country cooperation network map above. Centrality is one of the main factors that can reflect the influence of an institution in the research field (Geng and Maimaituerxun, 2022). The institution with higher centrality is Chinese Academy of Sciences (CAS) (0.11), while the centrality of others is low. As one of the key institutions in the field of source apportionment of heavy metals, CAS has significant academic influence and has frequent exchanges and cooperation with many other institutions. Institutions that have played a leading role in the early development of this field include the CAS (2004), the Council of Scientific and Industrial Research (2005), Quaid I Azam University (2006) and the Chinese Research Academy of Environmental Sciences (2009).

CAS has both the highest number of publications and the highest centrality, and it is also the first institution to publish relevant literature. And as shown in Figure 4, the main body of the institutional cooperation network is the group centered on the CAS, which means that it is undoubtedly the leading institution in this field. Therefore, scholars should keep an eye on the latest relevant literature published by CAS to better follow the latest developments in this field, and accurately predict the future development trend. The above analysis results show that inter-agency cooperation still needs to be further strengthened. Scholars in different institutions should communicate more to push the development of this field.

3.2.2 Author analysis

The author cooperation network can directly reflect the publication and cooperation of authors in a field, and suggest the most influential authors in the field. The cooperation between the authors who have never cooperated with each other might be the innovation and development direction of source apportionment of heavy metals research. Figure 5 shows a visual network diagram of author cooperation derived from CiteSpace, which contains 450 nodes and 967 links. The larger the nodes, the more papers published by the author; and the more links, the more frequent cooperation between authors (Rorissa and Yuan, 2012).

There is no significant difference in the size of nodes in Figure 5, indicating the number of publications by different authors is in a similar level. In addition, there are many collaborative groups among authors in this field, the largest of which are groups centered on X Querol and A Alastuey, and the number of

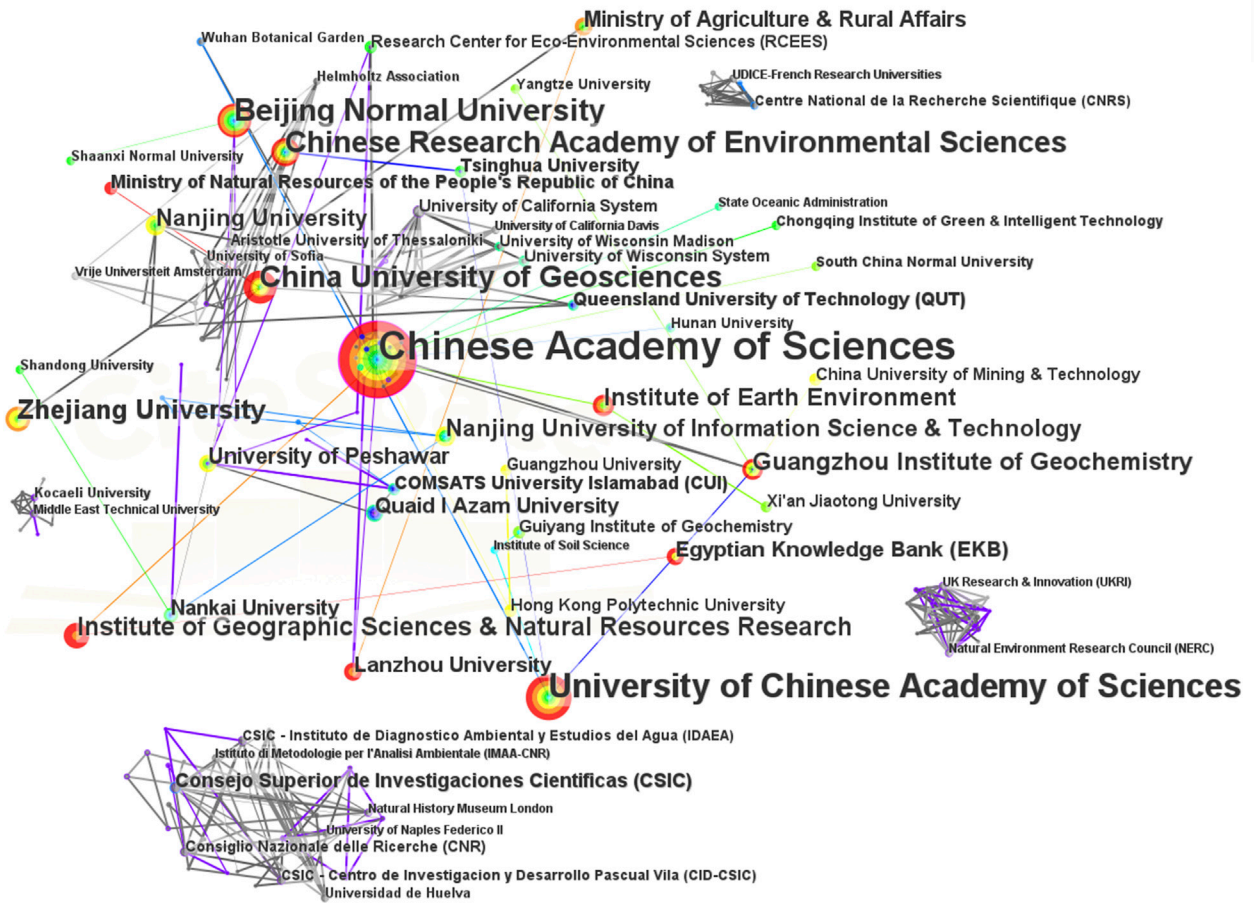

FIGURE 4
The cooperation network of institutions.

collaborators in the remaining groups is relatively small. Also, there is a lack of communication between groups, similar to the institutional collaboration described above. As such, scholars should strengthen exchanges and try interdisciplinary cooperation, in order to make greater breakthroughs in the analysis methods of source apportionment of heavy metals and their application. The top 10 authors in this field are listed in Table 6.

Among the top 10 authors, seven are from China, and the other three are from Pakistan and Saudi Arabia (Table 6). This is consistent with the above results of the country cooperation analysis. There is no significant gap in the number of publications between these authors. Authors with the maximum published literatures are Said Muhammad and Xinwei Lu. In the second tier are Idris Abubakr M, Junji Cao, and Yan Li. They are the major contributors to the publications in the field of source apportionment of heavy metals and have applied a number of representative methods for source apportionment study in soil, atmosphere and water environment, including PCA, PMF, isotopic tracer, among others (Du and Lu, 2022; Muhammad and Usman, 2022; Li N. et al., 2023; Liu S. et al., 2023; Proshad et al., 2023). For example, Said Muhammad et al. applied CA, PCI and PCA to analyze the pollution sources in the lake ecosystem (Tokatlı et al., 2024). Xinwei Lu et al. obtained the distribution of heavy metals sources in urban road dust using the PMF model (Hao et al., 2023).

The centrality values are all 0, which means that there is a lack of scholars with high influence in this field, and the cooperative relationship between scholars especially from different groups should be strengthened. In addition, the reason why most authors cooperate with fixed teams is also largely ascribed to regions, institutions, and research fields. For example, Said Muhammad mainly works in drinking water environment in Pakistan in source appointment of heavy metals research (Muhammad et al., 2011; Khan et al., 2015; Khan et al., 2016; Rehman et al., 2018; Jehan et al., 2019; Abeer et al., 2020). Xinwei Lu's collaboration focuses on source apportionment of heavy metals in Xi'an (Pan et al., 2017; Chen and Lu, 2018; Fan et al., 2021; Yu et al., 2021; Yu et al., 2023). Scholars can make use of the international exchange platform to promote more academic exchanges and cooperation.

During the top authors in Table 6, Said Muhammad and Sardar Khan are the scholars to publish the earliest relevant articles. However, the literature publication years by all the top authors are relatively late. Since 2010, the study of source apportionment of heavy metals has entered a stage of rapid development, so they did not make contributions to the initial research exploration of this

TABLE 5 Top 15 contributing institutions.

Rank	Institution	Country	Number of publications	Centrality	Year
1	Chinese Academy of Sciences	China	377	0.11	2004
2	University of Chinese Academy of Sciences	China	148	0.07	2011
3	Beijing Normal University	China	78	0.01	2010
4	China University of Geosciences	China	72	0.02	2011
5	Chinese Research Academy of Environmental Sciences	China	65	0.08	2009
6	Zhejiang University	China	43	0	2011
7	Institute of Geographic Sciences & Natural Resources Research	China	39	0	2021
8	Institute of Earth Environment	China	31	0	2019
9	Guangzhou Institute of Geochemistry	China	30	0.04	2010
10	Nanjing University of Information Science & Technology	China	28	0.01	2015
11	Nanjing University	China	26	0	2010
12	Ministry of Agriculture & Rural Affairs	China	22	0	2011
13	University of Peshawar	Pakistan	22	0.01	2011
14	Quaid I Azam University	Pakistan	21	0	2006
15	Council of Scientific & Industrial Research (CSIR) - India	India	20	0	2005

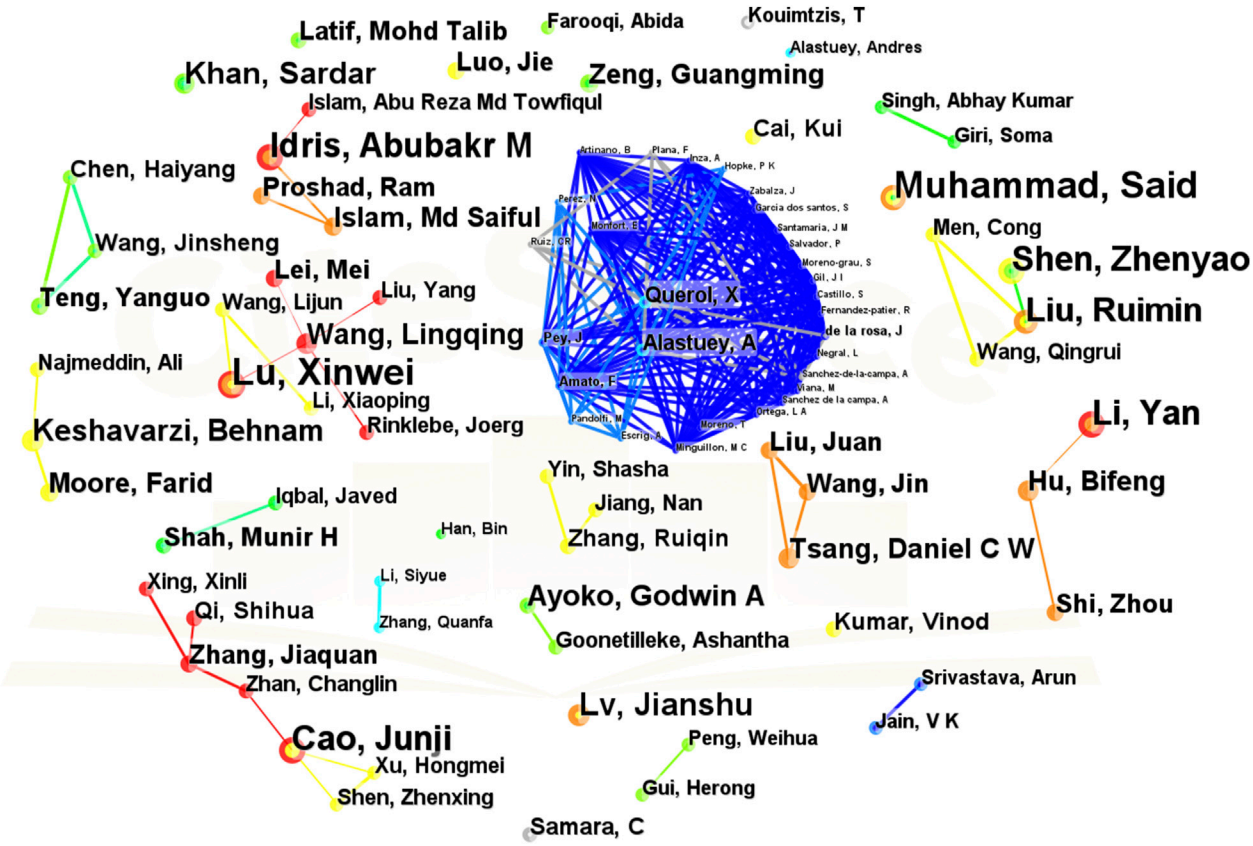

FIGURE 5
Author cooperation network.

TABLE 6 Top 10 authors in terms of number of publications.

Rank	Authors	Number of publications	Centrality	Year	Country
1	Muhammad, Said	21	0	2011	Pakistan
2	Lu, Xinwei	21	0	2018	China
3	Idris, Abubakr M	16	0	2020	Saudi Arabia
4	Cao, Junji	16	0	2018	China
5	Li, Yan	16	0	2020	China
6	Shen, Zhenyao	16	0	2015	China
7	Liu, Ruimin	15	0	2015	China
8	Lv, Jianshu	13	0	2018	China
9	Khan, Sardar	12	0	2011	Pakistan
10	Keshavarzi, Behnam	11	0	2018	Iran

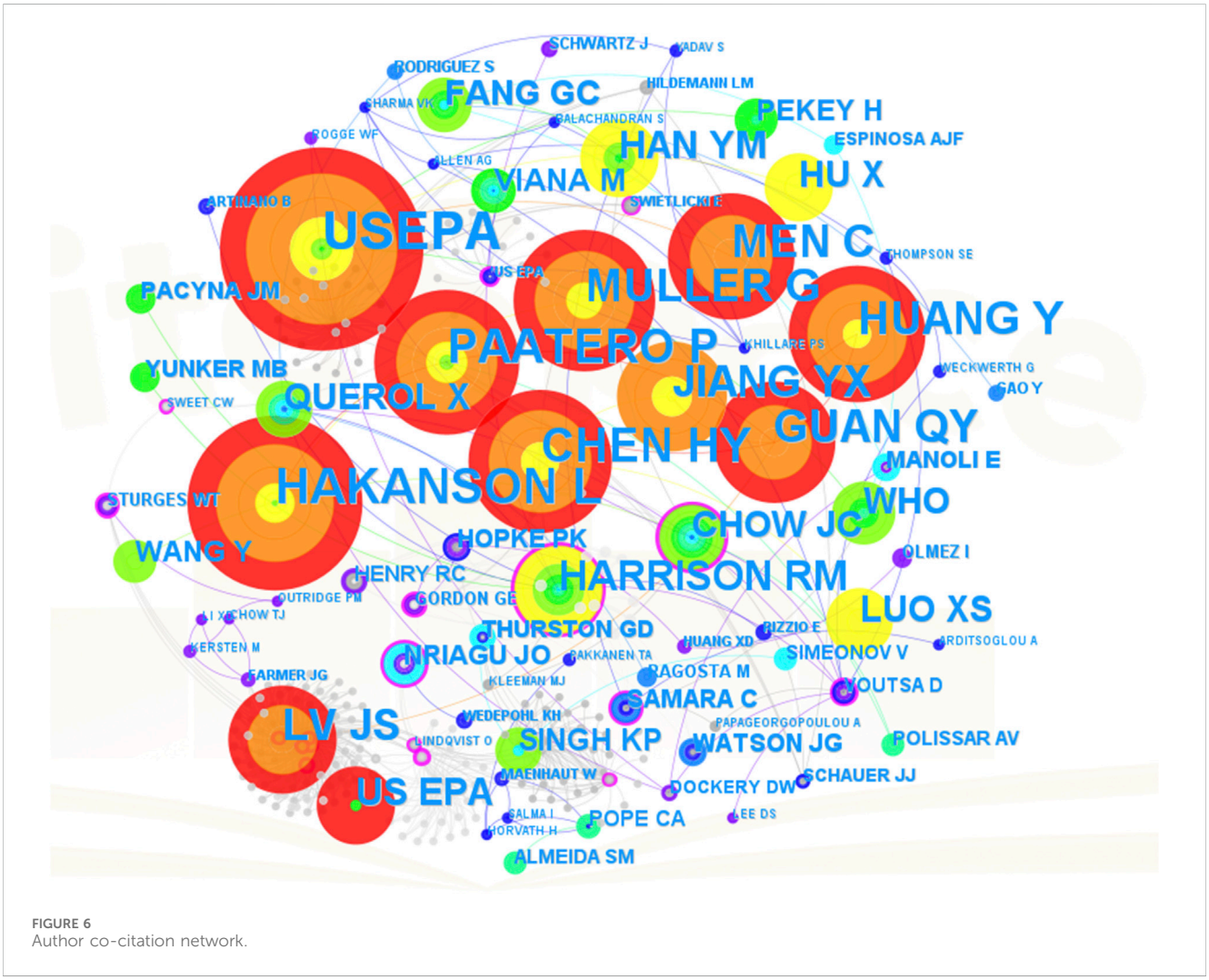

FIGURE 6
Author co-citation network.

field. The above analysis shows that authors need to promote cooperation with other teams, participate more in international exchanges, and communicate with scholars in different disciplines to contribute to new breakthroughs in research.

The author co-citation network reflects the influence of each author and help scholars quickly learn about the leading figure in a field. Figure 6 shows the author co-citation network derived from CiteSpace, which contains 323 nodes and 924 links. Nodes with

TABLE 7 Top 10 authors in terms of citations.

Rank	Cited authors	Number of co-citation frequency	Centrality	Year	Country
1	USEPA	635	0.03	2014	United States
2	HAKANSON L	460	0.01	2016	Sweden
3	PAATERO P	345	0.09	2012	Finland
4	CHEN HY	308	0.01	2018	China
5	MULLER G	303	0	2018	United States
6	HUANG Y	285	0	2018	China
7	MEN C	241	0	2020	China
8	GUAN QY	222	0.05	2020	China
9	JIANG YX	186	0.02	2018	China
10	LV JS	178	0	2020	China

purple outer rings have higher centrality. Table 7 shows the top 10 authors ranked according to the number of co-citations, including one organization (USEPA) and the rest individual authors. The highest co-citation frequency is the United States Environmental Protection Agency (USEPA), which is directly related to its concern about environmental pollution by heavy metals. The top individual authors who ranked behind USEPA are HAKANSON L (460), PAATERO P (345), CHEN HY (308), and MULLER G (303), indicating that the literature published by these authors has been recognized by many scholars. All the ten authors listed in Table 7 have a low centrality, and the highest centrality value is only 0.09. In addition, as shown in Figure 6, authors with high centrality do not have high co-citation frequency. Scholars should consider these two factors comprehensively when judging the influence of authors. As shown in Table 7, authors' co-citation time is generally concentrated from 2012 to 2020, which indicates that this research field is in a rapid development stage in this time. Moreover, most of the authors in the table are from China, which is consistent with the analysis results of the national cooperation and author cooperation mentioned above.

3.2.3 Reference Co-citation

The importance of a paper can usually be measured by two metrics: citation frequency and centrality. The more frequently an article is cited, the higher its recognition in the research field and the greater its contribution to promoting research progress is (Ale Ebrahim et al., 2013; Yoshikane, 2013). Centrality, the ratio of the shortest path between two nodes to the sum of all shortest paths, can identify potential key nodes quantifiably (Freeman, 2002; Chen, 2006). There is no linear relationship between the above two indicators, that is, an article with high citation frequency does not necessarily have high centrality, and *vice versa*. Only when an article has high values of both indicators at the same time, it has a greater influence in the research field.

Through the analysis of co-cited literature, the research knowledge base of source apportionment of heavy metals can be obtained, to more effectively discover the hot topics and development trends in this field (Persson, 1994; Musa et al., 2018; Shi and Liu, 2019). CiteSpace can show the literature co-citation network of a certain research field, and has been used by many scholars for literature co-citation analysis (Birmili et al., 2006; Thorpe and Harrison, 2008; Viana et al., 2008). In order to get a more detailed understanding of the literature citation situation, Table 8 lists the relevant data of the top 15 literatures with high citation frequency derived from CiteSpace. As shown in Table 8, the top 15 literatures contain five reviews, and the rest are case studies. The paper published by Yanxue Jiang has the highest cited frequency (182 times), followed by Qingyu Guan (133 times), both of which are cited more than 100 times. However, the centrality of these 15 literatures is generally low.

Many methods of the source apportionment of heavy metals have been applied in the top 15 most-cited literatures, which can also reflect the development of this field. At the beginning of the study, multivariate statistical analysis was the primary method for determining the sources of heavy metals (Birmili et al., 2006; Thorpe and Harrison, 2008; Viana et al., 2008). With the deepening of research, geostatistical analysis and receptor model analysis methods have been recognized by more and more scholars and widely used in this field so far (Mijić et al., 2010; Pekey and Doğan, 2013; Guan et al., 2018). In addition, in order to comprehensively elaborate heavy metal pollution, scholars often incorporate environmental and health risk assessment while conducting source apportionment (Hu et al., 2012; Li Z. et al., 2014; Jiang et al., 2017; Men et al., 2018).

3.3 Research hotspots and emerging trends

3.3.1 Keyword co-occurrence

The keywords of a literature highly summarize the key content of the literature, and reflect a lot of information including methods, purposes, views, and so on. Therefore, keyword co-occurrence analysis is of great significance to investigate hot topics and set development direction of the field. Figure 7 is a visual network diagram of keyword co-occurrence analysis in the field of source appointment of heavy metals exported by CiteSpace, which contains 400 nodes and 1,591 links. Each node represents a keyword, and the size of the node is proportional to the frequency of the keyword. In addition, a node with a purple outer ring represents a higher centrality of the keyword and a higher level of attention in this field.

TABLE 8 Key papers about source appointment of heavy metals.

Rank	Cited references	Number of cited frequency	Centrality	Year
1	Jiang et al., 2017, CHEMOSPHERE, V168, P1658, DOI 10.1016/j.chemosphere.2016.11.088	182	0	2017
2	Guan et al., 2018, CHEMOSPHERE, V193, P189, DOI 10.1016/j.chemosphere.2017.10.151	133	0	2018
3	Men et al., 2018, SCI TOTAL ENVIRON, V612, P138, DOI 10.1016/j.scitotenv.2017.08.123	98	0	2018
4	Duan et al., 2013, ATMOS ENVIRON, V74, P93, DOI 10.1016/j.atmosenv.2013.03.031	40	0	2013
5	Li et al., 2020b, SCI TOTAL ENVIRON, V468, P843, DOI 10.1016/j.scitotenv.2013.08.090	40	0	2014
6	Viana et al., 2008, J AEROSOL SCI, V39, P827, DOI 10.1016/j.jaerosci.2008.05.007	12	0	2008
7	Hu et al., 2012, ATMOS ENVIRON, V57, P146, DOI 10.1016/j.atmosenv.2012.04.056	11	0	2012
8	Muhammad et al., 2011, MICROCHEM J, V98, P334, DOI 10.1016/j.microc.2011.03.003	9	0	2011
9	Pant and Harrison 2013, ATMOS ENVIRON, V77, P78, DOI 10.1016/j.atmosenv.2013.04.028	8	0	2013
10	Birmili et al., 2006, ENVIRON SCI TECHNOL, V40, P1144, DOI 10.1021/es0486925	7	0.01	2006
11	Thorpe and Harrison, 2008, SCI TOTAL ENVIRON, V400, P270, DOI 10.1016/j.scitotenv.2008.06.007	6	0	2008
12	Iqbal and Shah, 2011, J HAZARD MATER, V192, P887, DOI 10.1016/j.jhazmat.2011.05.105	6	0	2011
13	Mijić et al., 2010, ATMOS ENVIRON, V44, P3630, DOI 10.1016/j.atmosenv.2010.06.045	6	0	2010
14	Manoli et al., 2002, ATMOS ENVIRON, V36, P949, DOI 10.1016/S1352-2310 (01)00486-1	6	0.02	2002
15	Pekey and Doğan, 2013, MICROCHEM J, V106, P233, DOI 10.1016/j.microc.2012.07.007	6	0	2013

The top 30 keywords by frequency exported by CiteSpace are listed in Table 9, in which "source apportionment", "heavy metals", "source identification" and "pollution" are the four keywords with the high frequency. This is related to the fact that "heavy metals" and "source appointment" were used as search keywords in literature screening. In addition, keywords with high frequency include spatial distribution (538 times), particulate matter (466 times), health risk assessment (368 times), agricultural soils (271 times), and positive matrix factorization (253 times). This indicates that while studying the source appointment of heavy metals, the spatial distribution of heavy metals in the environment and the health risk assessment of heavy metal pollutants are also generally investigated. As the source appointment of heavy metals is mostly related to environmental media such as atmospheric particulate matters and agricultural soils, PMF model is one of the widely used research methods.

The centrality is related to the number of articles linked by a keyword, and it represents the academic influence of a keyword to a certain extent. As shown in Table 9, the keywords with high centrality are heavy metals (0.33), trace elements (0.12), and air pollution (0.12). Through the above analysis results, we also conclude that the keyword with high frequency does not inevitably have high centrality. Early (pre-21st century) keywords are "source apportionment", "heavy metals", "trace elements", "particulate matter", "risk assessment", "air" "pollution", indicating that the source appointment of heavy metals in atmospheric environmental media appeared earlier. Keywords with high frequency in the past decade include "spatial distribution", "health risk", "agricultural soils", "ecological risk", "surface sediments", "spatial distribution", "agricultural soils", and "street dust", suggesting that the source appointment of heavy metals in soil, sediment and street dust environmental media has been the research focus in the past decade. With the progress of society and the enhancement of people's environmental awareness, more and more researchers have paid attention to the health risks caused by heavy metal pollution to human beings and the ecological risks caused to the environment on which human beings depend for survival.

3.3.2 Keyword clustering analysis

Keyword cluster analysis is based on keyword co-occurrence analysis, using cluster statistical algorithm to simplify complex co-occurrence network into relatively simple inter-group relations,

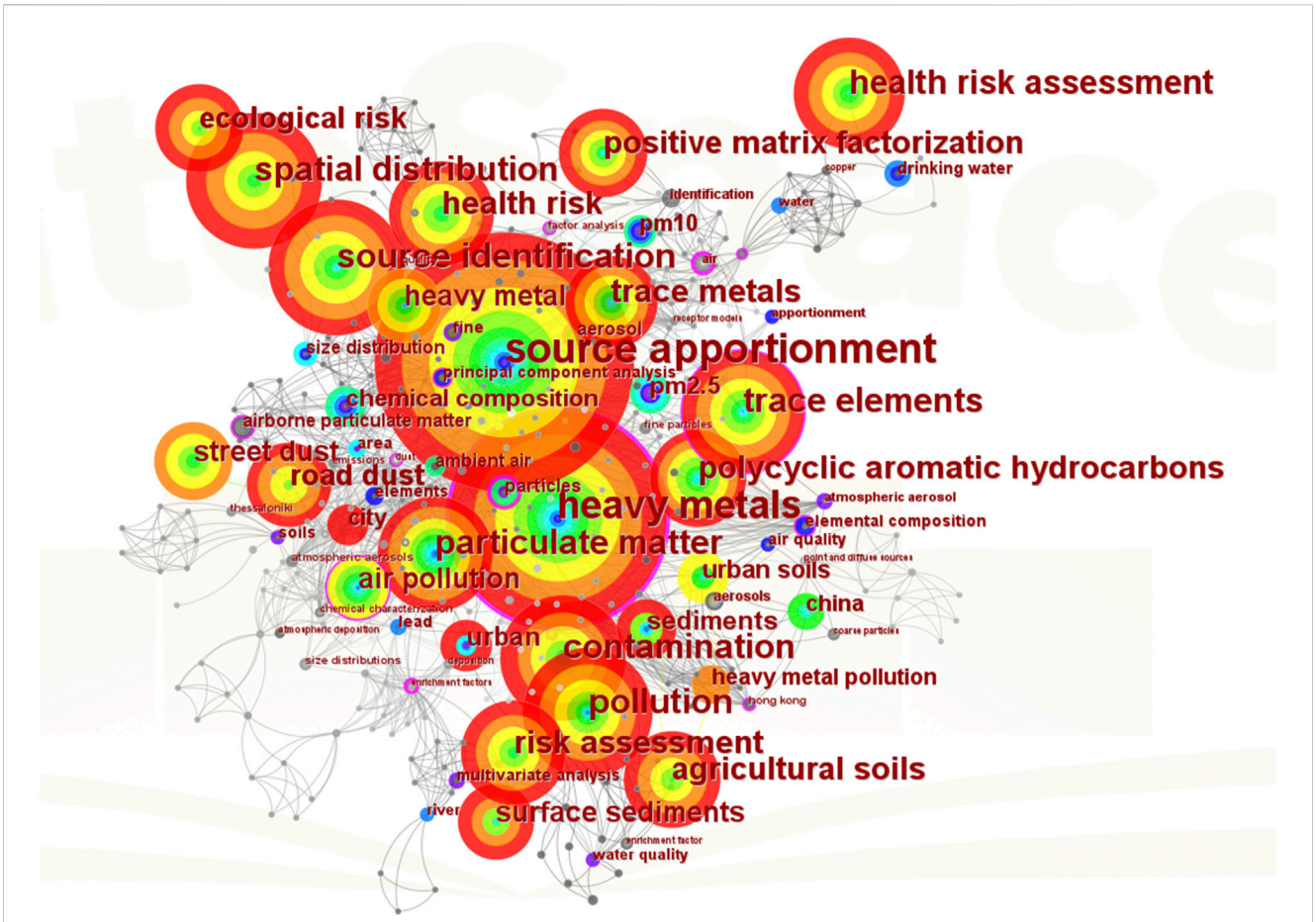

FIGURE 7
Keyword co-occurring network.

TABLE 9 Top 30 frequency keywords.

Rank	Keywords	Count	Centrality	Year	Rank	Keywords	Count	Centrality	Year
1	source apportionment	2007	0.01	1994	16	ecological risk	231	0	2018
2	heavy metals	1,461	0.33	1994	17	road dust	228	0.01	2003
3	source identification	576	0.03	2007	18	surface sediments	180	0	2015
4	pollution	558	0.09	2000	19	street dust	177	0	2016
5	spatial distribution	538	0.01	2014	20	heavy metal	172	0.01	2004
6	contamination	522	0.01	2000	21	air pollution	172	0.12	1996
7	trace elements	506	0.12	1997	22	sediments	117	0.03	2004
8	particulate matter	466	0.06	1999	23	urban	101	0.01	2005
9	health risk assessment	368	0	2011	24	urban soils	81	0.01	2004
10	polycyclic aromatic hydrocarbons	360	0.02	2002	25	chemical composition	72	0.09	2003
11	risk assessment	336	0.01	1998	26	PM2.5	70	0	2006
12	health risk	329	0	2015	27	city	54	0.03	2004
13	trace metals	314	0.05	2004	28	PM10	52	0.01	2002
14	agricultural soils	271	0	2018	29	heavy metal pollution	46	0.04	2004
15	positive matrix factorization	253	0	2008	30	china	44	0	2009

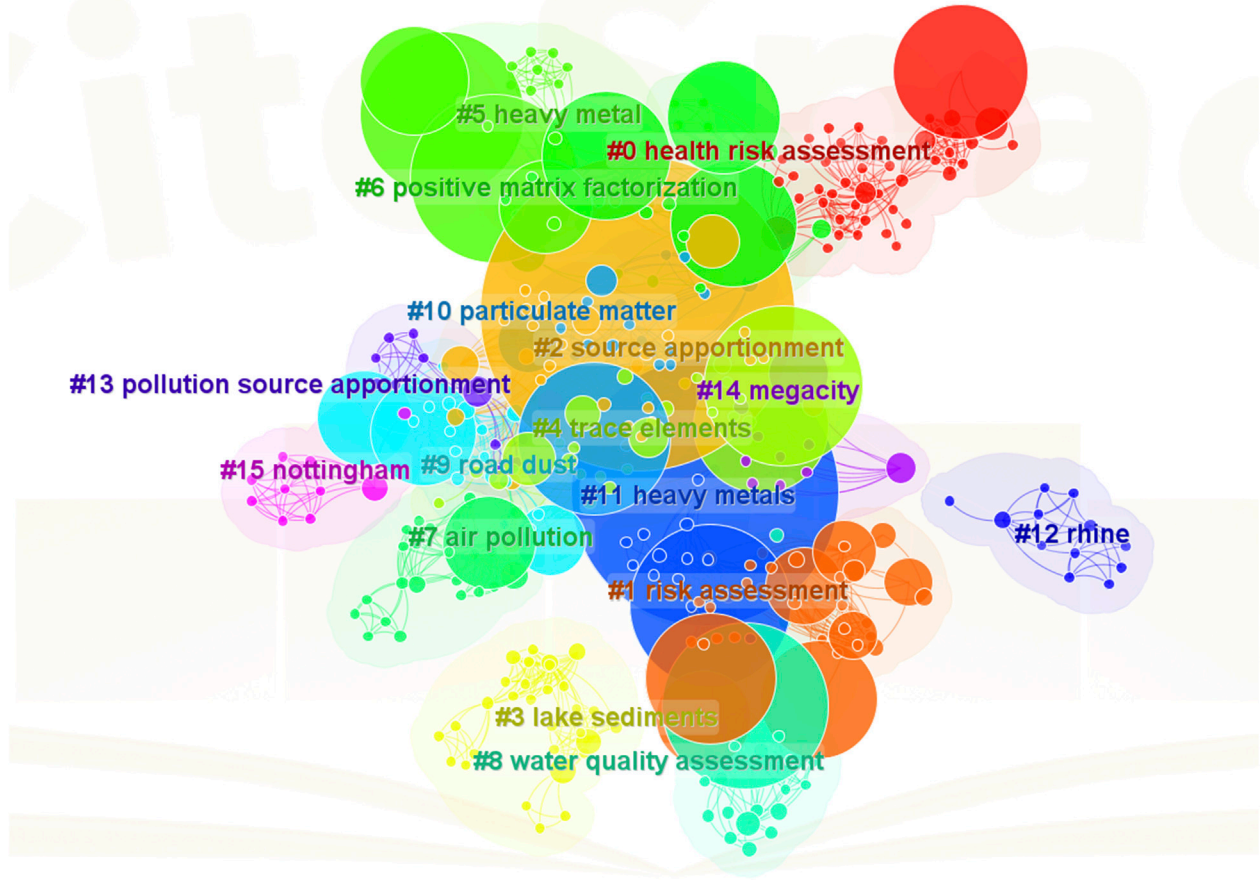

FIGURE 8
Main clusters labeled by keyword.

which can more comprehensively describe the research hot spots of source appointment of heavy metals. Figure 8 is the keyword cluster analysis map derived from CiteSpace, including 16 different clusters (#0 ~ #15). We need to combine the cluster names in Figure 8 with the main keywords contained in the clusters to analyze the network. Table 10 lists the details of the clusters, in order of ID from 0 to 15. The parameter Silhouette in the table is used to evaluate the clustering effect and was originally proposed by Rousseeuw (Rousseeuw, 1987). The closer the Silhouette value is to 1, the better the clustering effect will be. It is generally believed that when the value is greater than 0.7, the clustering results will be highly reliable (Sun et al., 2019).

The Cluster 0 and Cluster 1 are related to health risk assessment, and consist of air, aerosol, water, sediments, agricultural soils, urban soils and other keywords. The occurrence of heavy metals pollution in the atmosphere, water and soil environment may have adverse effects on the human body, so health risk assessment has been widely concerned by scholars all over the world in the research field of source apportionment of heavy metals (Li Y. et al., 2020; Wu et al., 2020; Wang J. et al., 2023; Zhu et al., 2023). The Cluster two and Cluster 13 are about pollution source apportionment, involving PM10, airborne particulate matter, principal component analysis, atmospheric aerosol, area, urban soil, power station, and so on. Particulate matter in the atmosphere includes PM10, PM2.5, *etc.*, which often carry heavy metal pollutants. And atmospheric environment is the early main research content of the field of source appointment of heavy metals, and till now, it is also one of the research hot spots (Vassilakos et al., 2007; Liu et al., 2021; Zhou et al., 2021). Principal component analysis (PCA) is one of the typical methods used in this field (Nguyen et al., 2020), which can transform a set of variables into unrelated components to represent system information (Borůvka et al., 2005; Shan et al., 2013). In addition, the flue gas and wastewater discharged by power stations usually contain heavy metals, which directly pollute the atmosphere and water, and can also migrate to the soil environment and cause soil pollution, among which the urban soil is greatly affected due to the close distance. These may seriously endanger the health of citizens. Therefore, the source apportionment of heavy metals in power station and urban soil has become the focus of many scholars (Li D. et al., 2023; Wang Y. et al., 2023; Khan and Shah, 2023; Ma et al., 2023; Zheng et al., 2023).

Cluster three and Cluster eight are about lake sediments and water quality assessment, containing multivariate analysis, river, enrichment factors, deposition, pollution, water quality, surface waters, and so on. The sediments in the surface waters play a role of storing, transporting and transporting heavy metals (Kipp et al., 2009; Li et al., 2017; Liang et al., 2019), and serve as both the sink and the source of heavy metals in aquatic ecosystem (Xu et al.,

TABLE 10 Top 15 clusters and the main keywords within the clusters.

Cluster ID	Silhouette value	Cluster name	Main keyword
0	1	health risk assessment	health risk assessment; aerosol; drinking water; water; air
1	0.952	risk assessment	risk assessment; agricultural soils; surface sediments; sediments; urban soils
2	0.791	source apportionment	source apportionment; PM10; airborne particulate matter; principal component analysis; atmospheric aerosol
3	0.938	lake sediments	multivariate analysis; river; enrichment factors; deposition; lake sediments
4	0.813	trace elements	trace elements; polycyclic aromatic hydrocarbons; city; particles; ambient air
5	0.927	heavy metal	source identification; spatial distribution; ecological risk; heavy metal; factor analysis
6	0.884	positive matrix factorization	health risk; trace metals; positive matrix factorization; size distribution; identification
7	0.901	air pollution	air pollution; metals; atmospheric deposition; chemical composition; pollution source
8	0.931	water quality assessment	pollution; water quality; enrichment factor; basin; surface waters
9	0.905	road dust	road dust; street dust; urban; emissions; dust
10	0.919	particulate matter	particulate matter; chemical composition; fine; elements; receptor models
11	0.96	heavy metals	heavy metals; contamination; aerosol source apportionment; atmospheric mercury; balance source apportionment
12	0.934	rhine	point and diffuse sources; heavy metal emissions; nutrients; heavy metal load; diffuse sources
13	0.991	pollution source apportionment	area; urban soil; information; power station; source origin
14	0.918	megacity	pm2.5; elemental composition; speciation; outdoor air; indoor fine particles
15	0.953	nottingham	soils; urban geochemistry; C13; natural environments; vegetation

2019). The source appointment of heavy metals in sediments has become the research objects of many scholars (Li N. et al., 2020; Emenike et al., 2020; Pastorino et al., 2020). Multivariate analysis and enrichment factor analysis are important methods for the source apportionment of heavy metals (Huang C.-C. et al., 2023; Jiang et al., 2023b; Wang P. et al., 2023; Fu et al., 2023; Saraswat et al., 2023; Xie et al., 2023). Water quality assessment is closely linked to the source appointment of heavy metals in water environment, as a result the matter of water quality assessment often appears in this field.

Cluster six focus on positive matrix factorization (PMF), including health risk, trace metals, size distribution, identification, among others. The PMF method was first proposed by Paatero (Paatero and Tapper, 1994), which is recommended by USEPA, and is a typical method in the field of source apportionment of heavy metals (Jiang et al., 2023a; Jung et al., 2023; Shiyi et al., 2023; Yang et al., 2023). The PMF method relies on iterative least squares to minimize the complex matrix and covariance matrix of multiple samples and associated heavy metal elements into a number of composite factors, accordingly the main pollution sources and their contribution ratios are determined. Moreover, this method can estimate the uncertainty by non-negative constraint factor load and score, reduce the data omission and error, and make the analysis results more reliable. In addition, when dealing with heavy metal pollution, researchers also assess the health risks caused by pollutants to humans, so health risk assessment appears frequently in this research field.

Cluster 7 focuses on air pollution, bringing in the keywords such as metals, atmospheric deposition, chemical composition, and pollution source. In this cluster, the researchers are motivated by atmospheric source apportionment of heavy metals, atmospheric dust fall, chemical composition, and heavy metal concentration. Atmospheric dust fall is the main way that heavy metals migrate from the atmosphere to water and soil, and atmospheric environment is also one of the main sources of heavy metal pollution (Bermudez et al., 2012), which has been widely concerned by many scholars (Samara and Voutsa, 2005; Bai et al., 2019; Li et al., 2022; Rabha et al., 2022; Wang et al., 2022).

Cluster 4 and Cluster 10 are about trace elements and particulate matter, absorbing city, particles, ambient air, chemical composition, elements, receptor models, and so on. In fact, particulate matter is a carrier of heavy metal pollutants in the atmosphere (Lee and Park, 2010; Li X. et al., 2014). Heavy metals can be attached to its surface, endangering the environment and human health (Li et al., 2015; Liu et al., 2015). And the receptor model is a common method employed in the study of source apportionment of heavy metals.

Cluster five and Cluster 11 are about heavy metals, regarding source identification, spatial distribution, ecological risk, factor analysis, contamination, and so on. The spatial distribution of heavy metal pollutants is an important prerequisite for source apportionment research (Xie et al., 2011). Factor analysis (FA) is one of the traditional methods (Meng et al., 2018; Ustaoğlu and Islam, 2020; Wang Z. et al., 2021; Jandacka et al., 2022). In addition, it is inevitable to carry out ecological risk assessment on

environmental pollution caused by heavy metals, thereafter the related research on risk assessment appears frequently in this field.

Cluster 9 is about road dust, concerning street dust, urban, emissions, and so on. One of the main sources of heavy metals in road dust is the emission of traffic exhaust gas. With the development of society, the problem of urban road pollution is becoming growingly serious. Recently, the source apportionment of heavy metals in road dust has attracted more and more scholars' attention (Wang Q. et al., 2023; Haghnazar et al., 2023; Shojaee Barjoee et al., 2023).

Cluster 12 and Cluster 15 are about Rhine and Nottingham, in relation to point and diffuse sources, heavy metal emissions, heavy metal load, diffuse sources, soils, urban geochemistry, natural environments, vegetation and other keywords. Rising from the foothills of the Alps in southeastern Switzerland, the Rhine River is 1,320 km long and is the longest river in Western Europe. The Rhine River flows through Liechtenstein, Austria, France, Germany, the Netherlands, and into the North Sea near Rotterdam. As it is one of the most important industrial transport arteries and one of the busiest rivers for shipping in the world, its ecological environment pollution is very serious. Because of the increasing pollution of the Rhine River, international attention is focused on its ecological protection (Wagenaar-Hart, 1994; Van Dijk et al., 1995), and scholars are no exception (Schebek et al., 1991; Leuven et al., 2009; Klaver et al., 2014; Li R. et al., 2020; Li et al., 2021). Nottingham is a city in Nottinghamshire, about 200 km north of London, and has a population of approximate 320,000. Environmental pollution there is very serious because of coal mining and smelting activities, which attracts great public concern (Hajat et al., 2007; Wang et al., 2020).

Cluster 14 is about megacity, including PM2.5, elemental composition, outdoor air, indoor fine particles, and so on. Thus it can be seen that many scholars pay more attention to the analysis of source apportionment of heavy metals in the air environment of megacity in this cluster (Huang W. et al., 2023; Chen et al., 2023; Hernández-López et al., 2023; Ke et al., 2023; Khobragade and Vikram Ahirwar, 2023).

3.3.3 Keyword bursts analysis

Keywords whose frequency increases sharply at a certain point in time are keywords with bursts, which can show research hotspots in different periods (Zhou et al., 2018). Analyzing its development trend can help predict the future direction (Li and Chen, 2016; He et al., 2022). Figure 9 presents the top 34 keywords in burst strength through the last nearly 30 years (1994–2022) by using CiteSpace, along with the strength and occurrence timespan. When the dark blue or red line begins to appear, the keyword begins to appear. The whole red line represents the burst period of the keyword (Zhou and Zhao, 2015). In addition, the light blue line represents the keyword with bursts has not shown up yet. It is clear that the research hot spot of the field has changed over time. The earliest keyword with bursts is "airborne particulate matter", "aerosol" and "principal component analysis", indicating that researchers have paid attention to the source apportionment of heavy metals in the atmospheric environment earlier, and PCA is a widely used source apportionment method model in the early stage of research. In terms of burst strength, PM2.5 had the highest burst strength (32.89), followed by chemical composition (31.98), PM10 (22.73), China (22.63), street dust (20.57), air pollution (18.23), urban (14.89), airborne particulate matter (14.72), and so on. In terms of burst time, the study in atmospheric environment appeared earliest in 1994 and lasted the longest (until about 2018). People's attention to heavy metals still mainly fell on the atmospheric environment, including inhalable particles, aerosols, among others until the beginning of the 21st century, during which the attention to aerosols began rather earlier, indicating that researchers' analysis of heavy metal sources in gaseous media remained at a relatively broad level. With the progress of traffic pollution and other pollution after 2000, we have gradually paid attention to the harm of heavy metals in inhalable particles to the human body, so PM10 has become a research hotspot. From 2003 to 2015, the research of water environment was a hot spot, early attention was paid to heavy metal pollution in rivers (2007–2015), followed by a greater focus on drinking water safety (2011–2015). From 2004 to 2013, the research of heavy metals in soil environment has been a hot spot. It shows that people's awareness of environmental protection is gradually increasing. The keywords with bursts in recent years are "particulate matter", "sediments", "China", "street dust", "heavy metal", and "road dust". Therefore, the future source apportionment of heavy metals research may continue pay attention to environmental media such as atmospheric particles, surface water sediments, and urban road dust. In conclusion, above analysis results help scholars quickly grab current frontiers, predict future research directions, avoid detours, and conduct research more efficiently.

4 Conclusion and perspective

This study presents a systematic bibliometric review of the field of source appointment of heavy metals, providing an overview and detailed insights into past, current, and future research trends in the field. This field has been developing for nearly 30 years, with a growing number of publications especially in recent years, and will continue develop in the future. The main categories have gradually changed, and become multifaceted and multidisciplinary due to the accelerated modernization and the emergence of new pollutants. The keywords have changed from "airborne particulate matteraeroso," "aerosol," "PCA," "air quality," and "water quality" during the early days to "soils," "urban," "multivariate analysis," "sediments," and "road dust" recently. The top journals in this field are Science of the Total Environment, Environmental Pollution, Journal of Hazardous Materials, Atmospheric Environment, and Chemosphere. In the last century, United States, Germany, and Canada have maintained the leading position in this field. While China's research is also playing an increasingly important role, during which Chinese Academy of Sciences is the leading institution in this field.

The reference co-citation analysis and keyword analysis reveal that there are three major points in this field so far: 1) the development of source appointment of heavy metals technology; 2) environmental and health risk assessment of heavy metal pollution; 3) environmental pollution prevention policies.

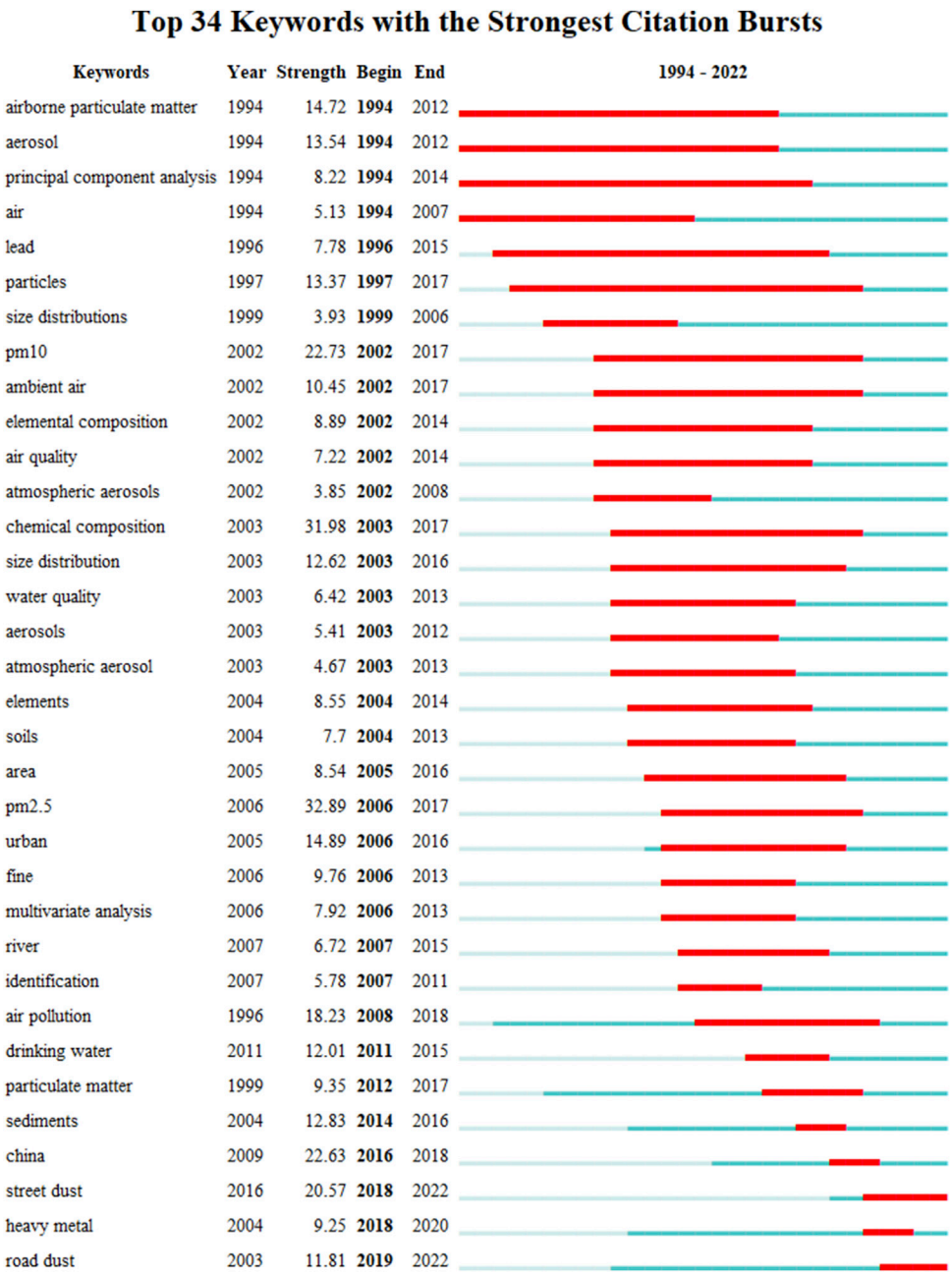

FIGURE 9
Keywords with bursts.

Combined with the results of literature metrology analysis and the overall development trend of research in the field of source apportionment of heavy metals, this field may show the following characteristics in the future: 1) More extensive application. The number of scholars who pay attention to this research field is still showing a rising trend, which signifies this field covers more and more disciplines, and the scope is becoming more and more widespread. In the future, the methods utilized in this field will be more diverse to solve more comprehensive and complex problems. 2) More advanced technologies. As artificial intelligence (AI) is developing rapidly, machine learning, computer vision, deep learning, natural language processing, Internet of Things, and other future research technologies in AI will continue to innovate the source apportionment of heavy metals research to promote new breakthroughs in this field. In the future, the more extensive application covering growing disciplines, the more advanced technologies such as artificial intelligence, the more comprehensive environmental and health risk assessment, as well as the more strengthened cooperation between various countries, institutions and authors continue to innovate the source apportionment of heavy metals research to promote new breakthroughs.

Author contributions

ZJ: Writing–original draft, Writing–review and editing, Conceptualization, Data curation, Software. AC: Writing–review and editing, Methodology. RL: Writing–review and editing, Investigation. XW: Investigation, Writing–review and editing. YL: Writing–review and editing, Methodology, Supervision, Validation, Writing–original draft.

Funding

The author(s) declare that financial support was received for the research, authorship, and/or publication of this article. This work was financed by the National Key Research and Development Program of China (2021YFD1700900), the Natural Science Foundation of Henan Province, the Talent Cultivation Program of Chinese Academy of Agricultural Sciences (NKYCQN-2021-028) and the Agricultural Science and Technology Innovation Program (ASTIP) of Chinese Academy of Agricultural Sciences.

Conflict of interest

The authors declare that the research was conducted in the absence of any commercial or financial relationships that could be construed as a potential conflict of interest.

Publisher's note

References

Abeer, N., Khan, S. A., Muhammad, S., Rasool, A., and Ahmad, I. (2020). Health risk assessment and provenance of arsenic and heavy metal in drinking water in Islamabad, Pakistan. *Environ. Technol. and innovation* 20, 101171. doi:10.1016/j.eti.2020.101171

Adgate, J. L., Willis, R. D., Buckley, T. J., Chow, J. C., Watson, J. G., Rhoads, G. G., et al. (1998). Chemical mass balance source apportionment of lead in house dust. *Environ. Sci. and Technol.* 32 (1), 108–114. doi:10.1021/es970052x

Ale Ebrahim, N., Salehi, H., Embi, M. A., Habibi, F., Gholizadeh, H., Motahar, S. M., et al. (2013). Effective strategies for increasing citation frequency. *Int. Educ. Stud.* 6 (11), 93–99. doi:10.5539/ies.v6n11p93

Aleixandre-Benavent, R., Aleixandre-Tudó, J. L., Castelló-Cogollos, L., and Aleixandre, J. L. (2017). Trends in scientific research on climate change in agriculture and forestry subject areas (2005–2014). *J. Clean. Prod.* 147, 406–418. doi:10.1016/j.jclepro.2017.01.112

Bai, L., He, Z., Ni, S., Chen, W., Li, N., and Sun, S. (2019). Investigation of PM2.5 absorbed with heavy metal elements, source apportionment and their health impacts in residential houses in the North-east region of China. *Sustain. Cities Soc.* 51, 101690. doi:10.1016/j.scs.2019.101690

Banerjee, S., Ghosh, S., Jha, S., Kumar, S., Mondal, G., Sarkar, D., et al. (2023). Assessing pollution and health risks from chromite mine tailings contaminated soils in India by employing synergistic statistical approaches. *Sci. Total Environ.* 880, 163228. doi:10.1016/j.scitotenv.2023.163228

Bao, L., Kusadokoro, M., Chitose, A., and Chen, C. (2023). Development of socially sustainable transport research: a bibliometric and visualization analysis. *Travel Behav. Soc.* 30, 60–73. doi:10.1016/j.tbs.2022.08.012

Batagelj, V., and Cerinšek, M. (2013). On bibliographic networks. *Scientometrics* 96 (3), 845–864. doi:10.1007/s11192-012-0940-1

Bermudez, G. M., Jasan, R., Plá, R., and Pignata, M. L. (2012). Heavy metals and trace elements in atmospheric fall-out: their relationship with topsoil and wheat element composition. *J. Hazard. Mater.* 213, 447–456. doi:10.1016/j.jhazmat.2012.02.023

Birmili, W., Allen, A. G., Bary, F., and Harrison, R. M. (2006). Trace metal concentrations and water solubility in size-fractionated atmospheric particles and influence of road traffic. *Environ. Sci. and Technol.* 40 (4), 1144–1153. doi:10.1021/es0486925

Borůvka, L., Vacek, O., and Jehlička, J. (2005). Principal component analysis as a tool to indicate the origin of potentially toxic elements in soils. *Geoderma* 128 (3-4), 289–300. doi:10.1016/j.geoderma.2005.04.010

Cai, Q., Long, M.-L., Zhu, M., Zhou, Q.-Z., Zhang, L., and Liu, J. (2009). Food chain transfer of cadmium and lead to cattle in a lead–zinc smelter in Guizhou, China. *Environ. Pollut.* 157 (11), 3078–3082. doi:10.1016/j.envpol.2009.05.048

Chary, N. S., Kamala, C., and Raj, D. S. S. (2008). Assessing risk of heavy metals from consuming food grown on sewage irrigated soils and food chain transfer. *Ecotoxicol. Environ. Saf.* 69 (3), 513–524. doi:10.1016/j.ecoenv.2007.04.013

Cheema, A. I., Liu, G., Yousaf, B., Abbas, Q., and Zhou, H. (2020). A comprehensive review of biogeochemical distribution and fractionation of lead isotopes for source tracing in distinct interactive environmental compartments. *Sci. total Environ.* 719, 135658. doi:10.1016/j.scitotenv.2019.135658

Chen, C. (2004). Searching for intellectual turning points: progressive knowledge domain visualization. *Proc. Natl. Acad. Sci.* 101 (suppl_1), 5303–5310. doi:10.1073/pnas.0307513100

Chen, C. (2006). CiteSpace II: detecting and visualizing emerging trends and transient patterns in scientific literature. *J. Am. Soc. Inf. Sci. Technol.* 57 (3), 359–377. doi:10.1002/asi.20317

Chen, C., and Song, M. (2019). Visualizing a field of research: a methodology of systematic scientometric reviews. *PloS one* 14 (10), e0223994. doi:10.1371/journal.pone.0223994

Chen, X., and Lu, X. (2018). Contamination characteristics and source apportionment of heavy metals in topsoil from an area in Xi'an city, China. *Ecotoxicol. Environ. Saf.* 151, 153–160. doi:10.1016/j.ecoenv.2018.01.010

Chen, Y., Ye, X., Yao, Y., Lv, Z., Fu, Z., Huang, C., et al. (2023). Characteristics and sources of PM2. 5-bound elements in Shanghai during autumn and winter of 2019: insight into the development of pollution episodes. *Sci. Total Environ.* 881, 163432. doi:10.1016/j.scitotenv.2023.163432

Chen, Z., Ding, Y., Jiang, X., Duan, H., Ruan, X., Li, Z., et al. (2022). Combination of UNMIX, PMF model and Pb-Zn-Cu isotopic compositions for quantitative source apportionment of heavy metals in suburban agricultural soils. *Ecotoxicol. Environ. Saf.* 234, 113369. doi:10.1016/j.ecoenv.2022.113369

Chi, P.-S., and Glänzel, W. (2017). An empirical investigation of the associations among usage, scientific collaboration and citation impact. *Scientometrics* 112, 403–412. doi:10.1007/s11192-017-2356-4

Chu, H., Liu, Y., Xu, N., and Xu, J. (2023). Concentration, sources, influencing factors and hazards of heavy metals in indoor and outdoor dust: a review. *Environ. Chem. Lett.* 21 (2), 1203–1230. doi:10.1007/s10311-022-01546-2

Davies, B. (1997). Heavy metal contaminated soils in an old industrial area of Wales, Great Britain: source identification through statistical data interpretation. *Water, Air, Soil Pollut.* 94, 85–98. doi:10.1007/bf02407095

De Temmerman, L., Vanongeval, L., Boon, W., Hoenig, M., and Geypens, M. (2003). Heavy metal content of arable soils in northern Belgium. *Water, Air, Soil Pollut.* 148, 61–76. doi:10.1023/a:1025498629671

Ding, X., and Yang, Z. (2022). Knowledge mapping of platform research: a visual analysis using VOSviewer and CiteSpace. *Electron. Commer. Res.* 22, 787–809. doi:10.1007/s10660-020-09410-7

Dong, B., Zhang, R., Gan, Y., Cai, L., Freidenreich, A., Wang, K., et al. (2019). Multiple methods for the identification of heavy metal sources in cropland soils from a resource-based region. *Sci. Total Environ.* 651, 3127–3138. doi:10.1016/j.scitotenv.2018.10.130

Donthu, N., Kumar, S., and Pattnaik, D. (2020). Forty-five years of journal of business research: a bibliometric analysis. *J. Bus. Res.* 109, 1–14. doi:10.1016/j.jbusres.2019.10.039

Du, H., and Lu, X. (2022). Source apportionment and probabilistic ecological risk of heavy metal (loid) s in sediments in the Mianyang section of the Fujiang River, China. *Minerals* 12 (12), 1513. doi:10.3390/min12121513

Duan, J., and Tan, J. (2013). Atmospheric heavy metals and Arsenic in China: situation, sources and control policies. *Atmos. Environ.* 74, 93–101. doi:10.1016/j.atmosenv.2013.03.031

Duan, Y., Zhang, Y., Li, S., Fang, Q., Miao, F., and Lin, Q. (2020). An integrated method of health risk assessment based on spatial interpolation and source apportionment. *J. Clean. Prod.* 276, 123218. doi:10.1016/j.jclepro.2020.123218

Ekundayo, T. C., and Okoh, A. I. (2018). A global bibliometric analysis of Plesiomonas-related research (1990–2017). *PloS one* 13 (11), e0207655. doi:10.1371/journal.pone.0207655

Emenike, P. C., Tenebe, I. T., Neris, J. B., Omole, D. O., Afolayan, O., Okeke, C. U., et al. (2020). An integrated assessment of land-use change impact, seasonal variation of pollution indices and human health risk of selected toxic elements in sediments of River Atuwara, Nigeria. *Environ. Pollut.* 265, 114795. doi:10.1016/j.envpol.2020.114795

Fan, X., Lu, X., Yu, B., Zuo, L., Fan, P., Yang, Y., et al. (2021). Risk and sources of heavy metals and metalloids in dust from university campuses: a case study of Xi'an, China. *Environ. Res.* 202, 111703. doi:10.1016/j.envres.2021.111703

Freeman, L. C. (2002). Centrality in social networks: Conceptual clarification. *Soc. Netw.* 1, 215–239. doi:10.1016/0378-8733(78)90021-7

Fu, L., Mao, S., Chen, F., Zhao, S., Su, W., Lai, G., et al. (2022). Graphene-based electrochemical sensors for antibiotic detection in water, food and soil: a scientometric analysis in CiteSpace (2011–2021). *Chemosphere* 297, 134127. doi:10.1016/j.chemosphere.2022.134127

Fu, Z., He, N., Ma, M., Bao, Z., Xie, S., and Gu, Y. (2023). Source apportionment and probabilistic risk assessment of heavy metals in selenium-rich soils in Hainan Province, China. *J. Geochem. Explor.* 251, 107241. doi:10.1016/j.gexplo.2023.107241

Geng, Y., and Maimaituerxun, M. (2022). Research progress of green marketing in sustainable consumption based on CiteSpace analysis. *Sage Open* 12 (3), 215824402211198. doi:10.1177/21582440221119835

Geng, Y., Zhang, N., and Zhu, R. (2023). Research progress analysis of sustainable smart grid based on CiteSpace. *Energy Strategy Rev.* 48, 101111. doi:10.1016/j.esr.2023.101111

Guan, Q., Wang, F., Xu, C., Pan, N., Lin, J., Zhao, R., et al. (2018). Source apportionment of heavy metals in agricultural soil based on PMF: a case study in Hexi Corridor, northwest China. *Chemosphere* 193, 189–197. doi:10.1016/j.chemosphere.2017.10.151

Gutiérrez-Salcedo, M., Martínez, M. Á., Moral-Munoz, J. A., Herrera-Viedma, E., and Cobo, M. J. (2018). Some bibliometric procedures for analyzing and evaluating research fields. *Appl. Intell.* 48, 1275–1287. doi:10.1007/s10489-017-1105-y

Haghnazar, H., Soltani-Gerdefaramarzi, S., Ghasemi, M., and Johannesson, K. H. (2023). Receptor model-based approach to estimate urban road dust pollution by heavy metal (loid) s exposed to desert dust storms in a rapid-growing city of Iran. *Environ. Earth Sci.* 82 (12), 316. doi:10.1007/s12665-023-11000-3

Hajat, S., Armstrong, B., Wilkinson, P., Busby, A., and Dolk, H. (2007). Outdoor air pollution and infant mortality: analysis of daily time-series data in 10 English cities. *J. Epidemiol. and Community Health* 61 (8), 719–722. doi:10.1136/jech.2006.053942

Hao, Q., Lu, X., Yu, B., Yang, Y., Lei, K., Pan, H., et al. (2023). Sources and probabilistic ecological-health risks of heavy metals in road dust from urban areas in a typical industrial city. *Urban Clim.* 52, 101730. doi:10.1016/j.uclim.2023.101730

He, Z., Huang, Y., and Zhao, C. (2022). A preliminary general framework for seismic resilience assessment of slope engineering. *Bull. Eng. Geol. Environ.* 81 (11), 463. doi:10.1007/s10064-022-02965-9

Henry, R. C., Lewis, C. W., Hopke, P. K., and Williamson, H. J. (1984). Review of receptor model fundamentals. *Atmos. Environ.* 18 (8), 1507–1515. doi:10.1016/0004-6981(84)90375-5

Hernández-López, A., Santos-Medina, G., Morton-Bermea, O., Hernández-Álvarez, E., Villalobos-Pietrini, R., and Amador-Muñoz, O. (2023). Chemical speciation of organic compounds and elemental compositions of PM2. 5 in Mexico City: Spatial-seasonal distribution, emission sources, and formation processes. *Atmos. Res.* 292, 106868. doi:10.1016/j.atmosres.2023.106868

Hirsch, J. E. (2005). An index to quantify an individual's scientific research output. *Proc. Natl. Acad. Sci.* 102 (46), 16569–16572. doi:10.1073/pnas.0507655102

Hu, X., Zhang, Y., Ding, Z., Wang, T., Lian, H., Sun, Y., et al. (2012). Bioaccessibility and health risk of arsenic and heavy metals (Cd, Co, Cr, Cu, Ni, Pb, Zn and Mn) in TSP and PM2. 5 in Nanjing, China. *Atmos. Environ.* 57, 146–152. doi:10.1016/j.atmosenv.2012.04.056

Huang, C.-C., Cai, L.-M., Xu, Y.-H., Jie, L., Hu, G.-C., Chen, L.-G., et al. (2023a). A comprehensive approach to quantify the source identification and human health risk assessment of toxic elements in park dust. *Environ. Geochem. Health* 45 (8), 5813–5827. doi:10.1007/s10653-023-01588-7

Huang, L., Zhou, M., Lv, J., and Chen, K. (2020). Trends in global research in forest carbon sequestration: a bibliometric analysis. *J. Clean. Prod.* 252, 119908. doi:10.1016/j.jclepro.2019.119908

Huang, W., Zhang, Z., Huang, J., Tao, J., Zhou, Z., Yuan, Z., et al. (2023b). High contribution of non-exhaust emission to health risk of PM2. 5-bound toxic metals in an urban atmosphere in south China. *Atmos. Environ.* 306, 119824. doi:10.1016/j.atmosenv.2023.119824

Huang, Y., Deng, M., Wu, S., Japenga, J., Li, T., Yang, X., et al. (2018). A modified receptor model for source apportionment of heavy metal pollution in soil. *J. Hazard. Mater.* 354, 161–169. doi:10.1016/j.jhazmat.2018.05.006

Iqbal, J., and Shah, M. H. (2011). Distribution, correlation and risk assessment of selected metals in urban soils from Islamabad, Pakistan. *J. Hazard. Mater.* 192 (2), 887–898. doi:10.1016/j.jhazmat.2011.05.105

Jacob, J. M., Karthik, C., Saratale, R. G., Kumar, S. S., Prabakar, D., Kadirvelu, K., et al. (2018). Biological approaches to tackle heavy metal pollution: a survey of literature. *J. Environ. Manag.* 217, 56–70. doi:10.1016/j.jenvman.2018.03.077

Jandacka, D., Durcanska, D., and Cibula, R. (2022). Concentration and inorganic elemental analysis of particulate matter in a road tunnel environment (Žilina, Slovakia): contribution of non-exhaust sources. *Front. Environ. Sci.* 10, 952577. doi:10.3389/fenvs.2022.952577

Jehan, S., Khan, S., Khattak, S. A., Muhammad, S., Rashid, A., and Muhammad, N. (2019). Hydrochemical properties of drinking water and their sources apportionment of pollution in Bajaur agency, Pakistan. *Measurement* 139, 249–257. doi:10.1016/j.measurement.2019.02.090

Ji, Q., Pang, X., and Zhao, X. (2014). A bibliometric analysis of research on Antarctica during 1993–2012. *Scientometrics* 101, 1925–1939. doi:10.1007/s11192-014-1332-5

Jiang, W., Chu, H., Liu, Y., Chen, B., Feng, Y., Lyu, J., et al. (2023a). Distribution of heavy metals in coastal sediments under the influence of multiple factors: a case study from the south coast of an industrialized harbor city (Tangshan, China). *Sci. Total Environ.* 889, 164208. doi:10.1016/j.scitotenv.2023.164208

Jiang, W., Meng, L., Liu, F., Sheng, Y., Chen, S., Yang, J., et al. (2023b). Distribution, source investigation, and risk assessment of topsoil heavy metals in areas with intensive anthropogenic activities using the positive matrix factorization (PMF) model coupled with self-organizing map (SOM). *Environ. Geochem. Health* 45 (8), 6353–6370. doi:10.1007/s10653-023-01587-8

Jiang, Y., Chao, S., Liu, J., Yang, Y., Chen, Y., Zhang, A., et al. (2017). Source apportionment and health risk assessment of heavy metals in soil for a township in Jiangsu Province, China. *Chemosphere* 168, 1658–1668. doi:10.1016/j.chemosphere.2016.11.088

Jung, J., Park, J., Choi, Y., Choe, J. K., An, J., and Nam, K. (2023). Environmental forensic approach towards unraveling contamination sources with receptor models: a case study in nakdong river, South Korea. *Sci. Total Environ.* 892, 164554. doi:10.1016/j.scitotenv.2023.164554

Ke, Y., Wang, H., Wu, Z., Liu, S., Zhao, T., and Yin, Y. (2023). Quantifying the pollution characteristics of chemical components in PM2. 5 in the North China Plain, China: spatiotemporal variation and health risk. *Atmos. Environ.* 307, 119860. doi:10.1016/j.atmosenv.2023.119860

Khan, M. B., Setu, S., Sultana, N., Gautam, S., Begum, B. A., Salam, M. A., et al. (2023). Street dust in the largest urban agglomeration: pollution characteristics, source apportionment and health risk assessment of potentially toxic trace elements. *Stoch. Environ. Res. risk Assess.* 37 (8), 3305–3324. doi:10.1007/s00477-023-02432-1

Khan, S., Rauf, R., Muhammad, S., Qasim, M., and Din, I. (2016). Arsenic and heavy metals health risk assessment through drinking water consumption in the Peshawar District, Pakistan. *Hum. Ecol. risk Assess. Int. J.* 22 (3), 581–596. doi:10.1080/10807039.2015.1083845

Khan, S., Shah, I. A., Muhammad, S., Malik, R. N., and Shah, M. T. (2015). Arsenic and heavy metal concentrations in drinking water in Pakistan and risk assessment: a case study. *Hum. Ecol. Risk Assess. Int. J.* 21 (4), 1020–1031. doi:10.1080/10807039.2014.950925

Khan, Y. K., and Shah, M. H. (2023). Fractionation, source apportionment, and health risk assessment of selected metals in the soil of public parks of Lahore, Pakistan. *Environ. Earth Sci.* 82 (12), 311. doi:10.1007/s12665-023-11013-y

Khobragade, P. P., and Vikram Ahirwar, A. (2023). Chemical and morphological characterization of PM2. 5 samples collected over an urban industrial region Raipur, Chhattisgarh. *Acta Geophys.* 71 (6), 3057–3076. doi:10.1007/s11600-023-01127-z

Kipp, G. G., Stone, J. J., and Stetler, L. D. (2009). Arsenic and uranium transport in sediments near abandoned uranium mines in Harding County, South Dakota. *Appl. Geochem.* 24 (12), 2246–2255. doi:10.1016/j.apgeochem.2009.09.017

Klaver, G., Verheul, M., Bakker, I., Petelet-Giraud, E., and Négrel, P. (2014). Anthropogenic rare earth element in rivers: gadolinium and lanthanum. Partitioning between the dissolved and particulate phases in the Rhine River and spatial propagation through the rhine-meuse delta (The Netherlands). *Appl. Geochem.* 47, 186–197. doi:10.1016/j.apgeochem.2014.05.020

Lee, B.-K., and Park, G.-H. (2010). Characteristics of heavy metals in airborne particulate matter on misty and clear days. *J. Hazard. Mater.* 184 (1-3), 406–416. doi:10.1016/j.jhazmat.2010.08.050

Lee, C.S.-l., Li, X., Shi, W., Cheung, S.C.-n., and Thornton, I. (2006). Metal contamination in urban, suburban, and country park soils of Hong Kong: a study based on GIS and multivariate statistics. *Sci. Total Environ.* 356 (1-3), 45–61. doi:10.1016/j.scitotenv.2005.03.024

Leuven, R. S., van der Velde, G., Baijens, I., Snijders, J., van der Zwart, C., Lenders, H. R., et al. (2009). The river Rhine: a global highway for dispersal of aquatic invasive species. *Biol. invasions* 11, 1989–2008. doi:10.1007/s10530-009-9491-7

Li, D., Lu, Q., Cai, L., Chen, L., and Wang, H. (2023a). Characteristics of soil heavy metal pollution and health risk assessment in urban parks at a megacity of Central China. *Toxics* 11 (3), 257. doi:10.3390/toxics11030257

Li, H., Wang, J., Wang, Q. g., Qian, X., Qian, Y., Yang, M., et al. (2015). Chemical fractionation of arsenic and heavy metals in fine particle matter and its implications for risk assessment: a case study in Nanjing, China. *Atmos. Environ.* 103, 339–346. doi:10.1016/j.atmosenv.2014.12.065

Li, J., and Chen, C. (2016). *CiteSpace: Text mining and visualization in scientific literature*. Beijing, China: Capital University of Economics and Business Press, 149–152.

Li, N., Li, Y., Wei, J., Liu, K., Wang, G., Zhang, H., et al. (2023b). Source-oriented ecological risk assessment of heavy metals in sediments of West Taihu Lake, China. *Environ. Sci. Pollut. Res.* 30 (6), 13909–13919. doi:10.1007/s11356-022-24766-z

Li, N., Zhou, Y., Liu, J., Tsang, D. C., Wang, J., She, J., et al. (2020a). Persistent thallium contamination in river sediments, source apportionment and environmental implications. *Ecotoxicol. Environ. Saf.* 202, 110874. doi:10.1016/j.ecoenv.2020.110874

Li, R., Hua, P., Zhang, J., and Krebs, P. (2020b). Effect of anthropogenic activities on the occurrence of polycyclic aromatic hydrocarbons in aquatic suspended particulate matter: evidence from Rhine and Elbe Rivers. *Water Res.* 179, 115901. doi:10.1016/j.watres.2020.115901

Li, X., Feng, L., Huang, C., Yan, X., and Zhang, X. (2014a). Potential hazardous elements (PHEs) in atmospheric particulate matter (APM) in the south of Xi'an during the dust episodes of 2001–2012 (NW China): chemical fractionation, ecological and health risk assessment. *Environ. earth Sci.* 71, 4115–4126. doi:10.1007/s12665-013-2800-6

Li, X., Xu, Y., Li, M., Ji, R., Dolf, R., and Gu, X. (2021). Water quality analysis of the Yangtze and the Rhine River: a comparative study based on monitoring data from 2007 to 2018. *Bull. Environ. Contam. Toxicol.* 106, 825–831. doi:10.1007/s00128-020-03055-w

Li, X., Yang, H., Zhang, C., Zeng, G., Liu, Y., Xu, W., et al. (2017). Spatial distribution and transport characteristics of heavy metals around an antimony mine area in central China. *Chemosphere* 170, 17–24. doi:10.1016/j.chemosphere.2016.12.011

Li, Y., Chen, H., and Teng, Y. (2020c). Source apportionment and source-oriented risk assessment of heavy metals in the sediments of an urban river-lake system. *Sci. Total Environ.* 737, 140310. doi:10.1016/j.scitotenv.2020.140310

Li, Y., Ma, L., Ge, Y., and Abuduwaili, J. (2022). Health risk of heavy metal exposure from dustfall and source apportionment with the PCA-MLR model: a case study in the Ebinur Lake Basin, China. *Atmos. Environ.* 272, 118950. doi:10.1016/j.atmosenv.2022.118950

Li, Z., Ma, Z., van der Kuijp, T. J., Yuan, Z., and Huang, L. (2014b). A review of soil heavy metal pollution from mines in China: pollution and health risk assessment. *Sci. total Environ.* 468, 843–853. doi:10.1016/j.scitotenv.2013.08.090

Liang, J., Liu, J., Xu, G., and Chen, B. (2019). Distribution and transport of heavy metals in surface sediments of the Zhejiang nearshore area, East China Sea: sedimentary environmental effects. *Mar. Pollut. Bull.* 146, 542–551. doi:10.1016/j.marpolbul.2019.07.001

Light, R. P., Polley, D. E., and Börner, K. (2014). Open data and open code for big science of science studies. *Scientometrics* 101, 1535–1551. doi:10.1007/s11192-014-1238-2

Liu, M., Li, W., Qiao, W., Liang, L., and Wang, Z. (2023a). Knowledge domain and emerging trends in HIV-MTB co-infection from 2017 to 2022: a scientometric analysis based on VOSviewer and CiteSpace. *Front. Public Health* 11, 1044426. doi:10.3389/fpubh.2023.1044426

Liu, S., Wu, T., Wang, Q., Zhang, Y., Tian, J., Ran, W., et al. (2023b). High time-resolution source apportionment and health risk assessment for PM2. 5-bound elements at an industrial city in northwest China. *Sci. Total Environ.* 870, 161907. doi:10.1016/j.scitotenv.2023.161907

Liu, W., Wang, J., Li, C., Chen, B., and Sun, Y. (2019). Using bibliometric analysis to understand the recent progress in agroecosystem services research. *Ecol. Econ.* 156, 293–305. doi:10.1016/j.ecolecon.2018.09.001

Liu, X., Zhai, Y., Zhu, Y., Liu, Y., Chen, H., Li, P., et al. (2015). Mass concentration and health risk assessment of heavy metals in size-segregated airborne particulate matter in Changsha. *Sci. Total Environ.* 517, 215–221. doi:10.1016/j.scitotenv.2015.02.066

Liu, Y., Hu, J., Wang, X., Jia, J., Li, J., Wang, L., et al. (2021). Distribution, bioaccessibility, and health risk assessment of heavy metals in PM2. 5 and PM10 during winter heating periods in five types of cities in Northeast China. *Ecotoxicol. Environ. Saf.* 214, 112071. doi:10.1016/j.ecoenv.2021.112071

Liu, Y., Li, Q., Li, W., Jia, L., and Pei, X. (2023c). Knowledge map and hotspot analysis in climate resilience infrastructure (CRI) from 1997 to 2022 through scientometric analysis. *Environ. Res.* 228, 115874. doi:10.1016/j.envres.2023.115874

Liu, Z., Cheng, Y., Wang, P., Yu, Y., and Long, Y. (2018). A method for remaining useful life prediction of crystal oscillators using the Bayesian approach and extreme learning machine under uncertainty. *Neurocomputing* 305, 27–38. doi:10.1016/j.neucom.2018.04.043

Lu, A., Wang, J., Qin, X., Wang, K., Han, P., and Zhang, S. (2012). Multivariate and geostatistical analyses of the spatial distribution and origin of heavy metals in the agricultural soils in Shunyi, Beijing, China. *Sci. total Environ.* 425, 66–74. doi:10.1016/j.scitotenv.2012.03.003

Ma, H., Mi, M., Wang, C., Wu, X., and Zhen, Z. (2023). The concentrations, sources, ecological, and human health risk assessment of heavy metals in roadside soils of six cities in Shanxi Province, China. *Environ. Toxicol. Chem.* 42 (7), 1485–1500. doi:10.1002/etc.5641

Manoli, E., Voutsa, D., and Samara, C. (2002). Chemical characterization and source identification/apportionment of fine and coarse air particles in Thessaloniki, Greece. *Atmos. Environ.* 36 (6), 949–961. doi:10.1016/S1352-2310(01)00486-1

Martínez, M. A., Cobo, M. J., Herrera, M., and Herrera-Viedma, E. (2015). Analyzing the scientific evolution of social work using science mapping. *Res. Soc. work Pract.* 25 (2), 257–277. doi:10.1177/1049731514522101

Meerow, S., Newell, J. P., and Stults, M. (2016). Defining urban resilience: a review. *Landsc. urban Plan.* 147, 38–49. doi:10.1016/j.landurbplan.2015.11.011

Men, C., Liu, R., Wang, Q., Guo, L., Miao, Y., and Shen, Z. (2019). Uncertainty analysis in source apportionment of heavy metals in road dust based on positive matrix factorization model and geographic information system. *Sci. total Environ.* 652, 27–39. doi:10.1016/j.scitotenv.2018.10.212

Men, C., Liu, R., Xu, F., Wang, Q., Guo, L., and Shen, Z. (2018). Pollution characteristics, risk assessment, and source apportionment of heavy metals in road dust in Beijing, China. *Sci. total Environ.* 612, 138–147. doi:10.1016/j.scitotenv.2017.08.123

Meng, L., Zuo, R., Wang, J.-s., Yang, J., Teng, Y.-g., Shi, R.-t., et al. (2018). Apportionment and evolution of pollution sources in a typical riverside groundwater resource area using PCA-APCS-MLR model. *J. Contam. hydrology* 218, 70–83. doi:10.1016/j.jconhyd.2018.10.005

Mijić, Z., Stojić, A., Perišić, M., Rajšić, S., Tasić, M., Radenković, M., et al. (2010). Seasonal variability and source apportionment of metals in the atmospheric deposition in Belgrade. *Atmos. Environ.* 44 (30), 3630–3637. doi:10.1016/j.atmosenv.2010.06.045

Muhammad, S., Shah, M. T., and Khan, S. (2011). Health risk assessment of heavy metals and their source apportionment in drinking water of Kohistan region, northern Pakistan. *Microchem. J.* 98 (2), 334–343. doi:10.1016/j.microc.2011.03.003

Muhammad, S., and Usman, Q. A. (2022). Heavy metal contamination in water of Indus River and its tributaries, Northern Pakistan: evaluation for potential risk and source apportionment. *Toxin Rev.* 41 (2), 380–388. doi:10.1080/15569543.2021.1882499

Musa, I., Park, H. W., Munkhdalai, L., and Ryu, K. H. (2018). Global research on syndromic surveillance from 1993 to 2017: bibliometric analysis and visualization. *Sustainability* 10 (10), 3414. doi:10.3390/su10103414

Nguyen, B. T., Do, D. D., Nguyen, T. X., Nguyen, V. N., Nguyen, D. T. P., Nguyen, M. H., et al. (2020). Seasonal, spatial variation, and pollution sources of heavy metals in the sediment of the Saigon River, Vietnam. *Environ. Pollut.* 256, 113412. doi:10.1016/j.envpol.2019.113412

Osinska, V., and Bala, P. (2015). Study of dynamics of structured knowledge: qualitative analysis of different mapping approaches. *J. Inf. Sci.* 41 (2), 197–208. doi:10.1177/0165551514559897

Paatero, P., and Tapper, U. (1994). Positive matrix factorization: a non-negative factor model with optimal utilization of error estimates of data values. *Environmetrics* 5 (2), 111–126. doi:10.1002/env.3170050203

Pan, H., Lu, X., and Lei, K. (2017). A comprehensive analysis of heavy metals in urban road dust of Xi'an, China: contamination, source apportionment and spatial distribution. *Sci. Total Environ.* 609, 1361–1369. doi:10.1016/j.scitotenv.2017.08.004

Pant, P., and Harrison, R. M. (2013). Estimation of the contribution of road traffic emissions to particulate matter concentrations from field measurements: a review. *Atmos. Environ.* 77, 78–97. doi:10.1016/j.atmosenv.2013.04.028

Pastorino, P., Prearo, M., Bertoli, M., Abete, M. C., Dondo, A., Salvi, G., et al. (2020). Accumulation of As, Cd, Pb, and Zn in sediment, chironomids and fish from a high-mountain lake: first insights from the Carnic Alps. *Sci. Total Environ.* 729, 139007. doi:10.1016/j.scitotenv.2020.139007

Pekey, H., and Doğan, G. (2013). Application of positive matrix factorisation for the source apportionment of heavy metals in sediments: a comparison with a previous factor analysis study. *Microchem. J.* 106, 233–237. doi:10.1016/j.microc.2012.07.007

Persson, O. (1994). The intellectual base and research fronts of JASIS 1986–1990. *J. Am. Soc. Inf. Sci.* 45 (1), 31–38. doi:10.1002/(sici)1097-4571(199401)45:1<31::aid-asi4>3.0.co;2-g

Proshad, R., Dey, H. C., Khan, M. S. U., Baroi, A., Kumar, S., and Idris, A. M. (2023). Source-oriented risks apportionment of toxic metals in river sediments of Bangladesh: a national wide application of PMF model and pollution indices. *Environ. Geochem. Health* 45 (9), 6769–6792. doi:10.1007/s10653-022-01455-x

Rabha, S., Subramanyam, K., Sawant, S. S., and Saikia, B. K. (2022). Rare-earth elements and heavy metals in atmospheric particulate matter in an urban area. *ACS Earth Space Chem.* 6 (7), 1725–1732. doi:10.1021/acsearthspacechem.2c00009

Rehman, U. u., Khan, S., and Muhammad, S. (2018). Associations of potentially toxic elements (PTEs) in drinking water and human biomarkers: a case study from five districts of Pakistan. *Environ. Sci. Pollut. Res.* 25 (28), 27912–27923. doi:10.1007/s11356-018-2755-y

Rorissa, A., and Yuan, X. (2012). Visualizing and mapping the intellectual structure of information retrieval. *Inf. Process. and Manag.* 48 (1), 120–135. doi:10.1016/j.ipm.2011.03.004

Rousseeuw, P. J. (1987). Silhouettes: a graphical aid to the interpretation and validation of cluster analysis. *J. Comput. Appl. Math.* 20, 53–65. doi:10.1016/0377-0427(87)90125-7

Samara, C., and Voutsa, D. (2005). Size distribution of airborne particulate matter and associated heavy metals in the roadside environment. *Chemosphere* 59 (8), 1197–1206. doi:10.1016/j.chemosphere.2004.11.061

Saraswat, A., Ram, S., Raza, M. B., Islam, S., Sharma, S., Omeka, M. E., et al. (2023). Potentially toxic metals contamination, health risk, and source apportionment in the agricultural soils around industrial areas, Firozabad, Uttar Pradesh, India: a multivariate statistical approach. *Environ. Monit. Assess.* 195 (7), 863. doi:10.1007/s10661-023-11476-3

Schebek, L., Andreae, M. O., and Tobschall, H. J. (1991). Methyl-and butyltin compounds in water and sediments of the Rhine River. *Environ. Sci. and Technol.* 25 (5), 871–878. doi:10.1021/es00017a007

Shan, Y., Tysklind, M., Hao, F., Ouyang, W., Chen, S., and Lin, C. (2013). Identification of sources of heavy metals in agricultural soils using multivariate analysis and GIS. *J. Soils Sediments* 13, 720–729. doi:10.1007/s11368-012-0637-3

Shen, Y.-W., Zhao, C.-X., Zhao, H., Dong, S.-F., Xie, J.-J., Lv, M.-L., et al. (2023). Decryption analysis of antimony pollution sources in PM2. 5 through a multi-source isotope mixing model based on lead isotopes. *Environ. Pollut.* 328, 121600. doi:10.1016/j.envpol.2023.121600

Shi, W., and Qin, B. (2023). Sediment and nutrient trapping by river dams: a critical review based on 15-year big data. *Curr. Pollut. Rep.* 9 (2), 165–173. doi:10.1007/s40726-023-00258-7

Shi, Y., and Liu, X. (2019). Research on the literature of green building based on the Web of Science: a scientometric analysis in CiteSpace (2002–2018). *Sustainability* 11 (13), 3716. doi:10.3390/su11133716

Shiyi, Y., Xiaonuo, L., and Weiping, C. (2023). High-resolution risk mapping of heavy metals in soil with an integrated static-dynamic interaction model: a case study in an industrial agglomeration area in China. *J. Hazard. Mater.* 455, 131650. doi:10.1016/j.jhazmat.2023.131650

Shojaee Barjoee, S., Azizi, M., Khaledi, A., Kouhkan, M., Soltani, M., and Farokhi, H. (2023). Street dust-bound metal (loid) s in industrial areas of Iran: moran's spatial autocorrelation distribution, eco-toxicological risk assessment, uncertainty and sensitivity analysis. *Int. J. Environ. Sci. Technol.* 20 (8), 8509–8536. doi:10.1007/s13762-023-05021-5

Simeonov, V., Einax, J., Tsakovski, S., and Kraft, J. (2005). Multivariate statistical assessment of polluted soils. *Open Chem.* 3 (1), 1–9. doi:10.2478/bf02476233

Song, M., Zhang, J., Liu, X., Zhang, L., Hao, X., and Li, M. (2023). Developments and trends in energy poverty research—literature visualization analysis based on CiteSpace. *Sustainability* 15 (3), 2576. doi:10.3390/su15032576

Sun, H., Zheng, Z., Chen, S., Cao, J., Guo, M., and Han, Y. (2023). Source apportionment of heavy metals and their effects on the species diversity of plant communities in the Caizi Lake wetland, China. *Environ. Sci. Pollut. Res.* 30 (21), 60854–60867. doi:10.1007/s11356-023-26815-7

Sun, X., Wang, H., Guo, Z., Lu, P., Song, F., Liu, L., et al. (2020). Positive matrix factorization on source apportionment for typical pollutants in different environmental media: a review. *Environ. Sci. Process. and Impacts* 22 (2), 239–255. doi:10.1039/c9em00529c

Sun, Y., Wu, S., and Gong, G. (2019). Trends of research on polycyclic aromatic hydrocarbons in food: a 20-year perspective from 1997 to 2017. *Trends food Sci. and Technol.* 83, 86–98. doi:10.1016/j.tifs.2018.11.015

Thorpe, A., and Harrison, R. M. (2008). Sources and properties of non-exhaust particulate matter from road traffic: a review. *Sci. total Environ.* 400 (1-3), 270–282. doi:10.1016/j.scitotenv.2008.06.007

Tokatlı, C., Islam, A. R. M. T., and Muhammad, S. (2024). Temporal variation of water quality parameters in the lacustrine of the Thrace Region, Northwest Türkiye. *Environ. Sci. Pollut. Res.* 31, 11832–11841. doi:10.1007/s11356-024-31912-2

Ustaoğlu, F., and Islam, M. S. (2020). Potential toxic elements in sediment of some rivers at Giresun, Northeast Turkey: a preliminary assessment for ecotoxicological status and health risk. *Ecol. Indic.* 113, 106237. doi:10.1016/j.ecolind.2020.106237

Van Dijk, G., Marteijn, E., and Schulte-Wülwer-Leidig, A. (1995). Ecological rehabilitation of the River Rhine: plans, progress and perspectives. *Regul. Rivers Res. and Manag.* 11 (3-4), 377–388. doi:10.1002/rrr.3450110311

Van Eck, N. J., and Waltman, L. (2014). CitNetExplorer: a new software tool for analyzing and visualizing citation networks. *J. Inf.* 8 (4), 802–823. doi:10.1016/j.joi.2014.07.006

Van Eck, N. J., and Waltman, L. (2017). Citation-based clustering of publications using CitNetExplorer and VOSviewer. *Scientometrics* 111, 1053–1070. doi:10.1007/s11192-017-2300-7

Vassilakos, C., Veros, D., Michopoulos, J., Maggos, T., and O'Connor, C. (2007). Estimation of selected heavy metals and arsenic in PM10 aerosols in the ambient air of the Greater Athens Area, Greece. *J. Hazard. Mater.* 140 (1-2), 389–398. doi:10.1016/j.jhazmat.2006.11.002

Viana, M., Kuhlbusch, T. A., Querol, X., Alastuey, A., Harrison, R. M., Hopke, P. K., et al. (2008). Source apportionment of particulate matter in Europe: a review of methods and results. *J. aerosol Sci.* 39 (10), 827–849. doi:10.1016/j.jaerosci.2008.05.007

Vink, R., Behrendt, H., and Salomons, W. (1999). Point and diffuse source analysis of heavy metals in the Elbe drainage area: comparing heavy metal emissions with transported river loads. *Hydrobiologia* 410, 307–314. doi:10.1007/978-94-017-2163-9_32

Wagenaar-Hart, A. (1994). International commission for the hydrology of the rhine basin (CHR). *Water Sci. Technol.* 29 (3), 375–378. doi:10.2166/wst.1994.0138

Wang, D., He, J., Tang, Y.-T., Higgitt, D., and Robinson, D. (2020). Life cycle assessment of municipal solid waste management in Nottingham, England: past and future perspectives. *J. Clean. Prod.* 251, 119636. doi:10.1016/j.jclepro.2019.119636

Wang, G., Yinglan, A., Jiang, H., Fu, Q., and Zheng, B. (2015). Modeling the source contribution of heavy metals in surficial sediment and analysis of their historical changes in the vertical sediments of a drinking water reservoir. *J. Hydrology* 520, 37–51. doi:10.1016/j.jhydrol.2014.11.034

Wang, J., Cai, Y., Yang, J., and Zhao, X. (2021a). Research trends and frontiers on source appointment of soil heavy metal: a scientometric review (2000–2020). *Environ. Sci. Pollut. Res.* 28 (38), 52764–52779. doi:10.1007/s11356-021-16151-z

Wang, J., Zheng, Y., Li, Y., and Wang, Y. (2023a). Potential risks, source apportionment, and health risk assessment of dissolved heavy metals in Zhoushan fishing ground, China. *Mar. Pollut. Bull.* 189, 114751. doi:10.1016/j.marpolbul.2023.114751

Wang, P., Huang, W., Ren, F., and Fan, D. (2023b). Pollution evaluation and source identification of heavy metals in soil around steel factories located in Lanshan District, Rizhao City, eastern China. *Environ. Monit. Assess.* 195 (6), 657. doi:10.1007/s10661-023-11230-9

Wang, Q., Chen, Q., Wang, C., Wang, R., Sha, T., Zhang, Q., et al. (2023c). Sources and health risk assessment of water-soluble and water-insoluble metals in road and foliar dust in Xi'an, Northwest China. *Sci. Total Environ.* 891, 164704. doi:10.1016/j.scitotenv.2023.164704

Wang, X., Liu, E., Yan, M., Zheng, S., Fan, Y., Sun, Y., et al. (2023d). Contamination and source apportionment of metals in urban road dust (Jinan, China) integrating the enrichment factor, receptor models (FA-NNC and PMF), local Moran's index, Pb isotopes and source-oriented health risk. *Sci. Total Environ.* 878, 163211. doi:10.1016/j.scitotenv.2023.163211

Wang, Y., Guo, G., Zhang, D., and Lei, M. (2021b). An integrated method for source apportionment of heavy metal (loid) s in agricultural soils and model uncertainty analysis. *Environ. Pollut.* 276, 116666. doi:10.1016/j.envpol.2021.116666

Wang, Y., Wu, L., Hu, W., Li, W., Shi, Z., Harrison, R. M., et al. (2022). Stable iron isotopic composition of atmospheric aerosols: an overview. *npj Clim. Atmos. Sci.* 5 (1), 75. doi:10.1038/s41612-022-00299-7

Wang, Y., Yu, H., Yi, M., Zhou, R., Li, H., Xu, S., et al. (2023e). Spatial distribution, sources, and risks of heavy metals in soil from industrial areas of Hangzhou, eastern China. *Environ. Earth Sci.* 82 (4), 95. doi:10.1007/s12665-023-10774-w

Wang, Z., Chen, X., Yu, D., Zhang, L., Wang, J., and Lv, J. (2021c). Source apportionment and spatial distribution of potentially toxic elements in soils: a new exploration on receptor and geostatistical models. *Sci. Total Environ.* 759, 143428. doi:10.1016/j.scitotenv.2020.143428

Wang, Z., Zhao, Y., and Wang, B. (2018). A bibliometric analysis of climate change adaptation based on massive research literature data. *J. Clean. Prod.* 199, 1072–1082. doi:10.1016/j.jclepro.2018.06.183

Watson, J. G., Zhu, T., Chow, J. C., Engelbrecht, J., Fujita, E. M., and Wilson, W. E. (2002). Receptor modeling application framework for particle source apportionment. *Chemosphere* 49 (9), 1093–1136. doi:10.1016/s0045-6535(02)00243-6

Wu, J., Li, J., Teng, Y., Chen, H., and Wang, Y. (2020). A partition computing-based positive matrix factorization (PC-PMF) approach for the source apportionment of agricultural soil heavy metal contents and associated health risks. *J. Hazard. Mater.* 388, 121766. doi:10.1016/j.jhazmat.2019.121766

Wu, M., Long, R., Bai, Y., and Chen, H. (2021). Knowledge mapping analysis of international research on environmental communication using bibliometrics. *J. Environ. Manag.* 298, 113475. doi:10.1016/j.jenvman.2021.113475

Xia, M., Chen, B., Fan, G., Weng, S., Qiu, R., Hong, Z., et al. (2023). The shifting research landscape for PAH bioremediation in water environment: a bibliometric analysis on three decades of development. *Environ. Sci. Pollut. Res.* 30 (27), 69711–69726. doi:10.1007/s11356-023-27404-4

Xie, L., Li, P., and Mu, D. (2023). Spatial distribution, source apportionment and potential ecological risk assessment of trace metals in surface soils in the upstream region of the Guanzhong Basin, China. *Environ. Res.* 234, 116527. doi:10.1016/j.envres.2023.116527

Xie, Y., Chen, T.-b., Lei, M., Yang, J., Guo, Q.-j., Song, B., et al. (2011). Spatial distribution of soil heavy metal pollution estimated by different interpolation methods: accuracy and uncertainty analysis. *Chemosphere* 82 (3), 468–476. doi:10.1016/j.chemosphere.2010.09.053

Xu, C., Lu, X., Huang, C., Sun, R., Gu, A., Pan, W., et al. (2023a). Positive matrix factorization as source apportionment of paddy soil heavy metals in black shale areas in western zhejiang Province, China. *Sustainability* 15 (5), 4547. doi:10.3390/su15054547

Xu, C., Yang, T., Wang, K., Guo, L., and Li, X. (2023b). Knowledge domain and hotspot trends in coal and gas outburst: a scientometric review based on CiteSpace

analysis. *Environ. Sci. Pollut. Res.* 30 (11), 29086–29099. doi:10.1007/s11356-022-23879-9

Xu, J., Xu, L., Zheng, L., Liu, B., Liu, J., and Wang, X. (2019). Distribution, risk assessment, and source analysis of heavy metals in sediment of rivers located in the hilly area of southern China. *J. soils sediments* 19, 3608–3619. doi:10.1007/s11368-019-02341-3

Xu, S., and Tao, S. (2004). Coregionalization analysis of heavy metals in the surface soil of Inner Mongolia. *Sci. total Environ.* 320 (1), 73–87. doi:10.1016/s0048-9697(03)00450-9

Xue, J.-l., Zhi, Y.-y., Yang, L.-p., Shi, J.-c., Zeng, L.-z., and Wu, L.-s. (2014). Positive matrix factorization as source apportionment of soil lead and cadmium around a battery plant (Changxing County, China). *Environ. Sci. Pollut. Res.* 21, 7698–7707. doi:10.1007/s11356-014-2726-x

Xue, S., Korna, R., Fan, J., Ke, W., Lou, W., Wang, J., et al. (2023). Spatial distribution, environmental risks, and sources of potentially toxic elements in soils from a typical abandoned antimony smelting site. *J. Environ. Sci.* 127, 780–790. doi:10.1016/j.jes.2022.07.009

Yang, J., Cheng, C., Shen, S., and Yang, S. (2017). "Comparison of complex network analysis software: citespace, SCI 2 and Gephi," in 2017 IEEE 2nd International conference on Big data analysis ICBDA*: ieee*, 169–172.

Yang, Z., Li, C., Chen, H., Shan, X., Chen, J., Zhang, J., et al. (2023). Source-oriented ecological and resistome risks associated with geochemical enrichment of heavy metals in river sediments. *Chemosphere* 336, 139119. doi:10.1016/j.chemosphere.2023.139119

Yoshikane, F. (2013). Multiple regression analysis of a patent's citation frequency and quantitative characteristics: the case of Japanese patents. *Scientometrics* 96, 365–379. doi:10.1007/s11192-013-0953-4

Yu, B., Lu, X., Fan, X., Fan, P., Zuo, L., Yang, Y., et al. (2021). Analyzing environmental risk, source and spatial distribution of potentially toxic elements in dust of residential area in Xi'an urban area, China. *Ecotoxicol. Environ. Saf.* 208, 111679. doi:10.1016/j.ecoenv.2020.111679

Yu, B., Lu, X., Wang, L., Liang, T., Fan, X., Yang, Y., et al. (2023). Potentially toxic elements in surface fine dust of residence communities in valley industrial cities. *Environ. Pollut.* 327, 121523. doi:10.1016/j.envpol.2023.121523

Zhang, J., Li, H., Zhou, Y., Dou, L., Cai, L., Mo, L., et al. (2018). Bioavailability and soil-to-crop transfer of heavy metals in farmland soils: a case study in the Pearl River Delta, South China. *Environ. Pollut.* 235, 710–719. doi:10.1016/j.envpol.2017.12.106

Zhang, X., Zhang, Y., Wang, Y., and Fath, B. D. (2021). Research progress and hotspot analysis for reactive nitrogen flows in macroscopic systems based on a CiteSpace analysis. *Ecol. Model.* 443, 109456. doi:10.1016/j.ecolmodel.2021.109456

Zhang, Y., Chen, W., and Gao, W. (2017). A survey on the development status and challenges of smart grids in main driver countries. *Renew. Sustain. Energy Rev.* 79, 137–147. doi:10.1016/j.rser.2017.05.032

Zhang, Y., Li, T., Guo, Z., Xie, H., Hu, Z., Ran, H., et al. (2023). Spatial heterogeneity and source apportionment of soil metal (loid) s in an abandoned lead/zinc smelter. *J. Environ. Sci.* 127, 519–529. doi:10.1016/j.jes.2022.06.015

Zheng, F., Guo, X., Tang, M., Zhu, D., Wang, H., Yang, X., et al. (2023). Variation in pollution status, sources, and risks of soil heavy metals in regions with different levels of urbanization. *Sci. Total Environ.* 866, 161355. doi:10.1016/j.scitotenv.2022.161355

Zhou, W., Kou, A., Chen, J., and Ding, B. (2018). A retrospective analysis with bibliometric of energy security in 2000–2017. *Energy Rep.* 4, 724–732. doi:10.1016/j.egyr.2018.10.012

Zhou, X., Li, Z., Zhang, T., Wang, F., Tao, Y., Zhang, X., et al. (2021). Chemical nature and predominant sources of PM10 and PM2. 5 from multiple sites on the Silk Road, Northwest China. *Atmos. Pollut. Res.* 12 (1), 425–436. doi:10.1016/j.apr.2020.10.001

Zhou, X., Xie, M., Zhao, M., Wang, Y., Luo, J., Lu, S., et al. (2023). Pollution characteristics and human health risks of PM2. 5-bound heavy metals: a 3-year observation in Suzhou, China. *Environ. Geochem. Health* 45 (7), 5145–5162. doi:10.1007/s10653-023-01568-x

Zhou, X., and Zhao, G. (2015). Global liposome research in the period of 1995–2014: a bibliometric analysis. *Scientometrics* 105, 231–248. doi:10.1007/s11192-015-1659-6

Zhu, Y., Chen, Q., Li, G., She, J., Zhu, Y., Sun, W., et al. (2023). Source and health risk apportionment of PM10 based on heavy metals in a city on the edge of the Tengger Desert. *Air Qual. Atmos. and Health* 16 (2), 391–399. doi:10.1007/s11869-022-01279-9

Zou, H., Ren, B., Deng, X., and Li, T. (2023). Geographic distribution, source analysis, and ecological risk assessment of PTEs in the topsoil of different land uses around the antimony tailings tank: a case study of Longwangchi tailings pond, Hunan, China. *Ecol. Indic.* 150, 110205. doi:10.1016/j.ecolind.2023.110205

frontiers | Frontiers in Environmental Science

TYPE Original Research
PUBLISHED 18 September 2024
DOI 10.3389/fenvs.2024.1471160

OPEN ACCESS

EDITED BY
Yaoguang Guo,
Shanghai Polytechnic University, China

REVIEWED BY
Chang Liu,
Anhui Normal University, China
Baoyi Lv,
Shanghai Maritime University, China

*CORRESPONDENCE
Xianfei Huang,
hxfswjs@gznu.edu.cn

†These authors have contributed equally to this work

RECEIVED 26 July 2024
ACCEPTED 28 August 2024
PUBLISHED 18 September 2024

CITATION
Jiang X, Wang X, Liu Y, Huang Y and Huang X (2024) Heavy metal changes related to land use changes in a karst area: a case study in Changshun, Guizhou Province, China. *Front. Environ. Sci.* 12:1471160. doi: 10.3389/fenvs.2024.1471160

Heavy metal changes related to land use changes in a karst area: a case study in Changshun, Guizhou Province, China

Xin Jiang[1†], Xingfu Wang[2,3†], Yi Liu[2], Yu Huang[2] and Xianfei Huang[1*]

[1]Guizhou Provincial Key Laboratory for Protection of Ecological Environment, Guizhou Normal University, Guiyang, China, [2]School of Health Management, Guiyang Healthcare Vocational University, Guiyang, China, [3]Guizhou Provincial Engineering Research Center of Medical Resourceful Healthcare Products, Guiyang Healthcare Vocational University, Guiyang, China

Karst areas are often characterized by fragile ecological systems, and environmental pollution has increased the pressures on people living in such regions. This study aimed to investigate the status of pollution caused by heavy metals (Pb, Cd, Hg, As, and Cu) in soils based on different land uses in Changshun County, a karst area in southwestern China. Soil samples were collected from natural forestlands (NFLs), natural brush lands (NBLs), natural pasture lands (NPLs), artificial forestlands (AFLs), artificial brush lands (ABLs), and artificial pasture lands (APLs) for evaluation. The results suggest that the soil profile characteristics of the heavy metals studied herein vary significantly among different land uses. The heavy metal concentrations in all soil samples collected from NFLs were lower than those in samples from other land uses. Forest trees can protect soil from heavy metal pollution caused by atmospheric deposition; this is especially true for Hg. In cultivated forestlands and brush lands, special attention should be devoted to Cd pollution in the soil, which may be caused by the use of fertilizers. Changing both natural and artificial pastoral lands to forestlands could benefit the local ecosystems as it may reduce Hg contamination.

KEYWORDS

land use, heavy metals, pollution, profile characteristics, karst area, southwestern China

1 Introduction

Heavy metal pollution of soil is a significant environmental concern owing to its long-lasting impacts on the ecosystems and human health (Wei et al., 2023). The heavy metals present in soil affect plant growth, soil ecosystems, and human health through direct exposure as well as consumption of contaminated food (Shukla and Jain, 2022; Wen et al., 2022). Heavy metal pollution of soil has been a persistent global problem for over half a century and is an important threat to all life; for instance, some of the important causes underlying many diseases in humans, such as cancer, are attributable to heavy metal pollution (Milner and Kochian, 2008). This type of pollution arises from various human activities, such as industrial processes, mining, agriculture, and improper waste disposal (Shakoor et al., 2013; Huang et al., 2017). Industrial developments are profitable and have made life convenient; however, they also cause many environmental problems (Ma et al., 2024; Roy et al., 2014; Haddou et al., 2014; Rainio et al., 2015; Wang et al., 2015). When crops absorb and accumulate toxic metals from contaminated soils, they may harm animal and human health as these pollutants move up the

food chain (Olawotin et al., 2012; Wang et al., 2020; Ahmed et al., 2013). Heavy metals like Cd can lead to cardiovascular diseases (Jin and Zhou, 2012); Pd can cause severe damage to the brain and central nervous system (Zhu et al., 2018); As can cause cancers (Yan and Zhang, 2021); Hg poses threats to the development of fetuses and young children (Clarkson et al., 2003); excess Cu in the environment may cause respiratory and digestive diseases (Geest et al., 2000).

The high geological background coupled with rocky desertification has led to prominent heavy metal soil pollution problems in the southwestern karst regions of China, which are important factors affecting the security of the ecological environments of these karst regions. There are large discrepancies in the soil heavy metal concentrations in karst mountain areas, and their impact factors are more complex than those in non-karst areas. Wang et al. (2021) noted that the levels of As, Cu, Pb, Cd, Cr, and Zn in the farmland soil around a Ni–Mo mining area in Guizhou were generally higher than the background values. Among these, Cd has been identified as a key factor contributing to soil heavy metal pollution. In addition, the Cd content in crops was between 0.02 and 1.28 mg kg^{-1}, and Cd levels were highly enriched in chili peppers (Wang et al., 2020). Zhang et al. (2022a) indicated that the potential ecological hazards of heavy metals in farmland soil decreased in the order of Hg > Cd > As > Pb > Cr in central Guizhou Province. The areas in which high Hg values were observed were distributed in a planar pattern, while areas with high values of Cd, As, Pb, and Cr were mostly distributed in dotted patterns. Atmospheric deposition and industrial activities are the main causes of heavy metal pollution in cultivated soils. Zhang et al. (2022b) showed that the levels of Sb, As, Cd, Pb, and Cu in the soil along the banks of the Duliu River caused mild pollution; the human health risks from heavy metals in the soil in the research areas were generally low, with children having greater health risks than adults. Cd and Sb were the main elements influencing human health, and it was shown that the risks to human health based on soil Cd levels could be spatially differentiated in the order of soil type > altitude > distance from river > land use type > slope.

Over the past few decades, Guizhou has experienced serious environmental problems, such as desertification, deforestation, organic and inorganic pollution, and persistent water shortages (Wang et al., 2022; Chen et al., 2022). The local government and some researchers have attempted to formulate strategies to lead the local people out of poverty and develop ecofriendly lifestyles. Since the beginning of the 21st century, the provincial government has been trying to develop the local tourism industry, for which environmental quality improvement is a key step. Some of the croplands have been or are in the process of being rearranged as pasture lands or forestlands. The changes that have occurred to the soil pollutants during this period and considerations that require special attention need to be identified. The aims of the present study are as follows: (a) to comparatively study the heavy metals in the soils from both natural and artificial forestlands and pasture lands; (b) to analyze the incidental heavy metal pollution problems caused by human activities.

2 Materials and methods

2.1 Study region

Guizhou is a typical karst area located on the Yunnan–Guizhou Plateau and has a subtropical humid climate with annual average temperatures of approximately 12°C–25°C; the January temperatures range from −2°C to 12°C and July temperatures range from 20°C to 29°C. Changshun County (106°12′32″–106°38′48″E, 25°39′28″–26°17′17″N) is a typical karst region in Guizhou Province in southwestern China and covers an area of 1554.6 km^2. The study area belongs to a humid zone in the mid-subtropical monsoon climate region and has obvious three-dimensional climatic characteristics. The mean annual temperature ranges from 13.4°C to 19.5°C and mean annual precipitation ranges from 1250 mm to 1400 mm, with four clearly evident seasons. The vegetation in this area includes broad-leaved mixed forests, evergreen broad-leaved forests, and montane elfin forests. Sufficient availability of water in this region promotes conditions for karst erosion and general erosion, and the desert area accounts for 77.9% of the total area. No obvious point pollution sources are noted in the study area.

2.2 Sampling

From March to June of 2022, eighteen soil profiles consisting of 120 soil samples were collected from natural forestlands (NFLs), natural brush lands (NBLs), natural pasture lands (NPLs), artificial forestlands (AFLs), artificial brush lands (ABLs), and artificial pasture lands (APLs) in Changshun County (Figure 1). These sampling areas have the same soil formation processes and similar geochemical backgrounds. All artificial areas (AFLs, ABLs, and APLs) were transferred from farmlands that were used for food production to the currently used types over a decade ago. The detailed information for each sampling site is listed in Table 1. Each soil profile was sampled at seven layers (0–10, 10–20, 20–30, 30–40, 40–50, 50–70, and 70–90 cm) if the soil depth was equal to or greater than 90 cm. Otherwise, sampling was carried out to the actual depth of the soil. For example, four samplings were performed if the soil depth was between 40 cm and 50 cm. The soil samples were transferred to the lab and dried at room temperature (ca. 28°C) before being ground and passed through a sieve (0.22 mm). The collected samples were stored in Ziploc bags for the analysis of heavy metals.

2.3 Analytical procedures

For analysis of Pb, Cd, and Cu, about 1 g (accurate to 0.0001 g) of each soil sample was weighed and digested with 30 mL of a digesting mixture composed of HNO_3, $HClO_4$, and HCl (HNO_3:$HClO_4$:HCl = 4:1:5 v/v/v). The Pb, Cd, and Cu contents were then determined with inductively coupled plasma atomic emission spectrometry (5300V, Perkin Elmer Corporation, Waltham, MA, USA) (Wang et al., 2020; Wang et al., 2021). For determination of As and Hg, about 0.3 g (accurate to 0.0001 g) of the soil sample was weighed and transferred to a 50-mL tube, followed by addition of 10 mL of a digesting solution composed of HCl, HNO_3, and H_2O (HCl:HNO_3:H_2O = 3:1:4 v/v/v) (Tokumoto et al., 2014). The tubes were then placed in a boiling water bath for 3 h and shaken at intervals of 30 min. The solutions were next transferred to 50-mL volumetric flasks and 5 mL of a reducing agent (10% thiourea solution) was added to each flask, followed by dilution to volume with 5% HCl (v/v). The As and Hg

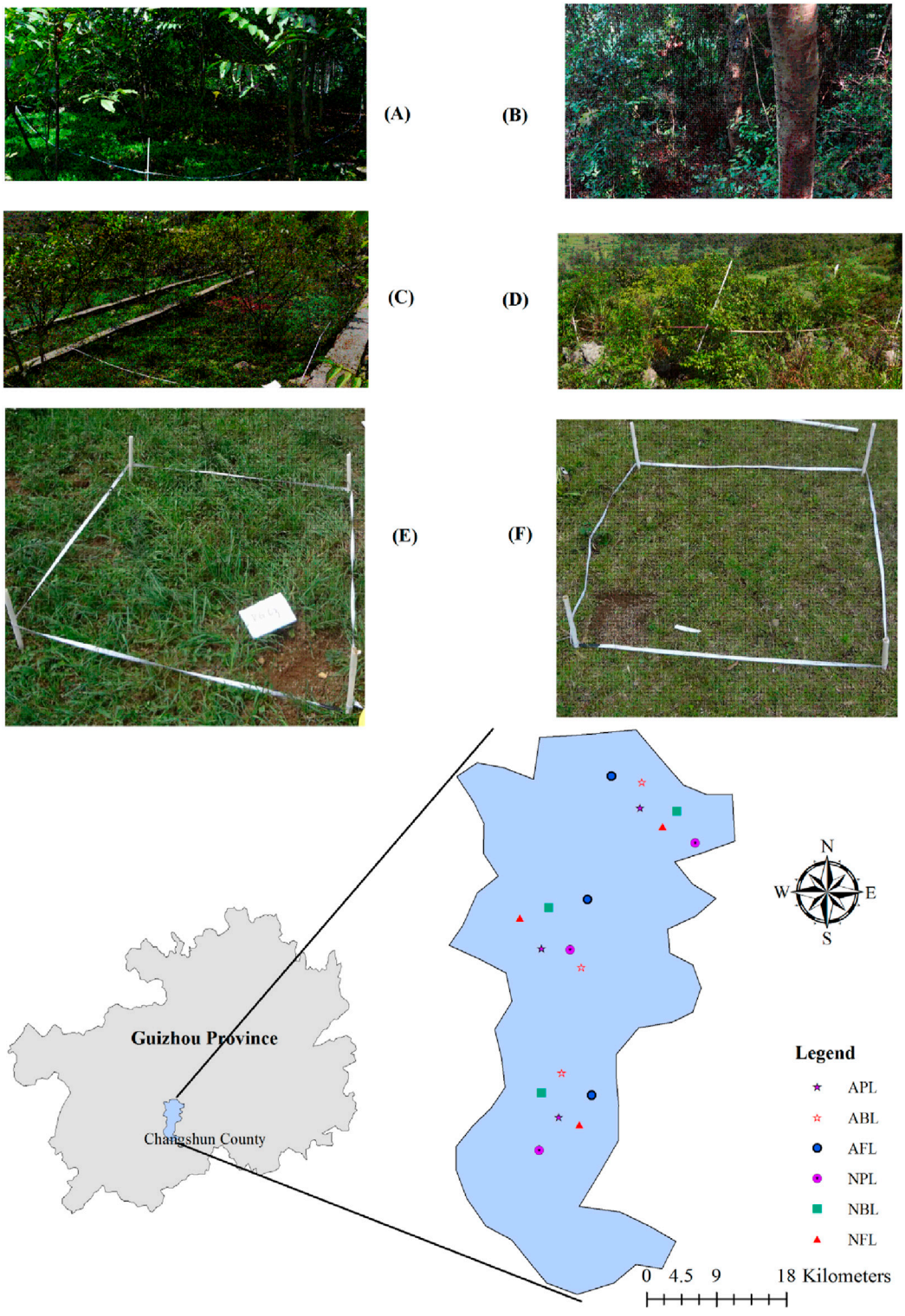

FIGURE 1
Study region and different types of land use: **(A)** artificial forest land; **(B)** natural forest land; **(C)** artificial brush land; **(D)** natural brush land; **(E)** artificial pasture land; **(F)** natural pasture land.

levels were determined using atomic fluorescence spectroscopy (AFS-933, Jitian Corporation, Shanghai, China). The quality of the analytical procedure was controlled using the certified reference material GBW 07403, which was analyzed in triplicate while the soil samples were replicated at a 20% level. The uncertainty of the analytical procedure was thus found to be within 10%. Analytical blanks were provided for all determinations (Huang et al., 2018; Huang et al., 2017). In addition, the other soil

TABLE 1 General information for each sampling site.

Sampling sites	Longitude and latitude	Soil types	Range of pH	Main plants
NFL1	N:25°56′48″ E:106°24′21″	Yellow soil	5.10–6.13	*Aralia chinensis, Betula luminifera, Quercus fabri*
NFL2	N:25°56′47″ E:106°24′21″	Yellow soil	5.52–6.40	*Quercus fabri, Aralia chinensis, Quercus acutissima* Carruth, *Fructus mori*
NFL3	N:25°56′49″ E:106°24′22″	Yellow soil	5.70–6.33	*Schefflera delavayi, Lindera communis, Betula luminifera*
NBL1	N:25°56′53″ E:106°24′17″	Yellow soil	4.94–6.70	*Coriaria nepalensis* Wall, *Pyracantha fortuneana, Viburnum foetidum -var*
NBL2	N:25°56′54″ E:106°24′16″	Yellow soil	4.62–6.34	*Rhus punjabensis* Stewart var, *Toddalia asiatica, Lindera communis*
NBL3	N:25°56′53″ E:106°24′14″	Yellow soil	5.41–6.52	*Betula luminifera, Quercus fabri*
NPL1	N:26°03′29″ E:106°27′03″	Yellow soil	5.70–6.39	*Cynodondactylon, Eremochloa ophiuroides*
NPL2	N:26°03′29″ E:106°27′02″	Yellow soil	5.86–6.35	*Cynodondactylon, Eremochloa ophiuroides*
NPL3	N:26°03′27″ E:106°27′04″	Yellow soil	5.19–6.35	*Cynodondactylon, Eremochloa ophiuroides*
AFL1	N:25°57′40″ E:106°25′09″	Yellow soil	4.95–6.35	*Juglans regia, Rosa roxburghii, Dactylis glomerata*
AFL2	N:25°57′40″ E:106°25′10″	Yellow soil	5.59–6.86	*Juglans regia, Rosa roxburghii, Dactylis glomerata*
AFL3	N:25°57′41″ E:106°25′09″	Yellow soil	5.19–7.16	*Juglans regia, Rosa roxburghii, Dactylis glomerata*
ABL1	N:25°57′35″ E:106°24′49″	Yellow soil	5.21–6.67	*Juglans regia, Rosa roxburghii, Dactylis glomerata*
ABL2	N:25°57′35″ E:106°24′48″	Yellow soil	6.60–6.65	*Juglans regia, Rosa roxburghii, Dactylis glomerata*
ABL3	N:25°57′35″ E:106°24′47″	Yellow soil	4.97–6.52	*Juglans regia, Rosa roxburghii, Dactylis glomerata*
APL1	N:26°03′28″ E:106°27′04″	Yellow soil	5.60–6.13	*Dactylis glomerata, Trifolium repens*
APL2	N:26°03′28″ E:106°27′04″	Yellow soil	6.00–7.68	*Dactylis glomerata, Trifolium repens*
APL3	N:26°03′29″ E:106°27′03″	Yellow soil	5.68–6.31	*Dactylis glomerata, Trifolium repens*

chemical indicators, such as total phosphorus (TP), total nitrogen (TN), and total potassium (TK), were tested simultaneously (Wang et al., 2022; Huang et al., 2018).

2.4 Assessment of heavy metals with gray clustering analysis

The heavy metal pollution at each study site was evaluated by gray clustering analysis, and the weight of each heavy metal in the clustering was determined. The basic theory of this analytical method can be found in literature (Pan et al., 2009; Fan et al., 2016). In the present study, five pollution indices (Pb, Cd, Hg, As, and Cu) were selected as the clustering indices to evaluate the pollution status at each studied site. The evaluation criteria were based on those recommended by the Ministry of Ecology and Environment of the People's Republic of China (GB15618-2018) (Wang et al., 2021; Fan et al., 2016; Fan et al., 2012; Zhang et al., 2019) (Table 2).

2.4.1 Gray whitening function

In the present study, the whitening functions of the *i*th clustering object's pollution index j are displayed as follows:

2.4.1.1 Class I

$$f(x_i) = \begin{cases} 1 & x_i \le a_i \\ (b_i - x_i)/(b_i - a_i) & a_i < x_i \le b_i \\ 0 & b_i < x_i \end{cases} \quad (1)$$

TABLE 2 Environmental quality of the soil standards in China.

Elements	Land use	Limiting value (mg·kg^{-1})			
		pH ≤ 5.5	5.5 < pH ≤ 6.5	6.5 < pH ≤ 7.5	pH > 7.5
Pb	Paddy land	80	100	140	240
	Other land	70	90	120	170
Cd	Paddy land	0.3	0.4	0.6	0.8
	Other land	0.3	0.3	0.3	0.6
Hg	Paddy land	0.5	0.5	0.6	1.0
	Other land	1.3	1.8	2.4	3.4
As	Paddy land	30	30	25	20
	Other land	40	40	30	25
Cu	Paddy land	150	150	200	200
	Other land	50	50	100	100

2.4.1.2 Class II

$$f(x_i) = \begin{cases} 0 & x_i < a_i \\ (x_i - a_i)/(b_i - a_i) & a_i \le x_i < b_i \\ (c_i - x_i)/(c_i - b_i) & b_i \le x_i < c_i \\ 0 & x_i \ge c_i \end{cases} \quad (2)$$

2.4.1.3 Class III

$$f(x_i) = \begin{cases} 0 & x_i \le b_i \\ (x_i - b_i)/(c_i - b_i) & b_i < x_i \le c_i \\ 1 & x_i < c_i \end{cases} \quad (3)$$

where x_i is the ith concentration of the heavy metal in the soil sample; a_i, b_i, and c_i are the criteria related to classes I, II, and III, respectively.

2.4.2 Clustering weight of each heavy metal in each classification

The measured content and biological toxicity index of each heavy metal were weighted, superimposed, and normalized. The biological toxicity indices of Pb, Cd, Hg, As, and Cu were found to be 4, 2, 1, 3, and 4, respectively (Fan et al., 2016; Fan et al., 2012). Then, the clustering weight of each heavy metal was calculated through the following formulas:

$$W_i = \frac{\frac{x_i}{S_i}}{\sum_{i=1}^{n} \frac{x_i}{S_i}} \quad (4)$$

$$\alpha_i = \frac{\frac{W_i}{K_i}}{\sum_{i=1}^{n} \frac{W_i}{K_i}} \quad (5)$$

where W_i is the clustering weight of the ith heavy metal, n is the number of heavy metals studied, x_i is the calculated concentration of the ith heavy metal in the soil sample, S_i is the mean value of the ith heavy metal in the evaluation criteria, and K_i is the biological toxicity index of the ith heavy metal. The weighted values of each soil sample were calculated to obtain the corresponding weight value matrix α_i.

2.4.3 Clustering coefficient and pollution degree

The clustering coefficients were calculated using the gray whitening functions and clustering weights, and these reflect the relationships between the clustering samples and gray classifications. The formula for calculation is as follows:

$$\delta_j = \sum_{i=1}^{n} R_{ij}\alpha_i \quad j = 1, 2, 3 \quad (6)$$

The value of δ determines the classification of the clustering sample site based on the clustering coefficient, where R_{ij} is the gray whitening function, and α_i is the weight of the ith indicator in the comprehensive clustering. The clustering sample site belongs to the classification with the maximum clustering coefficient.

2.5 Statistical analysis

Statistical analyses were conducted using Microsoft Excel 2003, SPSS 13.0 for Windows, and Origin 6.1 software.

3 Results and analyses

3.1 Characteristics of heavy metals under different land uses

The levels of heavy metals observed in the soil profiles from each land use are presented in Figure 2 and Table 3. The profile characteristics of these heavy metals clearly vary significantly among different land uses. As shown in Figure 2, the concentrations of Pb in the soil samples ranged from 2.99 to 84.44 mg kg^{-1}, with a mean value of 38.73 mg kg^{-1}. The concentrations of Cd in the soil samples ranged from 0.03 to

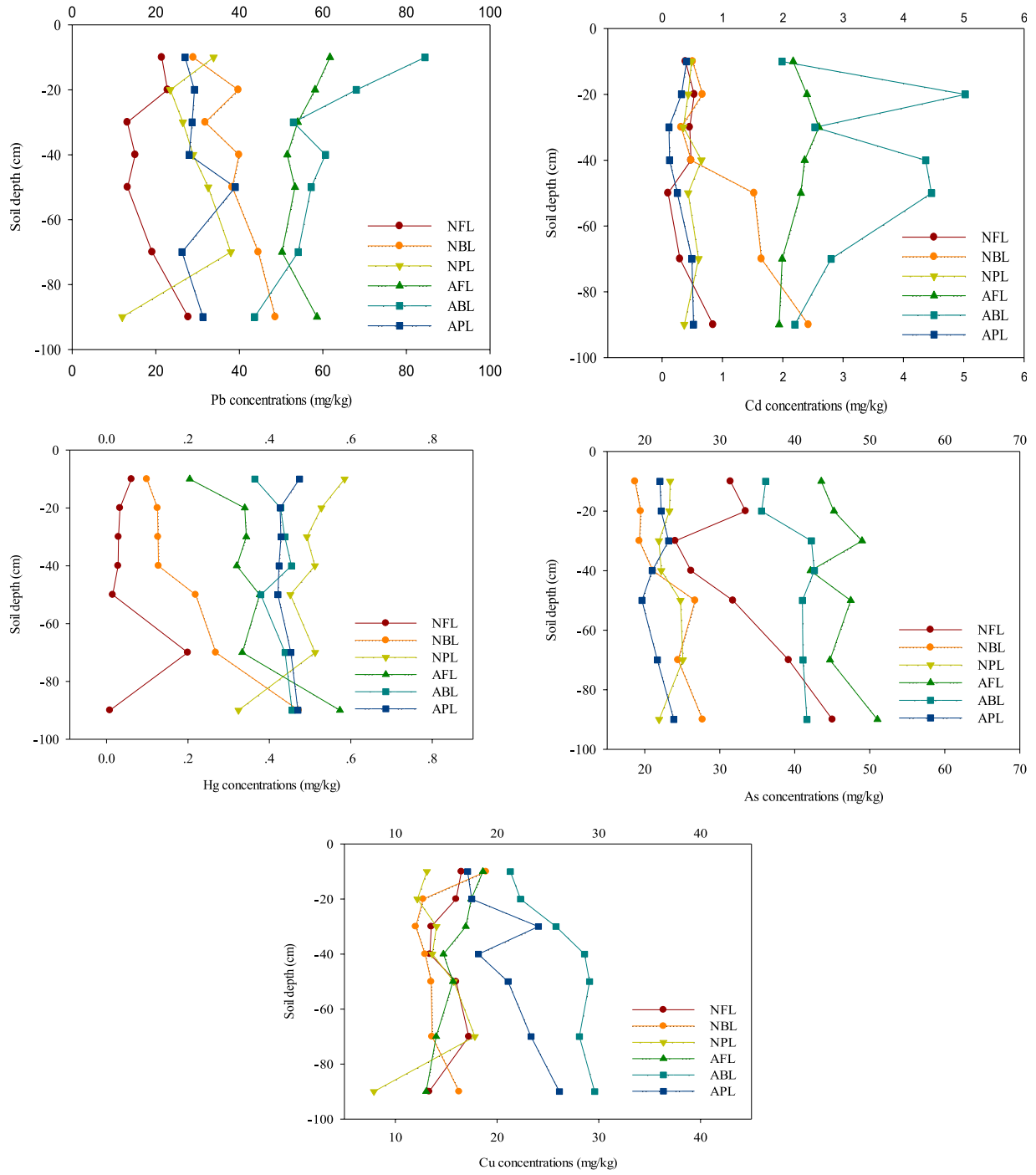

FIGURE 2
Soil profile characteristics of Pb, Cd, Hg, As, and Cu under different types of land use.

10.75 mg kg^{-1}, with a mean value of 1.33 mg kg^{-1}. The concentrations of Hg in the soil samples for different studied land uses ranged from ND (not detected given a detection limit of 0.005 mg kg^{-1}) to 0.71 mg kg^{-1}, with a mean value of 0.35 mg kg^{-1}. The As concentrations in the soil samples from the NFLs showed a similar distribution as that of Pb for this type of land use; the mean concentration decreased from 31.42 mg kg^{-1} in the top 10 cm of the surface soil to 24.07 mg kg^{-1} in soil samples at 20–30 cm depth after a small increase (33.44 mg kg^{-1} in soil samples at 10–20 cm depth) and then increased gradually to 45.03 mg kg^{-1}. In the soil samples from the NBLs, the As concentrations increased generally with depth, except for a weak decrease at a soil depth of 50–70 cm. For the NFLs and NPLs, the mean concentrations of As fluctuated irregularly, similar to those of Pb, with increase in soil depth. For the ABLs, AFLs, APLs, and NPLs, no obvious patterns of variation were found with changes in the soil depth. The concentrations of Cu in the soil samples ranged from 7.90 to 29.60 mg kg^{-1}, with a mean value of 18.94 mg kg^{-1}.

TABLE 3 Statistical analysis of the heavy metals under different types of land use (mg·kg^{-1}).

Metals	Land use	0–10	10–20	20–30	30–40	40–50	50–70	70–90
		cm						
Pb	NFL	21.43 ± 4.94Ab	22.82 ± 3.27Ab	13.19 ± 7.77Aa	15.06 ± 5.35Aa	13.23 ± 3.94Aa	19.13 ± 2.63Ab	27.75Bc
	NBL	28.97 ± 5.43Ba	39.75 ± 6.18Bb	31.84 ± 4.67Ca	39.92 ± 7.05Cb	38.30 ± 7.95BCb	44.55 ± 7.31Cbc	48.61 ± 13.17Cc
	NPL	33.83 ± 11.02Bc	23.46 ± 9.23Ab	26.48 ± 3.53Bb	28.92 ± 3.88Bbc	32.55 ± 5.62Bc	37.94 ± 3.77Cc	11.97Aa
	AFL	61.71 ± 3.48Cb	58.12 ± 5.82Cb	54.00 ± 3.61Da	51.48 ± 4.54Da	53.34 ± 6.69Da	50.25 ± 6.30Da	58.59 ± 9.91Db
	ABL	73.21 ± 6.60Dd	59.35 ± 4.40Cc	61.99 ± 7.74Ec	61.74 ± 3.45Ec	51.07 ± 8.57Db	57.97 ± 3.56Ec	44.96 ± 1.43Ca
	APL	27.00 ± 5.80Ba	29.23 ± 7.70Aa	28.68 ± 3.09BCa	27.98 ± 4.57Ba	39.00 ± 4.21Cb	26.26 ± 6.93Ba	31.28 ± 5.53Ba
Cd	NFL	0.39 ± 0.14Ab	0.39 ± 0.05Ab	0.53 ± 0.21Bc	0.46 ± 0.18Cbc	0.48 ± 0.02Bbc	0.10 ± 0.15Aa	0.30Ab
	NBL	0.51 ± 0.14Abc	0.51 ± 0.23Abc	0.67 ± 0.04Cc	0.32 ± 0.06Ba	0.48 ± 0.07Bb	1.53 ± 0.19Cd	1.65 ± 1.01Bd
	NPL	0.49 ± 0.17Aa	0.49 ± 0.16Aa	0.43 ± 0.09Ba	0.35 ± 0.20BCa	0.65 ± 0.07Cb	0.43 ± 0.14Ba	0.60Ab
	AFL	2.17 ± 0.08Bab	2.17 ± 0.20Bab	2.40 ± 0.39Dbc	2.60 ± 0.27Dc	2.36 ± 0.19Db	2.30 ± 0.14Db	1.99 ± 0.21Ba
	ABL	1.99 ± 0.10Ba	1.99 ± 2.86Ba	5.03 ± 0.38Ed	2.53 ± 0.26Db	4.37 ± 0.43Ec	4.47 ± 0.58Ec	2.80 ± 0.01Cc
	APL	0.40 ± 0.14Abc	0.40 ± 0.14Abc	0.32 ± 0.06Abc	0.11 ± 0.03Aa	0.12 ± 0.02Aa	0.25 ± 0.24Ab	0.49 ± 0.24Ac
Hg	NFL	0.06 ± 0.05Ad	0.03 ± 0.02Ac	0.03 ± 0.03Ac	0.03 ± 0.11Abc	0.02 ± 0.01Abc	0.20 ± 0.14Aab	0.01Aa
	NBL	0.10 ± 0.05Aa	0.12 ± 0.07Ba	0.13 ± 0.09Ba	0.13 ± 0.01Ba	0.22 ± 0.17Bb	0.27 ± 0.16AAb	0.47C ± 0.22c
	NPL	0.59 ± 0.04 Eb	0.53 ± 0.06 Eb	0.49 ± 0.09 Eb	0.51 ± 0.07 Eb	0.45 ± 0.03Db	0.51 ± 0.11Db	0.32Ba
	AFL	0.20 ± 0.01Ba	0.34 ± 0.07Cb	0.34 ± 0.07Cb	0.32 ± 0.03Cb	0.38 ± 0.05Cb	0.33 ± 0.09Bb	0.57D±0.00c
	ABL	0.36 ± 0.03Ca	0.43 ± 0.03Db	0.44 ± 0.04Db	0.45 ± 0.02DEb	0.38 ± 0.04Ca	0.44 ± 0.05Cb	0.46C ± 0.01b
	APL	0.47 ± 0.04Da	0.43 ± 0.07Da	0.43 ± 0.04Da	0.42 ± 0.11Da	0.42 ± 0.10Ca	0.45 ± 0.09Ca	0.47C ± 0.05a
As	NFL	31.42 ± 2.95Cb	33.44 ± 0.87Cb	24.07 ± 1.70Ca	26.18 ± 2.40Ba	31.76 ± 1.88Cb	39.18 ± 3.48Cc	45.03Cd
	NBL	18.70 ± 1.81Aa	19.45 ± 1.96Aa	19.29 ± 1.31Aa	21.07 ± 2.85Aa	26.72 ± 5.31Bb	24.44 ± 5.94Bab	27.70 ± 2.15Bb
	NPL	23.39 ± 1.46Ba	23.29 ± 1.50Ba	21.89 ± 1.31Ba	22.20 ± 0.63Aa	24.76 ± 1.11Bab	25.07 ± 0.99Bb	21.91Aa
	AFL	43.54 ± 3.38Ea	45.23 ± 2.73Da	48.97 ± 5.78Dab	42.11 ± 3.90Ca	47.46 ± 5.51Eab	44.70 ± 5.76Ca	51.02 ± 3.66Db
	ABL	36.12 ± 2.08Da	35.57 ± 3.01Ca	42.23 ± 7.22Db	42.62 ± 3.41Cb	41.02 ± 4.07Db	41.11 ± 4.67Cb	41.63 ± 4.58Cb
	APL	22.03 ± 1.02Bb	22.20 ± 1.90Bb	23.18 ± 2.16Cb	20.99 ± 1.76Aa	19.62 ± 2.46Aa	21.67 ± 1.87Aab	23.87 ± 0.44Ab
Cu	NFL	16.50 ± 2.61Bbc	15.97 ± 2.00Bb	13.53 ± 1.45Aa	13.40 ± 1.56Aa	15.97 ± 0.55Ab	17.22 ± 0.99Bc	13.32Ba
	NBL	18.90 ± 7.00Bb	12.73 ± 0.22Aa	12.00 ± 0.85Aa	12.92 ± 1.30Aa	13.52 ± 2.86Aa	13.61 ± 1.84Aa	16.26 ± 3.75Bb
	NPL	13.10 ± 3.50Ab	12.17 ± 2.30Ab	14.05 ± 3.64Ab	13.63 ± 4.80Ab	15.75 ± 4.51Ac	17.81 ± 5.94Bc	7.90Aa
	AFL	18.60 ± 2.96Bc	17.46 ± 1.86Cbc	16.92 ± 2.30Bb	14.72 ± 1.84Aa	15.66 ± 1.62Aab	14.01 ± 3.14Aa	13.03 ± 2.49Ba
	ABL	21.30 ± 2.19Ca	22.30 ± 1.94Da	25.80 ± 4.13Cb	28.60 ± 2.99Cc	29.10 ± 3.47Cc	28.10 ± 6.46Dc	29.60 ± 6.40Cc
	APL	17.10 ± 2.17Ba	17.50 ± 2.89Ca	24.07 ± 2.58Cb	18.15 ± 5.25Ba	21.07 ± 4.46Bb	23.34 ± 5.64Cb	26.13 ± 4.29Cb

In each row, values followed by the same lowercase letters (a–d) are not significantly different ($p < 0.05$) among the soil horizons for the same type of land use; in each column, values followed by the same uppercase letters (A–D) are not significantly different ($p < 0.05$) among the same soil horizon under different types of land use.

Overall, there were no regularity or significant distributions of all heavy metals from the surface to subsoil layers, and the distribution trends of each of the heavy elements in the same soil layer varied for different land uses (Table 3). The average values of Pb for different land uses decreased in the order of ABL > AFL > NBL > APL > NPL > NFL, among which the values for ABL and AFL were significant higher than the others. The distribution characteristics of Cd were in the order of ABL > AFL > NBL > NPL > NFL > APL, where the values in ABL and AFL were distinctly higher than in other land uses. There were minimal differences in the Cd content in NFL, NBL, NPL, and APL in the soil layers of depths 0–50 cm. The distribution of Hg decreased in the order of NPL > APL > ABL > AFL > NBL > NFL, and the discrepancies in the Hg values in each of the soil layers among the different land uses were large. The distribution of As decreased in the order of AFL > ABL > NFL > NPL > NBL > APL, among which the values in AFL

and ABL were significantly higher than those in the NPL, NBL, and APL. The average values of Cu for different land use cased decreased in the order of ABL > APL > AFL > NFL > NBL > NPL, with only slight differences in soil layers at depths of 0–30 cm. However, there were large differences in Cu values in soil layers at depths of 30–90 cm. In summary, each of the heavy metals were present at higher concentrations in the artificial land use cases than under natural land use; this implies that human interference maybe an important factor in heavy metal pollution.

3.2 Heavy metal contamination under different land uses

According to the Environmental Quality of Soil Standards of China, the limits for the studied heavy metals are listed in Table 2 (Fan et al., 2016). There are three limiting values for each element based on soil acidity. In the present study, all soil samples had pH values less than 7.5. Therefore, two groups of the class II limit values were applied.

In the soil samples from the NFLs, all concentrations of Pb and Hg met the limits under class I. About 36% of the Cd concentrations met the limits under class I, 31.58% met the limits under class II, and the rest met the limits under class III. All of the Hg concentrations in the 0–40 cm depth range were very low and met the limits under class I. However, the Hg concentrations at depths greater than 40 cm exceeded 0.15 mg kg^{-1} and sometimes exceeded 0.30 mg kg^{-1}. All of the As concentrations exceeded the limits under class I but were within the limits of class II, except the soil samples collected at depths of 40–90 cm, whose concentrations exceeded 25 mg kg^{-1}. All concentrations of Cu met the limits under class I.

In the soil samples from NBLs, about 36.84% of the Pb concentrations met the limits under class I, and the rest were within the limits of class II. In both NPLs and APLs, most of the Pb concentrations were below 35 mg kg^{-1}. It is worth noting that all concentrations of Hg exceeding 0.30 mg kg^{-1} (with some sample concentrations greater than 0.5 mg kg^{-1}) were beyond the limits of class II. In the AFLs, all of the Pb concentrations exceeded the limits under class I, and all of the As concentrations exceeded the limits under class II. Most of the Hg concentrations exceed the limits under class II. In the soils from both AFLs and ABLs, all Cd concentrations exceeded 1.00 mg kg^{-1}, which was beyond the limits of class III.

3.3 Clustering analysis of heavy metal pollution in soils under different land uses

According to the Equations 1–6, the heavy metals clustering weights under the different land use types was calculated. This results shown in Figure 3, Pb and Cu contributed little to the heavy metal concentrations under all kinds of land use based on the clustering weights. In the NBLs, AFLs, and ABLs, the clustering weights of Cd were greater than 50% of the total. In the NFLs and NPLs, the clustering weights of Cd were still greater than those of the other heavy metals. However, the clustering weights of Hg were largest among all the heavy metals studied in the APLs. Generally, the clustering weights of Hg in the pasture lands were greater than those in the brush lands, followed by forestlands. It was also found that the clustering weights of As accounted for a considerable portion of the heavy metal concentrations under all types of land use in this study and especially in the NFLs. The pollution degree of each sampling site is listed in Table 4. The soils from the NFLs, NPLs, and APLs belonged to class II, while those from NPL-3 belonged to class I. The soils from the NBLs, AFLs, and ABLs belonged to class III.

4 Discussion

4.1 Sources of heavy metals in the study area

The environmental fates of pollutants are determined by many factors. However, the physicochemical properties, geochemical baselines, anthropic activities, and microcircumstances are critical for determining the pollution levels and environmental behaviors of heavy metals (Teng et al., 2022). Based on field investigations and heavy metal distribution characteristics under different land uses, we hypothesized that the heavy metals in soils under different land uses would have different pollution sources. The baseline values (soil formation), application of fertilizers, and atmospheric deposition were considered as the critical sources in study area since there were no local mining or refining industries that would cause significant heavy metal pollution. Based on the Pearson correlation analysis, there were significant correlations between Pb and TK, Cd and TP, as well as As and TN; however, there were no significant correlations among Cu, Hg, and the soil nutrient elements (Table 5).

The Cu concentrations were very low in all soil samples; however, in the deeper layers, Cu concentrations in soils from APLs and ABLs were obviously higher than those from the other samples under study. In addition, the background value of Cu in the karst mountain area has been reported to be high (Wang et al., 2021). This finding indicates that Cu pollution is mainly from soil formation. The ABLs and AFLs were developed for growing different types of fruits; to promote good production, the land owners were reported to have applied different fertilizers that could cause heavy metal pollution. Previous studies have suggested that Cd, Pb, and As concentrations are higher in cultivated soils owing to fertilizer application (Atafar et al., 2010; Wang et al., 2012); these results indicate that fertilizer application is an important source of heavy metal pollution (Cd, Pb, and As) in ABLs and AFLs. According to the information listed in Tables 2, 3 and the GB15618-2018 standards, there were some samples in which the Hg contents were higher than the limiting value for paddy lands but lower than those for other land types. The production of Hg in Guizhou is known globally. Hg pollution in Guizhou Province has been a severe problem for a long time (Feng et al., 2008; Streets et al., 2005). It is well known that karst landforms have unique water ecological systems with dual above ground and underground structures; moreover, the underground water system is highly developed. Xu et al. (2020) noted that there was a significant positive correlation between Cd and Hg levels in underground water in karst mountain areas. In addition, the Cd content is relatively stable in the underground water in karst areas related to mining areas (Liao et al., 2023). Although there were no Hg mining or refining industries in the studied region, the groundwater

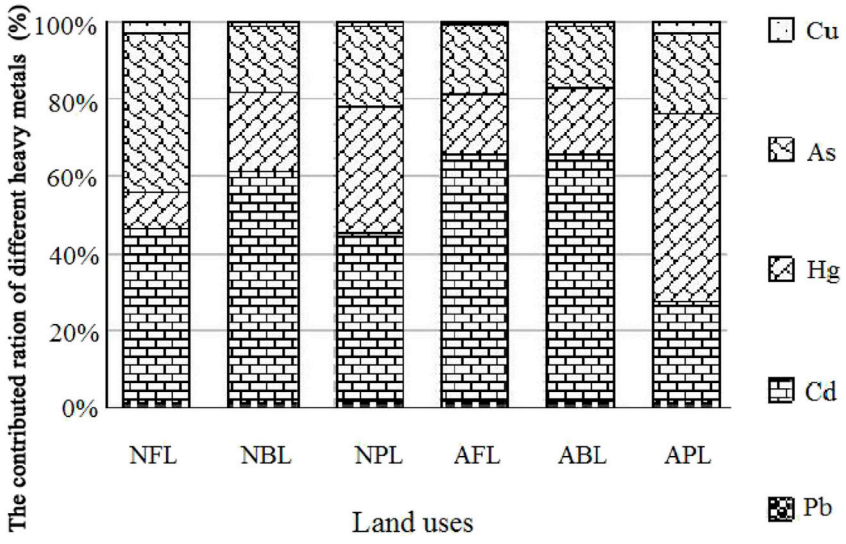

FIGURE 3
Heavy metal clustering weights under the different types of land use.

TABLE 4 Clustering coefficients for the different sampling sites.

Sampling sites	Class I	Class II	Class III	Clustering results
NFL-1	0.34	0.52	0.13	Class II
NFL-2	0.11	0.76	0.13	Class II
NFL-3	0.07	0.61	0.32	Class II
NBL-1	0.16	0.21	0.63	Class III
NBL-2	0.37	0.40	0.23	Class III
NBL-3	0.23	0.18	0.59	Class III
NPL-1	0.09	0.75	0.16	Class II
NPL-2	0.25	0.51	0.24	Class II
NPL-3	0.24	0.43	0.32	Class II
AFL-1	0.09	0.04	0.87	Class III
AFL-2	0.09	0.07	0.84	Class III
AFL-3	0.15	0.21	0.64	Class III
ABL-1	0.07	0.19	0.75	Class III
ABL-2	0.12	0.12	0.76	Class III
ABL-3	0.07	0.14	0.79	Class III
APL-1	0.29	0.67	0.03	Class II
APL-2	0.14	0.77	0.08	Class II
APL-3	0.54	0.46	0.00	Class I

could also be an important factor in the presence of heavy metals. Guo et al. (2024) showed that atmospheric deposition contributes to accumulation of heavy metals in soil. These results indicate that Hg pollution in this area may be caused by the underground water and atmospheric deposition (Feng et al., 2008).

4.2 Effects of land use changes on soil heavy metal pollution

Land use change is a significant factor affecting the sources and environmental behaviors of heavy metals. Atafar et al. (2010)

TABLE 5 Pearson correlation analysis results of the soil physicochemical properties.

	Pb	Cd	Hg	As	Cu	TP	TN
Cd	0.512	1					
Hg	0.361	0.177[b]	1				
As	0.519	0.441	−0.041	1			
Cu	0.425	0.427	0.156	0.268	1		
TP	0.515	0.741[b]	0.126	0.357	0.226[b]	1	
TN	0.263	0.487	0.057	0.389[b]	0.363	0.434[b]	1
TK	0.190[b]	−0.131	−0.212	0.133	0.159	0.377[a]	0.251[b]

[a]Correlation is significant at the 0.01 level.
[b]Correlation is significant at the 0.05 level.

reported that fertilizer application resulted in significantly higher concentrations of Cd, Pb, and As in cultivated soils (p-value <0.05). The clustering analysis results indicate that heavy metal pollution in the AFLs, ABLs, and NBLs are significantly higher than in other types of land use.

The Cd concentrations in the soil samples from the AFLs and ABLs were obviously higher than those from other types of land use in this study. This suggests that fertilizer application increased the concentrations of Cd, Pb, Cu, and As in the cultivated soils. The concentrations of Hg in the soil samples from NPLs were generally higher than those from the other types of land use. As these lands share the same soil formation processes and similar geochemical baselines, we believe that pollution caused by fertilizer application was the main reason for the increased Hg concentrations in soils from ABLs, which were higher than those from NBLs.

The results of this study show that there is a strong correlation between the soil Hg concentration and application of manure or compost. In forestlands, large tree canopies reduce Hg pollution caused by atmospheric deposition, which may be the main reason why Hg concentrations in the soil samples from NFLs were much lower than those from NBLs, APLs, and NPLs. Furthermore, Hg concentrations in soil samples from NBLs were slightly higher than those from APLs. We inferred that these were possibly the effects of management activities. The local farmers spread grass seeds to increase the grass quantity, and high levels of grazing also promote grass growth rates. Therefore, Hg concentrations in soils from APLs were generally lower than those in NPLs. This may be due to the fact that artificial grass planting has a certain alleviating effect on Hg pollution (Pacyna and Pacyna, 2001).

5 Conclusion

There were large variations in the concentrations of five types of heavy metals for different types of land use, and these concentrations were generally higher in artificial land uses than natural land use modes. NFLs can suppress Pb and Cu pollution to a certain degree, and the Cd and As levels in APLs are generally low. The lowest Cu concentrations were found in soils from NPLs. Exogenous introduction is an important method of heavy metal pollution, and land use change is a common practice in land resource management. Many positive and negative effects may arise during the process of land use change. In the study region, the soils were polluted by As and Cd to some extent, and fertilizer application was the main contributor in these two cases. Hg pollution is a serious issue in Guizhou Province, where soil concentrations often reach up to 0.59 mg kg^{-1} in NPLs, 0.47 mg kg^{-1} in APLs, 0.20 mg kg^{-1} in AFLs, and 0.36 mg kg^{-1} in ABLs. However, trees and brush plants play important roles in protecting soil from contamination by Hg through atmospheric deposition. Thus, changing both NPLs and APLs to forestlands could benefit the local ecosystems as these reduce Hg contamination. In addition, pastoral cultivation is a feasible method of alleviating soil Cd pollution. In the process of cultivating forestlands and brush lands, special attention should be devoted to Cd pollution of the soil.

Data availability statement

The original contributions presented in this study are included in the article/supplementary material, and any further inquiries may be directed to the corresponding author.

Author contributions

XJ: Conceptualization, Data curation, Formal analysis, Investigation, Methodology, Software, Writing–original draft. XW: Conceptualization, Data curation, Formal analysis, Funding acquisition, Investigation, Methodology, Project administration, Resources, Software, Supervision, Validation, Visualization, Writing–original draft, Writing–review and editing. YL: Investigation, Software, Writing–review and editing. YH: Investigation, Software, Writing–review and editing. XH: Conceptualization, Formal analysis, Funding acquisition, Investigation, Methodology, Project administration, Supervision, Writing–review and editing.

Funding

The authors declare that financial support was received for the research, authorship, and/or publication of this article. This research was funded by Guizhou Provincial Science and Technology Projects (nos. QKHZC[2023]YB215 and QKHZC[2023]YB141), Doctoral Research Fund of Guiyang Healthcare Vocational University (no. K2023-8), Department of Science and Technology of Guizhou Province (nos. LH[2017]7371, [2019]1217, [2016]2595-2, and [2019]2840), Department of Forestry of Guizhou Province (no. QLKH[2017]17), and Department of Education of Guizhou Province (no. KY[2021]302).

Conflict of interest

The authors declare that the research was conducted in the absence of any commercial or financial relationships that could be construed as a potential conflict of interest.

Publisher's note

References

Ahmed, M. K., Habibullah-Al-Mamun, M., Parvin, E., Akter, M. S., and Khan, M. S. (2013). Arsenic induced toxicity and histopathological changes in gill and liver tissue of freshwater fish, tilapia (*Oreochromis mossambicus*). *Exp. Toxicol. Pathology* 65, 903–909. doi:10.1016/j.etp.2013.01.003

Atafar, Z., Mesdaghinia, A., Nouri, J., Homaee, M., Yunesian, M., Ahmadimoghaddam, M., et al. (2010). Effect of fertilizer application on soil heavy metal concentration. *Environ. Monit. Assess.* 160, 83–89. doi:10.1007/s10661-008-0659-x

Chen, L. S., Xiong, K. N., Chen, Q. W., Shu, T., and Wu, J. (2022). Response mechanism of soil conservation function to rocky desertification under eco-environmental harness of karst areas. *Resour. Environ. Yangtze Basin* 29, 499–510. Available at: https://xueshu.baidu.com/usercenter/paper/show?paperid=1a3g0e602f4s0vu0qa6a00k087435300&sc_from=pingtai4&cmd=paper_forward&wise=0

Clarkson, T. W., Magos, L., and Myers, G. J. (2003). Human exposure to mercury: the three modern dilemmas. *J. Trace Elem. Exp. Med.* 16, 321–343. doi:10.1002/jtra.10050

Fan, L., Chen, F., and Fan, Y. (2012). Comprehensive assessment of soil environmental quality with improved grey clustering method: a case study of soil heavy metals pollution. *J. Agric. Sci. Appl.* 1, 67–73. doi:10.14511/jasa.2012.010302

Fan, M. Y., Yang, H., Huang, X. F., Cao, R. S., Zhang, Z. D., Hu, J. W., et al. (2016). Chemical forms and risk assessment of heavy metals in soils around a typical coal-fired power plant located in the mountainous area. *China Environ. Sci.* 36, 2425–2436. doi:10.3969/j.issn.1000-6923.2016.08.024

Feng, X. B., Li, P., Qiu, G. L., Wang, S. F., Li, G. H., Shang, L. H., et al. (2008). Human exposure to methylmercury through rice intake in mercury mining areas, Guizhou Province, China. *Environ. Sci. and Technol.* 42, 326–332. doi:10.1021/es071948x

Geest, H. G. V., Greve, G. D., Boivin, M. E., Kraak, M. H. S., and van Gestel, C. A. M. (2000). Mixture toxicity of copper and diazinon to larvae of the mayfly (ephoron virgo) judging additivity at different effect levels. *Environ. Toxicol. Chem.* 19, 2900–2905. doi:10.1002/etc.5620191208

Guo, B., Yang, G. F., and Liu, Q. (2024). Effect of atmospheric dry and wet deposition on heavy metal content in farmland in the Nanjing section of the Yangtze Rive. *J. Geol.* 48 (1), 85–91. Available at: https://kns.cnki.net/knavi/journals/JSDZ/detail?uniplatform=NZKPT.

Haddou, N., Ghezzar, M. R., Abdelmalek, F., Ognier, S., Martel, M., and Addou, A. (2014). Plasmacatalytic removal of lead acetate assisted by precipitation. *Chemosphere* 107, 304–310. doi:10.1016/j.chemosphere.2013.12.071

Huang, X. F., Hu, J. W., Qin, F. X., Quan, W. X., Cao, R. S., Fan, M. Y., et al. (2017). Heavy metal pollution and ecological assessment around the jinsha coal-fired power plant (China). *Int. J. Environ. Res. Public Health* 14, 1589. doi:10.3390/ijerph14121589

Huang, X. F., Zhou, Y. C., and Zhang, Z. M. (2018). Carbon sequestration anticipation response to land use change in a mountainous karst basin in China. Journal of Environmental Management. *J. Environ. Manage.* 228, 40–46. doi:10.1016/j.jenvman.2018.09.017

Jin, Z. G., and Zhou, M. Z. (2012). An assessment on contamination and potential ecological risk of cadmium and arsenic in the cultivated soils around the Ni-Mo mining area in Songli, Zunyi, China. *J. Agro-Environment Sci.* 31, 2367–2373. doi:10.1007/s11783-011-0280-z

Liao, H. W., Jiang, Z. C., Zhou, H., Qin, X. Q., Huang, Q. B., and Wu, H. Y. (2023). Heavy metal pollution and health risk assessment in karst basin around a lead-zinc mine. *Environ. Sci.* 44 (11), 6085–6094. doi:10.13227/j.hjkx.202210335

Ma, L., Zhang, L., Zhang, S., Zhou, M., Huang, W., Zou, X., et al. (2024). Soil protists are more resilient to the combined effect of microplastics and heavy metals than bacterial communities. *Sci. total Environ.* 906 (Jan.1), 167645. doi:10.1016/j.scitotenv.2023.167645

Milner, M. J., and Kochian, V. (2008). Investigating heavy-metal hyperaccumulation using Thlaspi caerulescens as a model system. *Ann. Bot.* 102, 3–13. doi:10.1093/aob/mcn063

Olawotin, R., Oyewole, S. A., and Grayson, R. L. (2012). Potential risk effect from elevated levels of soil heavy metals on human health in the Niger delta. *Ecotoxicol. Environ. Saf.* 85, 120–130. doi:10.1016/j.ecoenv.2012.08.004

Pacyna, J. M., and Pacyna, E. G. (2001). An assessment of global and regional emissions of trace metals to the atmosphere from anthropogenic sources worldwide. *Environ. Rev.* 9, 269–298. doi:10.1139/a01-012

Pan, A., Hu, L. H., Li, T. S., and Li, C. Z. (2009). Assessing the eutrophication of Shengzhong reservoir based on grey clustering method. Chinese Journal of Population. *Resour. Environ.* 7, 83–87. doi:10.1080/10042857.2009.10684929

Rainio, M. J., Eeva, T., Lilley, T., Stauffer, J., and Ruuskanen, S. (2015). Effects of early-life lead exposure on oxidative status and phagocytosis activity in great tits (*Parus major*). *Comp. Biochem. Physiology C-Toxicology and Pharmacol.* 167, 24–34. doi:10.1016/j.cbpc.2014.08.004

Roy, N. M., DeWolf, S., Schutt, A., Wright, A., and Steele, L. (2014). Neural alterations from lead exposure in zebrafish. *Neurotoxicology Teratol.* 46, 40–48. doi:10.1016/j.ntt.2014.08.008

Shakoor, M. B., Ali, S., Farid, M., Farooq, M. A., and Bharwana, S. A. (2013). Heavy metal pollution, a global problem and its remediation by chemically enhanced phytoremediation: a review. *J. Biodivers. Environ. Sci.* 3, 12–20. Available at: https://www.academia.edu/26062642/.

Shukla, L., and Jain, N. (2022). A review on soil heavy metals contamination: effects, sources and remedies. *Appl. Ecol. Environ. Sci.* 10, 15–18. doi:10.1080/15320383.2019.1592108

Streets, D. G., Hao, J. M., Wu, Y., Jiang, J. K., Chan, M., Tian, H. Z., et al. (2005). Anthropogenic mercury emissions in China. *Atmos. Environ.* 39, 7789–7806. doi:10.1016/j.atmosenv.2005.08.029

Teng, Y. G., Ni, S. J., Tuo, X. G., Zhang, C. J., and Ma, Y. X. (2022). Geochemical baseline and trace metal pollution of soil in Panzhihua mining area. *Chin. J. Geochem.* 21, 274–281. doi:10.1007/BF02831093

Tokumoto, M., Kutsukake, N., Yamanishi, E., Katsuta, D., Anan, Y., and Ogra, Y. (2014). Arsenic (+3 oxidation state) methyltransferase is a specific but replaceable factor against arsenic toxicity. *Toxicol. Rep.* 1, 589–595. doi:10.1016/j.toxrep.2014.08.011

Wang, F., Zhao, L., Shen, Y., Meng, H., Xiang, X., Cheng, H., et al. (2012). Analysis of heavy metal contents and source tracing in organic fertilizer from livestock manure in North China. *Trans. Chin. Soc. Agric. Eng.* 29, 202–208. doi:10.3969/j.issn.1002-6819.2013.19.025

Wang, X. F., Cao, R. S., Wu, X. L., Zhang, Z. M., and Huang, X. F. (2021). Study on heavy metals pollution assessment method of soil around a wasted mining in Karst mountain area. *J. Guizhou Normal Univ. Nat. Sci.* 39, 29–35. doi:10.16614/j.gznuj.zrb.2021.05.005

Wang, X. F., Huang, X. F., Hu, J. W., Wu, X. L., and Yao, S. M. (2020). Cadmium pollution and Bioconcentration characteristic in crops around the abandon Ni-Mo mining area in the karst mountainous. *Environ. Chem.* 39, 1872–1882. doi:10.7524/j.issn.0254-6108.2019051301

Wang, X. F., Huang, X. F., Xiong, K. N., Hu, J. W., Zhang, Z. M., and Zhang, J. C. (2022). Mechanism and evolution of soil organic carbon coupling with rocky desertification in south China karst. *Forests* 13, 28. doi:10.3390/f13010028

Wang, Y. Y., Wang, D. Z., Lin, L., and Wang, M. H. (2015). Quantitative proteomic analysis reveals proteins involved in the neurotoxicity of marine medaka Oryzias melastigma chronically exposed to inorganic mercury. *Chemosphere* 119, 1126–1133. doi:10.1016/j.chemosphere.2014.09.053

Wei, M., Pan, A., Ma, R., and Wang, H. (2023). Distribution characteristics, source analysis and health risk assessment of heavy metals in farmland soil in shiquan county, shaanxi province. *Process Saf. Environ. Prot.* 171, 225–237. doi:10.1016/j.psep.2022.12.089

Wen, M., Ma, Z., Bgingerich, D., Zhao, X., and Zhao, D. (2022). Heavy metals in agricultural soil in China: a systematic review and meta-analysis. *Eco-environment and Health* 1, 219–228. doi:10.1016/j.eehl.2022.10.004

Xu, C. X., Yan, H. L., Zhang, S. Q., Lei, L. S., and Hu, B. L. (2020). Heavy metal content and health risk assessment in water of karst cave in libo, Guizhou. *Environ. Sci. and Technol.* 43 (2), 204–212. doi:10.19672/j.cnki.1003-6504.2020.02.030

Yan, B., and Zhang, X. (2021). Current status, causes and harm of soil arsenic pollution. *IOP Conf. Ser. Earth Environ. Sci.* 769, 022034. doi:10.1088/1755-1315/769/2/022034

Zhang, D., Zhou, M. Z., Xiong, K. N., Gu, B. Q., and Yang, H. (2019). Risk assessment of nickel in soils and crops around the Ni-Mo polymetallic mining area in Song-lin, Zunyi, China. *J. Agro-Environment Sci.* 38, 356–365. doi:10.11654/jaes.2018-0746

Zhang, H. Z., Cui, W. G., Huang, Y. M., Li, Y. L., Zhong, X., and Wang, L. (2022a). Evaluation and source analysis of heavy metal pollution of farmland soil around the mining area of karst region of central Guizhou Province. *Acta Sci. Circumstantiae* 42, 412–421. doi:10.13671/j.hjkxxb.2021.0319

Zhang, S. Y., Wu, L. N., Zhang, G. Y., Wang, D., and Wu, P. (2022b). Soil heavy metal pollution analysis and health risk assessment in Karst areas along the upper reaches of the Du Liujiang River. *Acta Sci. Circumstantiae* 42, 421–433. doi:10.13671/j.hjkxxb.2021.0474

Zhu, J. W., Lei, Y. Q., and Yuan, J. (2018). Study on improving the milling precision of rice milling machine and reducing the broken rice rates. *Grain Sci. Technol. Econ.* 43, 4. doi:10.16465/j.gste.cn431252ts.20180319

frontiers | Frontiers in Environmental Science

TYPE Original Research
PUBLISHED 30 October 2024
DOI 10.3389/fenvs.2024.1482766

OPEN ACCESS

EDITED BY
Nnanake-Abasi O. Offiong,
Topfaith University, Nigeria

REVIEWED BY
Fei He,
Korea Institute of Energy Technology, Republic of Korea
Shreya Singh,
Cornell University, United States

*CORRESPONDENCE
Xiaojiao Zhang,
xjzhang@sspu.edu.cn
Yaoguang Guo,
ygguo@sspu.edu.cn

RECEIVED 18 August 2024
ACCEPTED 09 October 2024
PUBLISHED 30 October 2024

CITATION
Zhu X, Sui Y, Li X, Guan J, Zhang X, Zhang G and Guo Y (2024) Bibliometric analysis of photocatalytic oxidation of volatile organic compounds from 1998 to 2023.
Front. Environ. Sci. 12:1482766.
doi: 10.3389/fenvs.2024.1482766

Bibliometric analysis of photocatalytic oxidation of volatile organic compounds from 1998 to 2023

Xinjie Zhu[1], Yifan Sui[1], Xiuli Li[1], Jie Guan[1], Xiaojiao Zhang[1]*, Gangfeng Zhang[2] and Yaoguang Guo[1]*

[1]Shanghai Collaborative Innovation Centre for WEEE Recycling, School of Resources and Environmental Engineering, Shanghai Polytechnic University, Shanghai, China, [2]Shanghai Academy of Environmental Sciences, Shanghai, China

Introduction: Volatile organic compounds (VOCs) have attracted widespread attention due to their adverse effects on human health. Photocatalytic oxidation is an effective technology for degrading VOCs under ambient conditions.

Methods: In order to better understand the trends and development of global trends in photocatalytic oxidation of VOCs, the analysis of 2493 articles or reviews from the Science Citation Index Expanded (SCIE) in the Web of Science Core Collection, covering the period from 1998 to 2023, was conducted using CiteSpace and VOSviewer software.

Results and Discussion: The findings indicate significant growth in papers concerning photocatalytic oxidation of VOCs. China emerges as the most active country among the main drivers. Principal sources publishing relevant research are Applied Catalysis B-Environmental, Chemical Engineering Journal, Journal of Hazardous Materials, and Environmental Science and Technology. A relatively well-established theoretical framework has been developed for the study of photocatalytic oxidation of VOCs. In the field of VOCs photocatalytic oxidation, the focus is on the development and optimization of advanced photocatalysts with efficient charge separation, better adsorption performance, and a wider light response range. In addition, the in-depth study of the charge generation and transfer mechanisms within the photocatalysts, as well as the comprehensive understanding of the reaction kinetics and catalytic oxidation process, the optimization of the reaction conditions, and the improvement of the catalytic efficiency are at the forefront of the research in this field. This research system is advancing and becoming more refined, with its theoretical propositions, research findings, and methodologies increasingly employed and confirmed.

KEYWORDS

volatile organic compounds, photocatalytic oxidation, advanced photocatalysts, software, bibliometric analysis

1 Introduction

Volatile organic compounds (VOCs) are ubiquitous in the atmosphere and are key precursors of ground-level ozone (O_3), secondary organic aerosols (SOA), peroxyacetyl nitrate (PAN), and polycyclic aromatic hydrocarbons (PAHs), affecting the atmospheric environment, human health, and vegetation growth (Ou et al., 2022; Liu et al., 2022a). It is defined as an organic pollutant with a boiling point in the environmental range of 50°C–260°C (ISO, 2011; Sui et al., 2024). VOCs are mainly produced by the chemical, pharmaceutical, and tobacco industries, as well as by fuel combustion, composting, building renovation, and other production and living processes (Halios et al., 2022; Zhang et al., 2022; Emran et al., 2022). The most common volatile organic compounds are benzene, toluene, xylene, and ethylbenzene, collectively known as BTEX. Benzene causes immune cells to produce excessive inflammatory factors, leading to inflammatory responses and damage to the bone marrow and other hematopoietic tissues. Benzene and its metabolites also activate the intrinsic apoptotic pathway within cells, promoting programmed cell death of hematopoietic cells and causing hematotoxicity (Li et al., 2024). In BTEX compounds, the concentration of toluene is the highest. Long-term exposure to toluene in the human body can damage the central nervous system (Filley et al., 2004) and respiratory system (Yoon et al., 2010). Kim et al. coupled ultraviolet light with a Pd/TiO_2 photocatalyst to degrade toluene, with approximately 94.1% of toluene being converted into CO_2 and CO, with most intermediate products being benzaldehyde and formic acid. Common BTEX also includes xylene. During the photocatalytic process of xylene, intermediate compounds such as aromatic hydrocarbons, alkanes, and carbonyl compounds are produced. The health risks of the secondary products generated during the process are at least 4.5 times lower than those of degraded xylene, but the secondary pollution and health risks of xylene photodegradation products cannot be ignored. These isomerization products not only contribute about 97% and 91% to the formation potential of O_3 (OFP) and secondary organic aerosol (SOAFP) but also show obvious non-carcinogenic risks (Chen et al., 2024).

Other common VOC pollutants include ethyl acetate, styrene, and formaldehyde. Ethyl acetate (EA) is a colorless, transparent, fragrant liquid with low toxicity and sweet smell. It has a pungent odor and is highly volatile at high concentrations (Deng et al., 2021). Ethyl acetate is commonly used in the paint, ink, pharmaceutical, and automotive manufacturing industries. Intermediate products formed during the photodegradation of ethyl acetate include acetic acid, ethanol, and formaldehyde, which ultimately degrade into CO_2 and H_2O (Wang et al., 2023). Formaldehyde is the most representative indoor VOC pollutant, with a boiling point of only −19.5°C. As long as the indoor temperature is above −19.5°C, the free formaldehyde generated from decorative materials and furniture will continuously volatilize into the air, with a release period of 3–15 years, and cannot be removed in a short time. The diffusion speed of formaldehyde will be increased in high temperature and high humidity weather conditions, aggravating indoor air pollution. Released formaldehyde enters the body through breathing, dietary intake, or skin contact. Formaldehyde that enters the body is usually converted into a non-toxic chemical substance called formate, which is excreted through urine and exhaled as carbon dioxide. Unreacted formaldehyde will adhere to DNA or proteins in the body (Kim et al., 2011). Formaldehyde can cause neurotoxicity (Songur et al., 2010), respiratory system damage, and reproductive and genetic toxicity (Jakab et al., 2010). Formaldehyde also has carcinogenicity, and the International Agency for Research on Cancer (IARC) classifies formaldehyde as a human carcinogen that can cause nasopharyngeal cancer. Styrene is commonly used in automotive and motorcycle maintenance and repair services, the manufacture of other chemical products, ship and boat manufacturing, basic chemical manufacturing, and the manufacture of plastic products (Hahm et al., 2016); long-term exposure to styrene can cause serious health problems. Styrene has ear toxicity and may cause hearing loss, which may increase the likelihood of ear toxicity in combination with exposure to multiple chemicals and noise (Chen et al., 2009). Styrene also has lung function impairment effects, with studies showing that the average level of serum cytochrome c in styrene-exposed workers was 1.1 ng/mL (0.89–1.89), while the control group had levels below the detection limit (0.05 ng/mL), indicating that workers exposed to styrene have increased oxidative stress levels, which should be the cause of lung injury (Sati et al., 2011). Multiple reports have also verified the cancer-inducing risk of styrene exposure. In the photocatalytic degradation process, styrene is converted into intermediate products such as benzene, benzaldehyde, and benzoic acid, thereby reducing health risks (Hamada et al., 2022). The common VOCs in human production and life and their main sources and hazards are shown in Table 1. In recent years, adsorption, thermal oxidation, and photocatalytic oxidation have been researched and developed for the effective and rapid removal of VOCs (Rong et al., 2023; Sun et al., 2019; Song et al., 2020; Qian et al., 2021; Enesca, 2020; Le et al., 2021).

Photocatalysts are typically triggered through the absorption of light, leading to the excitation of electrons from the occupied valence band (VB) to the unoccupied conduction band (CB), resulting in the generation of positive holes within the VB. The resultant electrons and positive holes serve as pivotal agents in driving the reduction and oxidation processes of molecules adsorbed onto the surface of the photocatalyst, respectively (Ohtani, 2008; Carp et al., 2004; Pelaez et al., 2012; Montini et al., 2016). These active electrons and holes will interact with oxygen to generate reactive oxygen species, such as hydroxyl radicals (·OH) and superoxide radicals ($\cdot O_2^-$). The VOC pollutant molecules will come into contact with the generated reactive species and decompose into lower molecular weight products, ultimately into CO_2, H_2O, and other by-products (Mamaghani et al., 2017; Shayegan et al., 2018), as shown in Figure 1. Notable features of this technology include operation at ambient temperature without significant energy input, environmental friendly end products (CO_2 and H_2O), and applicability to different types of pollutants (water and microplastics) (Mamaghani et al., 2017; Zhong et al., 2010; Ollis, 2000; Zhang et al., 2022; Moura et al., 2022). Taken together, the treatment of VOC pollution by photocatalytic technology has a broad and long-term impact on the management of the atmospheric environment, and the development and research trends in this field of study have a bearing on human safety and global environmental

TABLE 1 Common VOCs and their main sources and hazards.

Name	Chemical formula	Main sources	Potential health effects
Benzene (Rinsky, 1989)	C_6H_6	Vehicle exhaust, tobacco smoke, and paints	Cancer and central nervous system damage
Toluene (Rudel et al., 2003)	C_7H_8	Paints, adhesives, and fuels	Respiratory irritation and nervous system damage
Xylene (Chen et al., 2024)	C_8H_{10} (various isomers)	Paints, dyes, and fuel additives	Eye and skin irritation, and nervous system damage
1,2,4-Trimethylbenzene (Korsak et al., 1995)	C_9H_{12}	Paints, adhesives, and plastics	Eye and skin irritation, and respiratory problems
Formaldehyde (Wang et al., 2024)	CH_2O	Building materials, furniture, and tobacco smoke	Eye and respiratory irritation, and cancer
Ethyl acetate (Li et al., 2023a)	$C_4H_8O_2$	Paints, glues, and fragrances	Eye and respiratory irritation, and nervous system damage
Ethylene (Gaffney et al., 2012)	C_2H_4	Plastics manufacturing, and synthetic fibers	Respiratory problems, potentially carcinogenic
Ethylbenzene (Kamani et al., 2023)	C_8H_{10}	Plastics, paints, and synthetic rubber	Eye and skin irritation, and respiratory tract irritation
Propene (Cano-Casanova et al., 2021)	C_3H_6	Petrochemicals and foundry processes	Respiratory tract irritation, and headache
Styrene (Li et al., 2022a)	C_8H_8	Plastics manufacturing and synthetic rubber	Nervous system damage and respiratory problems

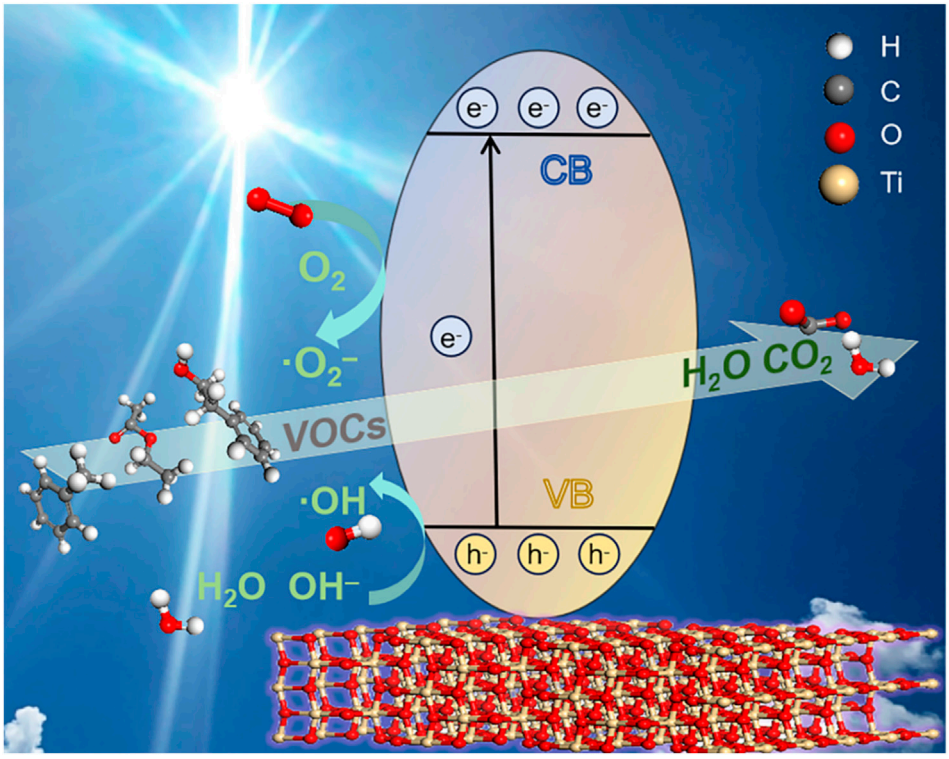

FIGURE 1
Scheme of illustration for photocatalytic oxidation of VOCs.

sustainability. Therefore, it is crucial to analyze the current status of this field. Mathematics and statistics are the main methods used in bibliometrics to analyze literature data, using knowledge mapping as an analytical tool to show the visual results of scientific knowledge and its relationship with each other more intuitively, quantitatively, and objectively, which is widely used in the field of scientometrics (Ni et al., 2022). The bibliometric analysis of VOC photocatalytic oxidation research is to use knowledge mapping as an analytical tool to study the trend of VOC photocatalytic oxidation research, the knowledge base, the hot frontiers, and their dynamic evolution relationship.

In this study, scientific knowledge mapping and comprehensive analysis of relevant literature information within the scope, including publication trends, source journals, authors'

TABLE 2 Article selection conditions and output results.

Filter condition		Language	Document type	Time interval	
		English	Article and review	1998.01.01–2023.12.01	
Result	Paper	Country	Institution	Journal	Author
	2,493	211	5,012	442	9,213

contributions and collaborations, keywords, research frontiers, and hotspots, were conducted with the help of software such as VOSviewer and CiteSpace. The analytical work identified and tracked research frontiers and hotspots in the field, captured the dynamic evolution of research topics and scientific priorities in the field, and highlighted established and emerging research directions. In addition, the analytical work contributes to a deeper understanding of the knowledge structure and developmental trajectory of the field and provides an intuitive scientific basis for subsequent research on photocatalytic oxidation of VOCs.

2 Data and methods

2.1 Data retrieval

The Web of Science Core Collection (WoSCC) database was used to collect data from articles on photocatalytic VOC oxidation studies. It is an important data source for bibliometric studies and the assessment of scientific papers and is considered to be highly reliable and widely used in the field of scientific metrics (Chen et al., 2023; Cheng et al., 2019). "Topic" (TS) as the search field: TS = ("photochemical catalysis" OR Photocatalysis OR photocatalytic OR photocatalyst OR "light cataly*" OR "photoredox catalysis" OR photodegradation OR photolytic OR photo-cataly* OR photooxidation OR "ultraviolet catalyzing" OR photoinduced OR "photo-assisted catalysis" OR "light catalyzing" OR "visible-light catalysis") AND TS = (VOCs OR VOC OR "volatile organic compounds" OR "volatile organics" OR "volatile organic components" OR "volatile organic matter" OR "volatility organic compounds" OR "volatile organic contaminants" OR "volatile organic matters"). The specific screening conditions are shown in Table 2, and the screening results were scrutinized to exclude irrelevant research topics and directions such as "Endocrinology Metabolism" and "Agronomy," and the final data are shown in Table 2.

2.2 Methods

The bibliometric analysis of data collected from the core WoS repositories, especially the number of publications, authors, institutions, countries/regions, citations, *etc.*, using mathematical and statistical methods, and visualization, often using CiteSpace and VOSviewer software (van Eck and Waltman, 2010; Pan et al., 2018; Chen, 2004; ŞEnocak and Arpaci, 2023). To determine the major contributions in the literature on photocatalytic oxidation of VOCs, we restricted our focus to authors, institutions, and countries with five or more publications, yielding 268 nodes, 245 nodes, and 49 nodes, respectively. The literature co-citation analysis considered works with a minimum of 50 citations and produced 83 nodes. Journals with more than 100 total citations were examined for co-citation, resulting in 184 nodes. In addition, 8,202 keywords were extracted from the WoSCC. The 163 keyword nodes were selected for visual analysis by selecting keywords with more than 25 occurrences. Furthermore, CiteSpace software was utilized to analyze the "20 most cited keywords" and the "keyword timeline".

3 Results and discussion

3.1 Trends in quantitative changes in research outputs

By statistically analyzing the number of papers published from 1998 to 2023, the development trend and the development and maturity of the scientific research results of VOC photocatalytic oxidation technology can be clearly understood. Figure 2 shows the distribution of research results on photocatalytic oxidation of VOCs based on time series. Between 1998 and 2000, less than 10 articles per year were published on the photocatalytic oxidation of VOCs. From 2001 to 2015, the overall trend of this field showed a slow growth, and in 2015, the annual number of articles in this field exceeded 100 for the first time. The research related to VOC photocatalytic oxidation has gradually become a hotspot, which is inseparable from the environmental protection policies of many countries. From 2016 to 2020, the number of published articles increased significantly, and the annual publication volume of 200 articles has been achieved in 5 years. By 2023, there have been 2,493 publications in the research area of photocatalytic oxidation of VOCs. The increasing volume of the literature in this domain implies that researchers are paying more attention to the photocatalytic oxidation of VOCs.

Figure 2 (inset) shows the contribution of the top 10 countries in terms of the number of articles published annually in the field of photocatalytic oxidation of VOCs. In 1998 and 2000, the United States, Spain, and Japan were among the top three countries in terms of contributing significantly to basic research on photocatalytic oxidation of VOCs. It should be noted that the number of relevant articles from China has increased significantly since 2001. Over the past 2 decades, Chinese researchers have made significant contributions to the study of VOC photocatalytic oxidation. Currently, the number of articles published by Chinese researchers has exceeded 40 percent and continues to increase, indicating their active participation and meaningful results. The increase could potentially be attributed to China's emphasis on air pollution control starting in the early 21st century.

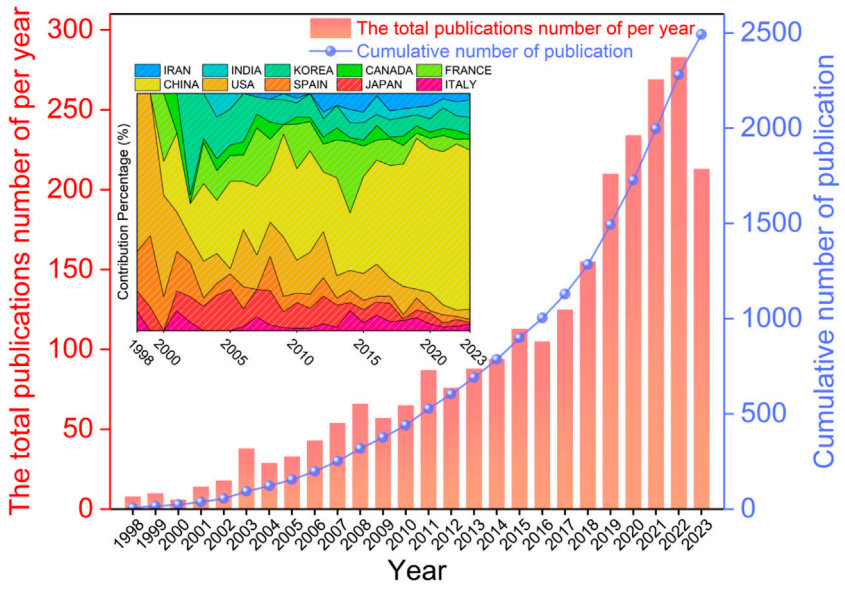

FIGURE 2
Annual and cumulative number of publications (inset: ratio of contributions from the top 10 countries in terms of number of publications per year).

TABLE 3 Top 10 source journals by journal h-index, 1998–2023.

Rank	Source journal	H①	TC②	NP③	CPP④	IF⑤
1	Appl. Catal. B-Environ	76	18105	181	100	22.6
2	Chem. Eng. J	48	7,935	176	45	15.1
3	J. Hazard. Mater	47	6,388	98	65	13.6
4	Chemosphere	29	2,963	71	42	8.8
5	J. Photoch. Photobio. A	28	2,363	62	38	4.3
6	Atmos. Environ	26	2,468	38	65	5
7	Environ. Sci. Technol	26	2,555	43	59	11.4
8	Appl. Surf. Sci	24	1,661	59	28	6.7
9	Build. Environ	24	2,647	47	56	7.4
10	Catal. Today	24	1790	41	44	5.3

① h-index; ② total Citation; ③ number of papers on photocatalytic oxidation of VOCs; ④ citations per paper (the number of citations per paper on average); ⑤ 2022 impact factor.

3.2 Analysis of journals published

Research field journals aid researchers in comprehending the primary scholarly resources and avenues of knowledge distribution in their field. The h-index is a hybrid quantitative metric that can be used to assess the volume and level of academic output, proposed in 2005 by George Hirsch, a physicist at the University of California, San Diego (Cheng et al., 2019). As shown in Table 3, the analysis of the journals resulted in the top 10 publications with the highest h-index on photocatalytic oxidation of VOCs.

Applied Catalysis B-Environmental (Appl. Catal. B-Environ.) is the most influential journal in the field (H = 76), focusing on the reaction mechanisms of photocatalytic processes and the fundamental understanding of photocatalysts, as applied to environmental problems. Moreover, Appl. Catal. B-Environ. published 181 papers on the research of photocatalytic oxidation of VOCs, with the highest number of papers. The second ranked journal is *Chemical Engineering Journal* (Chem. Eng. J., 176 papers, H = 48), which mainly researches about the synthesis and modification of photocatalyst materials in the field of photocatalytic oxidation of VOCs, as well as the mechanism of chemical reactions involved in the setup. The third ranked journal is *Journal of Hazardous Materials* (J. Hazard. Mater., 98 papers, H = 47), which is involved in the study of the development and modification of photocatalytic materials, the design of the light source, and the reactor. Other core journals also focus on the reaction mechanism, catalyst preparation, engineering design, and reaction products of photocatalytic oxidation of VOCs. Journal impact analysis in the field of photocatalytic oxidation technology for VOCs is pivotal for researchers and scholars as it

TABLE 4 Top 20 contributors in the field of photocatalytic oxidation of VOCs.

Author	Volume of publication	Organization	Country
An Taicheng	44	Guangdong University of Technology	China
Dong Fan	38	University of Electronic Science and Technology of China	China
Haghighat Fariborz	35	Concordia University	Canada
Huang Haibao	35	Sun Yat-Sen University	China
Li Guiying	33	Guangdong University of Technology	China
Sun Jing	33	Guangdong University of Technology	China
Leung Dennis Y C	31	University of Hong Kong	China
Xie Xiaofeng	25	Shanghai Institute of Ceramics	China
Lee Chang-Seo	24	Concordia University	Canada
Chen Jiangyao	22	Guangdong University of Technology	China
Jo Wan-Kuen	21	Kyungpook National University	South Korea
Li Yuanzhi	19	Wuhan University of Technology	China
Kim Ki-Hyun	18	Hanyang University	South Korea
Bouzaza Abdelkrim	17	Laboratoire Sciences Chimiques de Rennes	France
Mahmood Asad	17	Guangdong University of Technology	China
Wang Xiao	17	Guangdong University of Technology	China
Li Jieyuan	16	University of Electronic Science and Technology of China	China
Assadi Aymen Amine	15	Laboratoire Sciences Chimiques de Rennes	France
Sun Yanjuan	15	University of Electronic Science and Technology of China	China
Wang Hong	15	University of Electronic Science and Technology of China	China

illuminates the most influential and high-quality journals, thereby informing their publication choices and research trajectories, as well as significantly influencing the evolution of trends and the distribution of resources in this specialized domain.

3.3 Analysis of authors' contributions and collaborations

3.3.1 Author partnerships

Authors in a field of research and the collaborations between them are key elements in advancing scholarship and disseminating knowledge, and bibliometric analyses identify authors and their collaborations that contribute to a particular field of research (Kholidah et al., 2022). The 20 authors with the most publications in the field of photocatalytic oxidation of VOCs are shown in Table 4. Among them, 14 authors are from China, reflecting China's contribution to the field. An Taicheng from the Guangdong University of Technology, China, has the highest number of publications with 44 papers. One of his most influential papers was on the development of a modified ordered porous catalyst with high anti-coking properties by introducing oxygen vacancies into CeO_2 via simple redox and steam treatment ($ARCeO_2$) and its application to the efficient photothermal catalytic degradation of VOCs (Kong et al., 2020). This work highlights the importance of oxygen vacancy engineering in improving photothermal catalytic performance for VOC degradation and provides a facile and cost-effective strategy for the design and fabrication of CeO_2 catalysts with strong anti-coking potential. Dong Fan of Zhejiang University, China, came in second with 38 articles. The representative study of the second influential author involved the first preparation of mesoporous c-doped TiO_2 nanomaterials with the anatase phase using sucrose as the carbon doping source by green synthesis, thus improving the photocatalytic activity of the catalyst (Dong et al., 2011).

The distribution map of authors' collaboration can better reflect the collaboration and co-research among scholars in the field of photocatalytic oxidation of VOCs (Figure 3). The size of each node in the graph indicates the author's publication volume (the larger the node, the more productive the author), while the connecting lines indicate the collaborative relationship between authors. Figure 3 indicates the degree of author collaboration, with several clusters of authors working closely together appearing as shown, including An Taicheng, Dong Fan, Sun Jing, Li Guiying, and Huang Haibao. Moreover, they are the authors with the largest volume of articles. The strength of the linkages between the different authors is shown in Supplementary Figure S1 (Supplementary Material), indicating that international collaboration in this area currently needs to be strengthened. It is important to analyze the level of collaboration between researchers as such a collaboration not only helps pool

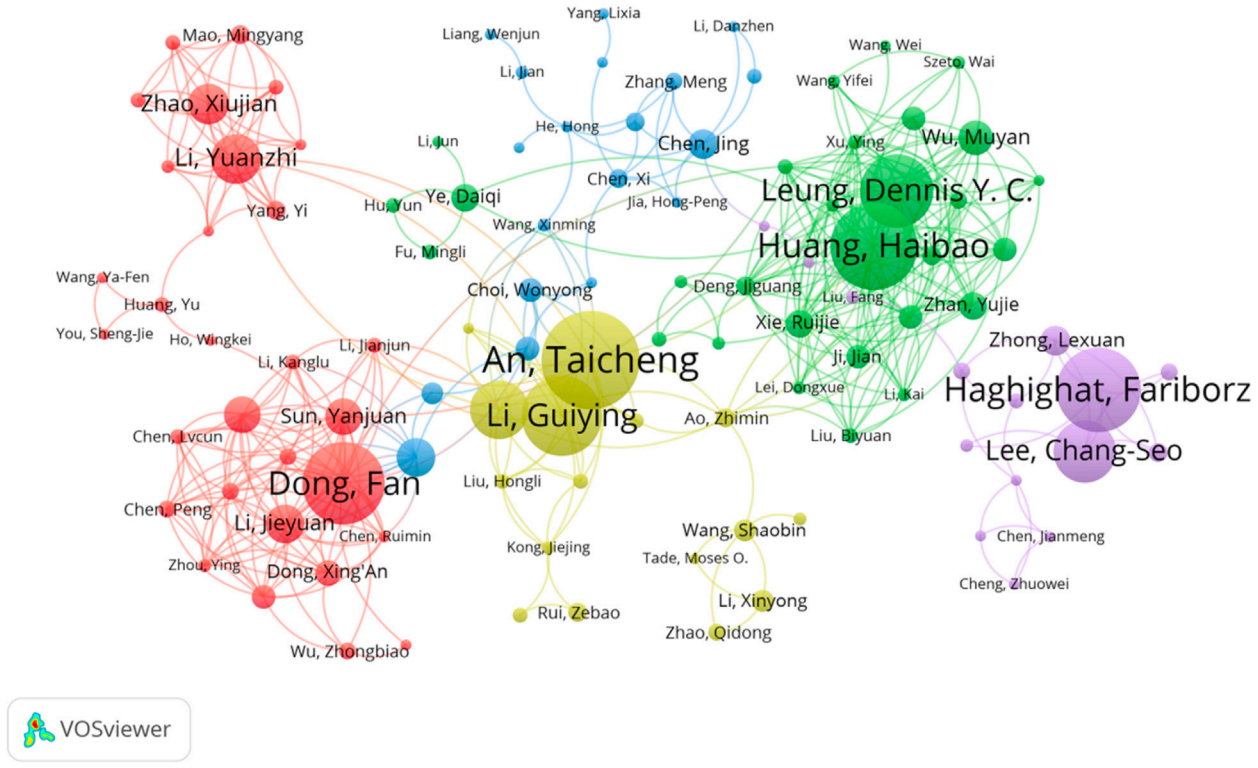

FIGURE 3
Network of collaboration of the author.

expertise from different disciplines and promote innovation and progress but also improves the efficiency, quality, and reliability of research through the sharing of resources, transfer of knowledge, and peer review. In addition, the collaboration promotes the internationalization of scientific research, helps address complex interdisciplinary issues, and accelerates the translation of research results into practical applications, in particular in the field of environmental protection and pollution control.

3.3.2 Analysis of institutions

The analysis of research institutions, which provides information on the research institutions with the greatest impact and highest research output in a given field of research, can help researchers better understand the state and trends of the field and provide guidance on how to address important issues and drive innovation (Li et al., 2023). Figure 4 illustrates a graph displaying the knowledge domains of collaborating organizations utilizing VOSviewer software. Each circular node denotes an organization, and the circle's dimensions indicate the number of papers published. Inter-institutional cooperation is indicated by a line between two nodes: the thicker the line, the closer the institutional cooperation. The Chinese Academy of Sciences (CAS) ranks the highest in terms of total linkage strength, boasting the largest number of publications and suggesting an expansive collaborative network and highly significant academic influence. The promotion of photocatalytic oxidation of gaseous pollutants on g-C_3N_4 is one of the most influential articles (Li et al., 2016). This strategy provides an easy and promising solution for combating air pollution through solar energy. In addition, as shown in Figure 4, there is a relatively close cooperation between CAS, University of Chinese Academy of Sciences (CASU), and Guangdong University of Technology. Their works mainly study the change in atmospheric carbonyl compounds in cities under light with time and the use of a polymer photocatalyst to decompose water.

3.3.3 Analysis of productivity and impact among countries

The problem of VOC air pollution is a global environmental issue; therefore, the analysis of international research cooperation in the field of photocatalytic oxidation of VOCs is of far-reaching importance for promoting global scientific progress, improving the quality and feasibility of research, and contributing to the sustainable development of global society (Zhang et al., 2023). China, the United States, France, South Korea, and India are the top five countries/regions with 1,144 (45.89%), 226 (9.07%), 205 (8.22%), 198 (7.94%), and 124 (4.79%) publications, respectively. Figure 5 shows the knowledge domains of the co-author countries, with the size of the nodes representing the number of national publications and the width of the connecting lines representing the strength of the links between the two countries. Through Figure 5 and Supplementary Table S1, it can be found that China, the United States, France, South Korea, and India have strong co-authorship links with other countries, with China working most closely with the United States, followed by Australia working with China.

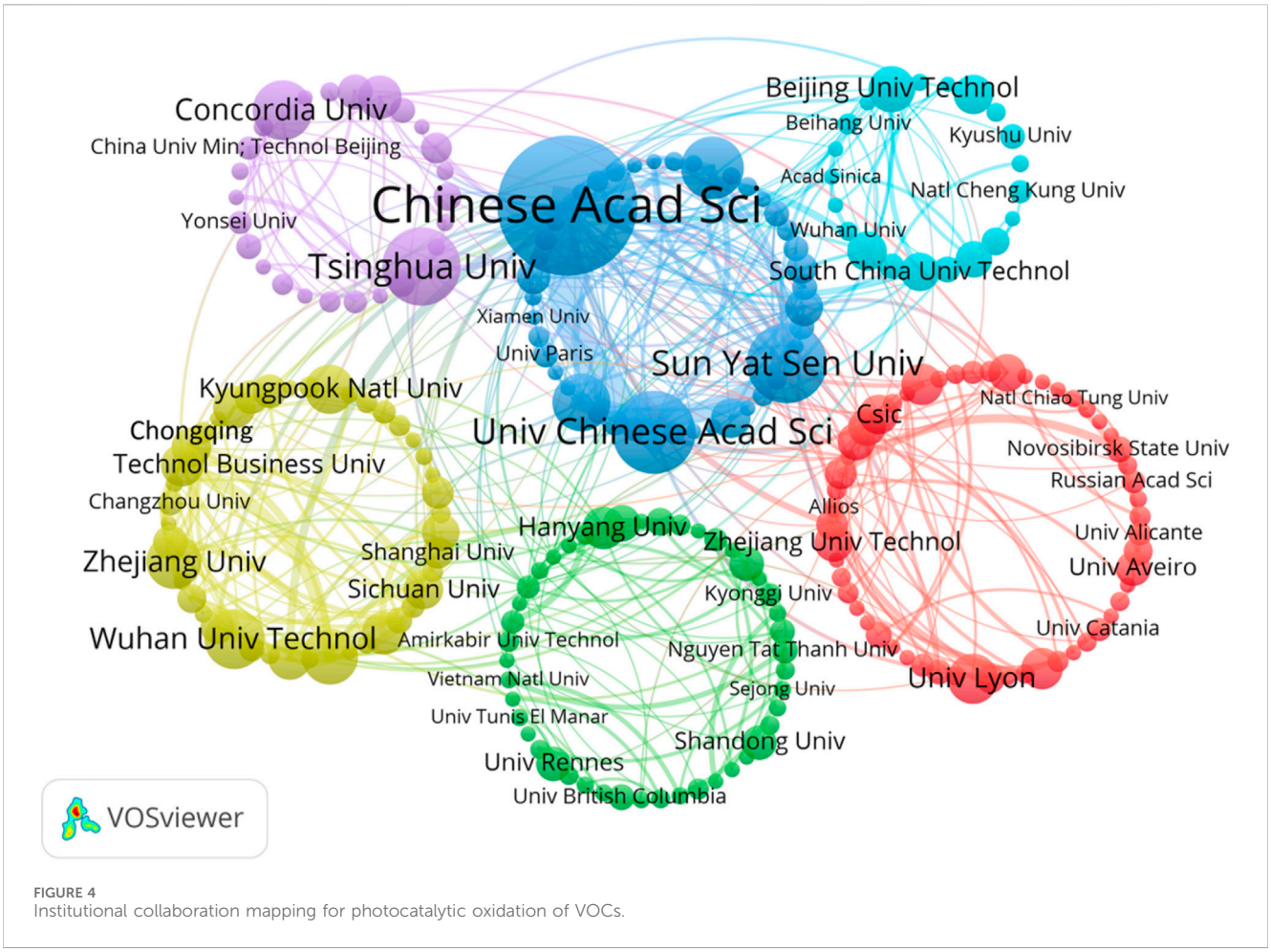

FIGURE 4
Institutional collaboration mapping for photocatalytic oxidation of VOCs.

3.4 Analysis of co-citation

To explore the links between academic publications and papers in the field of VOC photocatalytic oxidation research and to analyze the dynamics and direction of the field, journal co-citation and article co-citation analyses were performed (Farideh, 1996).

3.4.1 Analysis of journal co-citation

The research depicted in Figure 6 displays the journal co-citation mapping of the knowledge domain in the area of photocatalytic oxidation of VOCs, and the greater the number of connecting lines, the stronger the co-citation relationship between the two journals.

The orange cluster in Figure 6 mainly focuses on experimental and theoretical studies of photocatalytic oxidation of VOCs, including but not limited to the areas of photocatalyst characterization and VOC degradation, as represented by Appl. Catal. B-Environ., Catalysis Today, Chemosphere, Chem. Eng. J., and J. Hazard. Mater. In the latest research of this clustered journal, the main focus is on the latest hotspots of VOC photooxidation technology, with a major emphasis on the photocatalytic effects of modified porous materials and composite catalyst combination strategies. In recent studies, the focus is on the research of metal–organic frameworks (MOFs), with the study in Appl. Catal. B-Environ. focusing on the catalytic degradation mechanism of MOFs materials. Qin, JX. et al. prepared Fe-MOF derivatives with the MIL-100(Fe) precursor through thermal treatment, exposing the unsaturated Fe^{2+} active sites that could significantly promote the transfer of photoelectrons, enhancing the oxidation–reduction reaction and improving the photocatalytic performance (Qin et al., 2023). Chen, L. et al. designed the local charge imbalance of carboxylate ligands to regulate the Lewis acid–base sites in NaFe bimetal MOXs, thereby improving the adsorption of acetaldehyde or xylene and enhancing the production of oxidizing free radicals, thereby improving the photocatalytic performance (Chen et al., 2023). Research provided in Chem. Eng. J. primarily modifies MOF porous materials through pretreatment methods to enhance their photocatalytic performance while maintaining their adsorption effect for VOCs. Yu, X. et al. utilized the hotspot effect of MXene's absorption, designing an MXene/MOF high-performance photocatalytic performance aerogel, achieving a TOC removal rate of approximately 95% for acetone vapor within 60 min and demonstrating good stability (Yu et al., 2023). Chem. Eng. J. also focuses on composite catalyst combination strategies, and the S-scheme heterojunction is a recent research hotspot. Zhou, X. et al. synthesized an S-type $TiO_2/BaTiO_3$ heterojunction, where electrons pass through the Ti-O chain from $BaTiO_3$ to TiO_2 and form an internal electric field; it improved the efficiency of photogenerated carrier separation and electron transfer.

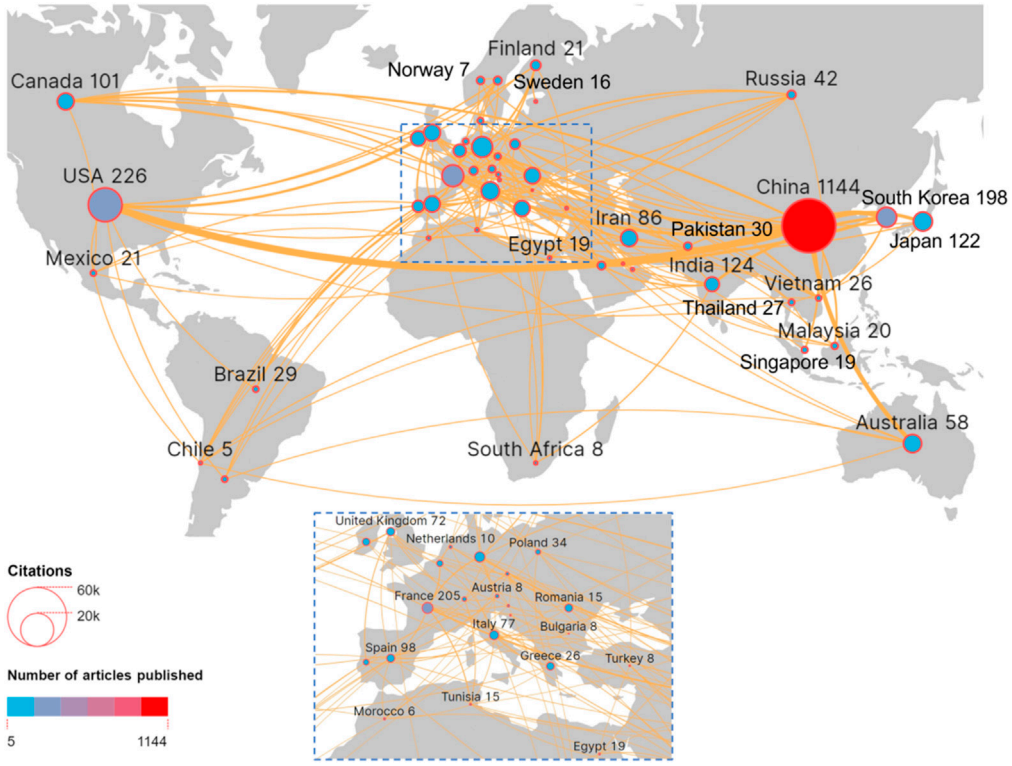

FIGURE 5
Literature distribution by country.

The *Journal of the American Chemical Society* (J. Am. Chem. Soc.), *Journal of Physical Chemistry C* (J. Phys. Chem. C), *Applied Surface Science* (Appl. Surf. Sci.), and *ACS Applied Materials & Interfaces* (ACS Appl. Mater. Interfaces) are affiliated with the Green Cluster. The cluster is dedicated in examining newly discovered catalyst materials, anticipating and observing new materials and surface properties, and studying material properties at a molecular and atomic level using specialized surface analysis techniques and computational methods. In this cluster of journals, the importance of material adsorption capacity and the formation and role of surface oxygen vacancies are emphasized. Appl. Surf. Sci. focuses on the adsorption of VOCs gases by catalysts. Zhao, SF. et al. used DFT calculations to simulate the adsorption ability of five prototype VOCs on transition metal-deposited graphene adsorbents and compared the enhancement effects of different metal depositions (Kunaseth et al., 2017). Kim, S. et al. modified activated carbon surfaces with polyethyleneimine (PEI) and MgO to regulate the adsorbent surface acidity and improve the adsorption of polar VOCs (Kim et al., 2023). Lin, ZF. et al. explored the impact of intermediate products on benzene photocatalytic oxidation in pulp mills, revealing the mechanism and cause of catalyst inactivation (Lin et al., 2020). ACS Appl. Mater. Interfaces. focuses on the activation of surface lattice oxygen and the formation of oxygen vacancies in its latest research. Chen, LC. et al. proved that $Sr_2Sb_2O_7$ is highly efficient and stable in photocatalytic oxidation of toluene compared to TiO_2, which is attributed to the large activation of surface lattice oxygen. The lattice oxygen promotes the adsorption and activation of O_2 and H_2O molecules, producing high-activity free radicals and enhancing the catalytic efficiency.

The blue cluster journals concentrate on the effects of chemical processes that form the foundation of photocatalytic VOC oxidation on human wellbeing, air quality, climate variation, and ecosystems such as *Environmental Science & Technology* (Environ. Sci. Technol.), *Atmospheric Environment* (Atmos. Environ.), and *Atmospheric Chemistry and Physics* (Atmos. Chem. Phys.). Environ. Sci. Technol. primarily focuses on solving real-world environmental problems. In recent studies, there has been a great interest in the environmental pollution caused by volatile organic compounds (VOCs) in solar evaporators. Ma, JX. et al. used a BiOBrI nanoflake with oxygen-rich vacancies to prepare porous sponges and used them as light-permeable solar evaporators with three-dimensional photocatalytic sites to boost VOC rejection for water purification (Ma et al., 2022). Zhou, S. et al. used Ag/AgCl particles to efficiently activate H_2O_2 to generate hydroxyl radicals, which rapidly degraded VOCs during steam generation, solving the VOC pollution problem in solar evaporators (Zhou et al., 2022). Atmos. Chem. Phys., on the other hand, primarily reveals some photochemical oxidation processes in the natural atmosphere. Wang, Y et al. studied the photochemical oxidation of α-pinene, isoprene, and o-cresol on hygroscopic ammonium sulfate seeds to reveal the trend of aerosol rebound (Wang et al., 2021). Li, JL. et al. studied the secondary organic aerosol production process from the photooxidation of mixed anthropogenic volatile organic compounds (Li et al., 2021).

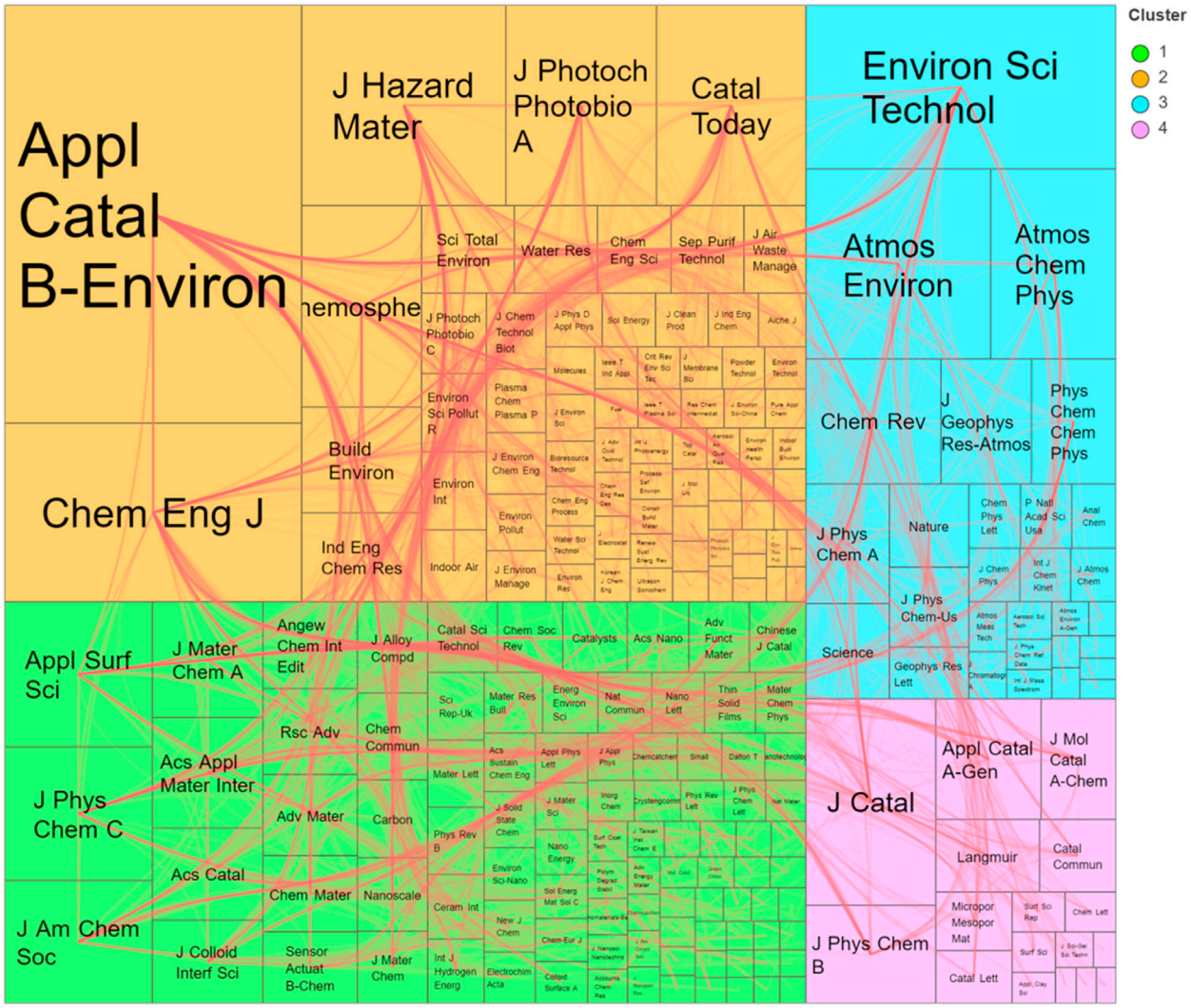

FIGURE 6
Graphic representation of the knowledge domains of journal co-citations in the field.

The Purple Cluster, spearheaded by the *Journal of Catalysis* (J. Catal.), *Journal of Physical Chemistry B* (J. Phys. Chem. B), and *Catalysis Communications* (Catal. Commun.), concentrates on the preparation, combination, and kinetic analysis of photocatalytic materials, along with employing spectroscopic techniques for catalyst characterization and theoretical models to explore probe–catalyst interactions and various theoretical methods. J. Catal. is dedicated to the study of the mechanism of VOC gas degradation. Song, BY. et al. explored the photocatalytic oxidation performance and mechanism of isoprene over titanium oxide by UV-Vis lights (Song et al., 2024). Krauter, J. et al. proved that partial photooxidation of 2-propanol not only is possible in the presence of oxygen but also in the absence of adsorbed water or even at room temperature below (Kräuter et al., 2022). The main research direction of Catal. Commun. in recent times is the modification strategy for titanium dioxide photocatalysts for the decomposition of VOCs (Higashimoto et al., 2020; Kovalevskiy et al., 2020).

As shown in Figure 6, Appl. Catal. B-Environ. has the largest share of area and is the most co-cited journal of all journals. Its significant impact on VOC photocatalytic oxidation research is mainly attributed to the journal prestige and the quantity of published articles. The journal has published 181 studies with photocatalytic oxidation of VOC topic, which is the largest number among all. Among the four clusters, Appl. Catal. B-Environ. and Chem. Eng. are included. Journals such as J. Catal. and Environ. Sci. Technol. are more widely cited, suggesting that journals dealing with the chemical processes involved in the photocatalytic oxidation of VOCs generally have a broader reach. Moreover, the connecting lines linking the aforementioned three journals are bolder, indicating a greater occurrence of co-citations among them.

In summary, studies on photocatalytic oxidation of VOCs have been published mainly in journals focusing on research and development of photocatalytic materials, analysis of VOC degradation processes, interfacial reactions, microscopic theoretical calculations, and macroscopic atmospheric environment. Journal co-citation analysis significantly reveals the network of key research and scholarly communication in the field of

TABLE 5 Top 10 most co-cited papers in the field of photocatalytic oxidation of VOCs.

No.	Title	Journal	Author	Year	Co-citation	Reference
1	Environmental Applications of Semiconductor Photocatalysis	Chem. Rev	Hoffmann, M.R., et al	1995	233	Hoffmann et al. (1995)
2	Determination and risk assessment of by-products resulting from photocatalytic oxidation of toluene	Appl. Catal. B-Environ	Mo, J., et al	2009	205	Mo et al. (2009)
3	TiO_2 photocatalyst for removal of volatile organic compounds in gas phase - A review	Chem. Eng. J	Shayegan, Z., et al	2018	203	Shayegan et al. (2018)
4	Photocatalytic oxidation technology for indoor environment air purification: The state-of-the-art	Appl. Catal. B-Environ	Mamaghani, A.H., et al	2017	201	Mamaghani et al. (2017)
5	Volatile organic compounds in indoor environment and photocatalytic oxidation: State of the art	Environ. Int	Wang, S., et al	2007	200	Wang et al. (2007)
6	Photocatalytic destruction of VOCs in the gas-phase using titanium dioxide	Appl. Catal. B-Environ	Alberici, R.M., et al	1997	181	Alberici and Jardim (1997)
7	TiO_2 Photocatalysis for Indoor Air Applications: Effects of Humidity and Trace Contaminant Levels on the Oxidation Rates of formaldehyde, Toluene, and 1,3-Butadiene	Environ. Sci. Technol	Obee, T.N., et al	1995	181	Obee and Brown (1995)
8	Photocatalytic oxidation for indoor air purification: a literature review	Build. Environ	Zhao, J., et al	2003	170	Zhao and Yang (2003)
9	Photocatalytic oxidation of toluene at indoor air levels (ppbv): Towards a better assessment of conversion, reaction intermediates and mineralization	Appl. Catal. B-Environ	Sleiman, M., et al	2009	143	Sleiman et al. (2009)
10	Kinetic study for photocatalytic degradation of volatile organic compounds in air using thin film TiO_2 photocatalyst	Appl. Catal. B-Environ	Kim, S.B., et al	2002	137	Kim and Hong (2002)

photocatalytic oxidation of VOCs, helping researchers to identify major trends, the core literature, and potential opportunities for interdisciplinary collaboration in the field.

3.4.2 Literature co-citation analysis

Both the number of co-citations and the number of citations are important indicators of the impact of scholarly articles, but there are differences in the emphasis and information reflected. Articles with a high number of co-citations (Table 5) emphasize the relevance of different studies and the concentration of research interests, whereas articles with a high number of citations (Supplementary Table S2) are more likely to highlight the broader impact and scientific contribution of an individual article. Table 5 displays the co-citations of the 10 most prominent papers in the scientific study of photocatalytic oxidation of VOCs. Seven of the top 10 most cited articles were published post-2000, indicating a remarkable advancement in the field over the last 2 decades. Of the 10 papers, five are reviews of photocatalytic oxidation of VOCs, two relate to the by-products of this process, and three discuss the degradation mechanism of photocatalytic oxidation, and titanium dioxide (TiO_2) was the photocatalyst used in their study.

The most co-cited paper was "Environmental Applications of Semiconductor Photocatalysis" by Hoffmann, et al., being co-cited 233 times. The aim of this review is to provide an overview of the fundamentals of semiconductor photocatalysis and its potential applications in environmental control technologies (Hoffmann et al., 1995). The analysis shows that semiconductor photocatalysis has extensive usage in environmental systems, including air purification. Furthermore, advancing research for this technology requires a new comprehension of the non-uniform photochemistry complexity of metal oxide systems in multiphase environments. The second ranked article is "Determination and risk assessment of by-products resulting from photocatalytic oxidation of toluene" (205 times). The article investigated the ppb-grade by-products generated during the photocatalytic oxidative decomposition of toluene using TiO_2 as a catalyst and concluded that the concentration of undesirable by-products generated during the photocatalytic oxidation process was low and would not have a negative impact on human health (Mo et al., 2009). Also of note are two research papers on the photocatalytic oxidation of VOCs by TiO_2, published before 2000, which provide a research base for the development of research in this field. "Photocatalytic destruction of VOCs in the gas-phase using titanium dioxide" has been co-cited 181 times and is ranked sixth. The gas-phase photocatalytic degradation of 17 VOCs by TiO_2 was investigated in this paper, and the results indicate the potential application of multiphase photocatalysis in the reduction of different classes of VOCs (Alberici and Jardim, 1997). The seventh-ranked article is "TiO_2 Photocatalysis for Indoor Air Applications: Effects of Humidity and Trace Contaminant Levels on the Oxidation Rates of Formaldehyde, Toluene, and 1,3-Butadiene" (181 times), which outlines how humidity and pollutant concentration impact the oxidation rate of VOCs in indoor air for TiO_2 photocatalytic applications (Obee and Brown, 1995). It attributes this relationship to the competitive adsorption to hydroxyl adsorption sites, as well as to changes in the quantity of hydroxyl radicals.

The four other articles reviewed the current state-of-the-art photocatalytic oxidation of VOCs in indoor air using TiO_2 as a photocatalyst (Wang et al., 2007), investigated the dependence of the

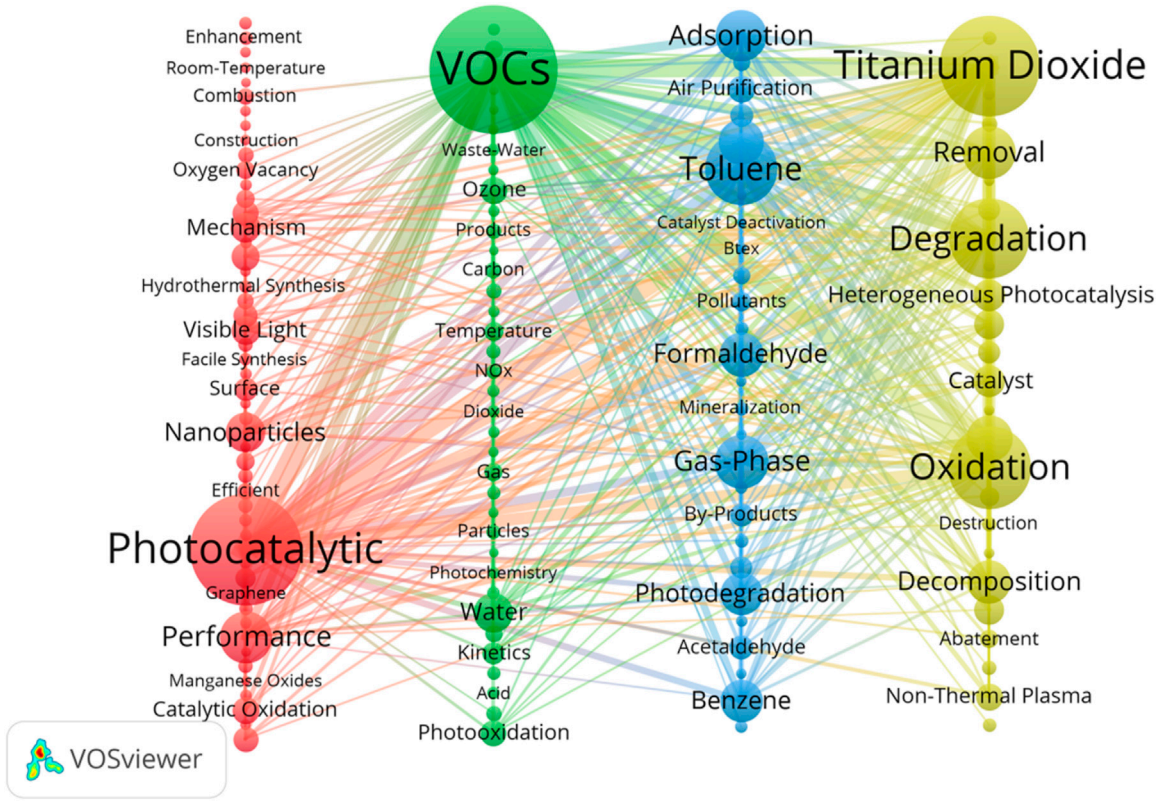

FIGURE 7
Keyword co-occurrence knowledge graph.

reaction rate on key factors through kinetic experiments and developed a kinetic model to assist in optimizing the reactor design (Zhao and Yang, 2003), and reviewed the removal of airborne VOCs by commercial TiO_2 photocatalysts for VOCs and reporting the results of a comprehensive literature review on TiO_2 modification technologies, including methods to overcome the inherent limitations of TiO_2 and improve the photocatalytic degradation of VOCs (Mamaghani et al., 2017; Shayegan et al., 2018). By synthesizing and analyzing research results on photocatalytic oxidation of VOCs, a comprehensive knowledge framework can be provided to researchers to help them understand the progress and challenges in the field. The study of the relationship between the reaction rate and key factors, as well as the development of kinetic models, can provide practical guidance for optimizing reactor design and further promote the application of this technology in production.

"Kinetic study for photocatalytic degradation of volatile organic compounds in air using thin film TiO_2 photocatalyst" and "Photocatalytic oxidation of toluene at indoor air levels (ppbv): Towards a better assessment of conversion, reaction intermediates, and mineralization" indicate that the degradation effect of photocatalytic oxidation of VOCs is impacted by various factors, including the initial concentration of VOCs, water vapor content, and photon flux of ultraviolet light (Sleiman et al., 2009; Kim and Hong, 2002). The thorough examination of the kinetics of the photocatalytic degradation process yields crucial insights into the degradation mechanism of VOCs on the catalyst surface. This information can be utilized to enhance the reaction conditions and enhance the efficiency of degradation. Furthermore, doing a comprehensive analysis of the intermediates generated throughout the reaction and the ultimate mineralization can provide valuable insights into the photocatalytic process, its safety implications, and its environmental effects.

3.5 Analysis of keyword co-occurrence

Keyword co-occurrence analysis facilitates comprehension of essential themes and concepts in the literature or dataset. It assists researchers in orientating their research, decision-making, and collaboration to achieve a fuller understanding of the challenges and opportunities of a specific field or topic.

From the results displayed in Figure 7, the analysis software application produced four clusters. Cluster 1 (red): as shown in Figure 7, the main nodes in the red cluster include "Photocatalytic," "Performance," "Nanoparticles," "Oxygen Vacancy," "Manganese Oxides," "Graphene," and "Hydrothermal Synthesis." Hence, the advancement of effective photocatalysts is a significant field of study in the research of photocatalytic oxidation of VOCs. This can be accomplished by altering the structure of nanomaterials like TiO_2, manganese oxides, and graphene through straightforward and efficient techniques such as hydrothermal synthesis. For instance, the introduction of oxygen vacancies can enhance the catalysts' capability to perform photocatalytic oxidation reactions at ambient

temperature. Supplementary Table S3 presents a concise overview of various photocatalysts, together with their associated modifying reagents, bandgaps, and target pollutants. Cluster 2 (green) with "VOCs," "Kinetics," "Acid," "Temperature," "Water," and "Dioxide" as the representative keyword indicates that photocatalytic oxidation of VOC technology is environmentally important in theory and practice and is an effective means of controlling air pollution and improving indoor and outdoor air quality. Photocatalysts catalyze the oxidative decomposition of VOCs under light conditions, converting them into more harmless substances such as carbon dioxide and water. Key factors in the treatment process include temperature, humidity, and pH conditions, which affect the reaction kinetics, the conversion efficiency of the pollutants, and the final degradation products. Cluster 3 (blue) of the keywords "Toluene," "Gas-Phase," "Benzene," "Formaldehyde," "By-Products," "Btex," "Catalyst Deactivation," and "Mineralization" indicates that photocatalytic technology is commonly used to remove Btex such as formaldehyde, acetaldehyde, benzene, and toluene from the air (Kamani et al., 2023). However, catalyst deactivation can occur due to the adsorption properties of the catalytic materials, and the photodegradation process can produce by-products that prevent complete mineralization of the pollutants. This requires a thorough understanding of the reaction mechanism in order to optimize reaction conditions and select suitable photocatalysts. Cluster 4 (yellow) represents the keywords "Titanium Dioxide," "Removal," "Degradation," "Oxidation," "Decomposition," and "Non-Thermal Plasma." Titanium dioxide is one of the most studied photocatalysts. The traditional titanium dioxide catalyst has a bandgap of 3.2 eV and can be excited by ultraviolet light to produce photogenerated electron hole pairs, which is the earliest discovered photocatalyst. However, because it can only be excited by ultraviolet light and the ultraviolet component of ambient sunlight only accounts for 5%, so it needs to be modified. Modified TiO_2 can effectively promote the degradation and mineralization of organic and inorganic pollutants. This process involves not only the direct decomposition of pollutants but also the in-depth treatment of their secondary decomposition products to ensure their complete harmlessness. On the other hand, non-thermal plasma technology, which decomposes pollutants by generating high-energy electrons, is particularly suitable for treating compounds that are difficult to degrade (Mu and Williams, 2022). This technology achieves efficient pollutant control at low temperatures, demonstrating unique advantages for treating low concentrations or stubborn pollutants. Combining these two technologies, the current research is not only focused on improving the efficiency and rate of pollutant treatment but also on optimizing the reaction conditions, lowering the operating costs, and reducing the generation of secondary pollutants. In addition, a deeper understanding and improvement of these technologies is scientifically and practically important for achieving more environmental friendly and cost-effective pollutant treatment methods.

3.6 Identification of research frontiers

As shown in Figure 8 , the keywords represent a node; the larger the node means that the keyword is more heavily researched, and some nodes means the keyword has high explosive power (Table 6); however, links between them indicate co-occurrence relationships (van Eck and Waltman, 2010). CiteSpace software was used to obtain nine clustering labels by the LLR (log-likelihood ratio) method: "#0 titanium dioxide," "#1 gas phase," "#2 dielectric barrier discharge," "#3 photocatalytic degradation," "#4 catalytic oxidation," "#5 air," "#6 performance," "#7 thin film," and "#8 carbon monoxide." The timeline clearly illustrates the development of the keywords within each of the representative clusters in the literature on the photocatalytic oxidation of VOCs over this time period (Seltenrich, 2015).

The keywords "Titanium Dioxide," "Formaldehyde," "Heterogeneous Photocatalysis," "Volatile Organic Compound," and "Air" appear in the 1998 timeline. From 2001 to 2003, the keywords include "Degradation," "Decomposition," "Photocatalytic Oxidation," "Indoor Air," "Activated Carbon," "Benzene," and "Thin-Film." In 2015, "Hydrothermal Synthesis," "Efficiency," "Low-Temperature," and "Nanocomposite" appeared. During 2020 to 2023, keywords involved "UV," "synergistic effect," "Enhanced Photocatalytic Activity," "Manganese Oxide," "Metal Organic Framework," "Efficient," "Charge Separation," "Hydrogen Production," "Carbon Nitride," and "Nanorod." Collectively, these keywords reflect the latest trends and advances in the field of inhomogeneous photocatalysis and provide directions for future research in material science, energy conversion, and environmental protection. Further progress in the efficiency and application of photocatalytic technology is expected through in-depth research in these key areas.

CiteSpace software counts the frequency of words in the identifiers of titles, abstracts, keywords, and bibliographic records of papers in related fields and identifies hot words based on the growth rate of word frequency of these words to reveal the research trend of photocatalytic oxidation of VOCs. As shown in Table 6, "Trichloroethylene," "Titanium Dioxide," "Heterogeneous," "Photocatalysis," "Air," and "Kinetics" have been a research buzzword from 1998 to 2015. In this stage, most of the studies used trichloroethylene as the target pollutant and TiO_2 as the photocatalyst to investigate the efficacy and kinetics of photocatalytic oxidation technology for VOCs. TiO_2, the cornerstone of photocatalysts, is the most popular photocatalyst, and its composites, with the combined advantages of their respective components, play an important role in different areas of pollution control (Belessiotis et al., 2022). Silvia Suárez et al. prepared hybrid-structured photocatalysts based on the adsorbents seafoam and TiO_2 by extruding ceramic dough and tested them for the photocatalytic degradation of the target volatile organic compound molecule trichloroethylene (Suárez et al., 2008). Khurram Shahzad Ayub et al. selected Co and Cu bimetallic oxides with high catalytic activity dispersed on TiO_2 and successfully prepared Co-Cu/TiO_2 catalysts, which were used in post-plasma catalysis for effective degradation of toluene (Ayub et al., 2022). The effects of TiO_2 content, zeolite structure, and silica/aluminum ratio on the textural properties, adsorption capacity, and photodegradation activity of zeolite/TiO_2 composites were investigated using formaldehyde and chlorinated hydrocarbon trichloroethane as model VOCs by Jansson et al. (2015). Xiaoqing Qiu et al. reported here that grafting nano-sized Cu_xO clusters onto TiO_2 produces an excellent indoor environmental risk reduction material. By

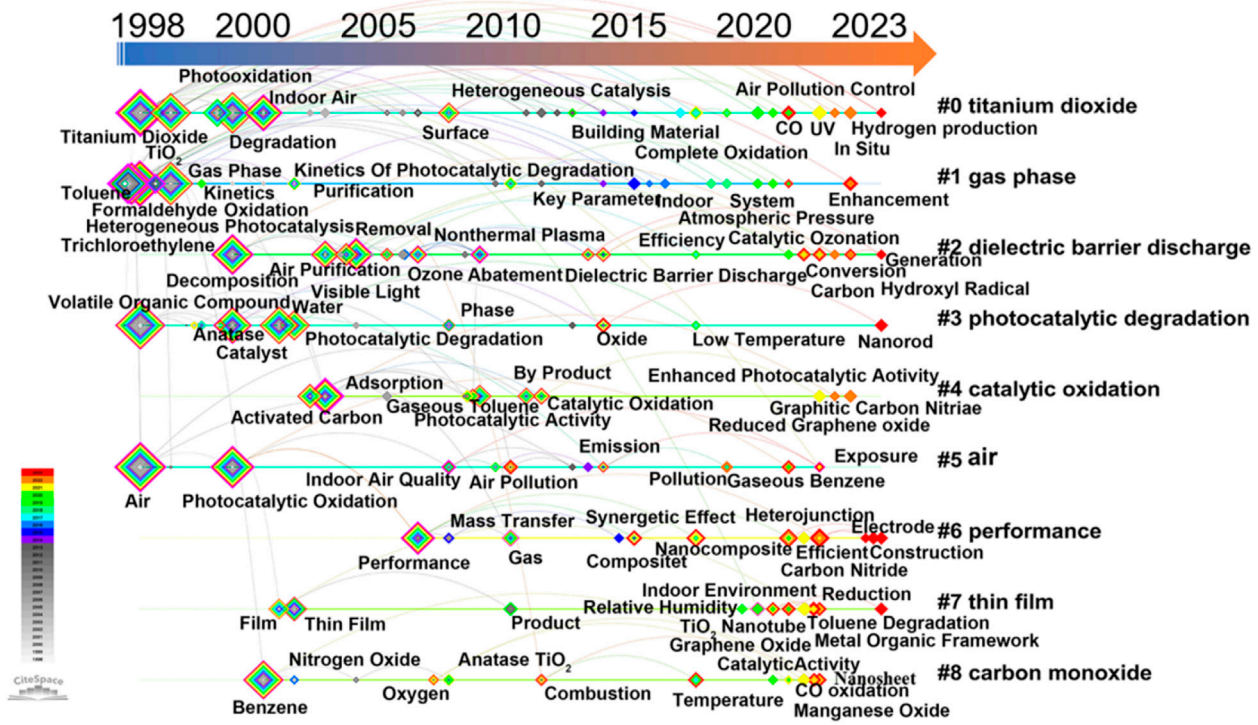

FIGURE 8
Timeline view of keyword clustering for photocatalytic oxidation studies of VOCs.

controlling the balance of Cu-I and Cu-II in Cu_xO, the Cu_xO/TiO_2 hybrid nanocomposites achieved efficient decomposition and anti-pathogenic activity (Qiu et al., 2012). Shuang Cao et al. prepared bimodal mesoporous TiO_2 catalysts doped with platinum, palladium, and ruthenium by wet impregnation for the catalytic combustion of dichloromethane, and the deactivation of Ru/TiO_2 catalysts was suppressed due to the fact that carbon and chlorine could be removed by RuO_2, which resulted in excellent catalytic activity (Cao et al., 2018). The research field of photocatalytic oxidation of VOCs has developed rapidly in the last 2 decades, and research on modified catalysts with TiO_2 catalysts as the cornerstone continues to be hot, with a deeper understanding of the photochemical mechanism and optimization of photocatalyst design, contributing to the reduction of air pollutants.

"Oxygen vacancies," "heterojunctions," "high efficiency," "nanosheets," "metal-organic frameworks," "manganese oxide," "carbon," "nanocomposites," "oxides," and "mechanism" are the burst keywords from 2019 to 2023.

3.6.1 Burst keyword "heterojunctions"

By adding the keyword "Heterojunction" to the Boolean operation search formula and conducting keyword analysis, Supplementary Figure S2 was obtained. It can be seen from the figure that the three keywords distributed over time, "p-n Heterojunction," "Z-scheme Heterojunction," and "S-scheme Heterojunction," imply the development of composite photocatalysts in the field of photocatalytic degradation of VOCs. According to the different positions of the energy band, the coupling of semiconductors can be divided into three types: broken gap, cross-border gap, and staggered gap (Che et al., 2023). In fact, only the heterojunction with staggered gaps can improve the charge transfer at the interface, thus attracting the attention of scholars. "p-n heterojunction" is a typical strategy of staggered-gap heterojunction. Since the main carriers of p-type semiconductors are positive charges and the main carriers of n-type heterojunctions are negative charges, the interface of p-n heterojunctions contains a built-in electric field and suppresses the recombination of carriers by separating the photogenerated electrons (e_{CB}^-) and holes (h_{VB}^+) (Zou et al., 2020). The formed heterojunction makes the spatial separation of photoinduced carriers possible and effectively inhibits the possibility of charge recombination. However, the separation efficiency of photogenerated electron–hole pairs is at the cost of reducing the oxidation ability of the two semiconductor photocatalysts.

The photocatalyst modified by the "Z-scheme Heterojunction" strategy not only has a strong redox ability to drive photocatalytic reactions but can also effectively separate photogenerated electrons and holes. The Z-type photocatalyst can help ensure the improvement of the utilization efficiency of solar energy while enhancing the redox ability of the photocatalyst and promoting the separation of charge carriers through its unique electron transfer (Li et al., 2022). In the Z-scheme heterojunction, electrons on the semiconductor with a lower CB move to the higher VB of the other semiconductor to combine with holes, thereby preventing the recombination of photogenerated carriers and maintaining the original maximum redox potential (Jia et al., 2023). The formation of Z-scheme heterojunctions can be proved by the production of high-energy free radicals. Yang, J. et al. coupled

TABLE 6 Chronological distribution of the top 20 highlight keywords.

Keyword	Year	Strength	Begin	End	1998–2023[a]
Trichloroethylene	1998	31.87	1998	2008	
Heterogeneous photocatalysis	1998	18.86	1998	2012	
Air	1998	15.73	1998	2014	
Reactor	1999	10.47	2007	2015	
Kinetics	1999	8.32	2007	2015	
Photodegradation	2003	10.73	2009	2013	
Purification	2004	8.13	2012	2017	
Gas	2013	9.09	2013	2019	
Nonthermal plasma	2009	12.26	2014	2016	
Oxygen vacancy	2019	11.86	2019	2023	
Heterojunction	2019	7.88	2019	2023	
Efficient	2020	12.61	2020	2023	
Nanosheet	2020	9.58	2020	2023	
Metal–organic Framework	2020	9.31	2020	2023	
Manganese oxide	2020	8.92	2020	2023	
Carbon	2013	8.98	2020	2023	
Nanocomposite	2016	7.83	2020	2023	
Oxide	2015	8.69	2021	2023	
Mechanism	2012	8.1	2021	2023	

[a]: Time period in which the keyword was normally followed; : time period in which the keyword was hotly followed; : time period in which the keyword was indifferently followed.

BiOCl with Bi_2WO_6 to form a heterojunction for efficient photocatalytic degradation of toluene; theoretically, the conduction band of BiOCl cannot reach the band condition for oxygen activation to superoxide radical (−0.33 eV). After the formation of composite free radicals, the existence of superoxide radicals was detected by EPR, proving that high-energy electrons can be retained on the conduction band of Bi_2WO_6 and form a Z-scheme heterojunction, effectively separating high-energy electrons from holes to improve the photocatalytic efficiency (Yang et al., 2023a). Based on the fact that Z-scheme heterojunctions can produce high-energy electrons or holes, many studies have adopted this approach to more efficiently generate free radicals. Li, X. et al. constructed a Z-scheme heterojunction formed by MnO_2 and C_3N_4, where low-energy electrons from the conduction band of C_3N_4 combine with holes on the valence band of MnO_2, retaining high-energy electrons on the low-conduction band of MnO_2, which is more conducive to the production of superoxide radicals, and improving the photocatalytic efficiency (Li et al., 2022). To further improve the photocatalytic efficiency of Z-scheme heterojunctions, researchers have proposed many modification strategies. Experimental evidence has shown that the surface plasmon resonance effect of Ag nanoparticles can assist in producing large amounts of active oxygen. Chen, JY. et al. introduced Ag nanoparticles into the heterojunction system of Cu_xO and $SrTiO_3$, achieving highly efficient degradation of toluene while also exhibiting excellent antibiosis against *E. coli* due to the chemical disinfection action of Cu and Ag (Chen et al., 2023). Yang, J. et al. chemically deposited AgCl on the surface of Bi_2WO_6 and synthesized $Ag/AgCl/Bi_2WO_6$ photocatalysts by photoreduction of Ag-0 nanoparticles under UV light, achieving nearly 100% toluene degradation efficiency under visible light irradiation (Yang et al., 2023b). There are also studies that combine three semiconductor materials to form a double Z-type heterojunction with overlapping band structures. Shi, L. et al. synthesized a tri-component Z-type heterojunction photocatalyst $BiPO_4/BiVO_4/g\text{-}C_3N_4$ by a one-step sol–gel method, exhibiting high catalytic performance (Shi et al., 2022).

The basic condition for the formation of the "S-scheme Heterojunction" strategy is that the conduction band (CB) position and Fermi level (Ef) of the reducing semiconductor (RP) should be higher than those of the oxidizing semiconductor (OP) (Li et al., 2023). Under illumination, the low-energy photoelectrons generated in the conduction band of OP are driven by the internal electric field to cross the interface, where they recombine with the photogenerated holes in the valence band of RP. Therefore, the photogenerated carriers with strong redox ability can accumulate at the high conduction band position of RP and the low valence band position of OP, respectively. This leads to the spatial separation of oxidation and reduction sites on both sides of the connection, greatly improving the utilization rate of photoinduced carriers and thereby greatly enhancing the production efficiency of photooxidation active substances for VOCs (Xu et al., 2022). The formation of S-scheme heterojunctions can be analyzed by photo-

irradiating a Kelvin probe and *in situ* X-ray photoelectron spectroscopy. Li. YW et al. synthesized $BiVO_4$/tubular g-C_3N_4 S-scheme heterojunction photocatalysts for formaldehyde degradation, and the elemental binding energy changes were observed through *in situ* X-ray irradiation. The surface morphology and potential were observed using a Kelvin probe force microscope, showing that electrons migrated from g-C_3N_4 to $BiVO_4$ in the dark, while electrons migrated from BiVO4 to g-C_3N_4 in the light, thus proving the formation of the S-scheme heterojunction (Li et al., 2023). The regulation of the interface charge transfer in S-scheme heterojunctions is of great importance, and recent research has used DFT (density functional theory) calculations to predict the formation strategies of S-scheme heterojunctions. Dong, YP. et al. predicted the formation of an S-scheme heterojunction by combining Cds with $InVO_4$ through DFT calculations and successfully loaded Cds quantum dots onto $InVO_4$. The transfer of electrons between Cds and $InVO_4$ was observed using a Kelvin probe force microscope, verifying the existence of the S-scheme heterojunction and achieving high-efficiency photocatalytic degradation of C_2H_4 (Dong et al., 2024). Xu, XY. et al. used DFT calculations to predict that an S-scheme heterojunction can be formed between CdS quantum dots and Bi_2MoO_6 monolayers and successfully fabricated the catalyst through *in situ* hydrothermal synthesis for highly efficient photocatalytic degradation of C_2H_4 under visible light (Xu et al., 2022).The high efficiency of charge separation and electron transfer in the S-scheme heterojunction is due to the bonding form between the semiconductors, which enhances the efficiency of electron transfer and inhibits the accumulation of degradation intermediates. Recent studies have reported that exposing more oxygen vacancies by forming S-scheme heterojunctions can enhance the catalyst's adsorption ability for VOC gases. Ying, TT. et al. prepared CeO_2/Cu_2O through a simple wet chemical method and found that the large number of oxygen vacancies on CeO_2 enhances the adsorption capacity for pollutants. The built-in electric field formed by the S-scheme heterojunction can improve the separation of photogenerated charges, enhancing the photocatalytic performance (Ying et al., 2024).

In Supplementary Table S4, the works of the above three heterojunction strategies including the S-type heterojunction in the field of modified photocatalytic degradation of VOCs are listed. The construction of heterojunctions is an effective strategy to improve the performance of photocatalysts by combining different semiconductor materials, which can achieve better charge separation and a wider range of light response.

In summary, monolithic semiconductor catalysts often exhibit poor photocatalytic activity due to limited light response, rapid photoinduced charge recombination, and weak oxidation–reduction ability. Therefore, designing heterojunctions between different semiconductors can overcome the disadvantages of monolithic semiconductor catalysts. By designing Z-scheme or S-scheme inhibition junctions, it is possible to effectively separate the photoelectron–hole pairs and enhance the oxidation–reduction ability of the electron and hole. However, the characterization techniques for Z-scheme heterojunctions are insufficient, and the charge transfer pathway between the semiconductors is still unclear. The synthesis requirements for S-scheme heterojunctions are certain, and there are sufficient characterization techniques, but there is still a need to explore efficient and unobstructed charge transfer pathways, and the stability and deactivation issues of the composite catalyst also need further research.

(1) Composite heterojunction photocatalysts can generate high oxidation–reduction potentials and rich photogenerated charges to enable various oxidation and reduction reactions. It is necessary to adjust the band structure and active centers of the semiconductor through targeted optimization to enhance specific oxidation–reduction reactions and improve the photocatalytic degradation efficiency.
(2) Building unobstructed and directed transfer channels at the interface of the heterojunction material is a top priority, and establishing stable chemical bonds is a reliable strategy. It is crucial to clarify the charge transfer pathway between different catalysts for the design of composite catalysts.
(3) For composite heterojunctions, it is necessary to consider the catalyst's activity and material stability. Therefore, composite catalysts with stronger interactions can be designed, such as chemical bonding, *in situ* growth, and high-temperature calcination, to ensure that the different semiconductor catalysts are in close contact.

3.6.2 Burst keyword "Metal Organic Framework"

MOFs have shown great potential in the design and synthesis of photocatalysts. Supplementary Figure S3 was obtained by adding the keyword "Metal Organic Framework" to the Boolean operation retrieval formula and conducting keyword analysis. It can be found in the figure that keywords such as "UiO-66," "ZIF-8," "Cu-btc," and "Mil-100(Fe)" are presented. These keywords represent different structural classifications of MOFs. "Uio-66" is composed of $[Zr_6O_4(OH)_4]$ coordinated with 12 terephthalic acid ligands to form a regular octahedral crystal structure. UiO (Universitetet i Oslo) belongs to coordination pillar layer (CPL) materials. Its synthesis method is simple, the material structure is flexible, and the pore size is adjustable. It has been widely applied in the fields of gas adsorption and energy storage (Marks et al., 2020). Zeolitic imidazolate frameworks (ZIFs) are self-assembled by Zn or Co ions bonded in a tetracoordinated manner to the N sites of the imidazole (or imidazole derivatives) ring. As a subclass of MOFs, ZIFs combine the advantages of zeolites and MOFs. Moreover, ZIFs also have higher chemical and thermal stability (Li et al., 2018). MIL (Materials Institute Lavoisier) is coordinated by trivalent transition metal ions (such as Fe, Al, and Cr) and carboxylic acid ligands (such as terephthalic acid and trimellitic acid), and usually has a high specific surface area and rich porosity. In conclusion, MOFs are a kind of porous crystalline multifunctional materials, which have received increasing attention due to their ultrahigh specific surface area. MOFs with different configurations have been studied and applied in photocatalytic degradation of VOCs (Zhao et al., 2020).

The structure of MOFs is adjustable, which is conducive to the implementation of modification strategies. Different functional groups (Yao et al., 2018; Zhang et al., 2020), metal clusters (Man et al., 2022; Wang et al., 2018), and nanoparticles (Zhang et al., 2022) can be incorporated through methods such as heat treatment and solvent exchange to improve the functionality and selectivity of the catalyst. The heterogeneous junction strategy can effectively separate photogenerated carriers to improve light utilization efficiency and photocatalytic performance (Chen et al., 2021). Atomic doping strategies can alter the bandgap of materials, improve light absorption ability, promote charge separation, and provide adsorption sites to enhance the adsorption capacity for specific

pollutants. Wang, X. et al. prepared MOF-derived Pd, N-co-doped TiO_2, where the incorporation of N and the loading of Pd nanoparticles reduced the bandgap and enhanced the light absorption efficiency, enhanced charge separation and charge transfer ability, resulting in high photocatalytic oxidation activity and exhibiting strong adsorption and degradation efficiency for ethyl acetate (Wang et al., 2023). Liu, Y. et al. successfully introduced Pt ions into MOFs, forming abundant atomic Pt and oxygen vacancy content on the surface, and maintained the selectivity of toluene and CO_2 products at 100% (Liu et al., 2022b). Metal nanoclusters and MOF materials can be combined to form MOF-nanoparticle composite materials, in which the metal nanoclusters can effectively separate charges and enhance the material's regenerative ability. Lin, LY. et al. successfully loaded Ti-based nanoclusters onto NH_2-UiO-66(Zr), not only providing extended visible light absorption and high charge mobility but also effectively converting key intermediates in the toluene degradation process (Lin et al., 2023). Carbon-based porous materials have stable structures and contain abundant mesopores and macropores, which can provide excellent diffusion channels for gas molecules when combined with MOFs, thereby significantly enhancing the material's gas adsorption capacity. Tan, HC. et al. successfully composite graphene aerogels with MOF materials; the open mesoporous structure of graphene aerogels helps molecules of reactants and products enter and exit, showing extremely strong formaldehyde adsorption capacity (Tan et al., 2019).

In summary, MOF is a porous crystalline multifunctional material that is increasingly gaining attention due to its ultrahigh specific surface area. However, truly efficient and highly selective catalytic effects achieved by MOF materials are still very limited. It is still necessary to design highly efficient MOF materials that can respond to visible light. The morphology design and surface microstructure control of MOFs are of great significance for exploring the crystal growth mechanism and developing novel nanomaterials with excellent performance and prospects for applications.

The applications of different configuration MOF modification strategies in the field of photocatalytic degradation of VOCs are listed in Supplementary Table S5.

3.6.3 Burst keyword "oxygen vacancy"

"Oxygen Vacancy": In photocatalytic materials, oxygen vacancies are essential for improving photocatalytic activity as they can act as electron capture centers, thus improving charge separation efficiency and enhancing the catalytic response (Zhou et al., 2023). The formation of oxygen vacancies is due to the destruction of oxygen atoms in the crystal lattice, with oxygen atoms being removed from their original lattice positions. In Supplementary Figure S4, the keywords "doping," "etching," and "combustion" can be found, which suggest different strategies for forming oxygen vacancies. Ion doping breaks the long-term periodicity of the crystal lattice oxygen by replacing existing atoms with cations or anions, thus producing oxygen vacancies and ensuring charge balance (Dong et al., 2020). Dong, C. et al. obtained two-dimensional MnO_2 catalysts with different oxygen vacancy concentrations by doping Cu^{2+}, and the oxygen vacancies enhanced the catalyst's reducibility and oxygen species activity, thereby improving the catalytic activity for toluene oxidation. Acid–base etching uses the corrosive action of strong acids or strong bases to dissolve metal elements, thereby forming many vacancy defects (Liu et al., 2019). Liu, Y. et al. used 0.2 M HNO_3 to modify MnO_2, and the increased acid sites and acidity on the catalyst surface after acid treatment promoted the adsorption and activation of gaseous benzene. The efficiency of benzene-related compound degradation was improved by the increased oxygen vacancies in the crystal lattice and surface-adsorbed oxygen due to the acid treatment-induced active oxygen species. Reduction strategies can produce oxygen vacancies by inducing oxygen atoms to escape from the material surface (Xu et al., 2021). Xu, Y. et al. synthesized Cu-Mn composite oxide catalysts by the hydrothermal method and then modified them by a solid-phase reaction with urea for improvement. The photocatalyst obtained has a large number of oxygen vacancies, which increases the number of surface-adsorbed oxygen and enhances the mobility of lattice oxygen, thereby improving the catalyst's reducibility and oxygen activity. High-temperature calcination causes the surface atoms of the material to vibrate violently, and surface lattice oxygen is easily diffused out, leading to the formation of oxygen vacancies (Liu et al., 2003). Liu, H. et al. pretreated TiO_2 with H_2 gas at a high temperature of 500°C–600°C and detected the presence of oxygen vacancies through the intensity of the electron paramagnetic resonance (EPR) signal. They found that the presence of oxygen vacancies enhanced the photocatalytic activity and facilitated the degradation of phenol.

In summary, oxygen vacancies play an important role in adsorption and catalysis in the field of photocatalytic VOCs. It is crucial to clarify the generation mechanism and distribution conditions of oxygen vacancies. Since oxygen vacancies can exist in different catalyst positions, such as the surface, lattice, or other positions, clarifying their distribution locations can help analyze their catalytic oxidation mechanism. Second, it is necessary to clarify the formation process and form change of oxygen vacancies in the catalytic process and clarify their catalytic role. Finally, it is necessary to clarify the role of different schemes of oxygen vacancies in the catalytic oxidation of VOCs, such as promoting adsorption and activation, promoting lattice oxygen and electron transfer, anchoring precious metals, and providing Lewis acid sites.

"Efficient": Improving photocatalytic efficiency is a central goal of the current research, especially in the fields of energy conversion and environmental remediation. "Nanosheet": Nanosheets with two-dimensional structure are promising materials for improving photocatalytic efficiency due to their high specific surface area and unique electronic properties (Ou et al., 2022). These keywords reflect the latest research trends in photocatalysis, highlighting innovations in material synthesis, structural design, and understanding of reaction mechanisms. These studies are of great significance for future applications in fields such as energy conversion, environmental remediation, and chemical synthesis.

4 Conclusion

(1) A bibliometric study was conducted on the WoSCC database for VOC photocatalytic oxidation research from 1998 to 2023. Using information visualization analysis, we generated a

knowledge map. From 2000 to 2015, research on VOC photocatalytic oxidation showed a gradual increase trend and then rapidly upgraded after 2016. The most studied VOC gases are still benzene derivatives and formaldehyde, while alkanes and ethyl acetate are also relatively popular VOC gases.

(2) The basic information relationship diagram can help researchers identify the countries that have made major contributions to the field, as well as the authors and institutions. It can be seen that China has the most prolific authors, with the most papers published, with the Guangdong University of Technology's An Taicheng team being the most productive team in China, focusing on the degradation effects and mechanisms of ring-shaped VOCs using modified photocatalysts. Canada has a relatively concentrated research force in this field, with 106 papers published, with Concordia University's Haghighat Fariborz and Lee Chang-Seo team publishing 59 papers, focusing on the modification strategies of TiO_2 photocatalysts. Some countries, such as China and the United States, have close cooperation in this field. However, the research cooperation of other countries is relatively independent, highlighting the potential for enhanced global cooperation.

(3) The journal map shows that different journals have different emphases. From the current journal publication information, the development of catalysts is a top priority, especially the modification strategies and design of composite catalysts, while the development of new materials is relatively less emphasized. In terms of the degradation of pollutants, more attention is paid to pollutants that have a significant impact on human health, while less attention is paid to the natural oxidation of volatile organic compounds. Appl. Catal. B-Environ. and similar journals mainly report on the photocatalytic effects of porous materials and the combination strategies of composite catalysts. Appl. Surf. Sci. and other journals focus on the adsorption of VOC gases by catalysts. Journals such as Environ. Sci. Technol. are mainly dedicated to solving real-world environmental problems. If readers want to understand the mechanism of VOC gas degradation, they can refer to related journals such as J. Catal. Analyzing the most highly cited research, it was determined that following research must be conducted in this field: the catalyst's adsorption capacity, the catalyst's degradation efficiency, and the analysis of intermediate products and their harmfulness.

(4) In the field of VOC photocatalytic oxidation, the focus of front-end development is on developing and optimizing advanced photocatalysts with a high charge separation efficiency, improved adsorption performance, and expanded light response range. In-depth research on the VOC degradation process focuses on the mechanisms of charge generation and transfer within the photocatalyst and the detailed mechanism of catalytic oxidation, which is crucial for optimizing reaction conditions and improving catalytic efficiency. At the same time, research has been conducted on the stability and durability of the photocatalyst in long-term use, as well as the secondary pollutants that may arise during the photocatalytic process, to ensure the environmental friendliness and sustainability of the technology. TiO_2 remains the most studied catalyst. In terms of catalyst modification strategies, emphasis has been placed on designing novel material structures, such as MOFs, heterojunctions, manganese oxides, and nanocomposites, to improve the photocatalytic oxidation efficiency of VOCs. It is worth noting that the surface engineering and adsorption capacity of the catalyst are also research priorities in this field, with oxygen vacancies being a major research topic. Of course, the key step toward commercialization and large-scale application of photocatalytic VOC oxidation technology is to transform laboratory research results into practical applications and conduct comprehensive evaluations of environmental impact and cost-effectiveness.

Despite the development of many methods to enhance the photocatalyst's degradation of VOCs, the application of photocatalysis in removing VOCs still faces significant challenges. First, a composite of multiple materials needs to be developed to produce a synergistic effect, which may result in better photocatalytic performance than that of a single semiconductor material. Second, the adsorption effect of gaseous organic compounds on the catalyst surface and its mechanism also need to be explored. Another challenge is to develop efficient photocatalysts to solve the real difficulties at industrial scale. To solve the problem of scaling up, more collaboration is needed between researcher groups from different disciplines to bridge the gap between laboratory testing and actual application. In addition, a series of strategies need to be developed to effectively utilize visible light photocatalysts and improve new materials or design structures to degrade toxic intermediates/by-products generated during the photocatalytic degradation of VOCs. Therefore, further research should be conducted to identify these created materials.

Data availability statement

The raw data supporting the conclusions of this article will be made available by the authors, without undue reservation.

Author contributions

XZu: Writing–original draft, Visualization, Investigation. YS: Software, Methodology, Writing–original draft, Investigation. XL: Writing–original draft, Methodology, Investigation. JG: Writing–review and editing, Resources, Funding acquisition. XZg: Writing–review and editing, Supervision. GZ: Writing–original draft, Methodology. YG: Writing–review and editing, Supervision, Investigation, Funding acquisition.

Funding

The author(s) declare that financial support was received for the research, authorship, and/or publication of this article. The present

work was financially supported by the Natural Science Foundation of China (52270129, 52070127, and 52370142), Oriental Talent Youth Program, Shanghai Shuguang Program (23SG52), and Guizhou Provincial Key Technology R&D Program (QKHZC(2024)153). Dr. Guo also thanks the financial support of Science and Technology Development Fund of Pudong New Area (PKJ2022-C07 and PKJ2022-C10).

Conflict of interest

The authors declare that the research was conducted in the absence of any commercial or financial relationships that could be construed as a potential conflict of interest.

Publisher's note

Supplementary material

The Supplementary Material for this article can be found online at: https://www.frontiersin.org/articles/10.3389/fenvs.2024.1482766/full#supplementary-material

References

Alberici, R. M., and Jardim, W. F. (1997). Photocatalytic destruction of VOCs in the gas-phase using titanium dioxide. *Appl. Catal. B Environ.* 14, 55–68. doi:10.1016/S0926-3373(97)00012-X

Ayub, K. S., Zaman, W. Q., Miran, W., Ali, M., Abbas, Z., Mushtaq, U., et al. (2022). Efficient post-plasma catalytic degradation of toluene via series of Co–Cu/TiO_2 catalysts. *Res. Chem. Intermed.* 48, 4227–4248. doi:10.1007/s11164-022-04805-7

Belessiotis, G. V., Falara, P. P., Ibrahim, I., and Kontos, A. G. (2022). Magnetic metal oxide-based photocatalysts with integrated silver for water treatment. *Materials* 15, 4629. doi:10.3390/ma15134629

Cano-Casanova, L., Amorós-Pérez, A., Ouzzine, M., Román-Martínez, M. C., and Lillo-Ródenas, M. A. (2021). Enhancement of the TiO_2 photoactivity for propene oxidation by carbon incorporation using saccharose in hydrothermal synthesis. *J. Environ. Chem. Eng.* 9, 104941. doi:10.1016/j.jece.2020.104941

Cao, S., Fei, X., Wen, Y., Sun, Z., Wang, H., and Wu, Z. (2018). Bimodal mesoporous TiO_2 supported Pt, Pd and Ru catalysts and their catalytic performance and deactivation mechanism for catalytic combustion of Dichloromethane (CH_2Cl_2). *Appl. Catal. A General* 550, 20–27. doi:10.1016/j.apcata.2017.10.006

Carp, O., Huisman, C. L., and Reller, A. (2004). Photoinduced reactivity of titanium dioxide. *Prog. Solid State Chem.* 32, 33–177. doi:10.1016/j.progsolidstchem.2004.08.001

Che, L., Pan, J. L., Cai, K. X., Cong, Y. Q., and Lv, S. W. (2023). The construction of p-n heterojunction for enhancing photocatalytic performance in environmental application: a review. *Sep. Purif. Technol.* 315, 123708. doi:10.1016/j.seppur.2023.123708

Chen, C. (2004). Searching for intellectual turning points: progressive knowledge domain visualization. *Proc. Natl. Acad. Sci.* 101, 5303–5310. doi:10.1073/pnas.0307513100

Chen, C. C., Duh, Y. S., and Shu, C. M. (2009). Thermal polymerization of uninhibited styrene investigated by using microcalorimetry. *J. Hazard. Mater.* 163, 1385–1390. doi:10.1016/j.jhazmat.2008.07.151

Chen, J. Y., Guo, X. M., Lang, L., Yin, X. L., Wang, A. M., and Rui, Z. B. (2023c). Multifunctional Z-scheme Cu_xO/Ag/$SrTiO_3$ heterojunction for photothermocatalytic VOCs degradation and antibiosis. *Appl. Surf. Sci.* 618, 153275. doi:10.1016/j.apsusc.2022.153275

Chen, L., Wang, X., Rao, Z. P., Tang, Z. X., Wang, Y., Shi, G. S., et al. (2021). *In-situ* synthesis of Z-Scheme MIL-100(Fe)/α-Fe_2O_3 heterojunction for enhanced adsorption and Visible-light photocatalytic oxidation of O-xylene. *Chem. Eng. J.* 416, 129112. doi:10.1016/j.cej.2021.129112

Chen, L., Wang, X., Shi, G. S., Lu, G. H., Wang, Y., Xie, X. F., et al. (2023b). The regulation of Lewis acid/basic sites in NaFe bimetal MOXs for the controllable photocatalytic degradation of electron-rich/deficient VOCs. *Appl. Catal. B-Environmental* 334, 122850. doi:10.1016/j.apcatb.2023.122850

Chen, X. Y., Zhu, W. K., Feng, S. F., and Chen, J. Y. (2024). Photodegradation of xylene isomers: kinetics, mechanism, secondary pollutant formation potential and health risk evaluation. *J. Environ. Sci.* 136, 658–669. doi:10.1016/j.jes.2022.12.034

Chen, Y.-H., Yin, M.-Q., Fan, L.-H., Jiang, X.-C., Xu, H.-F., Zhang, T., et al. (2023a). Bibliometric analysis of traditional Chinese medicine research on heart failure in the 21st century based on the WOS database. *Heliyon* 9, e12770. doi:10.1016/j.heliyon.2022.e12770

Cheng, S., Chang-Chien, G.-P., Huang, Q., Zhang, Y.-B., Yan, P., Zhang, J., et al. (2019). Global research trends in health effects of volatile organic compounds during the last 16 Years: a bibliometric analysis. *Aerosol Air Qual. Res.* 19, 1834–1843. doi:10.4209/aaqr.2019.06.0327

Deng, X., Zhang, D. Y., Lu, S. H., Bao, T., Yu, Z. M., and Deng, C. X. (2021). Green synthesis of Ag/g-C3N4 composite materials as a catalyst for DBD plasma in degradation of ethyl acetate. *Mater. Sci. Eng. B-Advanced Funct. Solid-State Mater.* 272, 115321. doi:10.1016/j.mseb.2021.115321

Dong, C., Qu, Z. P., Jiang, X., and Ren, Y. W. (2020). Tuning oxygen vacancy concentration of MnO_2 through metal doping for improved toluene oxidation. *J. Hazard. Mater.* 391, 122181. doi:10.1016/j.jhazmat.2020.122181

Dong, F., Guo, S., Wang, H., Li, X., and Wu, Z. (2011). Enhancement of the visible light photocatalytic activity of C-doped TiO_2 nanomaterials prepared by a green synthetic approach. *J. Phys. Chem. C* 115, 13285–13292. doi:10.1021/jp111916q

Dong, Y. P., Ji, P. Z., Xu, X. Y., Li, R., Wang, Y., Homewood, K. P., et al. (2024). Rational design and construction of a CdS QDs/$InVO_4$ atomic-layer (110)/(110) facet S-scheme heterojunction for highly efficient photocatalytic degradation of C_2H_4. *Energy and Environ. Mater.* 7. doi:10.1002/eem2.12643

Emran, M. Y., Miran, W., Gomaa, H., Ibrahim, I., Belessiotis, G. V., Abdelwahab, A. A., et al. (2022). "Biowaste materials for advanced biodegradable packaging technology," in *Handbook of biodegradable materials*. Editors G. A. M. Ali and A. S. H. Makhlouf (Cham: Springer International Publishing), 1–37.

Enesca, A. (2020). Enhancing the photocatalytic activity of SnO_2-TiO_2 and ZnO-TiO_2 tandem structures toward indoor air decontamination. *Front. Chem.* 8, 583270. doi:10.3389/fchem.2020.583270

Farideh, OSAREH (1996). Bibliometrics, citation analysis and Co-citation analysis: a review of literature I. *Libri* 46. doi:10.1515/libr.1996.46.3.149

Filley, C. M., Halliday, W., and Kleinschmidt-DeMasters, B. K. (2004). The effects of toluene on the central nervous system. *J. Neuropathology Exp. Neurology* 63, 1–12. doi:10.1093/jnen/63.1.1

Gaffney, J. S., Marley, N. A., and Blake, D. R. (2012). Baseline measurements of ethene in 2002: implications for increased ethanol use and biomass burning on air quality and ecosystems. *Atmos. Environ.* 56, 161–168. doi:10.1016/j.atmosenv.2012.04.002

Hahm, M., Lee, J., Lee, M. Y., and Byeon, S. H. (2016). Health risk assessment of occupational exposure to styrene depending on the type of industry: data from the Workplace Environmental Monitoring Program in Korea. *Hum. Ecol. Risk Assess.* 22, 1312–1322. doi:10.1080/10807039.2016.1168691

Halios, C. H., Landeg-Cox, C., Lowther, S. D., Middleton, A., Marczylo, T., and Dimitroulopoulou, S. (2022). Chemicals in European residences – Part I: a review of emissions, concentrations and health effects of volatile organic compounds (VOCs). *Sci. Total Environ.* 839, 156201. doi:10.1016/j.scitotenv.2022.156201

Hamada, K., Ochiai, T., Aoki, D., Akutsu, Y., and Hirabayashi, Y. (2022). Decomposition of gaseous styrene using photocatalyst and ozone treatment. *Catalysts* 12, 316. doi:10.3390/catal12030316

Higashimoto, S., Katsuura, K., Yamamoto, M., and Takahashi, M. (2020). Photocatalytic activity for decomposition of volatile organic compound on Pt-WO_3 enhanced by simple physical mixing with TiO2. *Catal. Commun.* 133, 105831. doi:10.1016/j.catcom.2019.105831

Hoffmann, M. R., Martin, S. T., Choi, W., and Bahnemann, D. W. (1995). Environmental applications of semiconductor photocatalysis. *Chem. Rev.* 95, 69–96. doi:10.1021/cr00033a004

Iso, I. (2011). 16000–6: 2011 indoor air—part. 6: determination of volatile organic compounds in indoor and test chamber air by active sampling on tenax TA sorbent, thermal desorption and gas chromatography using MS or MS-FID. *Therm. Desorption Gas Chromatogr. Using MS or MS-FID.*

Jakab, M. G., Klupp, T., Besenyei, K., Biró, A., Major, J., and Tompa, A. (2010). Formaldehyde-induced chromosomal aberrations and apoptosis in peripheral blood lymphocytes of personnel working in pathology departments. *Mutat. Research-Genetic Toxicol. Environ. Mutagen.* 698, 11–17. doi:10.1016/j.mrgentox.2010.02.015

Jansson, I., Suárez, S., Garcia-Garcia, F. J., and Sánchez, B. (2015). Zeolite–TiO_2 hybrid composites for pollutant degradation in gas phase. *Appl. Catal. B Environ.* 178, 100–107. doi:10.1016/j.apcatb.2014.10.022

Jia, Y., Zhang, X., Wang, R. Y., Yuan, J., Zheng, R. Z., Zhang, J. Q., et al. (2023). Energy band engineering of WO_3/Bi_2WO_6 direct Z-scheme for enhanced photocatalytic toluene degradation. *Appl. Surf. Sci.* 618, 156636. doi:10.1016/j.apsusc.2023.156636

Kamani, H., Baniasadi, M., Abdipour, H., Mohammadi, L., Rayegannakhost, S., Moein, H., et al. (2023). Health risk assessment of BTEX compounds (benzene, toluene, ethylbenzene and xylene) in different indoor air using Monte Carlo simulation in zahedan city, Iran. *Heliyon* 9, e20294. doi:10.1016/j.heliyon.2023.e20294

Kholidah, H., Hijriah, H. Y., Mawardi, I., Huda, N., Herianingrum, S., and Alkausar, B. (2022). A Bibliometric mapping of peer-to-peer lending research based on economic and business perspective. *Heliyon* 8, e11512. doi:10.1016/j.heliyon.2022.e11512

Kim, K. H., Jahan, S. A., and Lee, J. T. (2011). Exposure to formaldehyde and its potential human health hazards. *J. Environ. Sci. Health Part C-Environmental Carcinog. and Ecotoxicol. Rev.* 29, 277–299. doi:10.1080/10590501.2011.629972

Kim, S., Kim, S., and Lee, S. (2023). Activated carbon modified with polyethyleneimine and MgO: better adsorption of aldehyde and production of regenerative VOC adsorbent using a photocatalyst. *Appl. Surf. Sci.* 631, 157565. doi:10.1016/j.apsusc.2023.157565

Kim, S. B., and Hong, S. C. (2002). Kinetic study for photocatalytic degradation of volatile organic compounds in air using thin film TiO_2 photocatalyst. *Appl. Catal. B Environ.* 35, 305–315. doi:10.1016/S0926-3373(01)00274-0

Kong, J., Xiang, Z., Li, G., and An, T. (2020). Introduce oxygen vacancies into CeO_2 catalyst for enhanced coke resistance during photothermocatalytic oxidation of typical VOCs. *Appl. Catal. B Environ.* 269, 118755. doi:10.1016/j.apcatb.2020.118755

Korsak, Z., Rydzynski, K., Stetkiewicz, J., Świercz, R., and Jajte, J. (1995). Toxic effects of 1,2,4-trimethylbenzene (pseudocumene) after acute and subchronic inhalation exposure. *Toxicol. Lett.* 78, 49. doi:10.1016/0378-4274(95)94806-R

Kovalevskiy, N., Selishchev, D., Svintsitskiy, D., Selishcheva, S., Berezin, A., and Kozlov, D. (2020). Synergistic effect of polychromatic radiation on visible light activity of N-doped TiO_2 photocatalyst. *Catal. Commun.* 134, 105841. doi:10.1016/j.catcom.2019.105841

Kräuter, J., Franz, E., Waidhas, F., Brummel, O., Libuda, J., and Al-Shamery, K. (2022). The role of defects in the photoconversion of 2-propanol on rutile titania: operando spectroscopy combined with elementary studies. *J. Catal.* 406, 134–144. doi:10.1016/j.jcat.2021.12.025

Kunaseth, M., Poldorn, P., Junkeaw, A., Meeprasert, J., Rungnim, C., Namuangruk, S., et al. (2017). A DFT study of volatile organic compounds adsorption on transition metal deposited graphene. *Appl. Surf. Sci.* 396, 1712–1718. doi:10.1016/j.apsusc.2016.11.238

Le, M. C., Le, T. H., Thi, T. H. B., Nguyen, Q. D., Thi, T. H., and Thi, M. N. T. (2021). Synthesizing and evaluating the photocatalytic and antibacterial ability of TiO_2/SiO_2 nanocomposite for silicate coating. *Front. Chem.* 9, 738969. doi:10.3389/fchem.2021.738969

Li, H., Sun, Q. Y., Li, F., Wang, B. S., and Zhu, B. L. (2024). Metabolomics of benzene exposure and development of biomarkers for exposure hazard assessment. *Metabolites* 14, 377. doi:10.3390/metabo14070377

Li, J., Mo, S., Ding, X., Huang, L., Zhou, X., Fan, Y., et al. (2023a). Hollow cavity engineering of MOFs-derived hierarchical MnO_x structure for highly efficient photothermal degradation of ethyl acetate under light irradiation. *Chem. Eng. J.* 464, 142412. doi:10.1016/j.cej.2023.142412

Li, J. L., Li, H., Li, K., Chen, Y., Zhang, H., Zhang, X., et al. (2021). Enhanced secondary organic aerosol formation from the photo-oxidation of mixed anthropogenic volatile organic compounds. *Atmos. Chem. Phys.* 21, 7773–7789. doi:10.5194/acp-21-7773-2021

Li, M., Ma, L., Luo, L., Liu, Y., Xu, M., Zhou, H., et al. (2022a). Efficient photocatalytic epoxidation of styrene over a quantum-sized SnO_2 on carbon nitride as a heterostructured catalyst. *Appl. Catal. B Environ.* 309, 121268. doi:10.1016/j.apcatb.2022.121268

Li, X., Fang, G. G., Qian, X. R., and Tian, Q. W. (2022b). Z-scheme heterojunction of low conduction band potential MnO_2 and biochar-based g-C_3N_4 for efficient formaldehyde degradation. *Chem. Eng. J.* 428, 131052. doi:10.1016/j.cej.2021.131052

Li, X. Y., Li, J. A., Shi, Y., Zhang, M. M., Fan, S. Y., Yin, Z. F., et al. (2018). Rational design of cobalt and nitrogen co-doped carbon hollow frameworks for efficient photocatalytic degradation of gaseous toluene. *J. Colloid Interface Sci.* 528, 45–52. doi:10.1016/j.jcis.2018.05.067

Li, Y., Du, Q., Zhang, J., Jiang, Y., Zhou, J., and Ye, Z. (2023b). Visualizing the intellectual landscape and evolution of transportation system resilience: a bibliometric analysis in CiteSpace. *Dev. Built Environ.* 14, 100149. doi:10.1016/j.dibe.2023.100149

Li, Y., Ouyang, S., Xu, H., Wang, X., Bi, Y., Zhang, Y., et al. (2016). Constructing solid–gas-interfacial fenton reaction over alkalinized-C3N4 photocatalyst to achieve apparent quantum yield of 49% at 420 nm. *J. Am. Chem. Soc.* 138, 13289–13297. doi:10.1021/jacs.6b07272

Li, Y. W., Li, S. Z., Zhao, M. B., and Ma, W. L. (2023c). Decahedral $BiVO_4$/tubular g-C_3N_4 S-scheme heterojunction photocatalyst for formaldehyde removal: charge transfer pathway and deactivation mechanism. *Sep. Purif. Technol.* 327, 124966. doi:10.1016/j.seppur.2023.124966

Lin, L. Y., Liu, C. H., Dang, V. D., and Fu, H. T. (2023). Atomically dispersed Ti-O clusters anchored on NH_2-UiO-66(Zr) as efficient and deactivation-resistant photocatalyst for abatement of gaseous toluene under visible light. *J. Colloid Interface Sci.* 635, 323–335. doi:10.1016/j.jcis.2022.12.147

Lin, Z. F., Shen, W. H., Chen, X. Q., Corriou, J. P., and Xi, H. X. (2020). Impact of intermediate products on benzene photocatalytic oxidation in pulp mills: experimental and adsorption simulation study. *Appl. Surf. Sci.* 529, 147130. doi:10.1016/j.apsusc.2020.147130

Liu, H., Ma, H. T., Li, X. Z., Li, W. Z., Wu, M., and Bao, X. H. (2003). The enhancement of TiO_2 photocatalytic activity by hydrogen thermal treatment. *Chemosphere* 50, 39–46. doi:10.1016/s0045-6535(02)00486-1

Liu, Y., Chen, G. D., Chen, J. J., and Niu, H. J. Y. (2022b). Excellent catalytic performance of Ce-mof with abundant oxygen vacancies supported noble metal Pt in the oxidation of toluene. *Catalysts* 12, 775. doi:10.3390/catal12070775

Liu, Y., Cheng, Z., Liu, S., Ren, Y., Yuan, T., Zhang, X., et al. (2022a). A quantitative structure activity relationship (QSAR) model for predicting the rate constant of the reaction between VOCs and NO_3 radicals. *Chem. Eng. J.* 448, 136413. doi:10.1016/j.cej.2022.136413

Liu, Y., Zhou, H., Cao, R. R., Liu, X. Y., Zhang, P. Y., Zhan, J. J., et al. (2019). Facile and green synthetic strategy of birnessite-type MnO_2 with high efficiency for airborne benzene removal at low temperatures. *Appl. Catal. B-Environmental* 245, 569–582. doi:10.1016/j.apcatb.2019.01.023

Ma, J. X., An, L. Q., Liu, D. M., Yao, J. X., Qi, D. P., Xu, H. B., et al. (2022). A light-permeable solar evaporator with three-dimensional photocatalytic sites to boost volatile-organic-compound rejection for water purification. *Environ. Sci. and Technol.* 56, 9797–9805. doi:10.1021/acs.est.2c01874

Mamaghani, A. H., Haghighat, F., and Lee, C.-S. (2017). Photocatalytic oxidation technology for indoor environment air purification: the state-of-the-art. *Appl. Catal. B Environ.* 203, 247–269. doi:10.1016/j.apcatb.2016.10.037

Man, Z., Meng, Y., Lin, X. C., Dai, X. R., Wang, L. P., and Liu, D. Z. (2022). Assembling UiO-66@TiO_2 nanocomposites for efficient photocatalytic degradation of dimethyl sulfide. *Chem. Eng. J.* 431, 133952. doi:10.1016/j.cej.2021.133952

Marks, S. D., Riascos-Rodriguez, K., Arrieta-Pérez, R. R., Yakovenko, A. A., Exley, J., Evans, P. G., et al. (2020). Lattice expansion and ligand twist during CO_2 adsorption in flexible Cu bipyridine metal-organic frameworks. *J. Mater. Chem. A* 8, 18903–18915. doi:10.1039/d0ta03298k

Mo, J., Zhang, Y., Xu, Q., Zhu, Y., Lamson, J. J., and Zhao, R. (2009). Determination and risk assessment of by-products resulting from photocatalytic oxidation of toluene. *Appl. Catal. B Environ.* 89, 570–576. doi:10.1016/j.apcatb.2009.01.015

Montini, T., Melchionna, M., Monai, M., and Fornasiero, P. (2016). Fundamentals and catalytic applications of CeO_2-based materials. *Chem. Rev.* 116, 5987–6041. doi:10.1021/acs.chemrev.5b00603

Moura, L., and Picão, R. C. (2022). "Chapter 23 - removal of antimicrobial resistance determinants from wastewater: a risk perspective on conventional and emerging technologies," in *Emerging contaminants in the environment*. Editors H. Sarma, D. C. Dominguez, and W.-Y. Lee (Elsevier), 603–642.

Mu, Y., and Williams, P. T. (2022). Recent advances in the abatement of volatile organic compounds (VOCs) and chlorinated-VOCs by non-thermal plasma technology: a review. *Chemosphere* 308, 136481. doi:10.1016/j.chemosphere.2022.136481

Ni, Q., Amalfitano, N., Biasioli, F., Gallo, L., Tagliapietra, F., and Bittante, G. (2022). Bibliometric review on the volatile organic compounds in meat. *Foods* 11, 3574. doi:10.3390/foods11223574

Obee, T. N., and Brown, R. T. (1995). TiO_2 photocatalysis for indoor air applications: effects of humidity and Trace contaminant levels on the oxidation rates of formaldehyde, toluene, and 1,3-butadiene. *Environ. Sci. and Technol.* 29, 1223–1231. doi:10.1021/es00005a013

Ohtani, B. (2008). Preparing articles on photocatalysis—beyond the illusions, misconceptions, and speculation. *Chem. Lett.* 37, 216–229. doi:10.1246/cl.2008.216

Ollis, D. F. (2000). Photocatalytic purification and remediation of contaminated air and water. *Comptes Rendus l'Académie Sci. - Series IIC - Chemistry* 3, 405–411. doi:10.1016/S1387-1609(00)01169-5

Ou, K., Liu, J., Dou, Q., Zhou, Y., Zeng, Y., and Zhang, J. (2022). High-pressure modified mesoporous Zr-BTB nanosheets with enhanced photocatalyst activity. *Colloids Surfaces A Physicochem. Eng. Aspects* 649, 129511. doi:10.1016/j.colsurfa.2022.129511

Pan, X., Yan, E., Cui, M., and Hua, W. (2018). Examining the usage, citation, and diffusion patterns of bibliometric mapping software: a comparative study of three tools. *J. Inf.* 12, 481–493. doi:10.1016/j.joi.2018.03.005

Pelaez, M., Nolan, N. T., Pillai, S. C., Seery, M. K., Falaras, P., Kontos, A. G., et al. (2012). A review on the visible light active titanium dioxide photocatalysts for environmental applications. *Appl. Catal. B Environ.* 125, 331–349. doi:10.1016/j.apcatb.2012.05.036

Qian, Y. H., Ma, D. G., and Zhong, J. B. (2021). Metal-organic frameworks with variable valence metal-photoactive components: emerging platform for volatile organic compounds photocatalytic degradation. *Front. Chem.* 9, 749839. doi:10.3389/fchem.2021.749839

Qin, J. X., Pei, Y., Zheng, Y., Ye, D. Q., and Hu, Y. (2023). Fe-MOF derivative photocatalyst with advanced oxygen reduction capacity for indoor pollutants removal. *Appl. Catal. B-Environmental* 325, 122346. doi:10.1016/j.apcatb.2022.122346

Qiu, X., Miyauchi, M., Sunada, K., Minoshima, M., Liu, M., Lu, Y., et al. (2012). Hybrid Cu_xO/TiO_2 nanocomposites as risk-reduction materials in indoor environments. *ACS Nano* 6, 1609–1618. doi:10.1021/nn2045888

Rinsky, R. A. (1989). Benzene and leukemia: an epidemiologic risk assessment. *Environ. Health Perspect.* 82, 189–191. doi:10.1289/ehp.8982189

Rong, X., Cao, Q., Gao, Y., Du, X., Dou, H. W., Yan, M., et al. (2023). Performance optimization and kinetic analysis of HNO_3 coupled with microwave rapidly modified coconut shell activated carbon for VOCs adsorption. *Front. Energy Res.* 10. doi:10.3389/fenrg.2022.1047254

Rudel, R. A., Camann, D. E., Spengler, J. D., Korn, L. R., and Brody, J. G. (2003). Phthalates, alkylphenols, pesticides, polybrominated diphenyl ethers, and other endocrine-disrupting compounds in indoor air and dust. *Environ. Sci. and Technol.* 37, 4543–4553. doi:10.1021/es0264596

Sati, P. C., Khaliq, F., Vaney, N., Ahmed, T., Tripathi, A. K., and Banerjee, B. D. (2011). Pulmonary function and oxidative stress in workers exposed to styrene in plastic factory: occupational hazards in Styrene-exposed plastic factory workers. *Hum. and Exp. Toxicol.* 30, 1743–1750. doi:10.1177/0960327111401436

Seltenrich, N. (2015). New link in the food chain? Marine plastic pollution and seafood safety. *Environ. Health Perspect.* 123, A34–A41. doi:10.1289/ehp.123-A34

Şenocak, E., and Arpaci, İ. (2023). A bibliometric analysis on nanoscience and nanotechnology education research. *Turk. Kim. Dernegi Derg. Kısım C. Kim. Egitimi* 8, 1–30. doi:10.37995/jotcsc.1202851

Shayegan, Z., Lee, C.-S., and Haghighat, F. (2018). TiO_2 photocatalyst for removal of volatile organic compounds in gas phase – a review. *Chem. Eng. J.* 334, 2408–2439. doi:10.1016/j.cej.2017.09.153

Shi, L., Xue, J. Q., Xiao, W., Wang, P., Long, M. Y., and Bi, Q. (2022). Efficient degradation of VOCs using semi-coke activated carbon loaded ternary Z-scheme heterojunction photocatalyst $BiVO_4$-$BiPO_4$-g-C_3N_4 under visible light irradiation. *Phys. Chem. Chem. Phys.* 24, 22987–22997. doi:10.1039/d2cp03606a

Sleiman, M., Conchon, P., Ferronato, C., and Chovelon, J.-M. (2009). Photocatalytic oxidation of toluene at indoor air levels (ppbv): towards a better assessment of conversion, reaction intermediates and mineralization. *Appl. Catal. B Environ.* 86, 159–165. doi:10.1016/j.apcatb.2008.08.003

Song, B. Y., Wang, Z. C., Ma, W., Zhou, W. S., Tang, Q., Bao, X. L., et al. (2024). Photocatalytic oxidation mechanism of isoprene over titanium oxide by UV-Vis lights. *J. Catal.* 430, 115362. doi:10.1016/j.jcat.2024.115362

Song, S. N., Zhang, S. Y., Zhang, X. L., Verma, P., and Wen, M. C. (2020). Advances in catalytic oxidation of volatile organic compounds over Pd-supported catalysts: recent trends and challenges. *Front. Mater.* 7. doi:10.3389/fmats.2020.595667

Songur, A., Ozen, O. A., and Sarsilmaz, M. (2010). The toxic effects of formaldehyde on the nervous system, *Rev. Environ. Contam. Toxicol.* 203, 105–118. doi:10.1007/978-1-4419-1352-4_3

Suárez, S., Coronado, J. M., Portela, R., Martín, J. C., Yates, M., Avila, P., et al. (2008). On the preparation of TiO_2–Sepiolite hybrid materials for the photocatalytic degradation of TCE: influence of TiO_2 distribution in the mineralization. *Environ. Sci. and Technol.* 42, 5892–5896. doi:10.1021/es703257w

Sui, Y., Lu, D., Zhu, X., Guan, J., Li, F., Shen, J., et al. (2024). Insight into recycling spent power ternary cathode materials: towards preparation of Mn-based catalyst for efficient toluene removal. *Surfaces Interfaces* 46, 104086. doi:10.1016/j.surfin.2024.104086

Sun, X. J., Gu, X. L., Xu, W. T., Chen, W. J., Xia, Q. B., Pan, X. Y., et al. (2019). Novel hierarchical Fe(III)-Doped Cu-MOFs with enhanced adsorption of benzene vapor. *Front. Chem.* 7, 652. doi:10.3389/fchem.2019.00652

Tan, H. C., Chen, D. Y., Li, N. J., Xu, Q. F., Li, H., He, J. H., et al. (2019). Platinum-supported zirconia nanotube arrays supported on graphene aerogels modified with metal-organic frameworks: adsorption and oxidation of formaldehyde at room temperature. *Chemistry-a Eur. J.* 25, 16718–16724. doi:10.1002/chem.201904426

van Eck, N. J., and Waltman, L. (2010). Software survey: VOSviewer, a computer program for bibliometric mapping. *Scientometrics* 84, 523–538. doi:10.1007/s11192-009-0146-3

Wang, D. W., Li, Z. W., Zhou, J., Fang, H., He, X., Jena, P. R., et al. (2018). Simultaneous detection and removal of formaldehyde at room temperature: janus Au@ZnO@ZIF-8 nanoparticles. *Nano-Micro Lett.* 10, 4. doi:10.1007/s40820-017-0158-0

Wang, L., Tang, M., Jiang, H., Dai, J., Cheng, R., Luo, B., et al. (2024). Sustainable, efficient, and synergistic photocatalytic degradation toward organic dyes and formaldehyde gas via Cu_2O NPs@wood. *J. Environ. Manag.* 351, 119676. doi:10.1016/j.jenvman.2023.119676

Wang, S., Ang, H. M., and Tade, M. O. (2007). Volatile organic compounds in indoor environment and photocatalytic oxidation: state of the art. *Environ. Int.* 33, 694–705. doi:10.1016/j.envint.2007.02.011

Wang, X., Wu, L. K., Wang, Z. W., Feng, Y., Liu, Y. X., Dai, H. X., et al. (2023). Photothermal synergistic catalytic oxidation of ethyl acetate over MOFs-derived mesoporous N-TiO_2 supported Pd catalysts. *Appl. Catal. B-Environmental* 322, 122075. doi:10.1016/j.apcatb.2022.122075

Wang, Y., Voliotis, A., Shao, Y. Q., Zong, T. M., Meng, X. X. Y., Du, M., et al. (2021). Phase state of secondary organic aerosol in chamber photo-oxidation of mixed precursors. *Atmos. Chem. Phys.* 21, 11303–11316. doi:10.5194/acp-21-11303-2021

Xu, X. Y., Su, Y. H., Dong, Y. P., Luo, X., Wang, S. H., Zhou, W. Y., et al. (2022). Designing and fabricating a CdS QDs/Bi_2MoO_6 monolayer S-scheme heterojunction for highly efficient photocatalytic C2H4 degradation under visible light. *J. Hazard. Mater.* 424, 127685. doi:10.1016/j.jhazmat.2021.127685

Xu, Y., Qu, Z. P., Ren, Y. W., and Dong, C. (2021). Enhancement of toluene oxidation performance over Cu-Mn composite oxides by regulating oxygen vacancy. *Appl. Surf. Sci.* 560, 149983. doi:10.1016/j.apsusc.2021.149983

Yang, J., Li, L., Fu, F., Xu, H., Da, K., Cao, S. B., et al. (2023b). Construction of Z-scheme Ag/AgCl/Bi_2WO_6 photocatalysts with enhanced visible-light photocatalytic performance for gaseous toluene degradation. *Appl. Surf. Sci.* 610, 155598. doi:10.1016/j.apsusc.2022.155598

Yang, J., Yang, L., Fang, M., Li, L., Fu, F., Xu, H., et al. (2023a). A compact Z-scheme heterojunction of BiOCl/Bi_2WO_6 for efficiently photocatalytic degradation of gaseous toluene. *J. Colloid Interface Sci.* 631, 44–54. doi:10.1016/j.jcis.2022.11.023

Yao, P. Z., Liu, H. L., Wang, D. T., Chen, J. Y., Li, G. Y., and An, T. C. (2018). Enhanced visible-light photocatalytic activity to volatile organic compounds degradation and deactivation resistance mechanism of titania confined inside a metal-organic framework. *J. Colloid Interface Sci.* 522, 174–182. doi:10.1016/j.jcis.2018.03.075

Ying, T. T., Liu, W., Yang, L. X., Zhang, S. Q., Wu, Z. Y., Li, J. Y., et al. (2024). S-scheme construction boosts highly active self-supporting CeO_2/Cu_2O photocatalyst for efficient degradation of indoor VOCs. *Sep. Purif. Technol.* 330, 125272. doi:10.1016/j.seppur.2023.125272

Yoon, H. I., Hong, Y. C., Cho, S. H., Kim, H., Kim, Y. H., Sohn, J. R., et al. (2010). Exposure to volatile organic compounds and loss of pulmonary function in the elderly. *Eur. Respir. J.* 36, 1270–1276. doi:10.1183/09031936.00153509

Yu, X., Hu, Y., Luan, X. Q., Shah, S. J., Liu, L. M., Li, C. H., et al. (2023). Microwave-assisted construction of MXene/MOF aerogel via N-metal bonds for efficient photodegradation of vapor acetone under high humidity. *Chem. Eng. J.* 476, 146878. doi:10.1016/j.cej.2023.146878

Zhang, J. H., Hu, Y., Qin, J. X., Yang, Z. X., and Fu, M. L. (2020). TiO_2-UiO-66-NH_2 nanocomposites as efficient photocatalysts for the oxidation of VOCs. *Chem. Eng. J.* 385, 123814. doi:10.1016/j.cej.2019.123814

Zhang, X., Xiang, W., Miao, X., Li, F., Qi, G., Cao, C., et al. (2022a). Microwave biochars produced with activated carbon catalyst: characterization and sorption of volatile organic compounds (VOCs). *Sci. Total Environ.* 827, 153996. doi:10.1016/j.scitotenv.2022.153996

Zhang, X. D., Yue, K., Rao, R. Z., Chen, J. F., Liu, Q., Yang, Y., et al. (2022c). Synthesis of acidic MIL-125 from plastic waste: significant contribution of N orbital for efficient photocatalytic degradation of chlorobenzene and toluene. *Appl. Catal. B-Environmental* 310, 121300. doi:10.1016/j.apcatb.2022.121300

Zhang, Z., Wu, X., Liu, H., Huang, X., Chen, Q., Guo, X., et al. (2023). A systematic review of microplastics in the environment: sampling, separation, characterization and coexistence mechanisms with pollutants. *Sci. Total Environ.* 859, 160151. doi:10.1016/j.scitotenv.2022.160151

Zhang, Z., Wu, X., Zhang, J., and Huang, X. (2022b). Distribution and migration characteristics of microplastics in farmland soils, surface water and sediments in Caohai Lake, southwestern plateau of China. *J. Clean. Prod.* 366, 132912. doi:10.1016/j.jclepro.2022.132912

Zhao, C., Wang, Z. H., Chen, X., Chu, H. Y., Fu, H. F., and Wang, C. C. (2020). Robust photocatalytic benzene degradation using mesoporous disk-like N-TiO_2 derived from MIL-125(Ti). *Chin. J. Catal.* 41, 1186–1197. doi:10.1016/s1872-2067(19)63516-3

Zhao, J., and Yang, X. (2003). Photocatalytic oxidation for indoor air purification: a literature review. *Build. Environ.* 38, 645–654. doi:10.1016/S0360-1323(02)00212-3

Zhong, L., Haghighat, F., Blondeau, P., and Kozinski, J. (2010). Modeling and physical interpretation of photocatalytic oxidation efficiency in indoor air applications. *Build. Environ.* 45, 2689–2697. doi:10.1016/j.buildenv.2010.05.029

Zhou, H., Wang, Y., Wu, J., Zhou, W., Qi, Y., Liu, Q., et al. (2023). Enhanced photocatalytic reduction of CO_2 using a novel 2D/0D SnS_2/CeO_2 binary photocatalyst with Z-scheme heterojunction and oxygen vacancy. *J. CO2 Util.* 76, 102591. doi:10.1016/j.jcou.2023.102591

Zhou, S., He, R. H., Pei, J. C., Liu, W. P., Huang, Z. H., Liu, X. G., et al. (2022). Self-Regulating solar steam generators enable volatile organic compound removal through *in situ* H_2O_2 generation. *Environ. Sci. and Technol.* 56, 10474–10482. doi:10.1021/acs.est.2c02067

Zou, X. J., Dong, Y. Y., Ke, J., Ge, H., Chen, D., Sun, H. J., et al. (2020). Cobalt monoxide/tungsten trioxide p-n heterojunction boosting charge separation for efficient visible-light-driven gaseous toluene degradation. *Chem. Eng. J.* 400, 125919. doi:10.1016/j.cej.2020.125919

frontiers | Frontiers in Environmental Science

TYPE Original Research
PUBLISHED 05 November 2024
DOI 10.3389/fenvs.2024.1505162

OPEN ACCESS

EDITED BY
Yaoguang Guo,
Shanghai Polytechnic University, China

REVIEWED BY
Yiming Tang,
South China Normal University, China
Fei He,
Korea Institute of Energy Technology, Republic of Korea
Shuo Zhang,
King Abdullah University of Science and Technology, Saudi Arabia

*CORRESPONDENCE
Ying Huang,
huangyingdhu@163.com
Kan Wang,
wangkan@nbu.edu.cn

RECEIVED 02 October 2024
ACCEPTED 21 October 2024
PUBLISHED 05 November 2024

CITATION
Chen J, Wen H, Yu C, Yin Y, Zhang Y, Wang H, Huang Y and Wang K (2024) Photodegradation of clofibric acid in urban, town, and rural waters: important roles of dissolved organic matter composition.
Front. Environ. Sci. 12:1505162.
doi: 10.3389/fenvs.2024.1505162

Photodegradation of clofibric acid in urban, town, and rural waters: important roles of dissolved organic matter composition

Jingting Chen, Hairong Wen, Chunlei Yu, Yuxuan Yin, Yidi Zhang, Hongbin Wang, Ying Huang* and Kan Wang*

School of Civil and Environmental Engineering and Geography Science, Ningbo University, Ningbo, Zhejiang, China

Natural photolysis was the primary pathway for the transformation of pharmaceutical contaminants in surface water, whereas it could be easily influenced by dissolved organic matter (DOM). This study examined the complex effects of DOM on clofibric acid (CA) photodegradation in urban, town, and rural waters. Our results indicated rural water was the most conducive to CA photolysis followed by town water, then urban water. Quenching experiments revealed humic acid (HA) influenced the direct photolysis of CA mainly through two physical ways: internal filtering and active site competition. Reactive oxygen species were identified to be the main reason for CA photodegradation with fulvic acid (FA) or tyrosine (Tyr) involved, including hydroxyl radicals ($OH^{\bullet}$), singlet oxygen ($^1O_2$), and excited triplet DOM ($^3DOM^*$). We found that hydroxyl radical oxidation, C-O bond breaking, dechlorination, and rechlorination occurred in CA photolysis. Comparative eco-toxicity results showed that the toxicity of products during the CA natural photodegradation process with DOM involved was higher than CA itself, especially in urban waters. This finding emphasized the potential ecological risk of direct CA discharges in natural water and the need to develop risk management strategies that were critical to the health and sustainability of ecosystems.

KEYWORDS

DOM, clofibric acid, photodegradation, reactive oxygen species, ecotoxicity assessment

1 Introduction

Clofibric acid (CA) was a representative of high-risk PPCPs (pharmaceuticals and personal care products), which was an active metabolite of lipid-lowering drugs. It mainly entered natural water through domestic sewage, hospital wastewater, and industrial emissions (Andreozzi et al., 2003). CA existed in water over the long term with relatively low concentrations (ng/L-μg/L) (Li et al., 2012). It had adverse effects on human health and the ecological environment (Nakada et al., 2007; Yang et al., 2017).

The photolysis in natural water was the primary degradation pathway for a multitude of pollutants in surface water bodies. Photolysis had distinct advantages over alternative methods, including eco-friendliness and high efficiency (Yu et al., 2023; Pan et al., 2023).

Researchers reported that photodegradation played an important role in the migration of PPCPs (Cheng et al., 2024). Packer et al. (2003) found that CA underwent direct and indirect degradation under sunlight irradiation. Nevertheless, the photodegradation of CA could be influenced by various factors in natural water, such as pH, inorganic ions, and dissolved organic matter (DOM) (Guo Z. et al., 2023).

DOM in natural water was an important photosensitizer for indirect photolysis (Chen et al., 2009). DOM was a heterogeneous mixture derived from the biological and biochemical residues of animals and plants. DOM was able to generate reactive oxygen species (ROS) (e.g., $OH^{\bullet}$, $^1O_2$, and $^3DOM^*$) under solar irradiation, which impacted the photodegradation behavior of the organic pollutants (Zhang et al., 2014). Furthermore, DOM was characterized by its extensive distribution, complex compositions, and expansive absorption spectrum (Chen et al., 2022). The broad spectrum of DOM was likely to overlap with the absorption wavelengths of a majority of organic pollutants. This led to an internal filtering effect, which restrained the direct photodegradation of pollutants (Shi et al., 2022). Thus it was necessary to explore the significant role of DOM in the photolysis of organic pollutants. However, there was a notable lack of research exploring DOM's impact on the photodegradation of CA in natural water. Cai et al. observed the sources and compositions of DOM in China's Eastern Plain Lake region for a long time by the satellite (Cai et al., 2024). They discovered that the component structure of DOM varied among different area waters. Furthermore, other studies have revealed that the composition and structure of DOM influenced the effect of photolysis in natural water (Li et al., 2020; Awfa et al., 2020). Carena et al. found DOM composition in lake water could be affected by the season and depth of the lake water via modeling, which in turn influenced the photolytic effect of CA (Carena et al., 2024). Shi et al. explored the effect of DOM from different wastewater sources on CA degradation in the UV/H_2O_2 system, finding DOM generally hindered the CA photolysis degradation (Shi et al., 2022). However, the mechanism and eco-toxicity of DOM composition from different region waters on CA natural photolysis process were unclear and needed to be further explored.

In this study, Humic (HA), fulvic acid (FA), and tyrosine (Tyr) were chosen as three representative types of DOM. The natural photolysis process of CA in different water bodies was studied. The degradation kinetics of CA by single and combined DOM compositions were conducted. The mineralization degree in urban, town, and rural waters was assessed by measuring total organic carbon (TOC) removal. The photolysis mechanism was further investigated by ROS analysis and intermediates identification. Then, a potential degradation pathway of CA was proposed.

2 Materials and methods

2.1 Materials

Clofibric acid ($C_{10}H_{11}ClO_3$, >99%), humic acid, fulvic acid, and tyrosine were obtained from Acros Organics. L-histidine and sorbitol were obtained from Sigma-Aldrich. HPLC grade acetonitrile and methanol were supplied by Sinopharm Chemical Reagent Co., Ltd (Shanghai, China). $NaNO_2$, NaCl, NaOH, and H_2SO_4 were analytical grade without further purified. Milli-Q water (Millipore, France, >18.2 MΩ cm) was used for the preparation of all reagents and solvents.

2.2 Experimental procedure

Reactions were performed in 50 mL glass reactors for photochemical reactor and magnetically stirred (300 rpm) in the multi-port magnetic stirring reaction vessel at room temperature (25°C). To better study the photodegradable mechanism, the solution pH was set at 3.0 based on the initial pH of CA. Initially, reactions started by mixing different concentrations of DOM with a solution containing CA, or other chemicals. After the predetermined time, samples were taken for analysis. Methanol (for HPLC) or $NaNO_2$ (for GC-MS and TOC) was used as quenchers. To ensure repeatability, all tests were performed twice and the averages with error bars (±5%) were shown.

2.3 Analytical methods

The Atlantis® T3 Waters column (4.6 mm × 250 mm, 5 μm) of the Waters e2695 with 2489 UV/Vis detector was used to measure the residual CA concentrations at 227 nm. The limit of detection (LOD) was 50 ng/mL. The mobile phase was 0.5% phosphoric acid/methanol (15/85 (v/v)) at a flow rate of 1.0 mL min^{-1}. The sample solution injection volume was 20 μL. TOC analyzer (TOC-VCPH, Shimadzu, Japan) was employed to measure the TOC. GC-MS (Agilent 8860-GC/5977B-MSD, United States) was applied to analyze the intermediates of CA and the detailed operational parameters are provided in Text S1. For the assessment of eco-toxicity, the Ecological Structure Activity Relationships (ECOSAR) program was utilized to predict the acute and chronic toxicity levels of CA and its intermediates.

The pseudo-first-order kinetics via Equation 1 was applied to model the oxidation of CA.

$$C/C_0 = e^{-kt} \quad (1)$$

where C_0 and C represented the residual concentration of CA at 0 min and t min, respectively. *k* was the rate constant of pseudo-first-order (min^{-1}), and t represented reaction time.

3 Results and discussion

3.1 Effect of single DOM

3.1.1 Effect of HA concentration

The impact of different HA concentrations on CA degradation under simulated sunlight was illustrated in Figure 1A. It showed that the presence of HA inhibited the photodegradation process of CA. As the HA concentration increased from 0 to 15 mg C/L, the degradation efficiency of CA decreased from 94.3% to 50.8% (Supplementary Figure S1A), with the rate constant of CA degradation decreasing from 3.85 × 10^{-2} to 8.09 × 10^{-3} min^{-1}

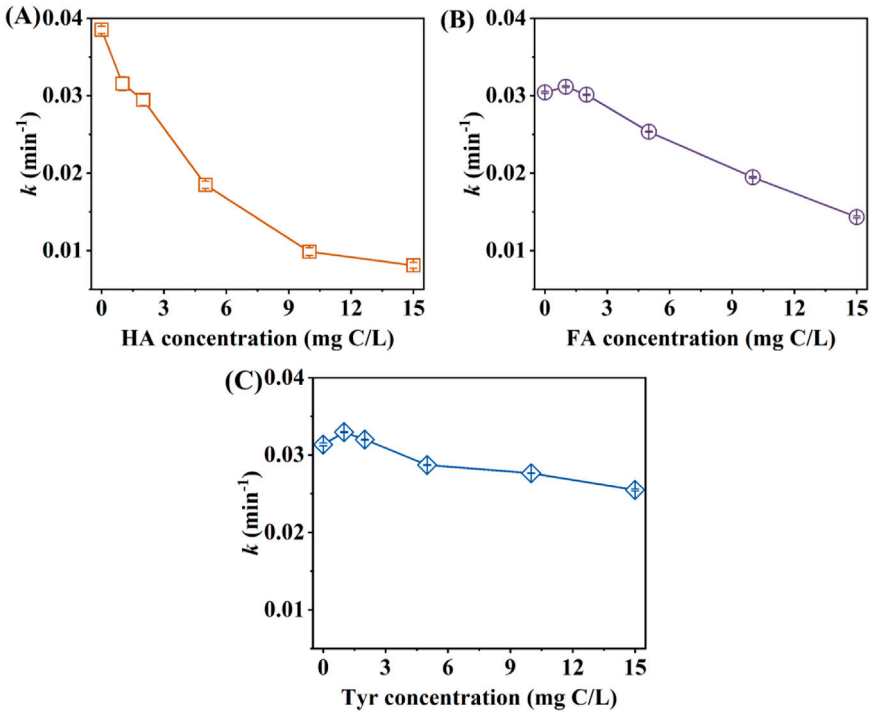

FIGURE 1
Effect of **(A)** HA, **(B)** FA, and **(C)** Tyr concentration on the rate constants *k* of CA photodegradation. Experimental conditions: $[CA]_0$ = 0.1 mM, pH = 3.0, 500 W xenon lamp.

(Figure 1A). This phenomenon could be attributed to two reasons. On the one hand, HA had a wide ultraviolet absorption band and could compete with organic pollutants in solution for photons (Chen et al., 2022). Due to the overlap of light absorption bands in the xenon emission spectrum, HA and CA could compete for photon absorption. On the other hand, CA was inhibited by internal filtration in the presence of HA (Shi et al., 2022; Guo et al., 2022). Ren et al. reported HA could reduce the contact opportunities between photons and the active sites of target pollutants, leading to an inhibitory effect on CA photocatalysis (Ren et al., 2018). Carlos et al. studied the natural photolysis of the emerging pollutants (EPs) in the presence of humus, including CA, amoxicillin, acetamiprid, acetaminophen, carbamazepine, and caffeine (Carlos et al., 2012). The authors found the increase of substance species in the mixed solution of HA reduced the exposure of photons to the target pollutants (Carlos et al., 2012).

3.1.2 Effect of FA concentration

As shown in Figure 1B and Supplementary Figure S1B, the impact of FA on CA degradation was first promoted and then inhibited, when the FA concentration increased. In the absence of FA, the rate constant *k* of CA oxidation was 3.04×10^{-2} min^{-1}, while *k* increased to 3.12×10^{-2} min^{-1} at 1 mg C/L FA (Figure 1B). However, the photodegradation rate decreased significantly with FA concentration further increased. The rate constant of CA degradation reduced from 3.01×10^{-2} to 1.43×10^{-2} min^{-1} as FA concentrations enhanced from 2 to 15 mg C/L (Figure 1B). Keum et al. found the degradation rate constant of PCBs peaked at 150 mg/L FA concentration (Keum and Li, 2004). At low concentrations of FA, the direct photolysis of CA might be the primary degradation pathway. Additionally, FA could absorb solar radiation to generate a range of photoactive intermediates, which might facilitate the photolysis of CA (Vaughan and Blough, 1998). Nevertheless, the chemical interaction between CA and high concentrations of FA altered the characteristics and functionality of FA, thereby inhibiting the degradation process of CA (Ren et al., 2019).

3.1.3 Effect of Tyr concentration

The impact of Tyr concentrations on CA photodegradation was investigated. As shown in Supplementary Figure S1C, there was no significant change in CA degradation with different Tyr concentrations. The degradation efficiency of CA was 93.23%, 94.71%, 94.23%, 92.34%, and 91.59%, at 0, 1, 5, 10, and 15 mg C/L Tyr concentration (Supplementary Figure S1C), corresponding to the rate constant of 3.13×10^{-2}, 3.30×10^{-2}, 3.20×10^{-2}, 2.88×10^{-2}, 2.77×10^{-2}, and 2.55×10^{-2} min^{-1}, respectively (Figure 1C). Compared with HA and FA, Tyr had less effect on CA photodegradation. Bianco et al. discovered that Try exhibited photochemical properties akin to those of HA and FA, whereas Tyr was limited to absorbing sunlight in the ultraviolet-B radiation (UVB) region (Berto et al., 2016). This result limited the photosensitivity of Tyr and reduced its competitive ability with CA for active sites and photons.

3.2 Effect of combined DOM

According to the literature on the composition of DOM in actual water body, we set the DOM concentration at 5 mg C/L in this study

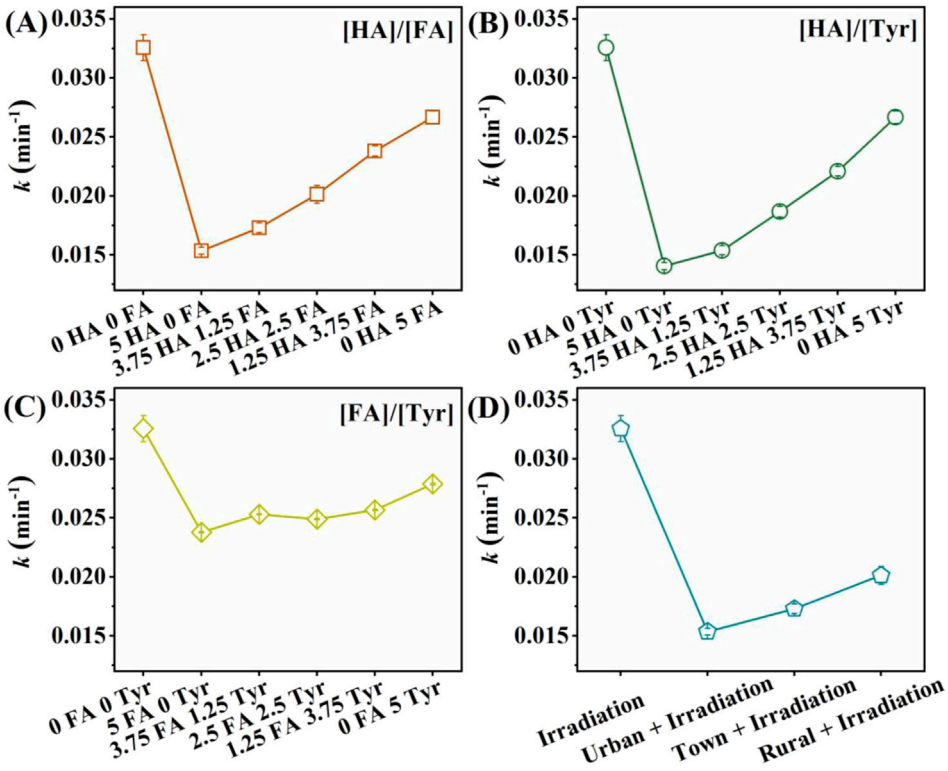

FIGURE 2
Effect of **(A)** [HA]/[FA], **(B)** [HA]/[Try], **(C)** [FA]/[Tyr] and **(D)** different region waters on the rate constants *k* of CA photodegradation. Experimental conditions: $[CA]_0$ = 0.1 mM, pH = 3.0, 500 W xenon lamp.

(Yu et al., 2018; Xu et al., 2022; Tang et al., 2019; Zeeshan et al., 2024). Xu et al. reported DOM concentrations in town, rural, and urban areas were 3.39 ± 0.60, 3.03 ± 1.26, and 3.02 ± 1.14 mg C/L, respectively (Xu et al., 2022). We explored the mechanism of CA degradation by adjusting the ratios of different DOM compositions. In the absence of combined DOM, the CA degradation rate constant was 3.26×10^{-2} min^{-1}. In general, the photolysis constant of CA decreased with the DOM involved (Figure 2).

As displayed in Figure 2A, the rate constant of CA degradation increased from 1.54×10^{-2} to 2.67×10^{-2} min^{-1} with a reduction in the [HA]/[FA] ratio (Figure 2A). Similarly, when the [HA]/[Tyr] ratio decreased, the CA degradation rate constant enhanced from 1.41×10^{-2} to 2.67×10^{-2} min^{-1} (Figure 2B). These results indicated a significant inhibition of CA photodegradation at high HA concentrations. As shown in Figure 2C, with the [FA]/[Tyr] ratio reduced, the rate constant of CA degradation increased from 2.38×10^{-2} to 2.79×10^{-2} min^{-1}. FA and Tyr had less impact on CA degradation compared to HA, therefore the [FA]/[Tyr] ratio posed a diminished inhibitory effect on CA degradation. The results in single or combined DOM indicated HA was the most effective inhibitor among three types of DOM composition. This could be attributed to the broad absorption spectrum of HA, which interfered with the photolysis process (Chen et al., 2022; Shi et al., 2022).

To observe the photodegradation of CA by DOM in actual water, we simulated the different DOM composition in urban, town, and rural water. Li et al. observed that urbanization levels had a notable impact on the concentration and composition of DOM from four watersheds with different levels of urbanization in Ningbo. Moreover, the DOM concentrations in urban, urban-rural combined, and rural areas were 3.18, 7.45 and 2.16–2.62 mg/L, respectively (Li et al., 2019). Therefore, we set the DOM composition as follows: in urban areas, [HA] = 1.272 mg C/L, [FA] = 0.636 mg C/L, [Tyr] = 1.2084 mg C/L; in towns, [HA] = 1.862 mg C/L, [FA] = 0.894 mg/L, [Tyr] = 4.47 mg C/L; in rural areas, [HA] = 0.84 mg C/L, [FA] = 0.72 mg/L, [Tyr] = 0.84 mg C/L.

As shown in Figure 2D, different regional water bodies exerted different degrees of suppression on the CA photolysis. Among them, the inhibition effect of rural water was the weakest. The rate constant of CA degradation in rural region was 2.01×10^{-2} min^{-1} with 82.83% of CA removal (Figure 2D). It could be attributed to the reason that HA concentration in rural water was lower than that in town and urban water bodies. These findings were consistent with the conclusions drawn from the impact of combined DOM on CA photodegradation (Figures 2A–C). Researchers had suggested that DOM exerted a dualistic influence (promotion or inhibition) on the CA degradation (Janssen et al., 2014). According to previous studies, DOM composition affected its molecular weight, functional group composition, and so on, thereby exerting DOM to exhibit complex and variable properties during photolysis (Wang J. et al., 2019; Janssen et al., 2014). Liu et al. (2023) discovered that DOM from different regions had different group compositions, which influenced the photodegradation of fluoroquinolone antibiotics. In our study, variations in the inhibitory effects of DOM from different regions on CA photolysis also could be attributed to these factors.

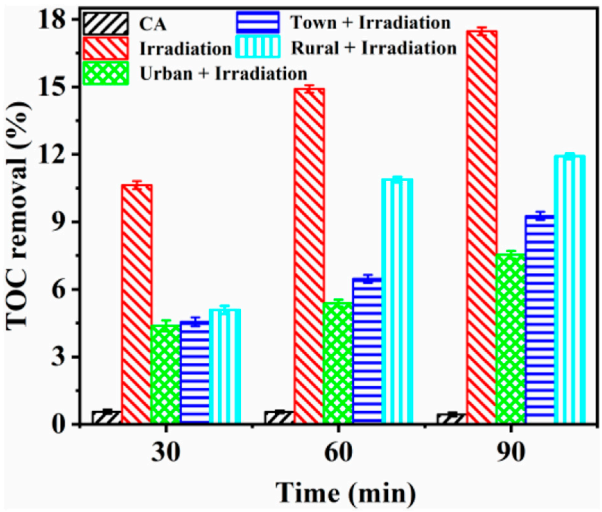

FIGURE 3
TOC removal of CA degradation with different DOM compositions at different reaction times. Experimental conditions: $[CA]_0$ = 0.1 mM, pH = 3.0.500 W xenon lamp.

3.3 Mineralization

However, the rapid degradation did not imply the complete mineralization of CA to CO_2, H_2O, and inorganic salts (Wang Y. et al., 2019). As depicted in Figure 3, CA had almost no mineralization without DOM and solar irradiation. Under irradiation, the mineralization of CA was 10.63%, 14.91%, and 17.47% after 30, 60, and 120 min, respectively. This implied a slight degradation of CA could occur under solar irradiation and the irradiation time might impact the natural photolysis of CA. However, TOC removal of CA in urban, town, and rural regions was reduced to 4.38%, 4.55%, and 5.09% after 30 min solar irradiation, respectively. The high CA photodegradation (Supplementary Figure S2D) but low TOC removal efficiency (Figure 3), might be ascribed to the formation of some refractory intermediates on CA photolysis process (Yuan et al., 2024). With the photolysis time enhanced, CA mineralization in rural water exhibited a significant increase compared to those in urban and town waters. The CA mineralization in rural water achieved 11.92% after 120 min irradiation. The difference in CA mineralization could be attributed to the complex chemical composition and structural characteristics of DOM (Sires et al., 2007). These characteristics

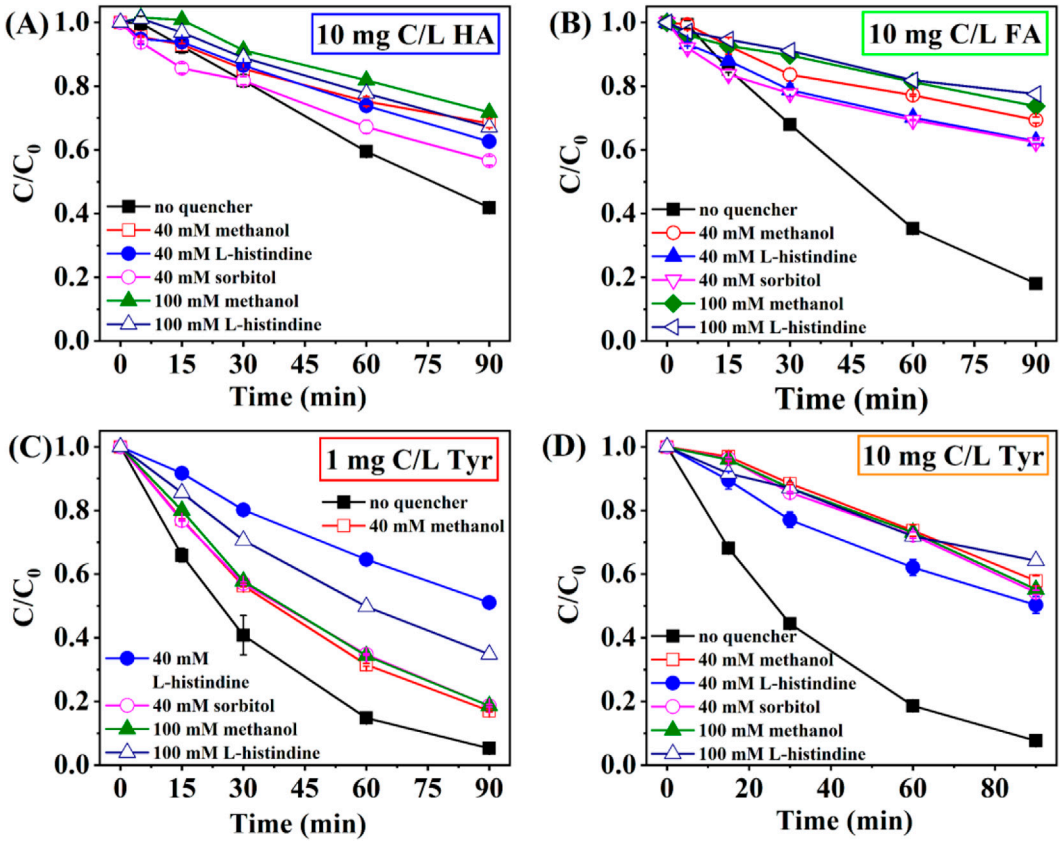

FIGURE 4
Effect of radical scavengers on CA photolysis in the presence of **(A)** 10 mg C/L HA, **(B)** 10 mg C/L FA, **(C)** 1 mg C/L Tyr, **(D)** 10 mg C/L Tyr. Experimental conditions: $[CA]_0$ = 0.1 mM, pH = 3.0, 500 W xenon lamp.

TABLE 1 Major products of CA degradation with different DOM compositions. Experimental conditions: $[CA]_0$ = 0.1 mM, pH = 3.0, 500 W xenon lamp.

NO.	Compound	Proposed structure	Formula	MW (g/mol)	Irradiation	Urban + Irradiation	Town + Irradiation	Rural + Irradiation
P1	Glycerol		$C_3H_8O_3$	92.09	√	√		
P2	Phenol	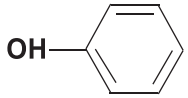	C_6H_6O	94.11	√	√		
P3	Hydroquinone	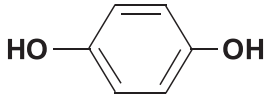	$C_6H_6O_2$	110.11	√	√		
P4	Resorcinol	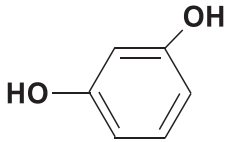	$C_6H_6O_2$	110.11	√			
P5	Catecho	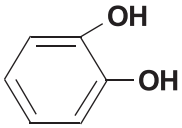	$C_6H_6O_2$	110.11	√			
P6	4-Chlorophenol	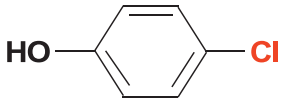	C_6H_5ClO	128.00	√			
P7	3-Chlorophenol	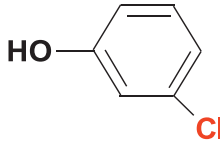	C_6H_5ClO	128.00	√	√	√	√
P8	4-Isopropyl phenol	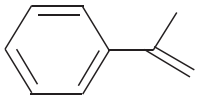	$C_9H_{10}O$	134.07		√	√	√
P9	Diglycolic acid		$C_4H_6O_5$	134.09	√			

(Continued on following page)

10.3389/fenvs.2024.1505162

TABLE 1 (*Continued*) Major products of CA degradation with different DOM compositions. Experimental conditions: $[CA]_0$ = 0.1 mM, pH = 3.0, 500 W xenon lamp.

NO.	Compound	Proposed structure	Formula	MW (g/mol)	Irradiation	Urban + Irradiation	Town + Irradiation	Rural + Irradiation
P10	6-Chloro-3-methyl-1-indanol	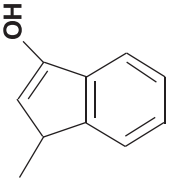	$C_{10}H_{11}ClO$	182.05		√		
P11	2-(4-chloro phenoxy) - 2-methyl propionate methyl ester	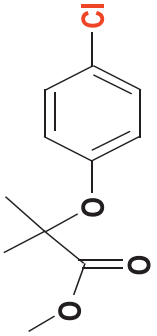	$C_{11}H_{13}ClO_3$	228.06		√	√	√

caused competing interactions and the formation of intermediate products, which collectively contributed to a reduction in the overall extent of mineralization (Li et al., 2009).

3.4 Reactive oxygen species identification

In natural water, DOM could absorb sunlight directly due to many chromophores, particularly in the ultraviolet spectrum (280–400 nm). The ground state of DOM could be excited and converted to the triplet state ^{3}DOM*. Furthermore, ^{3}DOM* had the potential to produce reactive oxygen species, which contributed to the indirect photodegradation of target organic pollutants (Jiao et al., 2008; Glover and Rosario-Ortiz, 2013; Leresche et al., 2016; Zeng and Arnold, 2013). Thus, we conducted quenching studies to explore the ROS during CA photodegradation in the presence of single DOM, namely, HA, FA, or Tyr. Methanol, L-histidine, and sorbitol served as scavengers for $OH^{\bullet}$, $^1O_2$, and ^{3}DOM*, respectively (Gao et al., 2022; Zhu et al., 2019).

As shown in Figure 4A, the photodegradation efficiency of CA was partially inhibited by methanol, L-histidine, and sorbitol presented in the presence of 10 mg C/L HA. Moreover, the quenching effect was not significantly improved with an increase in scavenger concentration. Raising methanol concentration from 40 to 100 mM slightly reduced CA photolysis efficiency from 31.67% to 28.23%. Similarly, CA photodegradation efficiency only reduced from 37.35% to 32.88% by varying L-histidine concentrations from 40 to 100 mM. This phenomenon indicated that $OH^{\bullet}$ and $^1O_2$ were not the primary ROS at 10 mg C/L HA. CA photolysis efficiency was 43.38% at 40 mM sorbitol. The inhibitory effect of sorbitol was the weakest, indicating the effect of ^{3}DOM* could be negligible. The result further proved that HA might inhibit CA photolysis through photon competition, reducing direct photolysis of CA rather than $OH^{\bullet}$, $^1O_2$, and ^{3}DOM* being the primary reactive free radicals.

As depicted in Figure 4B, the rate constant of CA degradation achieved 1.95×10^{-2} min^{-1} in the presence of 10 mg C/L FA without radical scavengers. The quenching effect of methanol and L-histidine was obvious. As methanol concentration rose from 40 to 100 mM, the rate constant for CA degradation decreased from 4.11×10^{-3} to 3.22×10^{-3} min^{-1}. Likewise, increasing L-histidine concentration from 40 to 100 mM caused a decline in the rate constant of CA photolysis from 4.96×10^{-3} to 2.85×10^{-3} min^{-1}. Sorbitol could restrain CA photolysis significantly. The photodegradation efficiency of CA decreased from 81.95% to 22.48% with 40 mM sorbitol. These findings highlighted the importance of $OH^{\bullet}$, $^1O_2$, and ^{3}DOM* in the photodegradation of CA at 10 mg C/L FA. The introduction of scavengers led to a notable decline in CA photolysis efficiency, indicating that FA might affect CA oxidation through indirect photolysis.

Since 1 and 10 mg C/L Tyr had an opposite effect on CA photodegradation, it was necessary to explore the mechanism. In the absence of scavengers, the photolysis efficiency of CA was 94.71% and 92.32% in 1 and 10 mg C/L Tyr solutions, respectively. In Figure 4C, methanol had a slight inhibitory effect on CA photodegradation at 1 mg C/L Tyr, whereas the inhibitory effects significantly enhanced with 10 mg C/L Tyr involved (Figure 4D). This indicated that the formation of $OH^{\bullet}$ increased with Tyr concentration enhancing. The photolysis efficiency of CA was

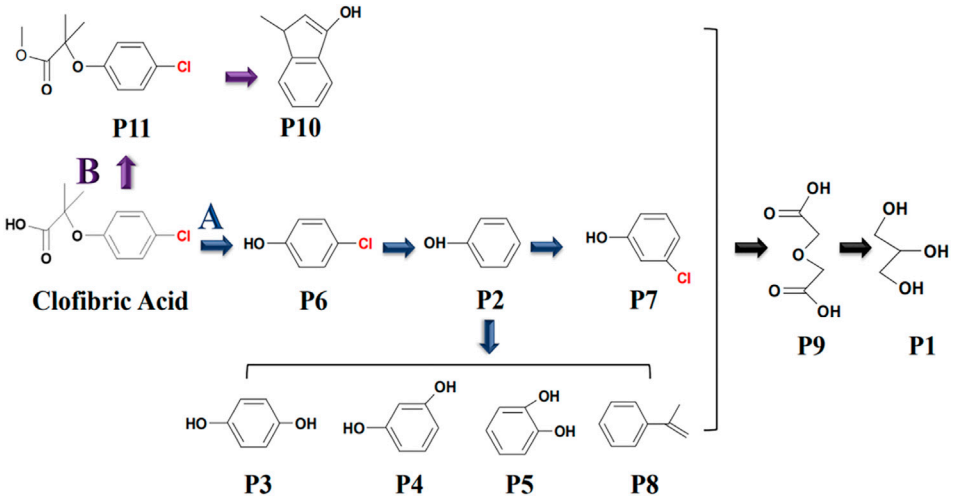

FIGURE 5
A possible degradation pathway of CA with DOM under solar irradiation. Experimental conditions: $[CA]_0$ = 0.1 mM, pH = 3.0, 500 W xenon lamp.

81.34% and 45.76% when 40 mM sorbitol was added to 1 and 10 mg C/L Tyr solutions, respectively. This suggested that a considerable quantity of ^{3}DOM* existed in the 10 mg C/L Tyr solution and participated in the CA photolysis reaction. Therefore, we could speculate that the increase in Tyr concentration was accompanied by an increase in the formation of $OH^•$ and ^{3}DOM*.

When L-histidine concentration varied from 40 to 100 mM, the photodegradation efficiency of CA increased from 48.9% to 65.16% at 1 mg C/L Tyr, but declined from 48.9% to 35.75% at 10 mg C/L Tyr. Excess L-histidine might trigger self-aggregation phenomena, which resulted in a reduced involvement of L-histidine in the reaction (Gao et al., 2022). Therefore, a low concentration of L-histidine (40 mM) exhibited a superior quenching effect. Tyr could only absorb sunlight in the UVB band, which limited its ability to compete for photons, and thus Tyr inhibited CA photolysis mainly through indirect photolysis (Ren et al., 2019). According to the quenching experiments, the inhibitory effect of Tyr on CA indirect photolysis was mainly achieved through the synergistic effect of $OH^•$, $^1O_2$, and ^{3}DOM*.

Due to the diversity of DOM components, the mechanism of different DOM composition on CA photolysis might be in diversity. Based on our findings, HA, FA, and Tyr all exerted their distinct influence on CA photodegradation process. HA predominantly impacted CA photolysis through physical interactions, characterized by photo-filtering and active site competition. Conversely, FA or Tyr inhibited the CA photodegradation mainly via the synergistic impact of various ROS.

3.5 Intermediates identification

To further elucidate the photodegradation mechanism of CA, we employed GC-MS to analyze the products of CA after a 120-min exposure to solar irradiation. Table 1 displayed eleven products identified during CA photodegradation.

The direct photolysis of CA after 120 min of irradiation yielded fewer and simpler products than those found in urban, town, and rural water. Some typical degradation products of CA was identified and their GC-MS spectra was shown in Supplementary Figure S3, such as phenol (P2), 4-chlorophenol (P6), and 3-chlorophenol (P7) (Zhang et al., 2018; Zhu et al., 2019). The presence of 3-chlorophenol (P7) in the system under irradiation confirmed the existence of dechlorination and subsequent rechlorination reactions during the CA photolytic process. In town and rural waters, the degradation products of CA were the same, namely, 3-chlorophenol (P7), 4-isopropyl phenol (P8), and 2-(4-chloro phenoxy)-2-methyl propionate methyl ester (P11). However, CA intermediates of CA in urban water were more complex than those in town and rural waters. Four additional products were identified, including glycerol (P1), phenol (P2), hydroquinone (P3), and 6-chloro-3-methyl-1-indanol (P10). The intermediates detected were consistent with the results obtained from the photolysis efficiency and mineralization of CA in urban, town, and rural waters. Among three regions, the photolysis efficiency and mineralization degree of CA were the lowest in urban water. This result further confirmed that the composition of DOM in different regions could influence the CA natural photolysis process comprehensively, including removal efficiency, mineralization and intermediates.

3.6 Degradation pathway proposed

Based on the major intermediates of CA and previous studies, a possible photodegradation pathway of CA was proposed in Figure 5. CA photodegradation might be carried out via two pathways in the presence of DOM (Zhu et al., 2019; Zhang et al., 2018).

Pathway A: the cleavage of the C-O bond in CA, resulted in the formation of 4-chlorophenol (P6). Then, P6 dechlorinated to yield phenol (P2). Phenol subsequently underwent a nucleophilic addition reaction, forming a chlorinated aromatic byproduct 3-chlorophenol (P7). Previous research had demonstrated that chlorine atoms on the benzene ring of CA could undergo dechlorination and re-chlorination processes (Zeng and Arnold, 2013). In addition, the ortho, meta, and para position of phenol

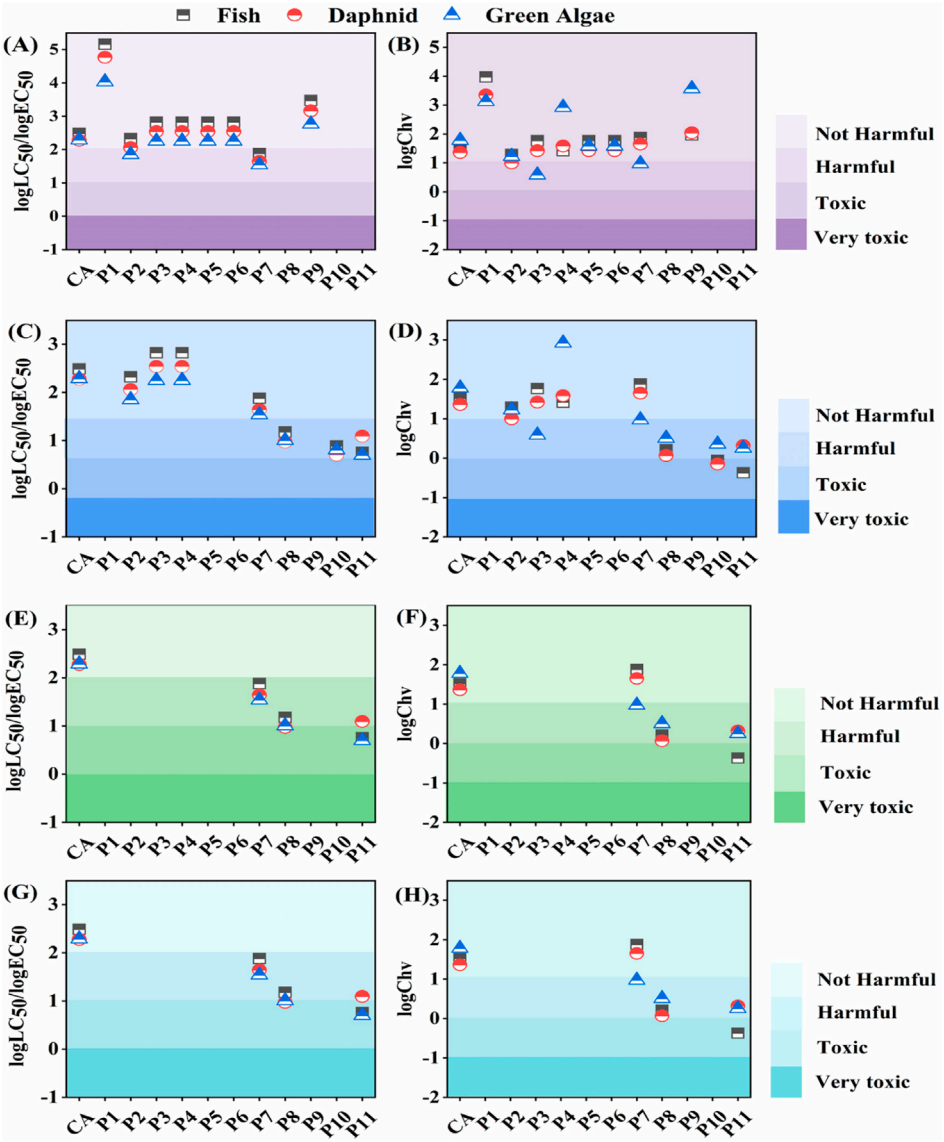

FIGURE 6
Acute toxicity ($logLC_{50}/logEC_{50}$) and chronic toxicity (logChv) under **(A, B)** irradiation, **(C, D)** urban + Irradiation, **(E, F)** town + Irradiation, **(G, H)** rural + Irradiation conditions. Experimental conditions: $[CA]_0$ = 0.1 mM, pH = 3.0, 500 W xenon lamp.

became active. Hydroquinone (P3), resorcinol (P4), catechol (P5), and 4-isopropyl phenol (P8) were further formed with ROS involved.

Pathway B: CA could also be reacted to form 2-(4-chlorophenoxy)-2-methylpropionate methyl ester (P11). Then, P11 cyclized to form 6-chloro-3-methyl-1-indanol (P10). Eventually, small molecule products were generated from two pathways, such as diglycolic acid (P9), glycerol (P1), and so on.

3.7 Eco-toxicity assessment

The ECOSAR programs could forecast toxicity metrics, namely, the lethal concentration (LC50), effective concentration (EC50), and chronic toxicity (Chv). Hence, the acute and chronic toxicity of CA and its products to aquatic organisms including fish, daphnia, and green algae were anticipated by employing the ECOSAR program. The European Union guidelines classify acute toxicity into four groups: very toxic (<1 mg/L), toxic (1–10 mg/L), harmful (10–100 mg/L), and not harmful (>100 mg/L) (Gao et al., 2014). Chronic toxicity levels were assessed according to the Chinese hazard chemical evaluation criteria, categorizing concentrations into very toxic (<0.1 mg/L), toxic (0.1–1 mg/L), harmful (1–10 mg/L), and not harmful (>10 mg/L) (HJ/TI 154–2004; Guo X. et al., 2023). For fish, daphnia, and green algae, CA was at a not harmful level of acute and chronic toxicity.

In Figure 6A, the acute toxicity of CA photolysis with irradiation was based on the values of LC50/EC50. Under irradiation, P2 was harmful to daphnia and green algae, while P7 was at a harmful level to fish, daphnia, and green algae. Other products remained at not harmful levels. In terms of chronic toxicity, P2 (to daphnia), P3 (to green algae), and P7 (to green algae) also reached harmful levels

(Figure 6B). The direct photodegradation of CA without DOM resulted in a minimal increase in ecotoxicity. In urban waters (Figure 6C), acute toxicity of P1, P2, P3, and P7 were at not harmful levels, whereas P8, P10 and P11 increased to harmful levels. Chronic toxicity was more complex (Figure 6D). The toxicity levels of products to fish were aggravated. Chv values of P10 and P11 to fish were 0.884 and 0.425 mg/L, reaching toxic concentrations. In the case of daphnid, P8 and P11 were identified at harmful levels, while P10 exhibited toxic levels. For green algae, a downward trend in Chv values suggested a general increase in toxicity to harmful levels. The eco-toxicity of intermediates in town and rural waters was the same (Figures 6E–H). The acute toxicity of P7 and P8 escalated to harmful levels. Notably, P11 exhibited toxicity to fish and green algae with an LC50 of 5.74 mg/L and EC50 of 4.99 mg/L, respectively. It also posed a harmful level to daphnids, with an EC50 of 12.4 mg/L. As for chronic toxicity, P7 was only harmful to green algae, whereas P8 and P11 were more poisonous to aquatic organisms. The Chv values of P8 (0.068 mg/L) and P11 (0.372 mg/L) achieved toxic levels to daphnids and fish, respectively. The eco-toxicity assessment under different conditions indicated that the natural photodegradation products of CA had a more adverse impact on the ecological environment and merited further attention. This might be due to the more complex structure of intermediates produced during CA photodegradation with DOM involved. It was worth noting that the photodegradation of CA in urban waters presented the highest ecological risk, due to the diversity of products and more toxic to aquatic organisms (e.g., P10 and P11).

4 Conclusion

In this study, we discovered that DOM had a complex effect on CA degradation, owing to its concentration and composition. HA, FA, and Tyr were selected as model DOM in this study. HA demonstrated the most significant inhibitory impact on CA photodegradation. Besides, the photodegradation efficiency, mineralization, and products of CA under natural photolysis conditions in urban, town, and rural waters were further investigated. The results showed that CA photolysis was inhibited in all three water bodies, especially in urban waters. Moreover, CA photodegradation intermediates in urban waters were more abundant and complex. Quenching experiments showed the formation of ROS was correlated with DOM components. HA affected the direct photolysis of CA mainly by filtration and active site competition. The reactions between FA or Tyr with CA were dominated by $OH^{\bullet}$, $^{1}O_{2,}$ and $^{3}DOM^{*}$. GC-MS analysis revealed the presence of some recalcitrant chlorinated organic compounds. The mechanism of CA photolysis included hydroxyl radical oxidation, C-O bond cleavage, dechlorination, re-chlorination, and so on. The degradation pathway of CA in the presence of DOM was further proposed. Eco-toxicological assessment indicated some degradation products might have higher toxicity levels than CA itself in urban, town, and rural waters. Our finding indicated the natural photolysis of pharmaceutical contaminants in natural water may have a detrimental impact on the ecological environment and safe disposal need to be conducted before discharge.

Data availability statement

The original contributions presented in the study are included in the article/Supplementary Material, further inquiries can be directed to the corresponding authors.

Author contributions

JC: Conceptualization, Data curation, Visualization, Writing–original draft. HW: Data curation, Resources, Writing–original draft. CY: Methodology, Resources, Writing–original draft. YY: Resources, Validation, Writing–original draft. YZ: Resources, Validation, Writing–original draft. HW: Data curation, Resources, Writing–original draft. YH: Conceptualization, Funding acquisition, Supervision, Writing–review and editing. KW: Methodology, Supervision, Writing–review and editing.

Funding

The author(s) declare that financial support was received for the research, authorship, and/or publication of this article. This work was supported by Natural Science Foundation of Ningbo (No. 202003N4135), the General Research Project of Zhejiang Provincial Department of Education (No. Y202043966) and the K. C. Wong Magna Fund in Ningbo University.

Conflict of interest

The authors declare that the research was conducted in the absence of any commercial or financial relationships that could be construed as a potential conflict of interest.

Generative AI statement

The author(s) declare that no Generative AI was used in the creation of this manuscript.

Publisher's note

Supplementary material

The Supplementary Material for this article can be found online at: https://www.frontiersin.org/articles/10.3389/fenvs.2024.1505162/full#supplementary-material

References

Andreozzi, R., Caprio, V., Marotta, R., and Radovnikovic, A. (2003). Ozonation and H_2O_2/UV treatment of clofibric acid in water: a kinetic investigation. *J. Hazard. Mater.* 103 (3), 233–246. doi:10.1016/j.jhazmat.2003.07.001

Awfa, D., Ateia, M., Fujii, M., and Yoshimura, C. (2020). Photocatalytic degradation of organic micropollutants: inhibition mechanisms by different fractions of natural organic matter. *Water Res.* 174, 115643. doi:10.1016/j.watres.2020.115643

Berto, S., De Laurentiis, E., Tota, T., Chiavazza, E., Daniele, P. G., Minella, M., et al. (2016). Properties of the humic-like material arising from the photo-transformation of L-tyrosine. *Sci. Total Environ.* 545-546, 434–444. doi:10.1016/j.scitotenv.2015.12.047

Cai, X. L., Lei, S. H., Li, Y. M., Li, J. Z., Xu, J., Lyu, H., et al. (2024). Humification levels of dissolved organic matter in the eastern plain lakes of China based on long-term satellite observations. *Water Res.* 250, 120991. doi:10.1016/j.watres.2023.120991

Carena, L., García-Gil, Á., Marugán, J., and Vione, D. (2024). Global modeling of photochemical reactions in lake water: a comparison between triplet sensitization and direct photolysis. *EEH*. doi:10.1016/j.eehl.2024.09.001

Carlos, L., Martire, D. O., Gonzalez, M. C., Gomis, J., Bernabeu, A., Amat, A. M., et al. (2012). Photochemical fate of a mixture of emerging pollutants in the presence of humic substances. *Water Res.* 46 (15), 4732–4740. doi:10.1016/j.watres.2012.06.022

Chen, M., Xu, J., Tang, R., Yuan, S., Min, Y., Xu, Q., et al. (2022). Roles of microplastic-derived dissolved organic matter on the photodegradation of organic micropollutants. *J. Hazard. Mater.* 440, 129784. doi:10.1016/j.jhazmat.2022.129784

Chen, Y., Hu, C., Hu, X., and Qu, J. (2009). Indirect photodegradation of amine drugs in aqueous solution under simulated sunlight. *Environ. Sci. Technol.* 43 (8), 2760–2765. doi:10.1021/es803325j

Cheng, F., Zhang, T., Yang, H., Liu, Y., Qu, J., Zhang, Y. N., et al. (2024). Effects of dissolved organic matter and halogen ions on phototransformation of pharmaceuticals and personal care products in aquatic environments. *J. Hazard. Mater.* 469, 134033. doi:10.1016/j.jhazmat.2024.134033

Gao, L. W., Guo, Y., Zhan, J. H., Yu, G., and Wang, Y. J. (2022). Assessment of the validity of the quenching method for evaluating the role of reactive species in pollutant abatement during the persulfate-based process. *Water Res.* 221, 118730. doi:10.1016/j.watres.2022.118730

Gao, Y., Ji, Y., Li, G., and An, T. (2014). Mechanism, kinetics and toxicity assessment of OH-initiated transformation of triclosan in aquatic environments. *Water Res.* 49, 360–370. doi:10.1016/j.watres.2013.10.027

Glover, C. M., and Rosario-Ortiz, F. L. (2013). Impact of halides on the photoproduction of reactive intermediates from organic matter. *Environ. Sci. Technol.* 47 (24), 13949–13956. doi:10.1021/es4026886

Guo, X., Zhang, H., Yao, Y. Y., Xiao, C. M., Yan, X., Chen, K., et al. (2023a). Derivatives of two-dimensional MXene-MOFs heterostructure for boosting peroxymonosulfate activation: enhanced performance and synergistic mechanism. *Appl. Catal. B* 323, 122136. doi:10.1016/j.apcatb.2022.122136

Guo, Y., Guo, Z., Wang, J., Ye, Z., Zhang, L., and Niu, J. (2022). Photodegradation of three antidepressants in natural waters: important roles of dissolved organic matter and nitrate. *Sci. Total Environ.* 802, 149825. doi:10.1016/j.scitotenv.2021.149825

Guo, Z., Kodikara, D., Albi, L. S., Hatano, Y., Chen, G., Yoshimura, C., et al. (2023b). Photodegradation of organic micropollutants in aquatic environment: importance, factors and processes. *Water Res.* 231, 118236. doi:10.1016/j.watres.2022.118236

Janssen, E. M. L., Erickson, P. R., and McNeill, K. (2014). Dual roles of dissolved organic matter as sensitizer and quencher in the photooxidation of tryptophan. *Environ. Sci. Technol.* 48 (9), 4916–4924. doi:10.1021/es500535a

Jiao, S., Zheng, S., Yin, D., Wang, L., and Chen, L. (2008). Aqueous photolysis of tetracycline and toxicity of photolytic products to luminescent bacteria. *Chemosphere* 73 (3), 377–382. doi:10.1016/j.chemosphere.2008.05.042

Keum, Y. S., and Li, Q. X. (2004). Copper dissociation as a mechanism of fungal laccase denaturation by humic acid. *Appl. Microbiol. Biotechnol.* 64 (4), 588–592. doi:10.1007/s00253-003-1460-y

Leresche, F., Gunten, U. v., and Canonica, S. (2016). Probing the Photosensitizing and inhibitory effects of dissolved organic matter by using N,N-dimethyl-4-cyanoaniline (DMABN). *Environ. Sci. Technol.* 50 (20), 10997–11007. doi:10.1021/acs.est.6b02868

Li, J., Zhang, X., Fan, W. Y., Yao, M. C., and Sheng, G. P. (2020). Dissolved organic matter dominating the photodegradation of free DNA bases in aquatic environments. *Water Res.* 179, 115885. doi:10.1016/j.watres.2020.115885

Li, W., Lu, S., Chen, N., Gu, X., Qiu, Z., Fan, J., et al. (2009). Photo-degradation of clofibric acid by ultraviolet light irradiation at 185 nm. *Water Sci. Technol.* 60 (11), 2983–2989. doi:10.2166/wst.2009.690

Li, W., Shi, Y., Gao, L., Liu, J., and Cai, Y. (2012). Occurrence of antibiotics in water, sediments, aquatic plants, and animals from Baiyangdian Lake in North China. *Chemosphere* 89 (11), 1307–1315. doi:10.1016/j.chemosphere.2012.05.079

Li, Y., Wei, H. J., Wang, K., Zhang, Z. Z., and Yu, X. B. (2019). Analysis of the relationship between dissolved organic matter (DOM) and watershed land-use based on three-dimensional fluorescence-parallel factor (EEM-PARAFAC) analysis. *Huan Jing Ke Xue* 40 (4), 1751–1759. doi:10.13227/j.hjkx.201808118

Liu, S., Cui, Z., Ding, D., Bai, Y., Chen, J., Cui, H., et al. (2023). Effect of the molecular weight of DOM on the indirect photodegradation of fluoroquinolone antibiotics. *J. Environ. Manage.* 348, 119192. doi:10.1016/j.jenvman.2023.119192

Nakada, N., Komori, K., Suzuki, Y., Konishi, C., Houwa, I., and Tanaka, H. (2007). Occurrence of 70 pharmaceutical and personal care products in Tone River basin in Japan. *Water Sci. Technol.* 56 (12), 133–140. doi:10.2166/wst.2007.801

Packer, J. L., Werner, J. J., Latch, D. E., McNeill, K., and Arnold, W. A. (2003). Photochemical fate of pharmaceuticals in the environment: naproxen, diclofenac, clofibric acid, and ibuprofen. *Aquat. Sci.* 65 (4), 342–351. doi:10.1007/s00027-003-0671-8

Pan, T., Tang, Y., Liao, Y., Chen, J., Li, Y., Wang, J., et al. (2023). $BiVO_4$ modifying with cobalt-phosphate cluster cocatalyst for persulfate assisted photoelectrocatalytic degradation of tetracycline. *Mol. Catal.* 549, 113527. doi:10.1016/j.mcat.2023.113527

Ren, D., Chen, F., Ren, Z., and Wang, Y. (2019). Different response of 17α-ethinylestradiol photodegradation induced by aquatic humic and fulvic acids to typical water matrixes. *Process Saf. Environ. Prot.* 121, 367–373. doi:10.1016/j.psep.2018.11.018

Ren, M., Drosos, M., and Frimmel, F. H. (2018). Inhibitory effect of NOM in photocatalysis process: explanation and resolution. *Chem. Eng. J.* 334, 968–975. doi:10.1016/j.cej.2017.10.099

Shi, Y., Geng, J., Li, X., Qian, Y., Li, H., Wang, L., et al. (2022). Effects of DOM characteristics from real wastewater on the degradation of pharmaceutically active compounds by the UV/H_2O_2 process. *J. Environ. Sci.* 116, 220–228. doi:10.1016/j.jes.2021.12.017

Sires, I., Arias, C., Cabot, P. L., Centellas, F., Garrido, J. A., Rodriguez, R. M., et al. (2007). Degradation of clofibric acid in acidic aqueous medium by electro-Fenton and photoelectro-Fenton. *Chemosphere* 66 (9), 1660–1669. doi:10.1016/j.chemosphere.2006.07.039

Tang, J., Li, X., Cao, C., Lin, M., Qiu, Q., Xu, Y., et al. (2019). Compositional variety of dissolved organic matter and its correlation with water quality in peri-urban and urban river watersheds. *Ecol. Indic.* 104, 459–469. doi:10.1016/j.ecolind.2019.05.025

Vaughan, P. P., and Blough, N. V. (1998). Photochemical Formation of hydroxyl radical by constituents of natural waters. *Environ. Sci. Technol.* 32 (19), 2947–2953. doi:10.1021/es9710417

Wang, J., Chen, J., Qiao, X., Zhang, Y. N., Uddin, M., and Guo, Z. (2019a). Disparate effects of DOM extracted from coastal seawaters and freshwaters on photodegradation of 2,4-Dihydroxybenzophenone. *Water Res.* 151, 280–287. doi:10.1016/j.watres.2018.12.045

Wang, Y., Li, H., Yi, P., and Zhang, H. (2019b). Degradation of clofibric acid by UV, O_3 and UV/O_3 processes: performance comparison and degradation pathways. *J. Hazard. Mater.* 379, 120771. doi:10.1016/j.jhazmat.2019.120771

Xu, W. N., Yu, H. B., Yang, F., Yang, F., Liu, D. P., Lu, K. T., et al. (2022). Second derivative UV-visible spectroscopy characterizing structural components of dissolved and particulate organic matter in an urbanized river. *Environ. Sci. Eur.* 34 (1), 29. doi:10.1186/s12302-022-00609-z

Yang, Y., Ok, Y. S., Kim, K. H., Kwon, E. E., and Tsang, Y. F. (2017). Occurrences and removal of pharmaceuticals and personal care products (PPCPs) in drinking water and water/sewage treatment plants: a review. *Sci. Total Environ.* 596-597, 303–320. doi:10.1016/j.scitotenv.2017.04.102

Yu, M., He, X., Liu, J., Wang, Y., Xi, B., Li, D., et al. (2018). Characterization of isolated fractions of dissolved organic matter derived from municipal solid waste compost. *Sci. Total Environ.* 635, 275–283. doi:10.1016/j.scitotenv.2018.04.140

Yu, M., Tang, Y., Liao, Y., He, W., Lu, X.-x., and Li, X. (2023). Defect-designed Mo-doped $BiVO_4$ photoanode for efficient photoelectrochemical degradation of phenol. *J. Mater. Sci. Technol.* 165, 225–234. doi:10.1016/j.jmst.2023.06.002

Yuan, Y., Zhang, J., Yin, W., Zhang, L., Li, L., Chen, T., et al. (2024). *In situ* coupling of reduction and oxidation processes with alternating current-driven bioelectrodes for efficient mineralization of refractory pollutants. *Engineering*. doi:10.1016/j.eng.2024.05.009

Zeeshan, M., Ali, O., Tabraiz, S., and Ruhl, A. S. (2024). Seasonal variations in dissolved organic matter concentration and composition in an outdoor system for bank filtration simulation. *J. Environ. Sci.* 135, 252–261. doi:10.1016/j.jes.2023.01.006

Zeng, T., and Arnold, W. A. (2013). Pesticide photolysis in prairie potholes: probing photosensitized processes. *Environ. Sci. Technol.* 47 (13), 6735–6745. doi:10.1021/es3030808

Zhang, D., Yan, S., and Song, W. (2014). Photochemically induced formation of reactive oxygen species (ROS) from effluent organic matter. *Environ. Sci. Technol.* 48 (21), 12645–12653. doi:10.1021/es5028663

Zhang, X., Liu, Z., Kong, Q., Liu, G., Lv, W., Li, F., et al. (2018). Aquatic photodegradation of clofibric acid under simulated sunlight irradiation: kinetics and mechanism analysis. *RSC Adv.* 8 (49), 27796–27804. doi:10.1039/c8ra03140a

Zhu, K., Wang, X., Geng, M., Chen, D., Lin, H., and Zhang, H. (2019). Catalytic oxidation of clofibric acid by peroxydisulfate activated with wood-based biochar: effect of biochar pyrolysis temperature, performance and mechanism. *Chem. Eng. J.* 374, 1253–1263. doi:10.1016/j.cej.2019.06.006

frontiers | Frontiers in Environmental Science

TYPE Original Research
PUBLISHED 09 January 2025
DOI 10.3389/fenvs.2024.1540638

OPEN ACCESS

EDITED BY
Yaoguang Guo,
Shanghai Polytechnic University, China

REVIEWED BY
Fang Li,
Donghua University, China
Huiqing Han,
Guizhou Institute of Technology, China
Fuxing Kang,
Nanjing Agricultural University, China

*CORRESPONDENCE
Yong Dai,
daiyong@cohl.com

RECEIVED 06 December 2024
ACCEPTED 26 December 2024
PUBLISHED 09 January 2025

CITATION
Dai Y, Zhao S and Zheng R (2025) Adsorption and removal of pentavalent antimony from water by biochar prepared from modified rosa roxburghii residue.
Front. Environ. Sci. 12:1540638.
doi: 10.3389/fenvs.2024.1540638

Adsorption and removal of pentavalent antimony from water by biochar prepared from modified rosa roxburghii residue

Yong Dai[1]*, Shengmao Zhao[2] and Ruyi Zheng[2]

[1]China Overseas Construction Limited, Shenzhen, Guangdong, China, [2]Key Laboratory of Karst Georesources and Environment, Ministry of Education, College of Resources and Environment Engineering, Guizhou University, Guiyang, China

In order to investigate the adsorption properties of modified rosa roxburghii residue biochar to antimony (Sb) in water, the modified rosa roxburghii residue biochar (BC-FeOOH) was prepared from rosa roxburghii residue factory in Guizhou Processing plant. The adsorption characteristics of BC-FeOOH on Sb(V) in water were investigated by batch test experiments with different pH, biochar dosage and adsorption time. The results showed that the best adsorption effect of BC-FeOOH on antimony was achieved at the dosage of 0.05 g and pH 2.0, and the adsorption amount reached 5.7 mg/g. The results of adsorption kinetic modeling showed that the equilibrium time of the adsorption of BC-FeOOH on Sb(V) in water was in the range of 8–10 h, and the mechanism of adsorption was mainly chemical adsorption. Langmuir model can better describe the adsorption process of BC-FeOOH on Sb(V), and the surface adsorption process is monomolecular layer chemisorption. The experimental results showed that BC-FeOOH is a good adsorbent for Sb pollution remediation in water. This study provides n ew insights for the development of Sb contamination removal strategies in water and offers a new way for the resource utilization of prickly pear pomace.

KEYWORDS

BC-FeOOH, Sb(V), adsorption, biochar, rosa roxburghii residue

1 Introduction

Antimony (Sb) is an emerging pollutant that has been shown to be highly toxic and carcinogenic (Deng et al., 2017). Excessive intake of antimony compounds is potentially toxic to the human immune, nervous system, genes and development (Cavallo et al., 2002). Sb exists in the natural environment mainly in two valence states, trivalent antimony (Sb(III)) and pentavalent antimony (Sb(V)), of which Sb(III) is about 10 times more toxic than Sb(V) (Shan et al., 2014). Increasing anthropogenic activities such as smelting, mining, fuel combustion and the widespread use of products containing Sb compounds (e.g., rubber, alloys) have resulted in the release of large amounts of Sb into the aquatic environment, posing a potential threat to human health (Jia et al., 2020). Sb pollution of water bodies has become a global environmental problem, in which the water environment of New Zealand, Australia, France, Japan, China and other countries are subject to varying degrees of Sb pollution (Druzbicka and Craw, 2015; Jia et al., 2020). Many countries have listed it as a priority pollutant for control. China is rich in Sb ore resources, and its reserves and production rank first in the world. China's Sb mining, extraction, smelting and waste water

discharge from abandoned Sb mines are important sources of Sb pollution in water bodies. In recent years, several river basins in China have suffered from Sb pollution incidents (Tang et al., 2023), such as the Duliu River pollution in 2009 and Sb contamination in the Sunshui River, where concentrations exceeded the standard for 38 months. These incidents have significantly impacted water quality, aquatic ecosystems, and drinking water supplies. Frequent Sb pollution problems in water bodies lead to serious impacts on regional water quality, and even adversely affect the drinking water of residents and the growth of aquatic plants and animals. Therefore, how to effectively remove Sb from water to provide a safe and reliable drinking water environment for human life has become the focus of research in countries around the world and the urgent need to solve the important environmental issues closely related to people's livelihood.

Currently, the main methods for the removal of Sb from wastewater include adsorption, coagulation, locculation, membrane separation, ion exchange, electrochemical and extraction (Li et al., 2018). Among them, adsorption method is widely used due to the advantages of low process requirements, high efficiency, low cost and simple operation, which is considered to be the most effective method to mitigate Sb pollution in water (Rahaman et al., 2008). Many scholars have used iron oxides (Liu et al., 2023), graphene and biochar as adsorbents for the removal of Sb from water. Among them, biochar, which has the characteristics of low cost, wide source, rich pore structure, abundant functional groups, and adjustable specific surface area, has been widely used for the removal of heavy metals, metalloids, and organic pollutants, etc., from water (Li et al., 2017), and is considered to be the most promising adsorbent. In addition, biochar can be modified by various advanced means to obtain modified biochar with more surface functions and high adsorption capacity, which has stronger adsorption and removal capacity of toxic elements in polluted water (Zhou et al., 2020). Studies have shown that the adsorption capacity of modified biomass charcoal for Sb was significantly improved, such as the adsorption capacity of magnetically modified biochar for Sb(V) was greatly improved, and its adsorption capacity increased from 2.22 mg/g to 18.92 mg/g at pH 7.0 (Wang C. et al., 2018); the maximum adsorption capacity of iron-containing cow dung biochar for Sb(V) was 58.3 mg/g, with a removal rate of 98.5% (Park et al., 2021); the saturated adsorption capacity of iron-modified rice husk hydrothermal carbon for Sb(V) was as high as 60.76 mg/g. This indicates that the adsorption removal of Sb from water by modified biochar has excellent application potential.

Rosa roxburghii residue, is an abundant and underutilized agricultural byproduct (Peidong et al., 2023). It has a high lignocellulosic content. Moreover. Rosa roxburghii residue contains significant amounts of phenolic compounds and other organic molecules (Xu et al., 2024), the biomass's composition is rich in oxygen-containing functional groups (such as carboxyl and hydroxyl groups) (Wang et al., 2021), which are known to facilitate the adsorption of heavy metals and other pollutants. However, Rosa roxburghii residues are often discarded as waste, making them a sustainable and cost-effective source for biochar production, promoting the principles of circular economy and waste valorization (Zhou et al., 2019). In recent years, Guizhou has experienced a significant increase in the production of prickly pear, which has led to the generation of a considerable amount of prickly pear pomace. According to statistical data, Guizhou can produce approximately 15,000 tons of prickly pear pomace annually (Li et al., 2022). Prickly pear pomace is typically discarded as waste, and the accumulation of prickly pear pomace is prone to decomposition, which not only represents a waste of resources but also produces hazardous substances that can pollute the environment (Jain et al., 2024). Therefore, exploring the resource utilization of prickly pear pomace not only can effectively alleviate the waste of prickly pear pomace but also has great significance in promoting the sustainable development of the prickly pear industry. While the use of biochar in environmental remediation is well-documented (Yi et al., 2020), our work uniquely focuses on the use of Rosa roxburghii, a lesser-explored biomass source, and the modification of its biochar to enhance its adsorption capacity for Sb(V). To our knowledge, no other study has explored this specific biomass source for the removal of antimony from aqueous environments, making this an innovative approach. Additionally, our study provides a detailed characterization of the biochar's surface properties, demonstrating how modifications influence its adsorption mechanisms and effectiveness. This combination of using a novel biomass source, modifying biochar, and targeting the specific removal of Sb(V) from water constitutes the distinctive contribution of this research. Based on this point or Based on this viewpoint, the present study selected prickly pear pomace as the raw material for the preparation of biochar, which was modified with hydroxyl iron oxide (Fe-OOH) by the hydrothermal method. The modified prickly pear pomace biochar (BC-FeOOH) was then subjected to kinetic adsorption and isothermal adsorption tests to investigate its removal of Sb(V) in water under varying conditions, including biochar dosage, pH, and adsorption time. The findings of this study will provide theoretical support for the removal of Sb in water and serve as a reference for the green utilization pathway of prickly pear pomace. The study investigated the availability of BC-FeOOH under different conditions, including varying biochar dosages, pH levels, and adsorption times. This research aimed to provide theoretical support for the removal of Sb in water and to establish a green resource utilization pathway for prickly pear.

2 Material and method

2.1 Main reagents and instruments

The principal reagents employed in this study were ferrous sulfate heptahydrate ($FeSO_4.7H_2O$, 99%, Sigma-Aldrich), ethylene glycol [$(CH_2OH)_2$, 99%, Sinopharm)], ethanol (C_2H_5OH, 99%, Sinopharm) sodium hydroxide (NaOH, 99%, Sinopharm), citric acid ($C_6H_8O_7$, 99%, Sinopharm), and antimony standard storage solution (Sb(V), 99%, Sinopharm). The reagents utilized in the test were analytically pure reagents, and the test water was ultrapure water.

The principal instruments employed in this study were a tubular muffle furnace (L 9/11, Nabertherm, China), a hydride generation atomic fluorescence spectrometer (HG-AFS9700, HAIGUANG INSTRUMENT, China), a pH meter (PHS-3C, Lei-ci, China), and a constant temperature oscillator.

2.2 Preparation and characterization of modified biochar

2.2.1 Preparation of biochar

Firstly, the prickly pear pomace, derived from the prickly pear processing plant, was subjected to a crushing process and subsequently placed in an oven at a temperature of 60°C for a period of 24 h. Following this, the material was removed and placed in a tube muffle furnace at a temperature of 450°C for a duration of 4 h, this temperature range effectively enhances the surface area and functional groups of biochar while maintaining the structural integrity of the biomass (Caidi et al., 2021; Fatouma et al., 2023; Hamzah et al., 2018), during which time it underwent a transformation into prickly pear pomace biochar (BC). After cooling, the material was ground and crushed through a 100-mesh sieve. It was then soaked in 1 mol/L HCl for 2 h to remove the ash on the surface of BC. The material was subsequently washed with deionized water on several occasions until the pH was neutral. Finally, the material was dried in an oven at 60°C for 24 h and then placed in a sealed bag for use.

2.2.2 Preparation of BC-FeOOH modification

5 g of BC were weighed and dispersed uniformly into an aqueous ethylene glycol solution (the volume ratio of ethylene glycol to water was 1:7). Subsequently, 0.111 g of $FeSO_4.7H_2O$ was added and stirred for 10 min before being transferred to a high-pressure reactor. The hydrothermal reaction was then carried out at 120°C for 12 h before being cooled down to room temperature. The biochar was washed with ethanol several times to achieve a neutral pH, and then dried under vacuum at 60°C for 12 h. The solid was ground into powder and sieved through a 100-mesh sieve, resulting in the modified biochar (An et al., 2020), which was recorded as BC-FeOOH. Two control experiments were conducted simultaneously. The first group lacked a Fe source and only contained ethylene glycol, designated as BC-$(CH_2OH)_2$. The second group lacked both a Fe source and ethylene glycol, serving as a blank control. This group was designated as BC-$(CH_2OH)_2$. The third group lacked both a Fe source and ethylene glycol and was used as a blank control. This group was designated as BC-blank control group and indicated by (BC-control) in the figure.

2.2.3 BC-FeOOH modification characterization

The specific surface area, average pore size, and pore volume of distinct biochar samples were quantified employing the Brunauer-Emmett-Teller system (BET, ASAP2020).

2.3 Batch experiment

2.3.1 Determination of optimal dosage

The biochar modified by the three methods of 0.05 g, 0.10 g, 0.20 g and 0.3 g was placed in a 50 mL centrifuge tube, and 40 mL of Sb(V) solution with an initial concentration of 10 mg/L was added, respectively. Oscillate at a constant speed of 200 r/min and 25°C for 24 h on a constant temperature oscillator. After the reaction, 2 mL was sampled with a needle syringe and filtered with a 0.45 μm aqueous filter membrane. The concentration of Sb(V) in the solution was determined by atomic fluorescence spectrometer, and the adsorption capacity and removal rate of Sb by the three adsorbents were calculated to determine the optimal dosage of biochar. Three parallel groups were set in each group to obtain the highest adsorption amount of biochar for subsequent tests.

2.3.2 Determination of optimal pH value

The optimal amount of biomass charcoal was weighed into a 50 mL centrifuge tube, and 40 mL of Sb(V) solution with an initial concentration of 10 mg/L was added. The pH of the reaction system was then adjusted to 2, 4, 6, and 7 with The reaction system was then treated with 0.1 mol/L HCl and NaOH, and shaken on a thermostatic oscillator at a constant temperature of 200 r/min and 25°C for 24 h. The optimal pH value was used as the control condition for the subsequent adsorption experiments.

2.3.3 Adsorption kinetics experiment

In the experiments, the reaction temperature was 25°C, and under the optimal biomass charcoal dosage and pH conditions, the biomass charcoal was dosed into 40 mL of 10 mg/L Sb(V) solution, which was shaken on a constant temperature oscillator at a constant speed of 200 rpm for 5, 10, 15, 30, 60, 300, 720, 960, 1,440, 1920 and 2,770 min, respectively, after the start of the experiments. To study the adsorption kinetic characteristics of Sb(V), samples of 2 mL were taken with a needle syringe, filtered, and then determined by atomic fluorescence spectrometer, and three parallel groups were set up during the experiment.

The adsorption of Sb in water by biochar, Q (mg/g), was calculated Equation 1:

$$Q = (C_0 - C_t) * V/m \quad (1)$$

where C_0 and C_t represent the concentration of Sb solution before and after adsorption by biochar in mg/L, respectively; Q represents the adsorption amount in mg/g; V is the volume of solution added (mL); m is the mass of adsorbent poured in g.

The removal rate of Sb from water by biochar was calculated Equation 2:

$$E = (C_0 - C_t)/C_0 * 100\% \quad (2)$$

The experimental results obtained were used to fit the adsorption kinetics using the fitted first-order equations as well as the fitted second-order equations calculated to fit the equations:

The fitted equations were modeled by the fitted first-order Equation 3:

$$Q_t = Q_e\left(1 - e^{k1t}\right) \quad (3)$$

Fitting a second-order fitted Equation 4:

$$Q_t = Q_e^2 k_2 t/(1 + Q_e K_2 t) \quad (4)$$

where Q_e represents the maximum adsorption amount of Sb by biochar when the adsorption reaches adsorption equilibrium, in mg/g; while Q_t denotes the adsorption amount of biomass char corresponding to the moment t; and k_1, k_2 represent the adsorption rate constants for the proposed primary kinetics and the adsorption rate constants for the proposed secondary kinetics, respectively.

TABLE 1 BET specific surface area of BC-FeOOH and its pore structure parameters.

Materials	Specific surface area/(m^2/g)	Mean aperture/(nm)	Pore volume/(cm^3/g)
BC	3.83	9.59	5.51×10^{-3}
BC-FeOOH	5.17	4.12	9.23×10^{-3}

2.3.4 Isothermal adsorption experiments

Under the conditions of optimal pH and optimal biochar dosage, the three modified BCs were sequentially added to 40 mL of Sb solution with mass concentrations of: 5, 10, 30, 50, and 80 mg/L. After adsorption for 15 min, the adsorption amount was calculated by constant temperature oscillation on a thermostatic oscillator at 200 rpm and 25 °C for 24 h, and the adsorption isotherm model was used to fit the experimental data.

According to the results obtained from the experiments, the adsorption thermodynamics was fitted to the experimental results, and the fitting models were: Langmuir equation and Freundlich equation, whose expressions are Equations 5, 6:

Langmuir isotherm:

$$Q_e = Q_{\max} k_L C_e / (1 + K_L C_e) \quad (5)$$

Freundlich isotherm:

$$Q_e = K_F C_e^{\frac{1}{n}} \quad (6)$$

where K_L and K_F are Langmuir and Freundlich constants in L/mg, respectively; C_e is the concentration at which the adsorption reaches equilibrium in mg/L; Q_e is the equilibrium adsorption capacity in mg/g; Q_{max} is the maximum adsorption capacity of the adsorbent; and 1/n is a dimensionless number representing the adsorption strength.

3 Results and analysis

3.1 Characteristics of specific surface area and pore size changes before and after biomass charcoal modification

As shown in Table 1, the BC-FeOOH pore size decreased from 9.59 nm to 4.12 nm, the BET specific surface area increased from 3.83 m^2/g to 5.17 m^2/g before modification, and the pore volume increased from 5.51×10^{-3} cm^3/g to 9.23×10^{-3} cm^3/g. The decrease in pore size of BC-FeOOH was mainly due to the fact that the biomass charcoal in the glycol and Fe(II) added during the modification process favored the increase in the number of micropores and adsorption sites, thus increasing its specific surface area and pore volume (Zeng et al., 2023). The BET results show a significant increase in surface area, providing more sites for Sb(V) molecules to be "physically adsorbed" or trapped within the pores. The micropores and mesopores (2–50 nm) are particularly important, as Sb(V) ions can be adsorbed through van der Waals forces and electrostatic interactions in these small spaces (Waldemar et al., 2020). Additionally, the high porosity of the biochar enhances the contact surface area between the adsorbent and the solution, further promoting the adsorption process.

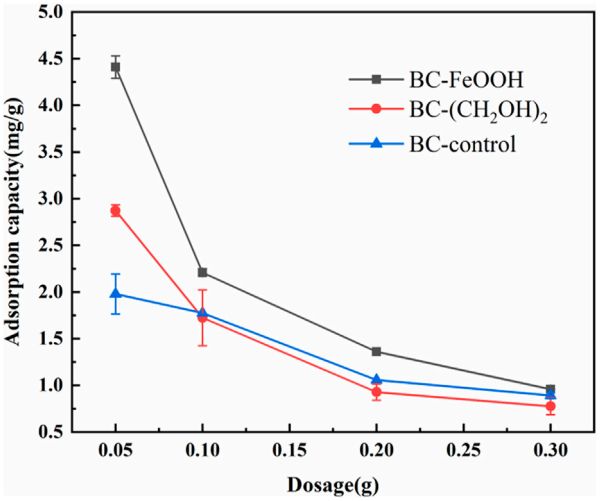

FIGURE 1
Effect of dosage on adsorption of antimony in water by biochar, the errors are based on the results of three parallel experiments.

3.2 Influence of biochar dosage on the adsorption effect of Sb

The adsorption performance of different dosages of the Sb(V) solution with an initial concentration of 10 mg/L was determined. As shown in Figure 1, with the increase of biochar dosage, the adsorption amount per unit mass of Sb by the three materials showed a decreasing trend. This indicates that their biochar dosage was inversely proportional to the adsorption amount. The reduction in adsorption capacity per unit mass of biochar with increasing biochar dosing was primarily attributable to the fact that the total quantity of Sb(V) in the water body was insufficient to saturate the adsorption process with excess biochar. Additionally, the decrease in adsorption capacity may be attributed to the aggregation of adsorption sites due to the increase in biochar, which results in the covering of some of the adsorption sites on the surface of the biochar, thereby reducing the adsorption capacity per unit mass (Mahdi et al., 2020). Throughout the adsorption process, the adsorption of Sb(V) onto biochar occurs through surface complexation and ion exchange. Oxygen-containing functional groups on the biochar surface, such as hydroxyl (-OH) and carboxyl (-COOH), interact with Sb(V) ions via electrostatic attraction or coordination, forming surface complexes that enhance adsorption. Additionally, ion exchange plays a key role, where exchangeable cations (e.g., Ca^{2+}, K^+) on the biochar are displaced by Sb(V) ions. This mechanism is pH-dependent (Trakal et al., 2014), with higher adsorption occurring in acidic conditions where the biochar surface carries a positive charge, promoting ion

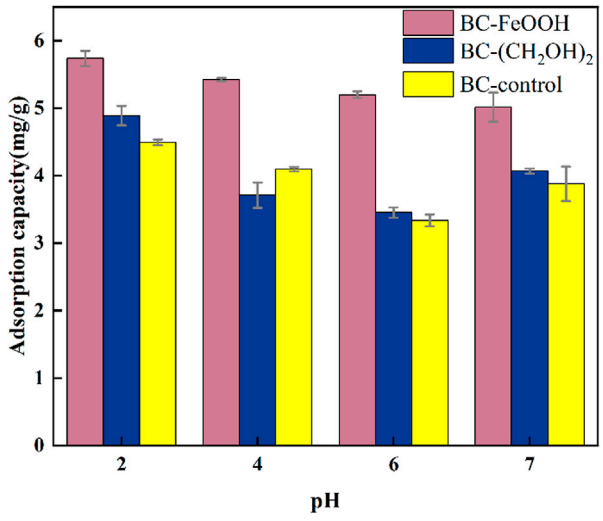

FIGURE 2
Effect of solution pH on adsorption of Sb(V) in water by biochar, the errors are based on the results of three parallel experiments.

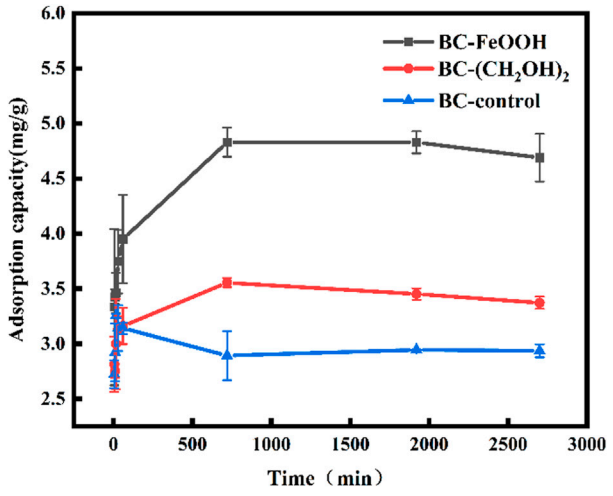

FIGURE 3
Effect of adsorption time on antimony adsorption by biochar, the errors are based on the results of three parallel experiments.

exchange and Sb(V) uptake. As illustrated in the figure, all three materials exhibited the highest adsorption capacity at a dosage of 0.05 g. The adsorption capacity of modified BC-FeOOH was up to 4.4 mg/g, which was significantly higher than that of ethylene glycol-modified biochar and unmodified biochar. Therefore, based on considerations of cost and removal effect, the optimal dosage of biochar was determined to be 0.05 g. Additionally, the maximum removal capacities of activated carbon and activated alumina for antimony generally range between 10–100 mg/g (Lee et al., 2024; Xu et al., 2001). While these adsorbents exhibit higher adsorption capacities compared to the 4.4 mg/g removal capacity of biochar modified with Rosa roxburghii residue, the relatively high costs associated with activated carbon and activated alumina may hinder their economic viability for large-scale applications. The adsorption capacities of silicate minerals, when used as adsorbents for antimony, exhibit significant variability. For instance, some silicate minerals, such as bentonite and kaolinite, have adsorption capacities of less than 1.0 mg/g (Xi et al., 2010). In contrast, the modified biochar derived from Rosa roxburghii residue demonstrates superior adsorption properties, outperforming these low-efficiency silicate minerals.

3.3 Effect of pH on adsorption properties of biochar

Solution pH represents a pivotal variable influencing the adsorption efficacy of solution Sb. pH exerts a dual influence on the biochar surface functional groups, affecting both their effectiveness and the morphology, existence, and chemical characteristics of Sb(V) in aqueous solution (Sun et al., 2011). The adsorption of Sb by the three types of biochar exhibited a slight decrease with an increase in pH (Figure 2). The maximum adsorption amount of the three types of biochar was observed at pH = 2, with the maximum adsorption amounts of BC-FeOOH, BC-(CH The adsorption amounts of the three biochars at pH 6 were 5.7 mg/g, 4.8 mg/g, and 4.5 mg/g, respectively. At pH 6, the adsorption amounts of the respective biochars reached the lowest values. The results of the present experimental study are in general agreement with those of previous studies. This may be due to the fact that the type of Sb(V) in the solution and the surface charge of the adsorbent are affected by pH (Deng et al., 2020). When the solution is acidic, the presence of a large amount of H+ in the solution induces the protonation of functional groups on the surface of the biochar, which in turn leads to an increase in the positive charge on the surface of the biochar. This contributes to the electrostatic attraction and complexation reactions between the Sb in the solution and the functional groups on the surface of the biochar (Di et al., 2021). Furthermore, it has been demonstrated that the surface of biochar is susceptible to positive charging under strong acidic conditions, and with increasing pH, the surface of biochar is negatively charged (Wan et al., 2020). Consequently, an increase in solution pH may result in an electrostatic repulsion effect between the surface of biochar and Sb(OH)- ions, which impairs the biochar's ability to adsorb and remove Sb (Li et al., 2022). Consequently, the adsorption of Sb by the three biochar species demonstrated a declining trend with increasing solution pH.

3.4 Adsorption kinetics

Adsorption kinetics can be employed as the primary criterion for evaluating the potential practical application of biochar adsorbents. In cases where the adsorption process is rapid and efficient, the associated costs can be reduced. Figure 3 illustrates the trends in adsorption amount and removal rate of Sb(V) in water over time for the three biochars. The adsorption amount increased rapidly during the initial two hours of the adsorption process, after which the growth slowed down to reach equilibrium after 10 ours. The equilibrium adsorption amounts of Sb(V) by biochar prepared from different modified materials were 4.8 mg/g, 3.6 mg/g, The

TABLE 2 Adsorption kinetic parameter model of antimony adsorption on biochar.

Sample	Pseudo-first-order model			Pseudo-second-order model		
	$K_1/(h^{-1})$	$Q_e/(mg/g)$	R^2	K_2 ($g{\cdot}mg^{-1}h^{-1}$)	$Q_e/(mg/g)$	R^2
BC-FeOOH	0.21	4.3	0.34	0.07	4.57	0.1
BC-$(CH_2OH)_2$	0.34	3.24	0.33	0.21	3.37	0.75
BC-control	0.42	3.08	0.49	0.63	3.17	0.31

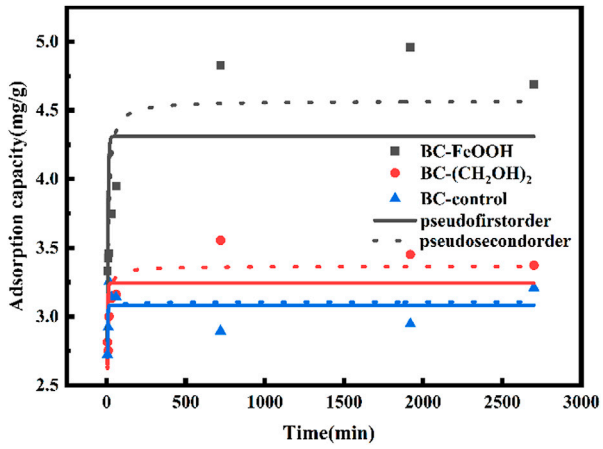

FIGURE 4
Dynamic adsorption equation model.

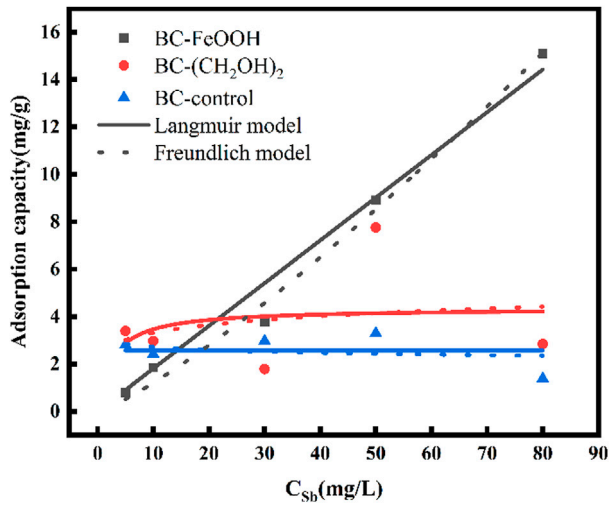

FIGURE 5
Isothermal adsorption curve equation model.

equilibrium adsorption amounts were 2.9 mg/g, and the equilibrium removal rates were 35%, 26.5%, and 22%, respectively. These results indicated that BC-FeOOH exhibited the best adsorption effect. The presence of FeOOH may provide additional adsorption sites, beyond those provided by surface functional groups, which could enhance the adsorption efficiency of BC-FeOOH. Furthermore, it was demonstrated that biochar with larger pores exhibited a higher rate of adsorption of Sb removal (Chen et al., 2022), indicating that the pore structure of the surface of prickly pear pomace modified biochar by Fe was enhanced, which accelerated the diffusion rate of Sb within the pores and resulted in a faster rate of BC-FeOOH adsorption.

During the adsorption of Sb from solution by biochar, there were more adsorption sites and functional groups on the surface of the adsorbent at the beginning stage of adsorption, and the competition between ions was minimal. Additionally, functional groups with high adsorption affinity on the adsorbent surface were occupied first, which led to a rapid increase in adsorption efficiency. However, as adsorption proceeds, the limited adsorption sites are gradually saturated, and heavy metal ions begin to diffuse into the interior of the adsorbent. This leads to a gradual increase in diffusion resistance and a decrease in diffusion rate. At the same time, the remaining adsorption sites with lower adsorption affinity begin to function, and gap diffusion may occur. The adsorption rate gradually slows down and eventually tends to adsorption equilibrium (Zhou et al., 2017).

The adsorption mechanism of Sb by prickly pear pomace biochar was further investigated based on the study of the adsorption amount and removal rate of Sb(V) in solution, as well as the effect of different adsorption times on the adsorption performance of biochar. The adsorption of Sb(V) by prickly pear pomace biochar was used in this study. Table 2 presents the fitting parameters of the proposed primary equation and the proposed secondary kinetic equation model for the adsorption of Sb(V) by prickly pear pomace biochar. Figure 4 depicts the results of the adsorption kinetic equation. The adsorption rate of the three biochar samples exhibited a trend of initial acceleration followed by a deceleration with increasing time, reaching equilibrium after approximately 8 h. The adsorption amount of BC-FeOOH was the highest at equilibrium, reaching 4.6 mg/g, while the adsorption amount of BC-control was the lowest, at 3.1 mg/g. The adsorption of Sb(V) in water by FeOOH-modified prickly pear pomace biochar was found to be the most effective.

The pseudo-primary kinetic fitted R^2 values of the three biochars were 0.34, 0.33, and 0.49, respectively, while the proposed secondary kinetic fitted R^2 values were 0.71, 0.75, and 0.31. These results indicated that the proposed secondary kinetic equations better responded to the adsorption mechanism of modified prickly pear pomace biochar on Sb(V), and also indicated that the surface adsorption energy of the modified prickly pear pomace biochar in the adsorption process was uniformly distributed. The proposed primary kinetic adsorption is physical adsorption, whose adsorption process is mainly controlled by diffusion, and the proposed

TABLE 3 Parameter model of isothermal adsorption curve for Biocarbon adsorption of antimony.

Sample	Langmuir model			Freundlich model		
	K_L/(L/m	Q_m/(mg/g)	R^2	K_F(L/mg)	n	R^2
BC-FeOOH	0.07	13.80	0.97	0.07	1.22	0.99
BC-$(CH_2OH)_2$	2.41	4.35	0.05	0.21	0.14	0.06
BC-control	3.19	2.57	0.3333	0.63	−0.07	−0.22

secondary equation is mainly chemical adsorption, whose adsorption process is mainly controlled by binding force (Fang et al., 2021). Therefore, the adsorption mechanism of Sb by the two biochars, BC-FeOOH and BC-$(CH_2OH)_2$, is mainly chemisorption, and BC-control's mainly exhibits physisorption.

3.5 Adsorption isothermal process

The adsorption isotherms of Sb in water by the three biochars are presented in Figure 5. It can be observed that the adsorption of Sb in water by BC-FeOOH increased with the increase of the initial concentration, and that the adsorption and removal capacity of Sb in solution was stronger. The adsorption amount of BC-control and BC-$(CH_2OH)_2$ was greater than that of BC-FeOOH when the concentration was lower, and the adsorption amount of BC-FeOOH exceeded that of BC-$(CH_2OH)_2$when the concentration reached up to 20 mg/L, with a greater adsorption capacity. This indicates that BC-$(CH_2OH)_2$ can be used for the treatment of low concentrations of Sb in water, while BC-FeOOH can be efficiently adsorbed to remove Sb from water. The parameters calculated by Langmuir and Freundlich models are shown in Table 3. The adsorption effects of BC-$(CH_2OH)_2$ and BC-control were not obvious. Therefore, these parameters are not discussed further. The Langmuir and Freundlich equations for BC-FeOOH both have R^2 values greater than 0.9, indicating that these isothermal adsorption equations can fit the experimental data better. This also indicates that the adsorption process of modified prickly pear pomace on Sb from water may be affected by a variety of adsorption mechanisms. The R^2 value of the Freundlich equation is greater than that of the Langmuir equation, indicating that the Langmuir equation more accurately describes the adsorption process of BC-FeOOH on Sb as homogeneous monolayer chemisorption (Zhou et al., 2016). Its 1/n is 0.81, which is less than 1, suggesting that this adsorption process is more facile (Wang L. et al., 2018).

4 Conclusion

In this study, modified prickly pear pomace biochar (BC-FeOOH) was prepared from prickly pear pomace as the raw material. The adsorption characteristics of modified prickly pear pomace biochar on Sb in water were investigated with different biochar dosages, pH values, and reaction times. The results confirmed the feasibility of the modified prickly pear pomace biochar for the removal of Sb in water. The experimental results demonstrated that the maximum adsorption of antimony in water was achieved at a biochar dosage of 0.05 g and a pH of 2.0. The kinetic and isothermal modeling indicated that the reaction kinetics of the adsorption process of Sb by BC-FeOOH conformed to the proposed second-order kinetic equation, and the isothermal adsorption curves conformed to the Langmuir model. The adsorption The adsorption of Sb in water by BC-FeOOH was a mono-molecular-layer chemical adsorption process. The adsorption of Sb in water by BC-FeOOH exhibited excellent adsorption performance, and it is an adsorbent with considerable potential for application. The application of BC-FeOOH to the adsorptive removal of Sb in water not only provides an efficient, inexpensive, and fast way to remove Sb from wastewater, but also realizes the efficient green resourcefulness and harmless utilization of prickly pear residue.

Data availability statement

The raw data supporting the conclusions of this article will be made available by the authors, without undue reservation.

Author contributions

YD: Formal Analysis, Funding acquisition, Writing–original draft. SZ: Supervision, Validation, Writing–review and editing. RZ: Investigation, Methodology, Writing–review and editing, Supervision.

Funding

The author(s) declare that no financial support was received for the research, authorship, and/or publication of this article.

Conflict of interest

Author YD was employed by China Overseas Construction Limited.

The remaining authors declare that the research was conducted in the absence of any commercial or financial relationships that could be construed as a potential conflict of interest.

Generative AI statement

The author(s) declare that no Generative AI was used in the creation of this manuscript.

Publisher's note

References

An, Q., Miao, Y., Zhao, B., Li, Z., and Zhu, S. (2020). An alkali modified biochar for enhancing Mn2+ adsorption: performance and chemical mechanism. *Mater. Chem. Phys.* 248, 122895. doi:10.1016/j.matchemphys.2020.122895

Caidi, Y., Jingjing, L., and Shenggao, L. (2021). Pyrolysis temperature affects pore characteristics of rice straw and canola stalk biochars and biochar-amended soils. *Geoderma*, 397. doi:10.1016/J.GEODERMA.2021.115097

Cavallo, D., Iavicoli, I., Setini, A., Marinaccio, A., Perniconi, B., Carelli, G., et al. (2002). Genotoxic risk and oxidative DNA damage in workers exposed to antimony trioxide. *Environ. Mol. Mutagen.* 40, 184–189. doi:10.1002/em.10102

Chen, H. B., Gao, Y. R., El-Naggar, A., Niazi, N. K., Sun, C. H., Shaheen, S. M., et al. (2022). Enhanced sorption of trivalent antimony by chitosan-loaded biochar in aqueous solutions: characterization, performance and mechanisms. *J. Hazard. Mater.*, 425. doi:10.1016/j.jhazmat.2021.127971

Deng, J. Q., Li, X. D., Wei, X., Liu, Y. G., Liang, J., Shao, Y. N., et al. (2020). Different adsorption behaviors and mechanisms of a novel amino-functionalized hydrothermal biochar for hexavalent chromium and pentavalent antimony. *Bioresour. Technol.* 310, 123438. doi:10.1016/j.biortech.2020.123438

Deng, R. J., Jin, C. S., Ren, B. Z., Hou, B. L., and Hursthouse, A. S. (2017). The potential for the treatment of antimony-containing wastewater by iron-based adsorbents. *Water* 9, 794. doi:10.3390/w9100794

Di, F. J., Zhang, C., Song, G. F., Jiang, S. X., Shan, B. Q., and Song, Z. X. (2021). The adsorption mechanism of kapok biochar on Cr(VI) in aqueous solution. *Acta Sci. Circumstantiae* 41 (05), 1891–1900.

Druzbicka, J., and Craw, D. (2015). Metalloid attenuation from runoff waters at an historic orogenic gold mine, New Zealand. *Mine Water Environ.* 34, 417–429. doi:10.1007/s10230-014-0316-2

Fang, Z., Suhua, H., Xu, L., Jian, F., Qi, L., Zhiwei, W., et al. (2021). Adsorption kinetics and thermodynamics of rare earth on Montmorillonite modified by sulfuric acid. *Colloids Surfaces a-Physicochemical Eng. Aspects* 627, 127063. doi:10.1016/j.colsurfa.2021.127063

Fatouma, A. M., Ayoub, A., Touria, H., Abbi, R., Achira, M., Abourriche, A., et al. (2023). Materials derived from olive pomace as effective bioadsorbents for the process of removing total phenols from oil mill effluents. *Molecules* 28 (11), 4310. doi:10.3390/molecules28114310

Hamzah, S., Razali, A. N., Yatim, I. N., Alias, M., Ali, A., Zaini, S. N., et al. (2018). Characterisation and performance of thermally treated rice husk as efficient adsorbent for phosphate removal. *J. Water Supply Res. Technology—AQUA* 67 (8), 766–778. doi:10.2166/aqua.2018.087

Jain, A., Sarsaiya, S., Gong, Q. H., Wu, Q., and Shi, J. S. (2024). Chemical diversity, traditional uses, and bioactivities of Rosa roxburghii Tratt: a comprehensive review. *Pharmacol. and Ther.*, 259. doi:10.1016/J.PHARMTHERA.2024.108657

Jia, X., Zhou, J., Liu, J., Liu, P., Yu, L., Wen, B., et al. (2020). The antimony sorption and transport mechanisms in removal experiment by Mn-coated biochar. *Sci. Total Environ.* 724, 138158. doi:10.1016/j.scitotenv.2020.138158

Lee, S. H., Chung, J., and Lee, Y. W. (2024). Adsorption removal characteristics of hazardous metalloids (antimony and arsenic) according to their ionic properties. *Water* 16 (5), 767. doi:10.3390/w16050767

Li, H., Dong, X., da Silva, E. B., de Oliveira, L. M., Chen, Y., and Ma, L. Q. (2017). Mechanisms of metal sorption by biochars: biochar characteristics and modifications. *Chemosphere* 178, 466–478. doi:10.1016/j.chemosphere.2017.03.072

Li, J., Zheng, B., He, Y., Zhou, Y., Chen, X., Ruan, S., et al. (2018). Antimony contamination, consequences and removal techniques: a review. *Ecotoxicol. Environ. Saf.* 156, 125–134. doi:10.1016/j.ecoenv.2018.03.024

Li, Q., Ma, X., Qi, C., Li, R., Zhang, W., Li, J., et al. (2022). Facile preparation of novel magnetic mesoporous Fe Mn binary oxides from Mn encapsulated carboxymethyl cellulose-Fe(III) hydrogel for antimony removal from water. *Sci. Total Environ.*, 821. doi:10.1016/J.SCITOTENV.2022.153529

Liu, Y., Zhong, D. J., Xu, Y. L., Chang, H. X., Dong, L., Han, Z. F., et al. (2023). Facile synthesis of lanthanum-doped Fe-based MOF for phosphate removal from water: high adsorption capacity, tuneability, and reproducibility. *Water Air Soil Pollut.* 234, 321. doi:10.1007/s11270-023-06340-6

Mahdi, Z., El Hanandeh, A., and Yu, Q. J. (2020). Electro-assisted adsorption of heavy metals from aqueous solutions by biochar. *Water Sci. Technol.* 81, 801–812. doi:10.2166/wst.2020.163

Park, S.-J., Lee, Y.-J., Kang, J.-K., Lee, J.-C., and Lee, C.-G. (2021). Application of Fe-impregnated biochar from cattle manure for removing pentavalent antimony from aqueous solution. *Appl. Sci.* 11, 9257. doi:10.3390/app11199257

Peidong, L., Chao, L., Xiong, F., Huang, Q., and Qing, C. (2023). Physicochemical, functional and biological properties of soluble dietary fibers obtained from Rosa roxburghii Tratt pomace using different extraction methods. *Process Biochem.*, 12840–12848. doi:10.1016/J.PROCBIO.2023.02.021

Rahaman, M. S., Basu, A., and Islam, M. R. (2008). The removal of As(III) and As(V) from aqueous solutions by waste materials. *Bioresour. Technol.* 99, 2815–2823. doi:10.1016/j.biortech.2007.06.038

Shan, C., Ma, Z., and Tong, M. (2014). Efficient removal of trace antimony(III) through adsorption by hematite modified magnetic nanoparticles. *J. Hazard. Mater.* 268, 229–236. doi:10.1016/j.jhazmat.2014.01.020

Sun, F. H., Wu, F. C., Liao, H. Q., and Xing, B. S. (2011). Biosorption of antimony(V) by freshwater cyanobacteria Microcystis biomass: chemical modification and biosorption mechanisms. *Chem. Eng. J.* 171, 1082–1090. doi:10.1016/j.cej.2011.05.004

Tang, H. Y., Hassan, M. U., Nawaz, M., Yang, W. T., Liu, Y., and Yang, B. J. (2023). A review on sources of soil antimony pollution and recent progress on remediation of antimony polluted soils. *Ecotoxicol. Environ. Saf.* 266, 115583. doi:10.1016/j.ecoenv.2023.115583

Trakal, L., Bingöl, D., Pohořelý, M., Hruška, M., and Komárek, M. (2014). Geochemical and spectroscopic investigations of Cd and Pb sorption mechanisms on contrasting biochars: engineering implications. *Bioresour. Technol.* 171, 171442–171451. doi:10.1016/j.biortech.2014.08.108

Waldemar, K., Malte, B., and Sergej, F. (2020). Measurement of sub-nanonewton forces inside a scanning electron microscope. *Rev. Sci. Instrum.* 91 (4), 043701. doi:10.1063/1.5144653

Wan, S., Qiu, L., Li, Y., Sun, J., Gao, B., He, F., et al. (2020). Accelerated antimony and copper removal by manganese oxide embedded in biochar with enlarged pore structure. *Chem. Eng. J.* 402, 126021. doi:10.1016/j.cej.2020.126021

Wang, C., Wang, H., and Cao, Y. (2018a). Pb(II) sorption by biochar derived from Cinnamomum camphora and its improvement with ultrasound-assisted alkali activation. *Colloids Surfaces A Physicochem. Eng. Aspects* 556, 177–184. doi:10.1016/j.colsurfa.2018.08.036

Wang, L., Wang, J., Wang, Z., He, C., Lyu, W., Yan, W., et al. (2018b). Enhanced antimonate (Sb(V)) removal from aqueous solution by La-doped magnetic biochars. *Chem. Eng. J.* 354, 623–632. doi:10.1016/j.cej.2018.08.074

Wang, L., Zhang, P., Chen, Y., Tian, Y., and Chen, J. (2021). Physicochemical characterization and *in vitro* biological activities of water-extracted polysaccharides fractionated by stepwise ethanol precipitation from Rosa roxburghii Tratt fruit. *J. Food Meas. Charact.* 16, 38–48. doi:10.1007/s11694-021-01125-z

Xi, J., He, M., and Lin, C. (2010). Adsorption of antimony(III) and antimony(V) on bentonite: kinetics, thermodynamics and anion competition. *Microchem. J.* 97 (1), 85–91. doi:10.1016/j.microc.2010.05.017

Xu, S., Deng, J., Wu, S., Fei, Q., Lin, D., Chen, H., et al. (2024). Dynamic changes of active components and volatile organic compounds in rosa roxburghii fruit during the process of maturity. *Foods Basel, Switz.* 13 (18), 2893. doi:10.3390/foods13182893

Xu, Y. H., Ohki, A., and Maeda, S. (2001). Adsorption and removal of antimony from aqueous solution by an activated alumina. *Toxicol. and Environ. Chem.* 80 (3-4), 133–144. doi:10.1080/02772240109359004

Yi, Y., Huang, Z., Lu, B., Xian, J., Tsang, E. P., Cheng, W., et al. (2020). Magnetic biochar for environmental remediation: a review. *Bioresour. Technol.* 298, 298122468. doi:10.1016/j.biortech.2019.122468

Zeng, W., Zhu, J., Guo, X. Q., and Yin, H. (2023). Adsorption effect of FeOOH loaded rosa roxburghii residue biomass carbon on fluorine (F^-) in water. *J. Sichuan Normal Univ.* 41 (04), 690–697. doi:10.16036/j.issn.1000-2650.202203175

Zhou, L., Liu, Y., Liu, S., Yin, Y., Zeng, G., Tan, X., et al. (2016). Investigation of the adsorption-reduction mechanisms of hexavalent chromium by ramie biochars of different pyrolytic temperatures. *Bioresour. Technol.* 218, 351–359. doi:10.1016/j.biortech.2016.06.102

Zhou, X., Zeng, Z., Zeng, G., Lai, C., Xiao, R., Liu, S., et al. (2020). Persulfate activation by swine bone char-derived hierarchical porous carbon: multiple mechanism system for organic pollutant degradation in aqueous media. *Chem. Eng. J.* 383, 123091. doi:10.1016/j.cej.2019.123091

Zhou, X., Zhu, G., Lu, Y., Du, B., Lin, D., and Ran, Z. (2019). Optimization of insoluble dietary fiber preparation technology from Rosa roxburghii Tratt pomace by enzyme method. *IOP Conf. Ser. Earth Environ. Sci.* 330 (4), 042052. doi:10.1088/1755-1315/330/4/042052

Zhou, Y. Y., Liu, X. C., Xiang, Y. J., Wang, P., Zhang, J. C., Zhang, F. F., et al. (2017). Modification of biochar derived from sawdust and its application in removal of tetracycline and copper from aqueous solution: adsorption mechanism and modelling. *Bioresour. Technol.* 245, 266–273. doi:10.1016/j.biortech.2017.08.178

frontiers | Frontiers in Environmental Science

TYPE Original Research
PUBLISHED 09 January 2025
DOI 10.3389/fenvs.2024.1539964

OPEN ACCESS

EDITED BY
Yaoguang Guo,
Shanghai Polytechnic University, China

REVIEWED BY
Chunqiao Xiao,
Wuhan Institute of Technology, China
Peng Zhang,
China University of Geosciences Wuhan, China
Yasir Al-Ani,
University of Anbar, Iraq

*CORRESPONDENCE
Rongxin Liu,
13595363067@163.com

RECEIVED 05 December 2024
ACCEPTED 23 December 2024
PUBLISHED 09 January 2025

CITATION
Liu R, Liu C, Du J, Wang C, Yuan Y and Zhang X (2025) Preparation of phosphogypsum ecological concrete and study on its phytogenic properties.
Front. Environ. Sci. 12:1539964.
doi: 10.3389/fenvs.2024.1539964

Preparation of phosphogypsum ecological concrete and study on its phytogenic properties

Rongxin Liu[1]*, Chunduo Liu[1], Jiang Du[1], Cheng Wang[1], Yonghui Yuan[1] and Xin Zhang[2]

[1]China Overseas Construction Limited, Guangdong Shenzhen, Shenzhen, China, [2]Resource and Environmental Engineering College, Guizhou University, Guiyang, Guizhou, China

In this study, vegetative eco-concrete was prepared based on electrolytic manganese slag/phosphogypsum composite cementitious material as binder and clayey ceramic grains as aggregate. Based on the conditions of porosity and water-cement ratio, the optimal proportion of phosphogypsum-based eco-concrete was investigated, and concrete specimens with good performance were prepared (14 days compressive strength: 3.49 MPa, permeability coefficient: 1.37, total porosity: 24.5%, Improved compressive strength by 15% and water retention by 20%). The nutrient matrix of vegetative eco-concrete with different phosphogypsum/electrolytic manganese slag ratios was designed and modified, and the vegetative performance of the eco-concrete was investigated using four-season grass, ryegrass, clippings and clover as the grass species. The results showed that the eco-concrete based on phosphogypsum as raw material was rich in nutrients such as nitrogen, phosphorus and potassium, which could meet the requirements of plant growth, Supporting plant growth with a 30% increase in root length and 25% improvement in biomass compared to control concrete. The addition of improvers had a good passivation effect on heavy metals such as As, Cu, Cr, Zn, Sb and Pb in the phytogenic substrate. The adaptability of different grass species to the planting substrate was Four Seasons > ryegrass > shepherd's purse > clover, alfalfa, dogbane; the application of electrolytic manganese slag substrate had the best performance of planting, and the planting substrate with the application of improver inhibited the growth of plants. The study addresses the challenge of using phosphogypsum as a binder in concrete, which has traditionally faced issues with strength and stability. By optimizing the mix ratio and curing process, we were able to achieve a concrete material that not only performs well mechanically but also supports plant growth.

KEYWORDS

ecological concrete, electrolytic manganese slag, phytogenic performance, phosphogypsum, planting substrate

1 Introduction

Phosphogypsum (PG), a byproduct of the phosphorus chemical industry, is characterized by high production and stockpiling volumes, along with a low rate of resource utilization (Liu et al., 2022). Globally, PG accumulations have reached approximately 6 billion tons, increasing by 150 million tons annually, while the overall utilization rate remains below 20% (Liu et al., 2022; Du et al., 2022). In China, annual PG production is around 75 million tons, with an estimated 40%

utilization rate. Notably, five provinces—Hubei, Yunnan, Guizhou, Sichuan, and Anhui—account for approximately 85% of the country's total PG production, largely due to their substantial phosphate fertilizer output (Cui et al., 2022). The primary component of PG is $CaSO_4{\cdot}2H_2O$, yet it also contains hazardous impurities such as calcium fluoride, acid-insoluble materials, soluble phosphorus, heavy metals, and radioactive elements, which pose health risks to humans and harm plant growth (Liu et al., 2022). PG disposal mainly relies on long-term stockpiling, which not only occupies significant land resources but also presents considerable environmental and safety risks. This situation exerts substantial pressure on China's ecological protection efforts and poses a significant obstacle to the sustainable development of phosphorus chemical enterprises. Consequently, enhancing the resource utilization of PG has become a critical issue urgently requiring industry solutions.

Currently, the resource utilization of PG is primarily applied in areas such as road construction, building materials, agriculture, and mine reclamation (Cui et al., 2022; Huang et al., 2023; Jin et al., 2024). Among these, the use of PG in the building materials industry—such as for producing bricks, lightweight aggregates, and binders—represents an effective large-scale approach to PG resource utilization (Huang et al., 2019; Junakova and Junak, 2017; Liang and Li, 2015). However, impurities like phosphorus and fluorine in PG may impact the performance of construction materials. To mitigate these effects, PG is typically calcined at high temperatures to produce hemihydrate or anhydrite gypsum, which is then used to manufacture cement and slag-based composite binders, addressing the impurity issues to a certain extent (Garg, 1995; Yang and Qian, 2011). For instance, Zhang Yi and colleagues successfully prepared gypsum-based binders with desirable mechanical properties using PG (Cao, 2018; Huang et al., 2016; Zhang et al., 2011). Therefore, developing innovative methods for preparing PG-based binders can significantly enhance the efficiency of PG utilization. Additionally, numerous studies have demonstrated effective modification of PG using quicklime, industrial alkaline wastes, and fly ash to produce cement retarders, with the resulting cement products meeting national standards (Yang et al., 2003; Li et al., 2002; Zhou et al., 2007). At present, the production of cement retarders from PG remains the primary method for large-scale PG consumption.

Ecological concrete, also known as "vegetative concrete," is an innovative concrete material distinct from conventional concrete, designed to support plant growth, regulate ecological balance, enhance environmental aesthetics, and provide protective functions (Chen, 2021). It is widely applied in ecological protection of slopes along highways, riverbanks, and reservoirs, as well as in municipal engineering, ecological landscaping, mountain restoration, and vertical greening (Ismaeel et al., 2023; M S et al., 2020; Yatesh et al., 2023; Said Awad et al., 2024a), playing a critical role in preventing soil erosion and enhancing environmental quality. This material offers promising application potential. Ecological concrete consists of coarse aggregate, binding materials, and water mixed in specific proportions, providing a high porosity that creates space and water cycling conditions conducive to plant growth (Song, 2009). Though traditionally cement is used as the primary binding material in most ecological concrete, its high energy consumption and elevated alkalinity are unfavorable for plant growth. To mitigate the environmental impacts associated with traditional cement, researchers have explored alternative materials that can enhance both the sustainability and performance of ecological concrete. One such material is phosphogypsum (PG), which, when incorporated as a binder, not only reduces the reliance on cement but also offers additional environmental benefits, such as waste recycling and reduced carbon footprint. Alongside PG, the ongoing challenge of managing waste materials, such as plastic waste, has spurred innovative solutions in the construction industry. Incorporating waste plastics into concrete not only addresses the growing issue of plastic pollution but also improves the material's thermal properties. Similar to the use of phosphogypsum in concrete, recycling plastic waste provides a sustainable alternative to traditional concrete, offering significant environmental benefits (Said et al., 2024b; Hameed et al., 2023; Jassam et al., 2023).

Research has demonstrated that electrolytic manganese residue (EMR) can be processed into a low-strength binder suitable for ecological concrete production, presenting a viable expansion path (Zhang, 2022). EMR has demonstrated versatility in construction materials, including cement, road bases, and ceramics, with the potential for direct incorporation into Portland cement without high-temperature pretreatment. This approach reduces costs and environmental impacts while functioning effectively as a low-strength binder in ecological concrete (Fu et al., 2023; Shichao et al., 2023). Research has also shown that EMR enhances concrete durability and performance, with its gypsum and sulfate content activating slag pozzolanic activity to improve the microstructure and overall properties (Wang et al., 2013). These findings highlight EMR's significant potential for sustainable construction practices. However, there has been limited research on using PG as a binder for ecological concrete. While the benefits of incorporating industrial by-products like phosphogypsum into concrete are known, most studies have focused solely on the material's mechanical properties. In contrast, this study examines its dual role—enhancing both the mechanical performance and ecological functions of concrete, specifically its superior water retention and its ability to promote plant growth. By building on our previous work, this study expands the scope to include the ecological impact of phosphogypsum-based concrete, addressing the research gap where few studies have investigated its combined effects on sustainability and plant growth.

This study aims to develop a plant-compatible ecological concrete using PG as a primary material, mixed with electrolytic manganese residue and slag powder to create composite binders at various PG-to-manganese residue ratios. This composite binder is then used to produce vegetative ecological concrete. The study examines the effects of different mix designs on the water absorption, porosity, and compressive strength of the ecological concrete. Additionally, PG and electrolytic manganese residue are blended with diatomaceous earth and straw biochar to create an improved planting substrate. The vegetative performance of common grass species is tested to explore novel pathways for PG resource utilization.

TABLE 1 Main chemical composition of phosphogypsum and electrolytic manganese residue (wt%).

Materials	SiO_2	CaO	SO_3	Al_2O_3	Fe_2O_3	MgO	K_2O	Na_2O	TiO	MnO	P_2O_5	∑
PG	4.87	52.20	39.02	0.88	1.25	0.17	0.13	0.26	0.16	—	0.86	99.8
EMR	40.72	14.41	18.78	11.10	5.49	2.16	2.29	1.18	0.54	2.99	—	99.6
GGBFS	32.49	35.28	1.62	19.22	0.52	8.76	0.40	0.61	0.63	0.19	—	99.9

Note: means below detection limit.

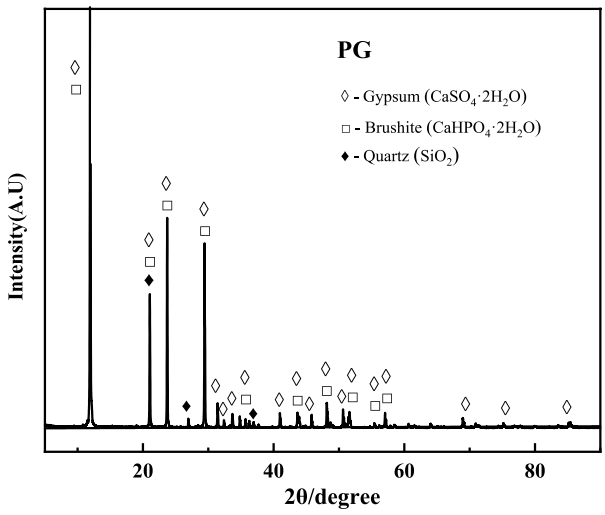

FIGURE 1
XRD patterns of PG.

2 Materials and methods

2.1 Materials

2.1.1 Test raw materials

PG was sourced from a phosphogypsum stockpile at a Wengfu facility. After thorough mixing, it was air-dried to a moisture content of ≤1%, ground to pass through a 0.25 mm sieve, and stored in a sealed container for later use. Electrolytic manganese residue was obtained from a stockpile in Songtao County, Guizhou Province. S95-grade ground granulated blast furnace slag (GGBFS) was purchased from Taiyuan Iron & Steel Group Co., Ltd. Ordinary Portland cement (P·O42.5), with a residue of 3.5% on a 180-mesh sieve, was commercially available. Lightweight clay ceramsite (particle size 1–1.5 mm, compressive strength 1.3 MPa) was acquired from the local market. Luminescent bacteria (from *Photobacterium phosphoreum*) were provided by Beijing Hamamatsu Photon Techniques Co., Ltd. All chemicals used in the experiments were of analytical grade, and distilled water was used as the experimental water source.

The chemical compositions of PG, EMR, and GGBFS are presented in Table 1. PG mainly consists of CaO, SO_3, and SiO_2, while EMR's primary components include SiO_2, SO_2, CaO, Fe_2O_3, and MgO. The main constituents of GGBFS are SiO_2, CaO, Al_2O_3, and MgO. The X-ray diffraction (XRD, BrukerAXSD8 Advance, Germany) pattern of PG is shown in Figure 1, indicating gypsum ($CaSO_4·2H_2O$), monetite ($CaHPO_4·2H_2O$), and quartz (SiO_2) as the primary mineral phases.

2.1.2 Composite cementitious material preparation

A composite cementitious material was prepared using PG, EMR and ground granulated blast furnace slag (GGBFS). In this experiment, a mass ratio of 50:10:20:10 was used for EMR, PG, slag powder, and cement to produce the EMR-PG composite binder, with an addition of 4% CaO (AR, 99%, Sinopharm). After combining the binder materials with EMR, 30% distilled water was added, and the mixture was stirred at a constant speed until thoroughly mixed. It was then left to stand in a ventilated area for 12 h before conducting a toxicity leaching test. The prepared EMR was dried at 40°C to a constant weight and passed through a 60-mesh sieve for later use. The materials were thoroughly mixed at a ratio of EMR:PG: slag = 50:20:20:10 and further blended with water at the standard consistency requirement. The resulting slurry was poured into molds measuring 40 mm × 40 mm × 40 mm. The molds were sealed with plastic film and cured at a constant temperature of 60°C and 95% ± 5% humidity for 12 h, followed by an additional 4 h at 60°C to remove excess surface moisture for easy demolding. Finally, the samples were cured at (25 ± 3)°C and 95% ± 5% humidity until the specified curing age was reached.

2.1.3 Eco-concrete mixing ratio

Ecological concrete was prepared according to the mix proportions shown in Table 2. The aggregate ceramsite was first combined with 50% of the mixing water and stirred for 30 s. Then, 50% of the composite binder, prepared as described in Section 2.1.2, was added and mixed thoroughly. The remaining 50% of the mixing water and binder were then added, and the mixture was stirred until homogenous. The mixture was then placed in molds measuring 70 mm × 70 mm × 70 mm in three layers, with each layer compacted to ensure even distribution. The surfaces of the specimens were smoothed, and the molds were wrapped in plastic film to retain moisture and prevent water evaporation. After curing for 14 days, the specimens were removed and set aside for further testing.

2.1.4 Method for determining the vegetative properties of eco-concrete

The molds used in this study had an outer diameter of 50 mm (with a wall thickness of 2 mm), a length of 150 mm, and were made of PVC. Three specimens were formed for each mix proportion. Additionally, an identical PVC pipe was prepared, with one end glued to a PVC joint to form the upper structure of a permeability testing device. The concrete was first thoroughly mixed according to the designated proportions, compacted, and leveled. To prevent moisture loss, the specimens were sealed with plastic film and

TABLE 2 Ecological concrete test mix ratio.

Ti	Design porosity (%)	Water consumption (kg/m^3)	Aggregate (kg/m^3)	Rubber-bone ratio (%)	Amount of cementitious material (kg/m^3)	Water cement ratio (%)
1	0.25	176.9	361	1.485	505.5	0.35
2	0.30	155.2	361	1.275	443.5	0.35
3	0.35	133.6	361	1.066	381.6	0.35

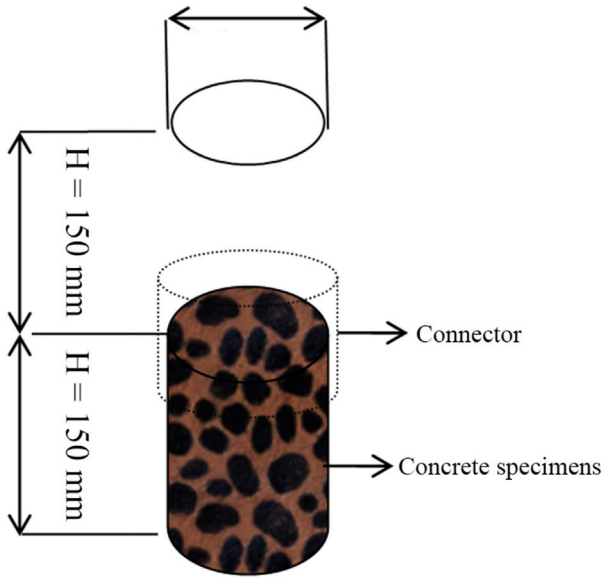

FIGURE 2
Permeability test installation.

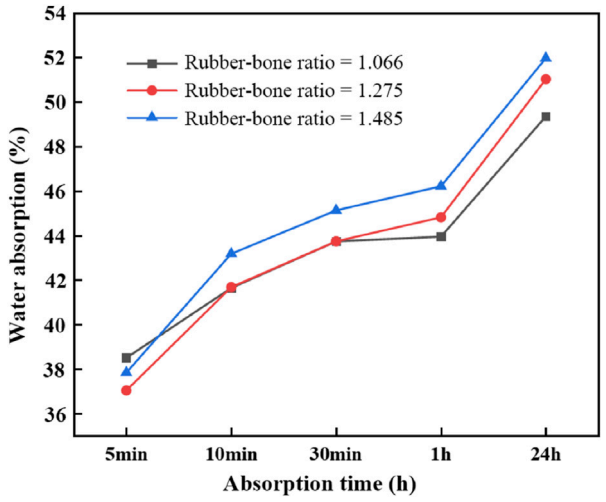

FIGURE 3
The effect of different rubber-bone ratio on water absorption.

TABLE 3 Experimental results of ecological concrete design mix ratio.

Formulation	Rubber-bone ratio (%)	Water-cement ratio (%)	Water permeability coefficient (cm/s)	14 days compressive strength (MPa)	Alkalinity	Porosity (%)	Total porosity (%)	Connected porosity (%)
1	1.485	0.33	1.37	3.49	10.15	0.25	24.5	0.235
2	1.275	0.33	2.75	2.58	9.87	0.30	28.1	0.278
3	1.066	0.33	4.13	1.29	10.43	0.35	34.7	0.342

cured at 60°C and 95% ± 5% humidity for 12 h. To facilitate demolding, excess surface moisture was removed by further curing the specimens at (25 ± 3)°C and 95% ± 5% humidity for 7 days. For the permeability test setup, a layer of petroleum jelly was applied to the top end of the mold containing the specimen and to the bottom end of an empty PVC pipe, which were then secured together with connectors. The structure of the permeability testing device is shown in Figure 2. To perform the test, 5 L of tap water was prepared, and water was introduced into the device, allowing the water level to gradually rise. When it reached 295 mm, additional water was added as needed to maintain a water level of 295 ± 5 mm throughout the experiment.

(1) The water permeability coefficient of concrete is calculated using Equation 1 below:

$$K_T = \frac{Q \cdot L}{A \cdot H \cdot (t_1 - t_2)} \quad (1)$$

In the formula: KT represents the permeability coefficient of ecological concrete at a water temperature of T °C, measured in cm/s. Q is the volume of water passing through the ecological concrete between time t_1 and t_2 measured in cm^3.L denotes the thickness of the permeable specimen.A is the cross-sectional area of the specimen, in cm^2. H represents the hydraulic head, in cm.t_1 is the

TABLE 4 Comparison of phosphogypsum concrete with other concrete.

Material	14-day compressive strength	Permeability coefficient	Total porosity	Water-retaining property
Conventional concrete	3.03 MPa	3.94	13.2%	1
Ecological concrete based on phosphogypsum	3.49 MPa	1.37	24.5%	Increase by 20%
Fly ash concrete (Rabatho et al., 2011; Araujo et al., 2004)	5.89 MPa	3.89	21.3%	Decrease by 24%
Slag concrete (Mun et al., 2005; Potgieter et al., 2003)	9.84 MPa	6.38	27.9%	Decrease by 18%

TABLE 5 Nutrient composition of plant substrate.

Name	PG	EMR	P:E = 1:9	P:E = 2:8	P:E = 3:7	P:E = 4:6	P:E = 5:5
pH	2.39	6.70	5.95	5.45	5.03	4.50	4.19
Alkaline dissolved nitrogen (mg/kg)	3.50	7,509.60	6,778.80	6,073.20	5,644.80	5,014.80	4,304.30
Quick-acting phosphorus (mg/kg)	4,295.9	585.30	141.10	364.20	694.20	1,290.70	1787.80
Quick-acting potassium (mg/kg)	471.6	408.50	442.90	418.10	439.20	432.50	412.30

Note: P:E indicates the mass ratio of PG to EMR delivery.

TABLE 6 Leaching of heavy metals in plant substrates under different ratios (mg/L).

Name	Pb	Cr	Zn	Sb	Mn	Cu	As	Cd
P:E = 1:9	—	0.010	0.091	0.005	1,350.05	0.182	0.018	0.003
P:E = 2:8	—	0.010	0.150	0.006	1,207.88	0.178	0.053	0.002
P:E = 3:7	—	0.011	0.228	0.008	1,131.62	0.171	0.108	0.002
P:E = 4:6	—	0.014	0.311	0.013	997.52	0.149	0.160	0.003
E:P = 5:5	—	0.022	0.405	0.019	894.94	0.167	0.248	0.004

Note: - is below the detection limit.

initial time of measurement, in seconds. t_2 is the final time of measurement, in seconds.

(2) Water absorption and porosity were calculated as shown in Equations 2–4, respectively:

The water absorption is determined as follows (Yu, 2016):

$$Q = \frac{W_x - W_0}{W_0} \quad (2)$$

In the formula: Q represents the water absorption rate after soaking for xxx time, expressed as a percentage (%); W_x denotes the mass of a single specimen after soaking for xxx time, in grams (g); W_0 is the mass of the specimen dried to a constant weight at 40°C, in grams (g).

The porosity test is conducted as follow (Peng et al., 2013):

$$P_1 = \left(1 - \frac{W_2 - W_1}{V}\right) \times 100\% \quad (3)$$

$$P_2 = \left(1 - \frac{W_2 - W_3}{V}\right) \times 100\% \quad (4)$$

In the formula: P_1 represents the total porosity of the specimen, expressed as a percentage (%); P_2 denotes the connected porosity of the specimen, expressed as a percentage (%); W_1 is the weight of the specimen after 24 h of soaking in water, in grams (g); W_2 represents the weight of the specimen in air after being removed from water and left to stand naturally for 24 h, in grams (g); W_3 is the weight of the specimen in water after standing naturally for 24 h, in grams (g).

2.2 Experimental design of planting substrate

2.2.1 Experiment on the proportion of planting substrate and its improvement

EMR and PG were passed through a 60-mesh sieve, then mixed at mass ratios of 9:1, 8:2, 7:3, 6:4, and 5:5. The EMR and PG mixtures, along with water and slag at a mass ratio of 10:1, were oscillated at a speed of 110 ± 10 rpm for 8 h and allowed to stand for 16 h before measuring the contents of alkali-hydrolyzable nitrogen, available phosphorus, and available potassium in the supernatant. To improve the planting substrate, 2.5% diatomaceous earth and

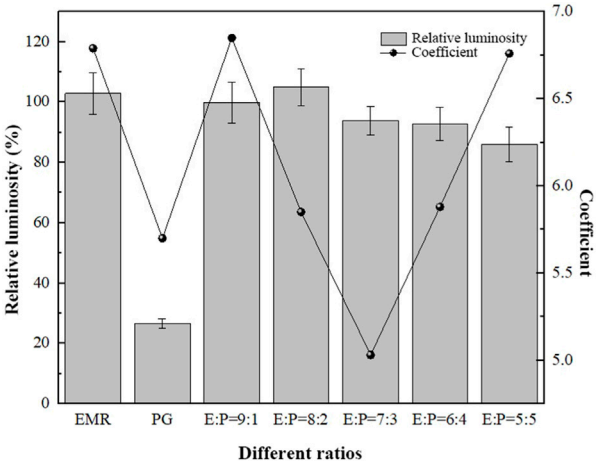

FIGURE 4
Relative luminosity of plant matrix leachate at different ratios.

2.5% straw biochar were added to each substrate (Lou et al., 2020). This modification aims to stabilize and adsorb metal ions released from EMR and PG, reducing their toxicity to plant growth and development.

2.2.2 Toxicity leaching test

In this study, the toxicity leaching test was conducted according to the method described in Leaching Toxicity Testing for Solid Waste—Horizontal Oscillation Method (HJ557-2010). A mixture of EMR and distilled water at a mass ratio of 1:10 was placed in a container, leached at 110 ± 10 rpm for 8 h, and then allowed to stand for 16 h. Additionally, To assess substrate toxicity, the sample pH (PHS-3C, Lei-ci, China), was initially adjusted to approximately 7.0 for testing with luminescent bacteria. Afterward, it was filtered, and the heavy metal content in the filtrate was measured.

Following Ma Mei's medium formula, a culture medium for luminescent bacteria was prepared (Ma, 2002). The luminescent bacteria were placed in an incubator for 15 min, to which 1 mL of bacterial recovery solution was added to activate the bacteria, followed by incubation for 12 h. This activation step was repeated three times before an appropriate amount of bacterial colonies was inoculated. The bacteria were then incubated in a constant-temperature shaker for 12–16 h for subsequent toxicity testing. Under the same conditions, second- and third-generation bacteria were obtained and preserved for future use. A standard white opaque 96-well enzyme-linked immunosorbent assay (ELISA) plate was used as the carrier. Into each well, 150 μL of the test sample and 50 μL of the cultured bacterial solution were added. The ELISA plate was placed in a microplate reader (Varioskan LUX, Thermofisher, US), shaken, and after 15 min of reaction, the luminescence intensity was measured. A 3% NaCl (AR, 99%, Sinopharm) solution served as the blank control, and each sample was tested in triplicate. The relative luminescence intensity was calculated using the Equations 5, 6:

$$L(\%) = \frac{L_i}{L_0} \times 100\% \quad (5)$$

$$1L(\%) = 100 - L \quad (6)$$

In the formula: L represents the relative luminescence of the sample. L_0 is the luminescence of the blank sample. L_i denotes the luminescence of the test sample. 1 L represents the inhibition rate of the sample's luminescence.

2.2.3 Selection of grass species and determination of their vegetative performance

Grass species adapted to the local substrate (clover, alfalfa, wild ryegrass, blackgrass, Bermuda grass, and holly) were selected for a seed germination experiment. Ten seeds were placed in a petri dish, and 2 mL of vegetation substrate leachate was added. The dishes were incubated at 25°C ± 1°C with light exposure, with daily water replenishment to compensate for evaporation. The germination rate and germination index of the seeds were measured.

According to the designed ecological concrete formulation, concrete was poured into transparent plastic pots and shaped, followed by demolding after 7 days of curing. Sixty seeds were mixed with 10 g of the improved vegetation substrate, and 5 g of mushroom compost was added to enhance the physical and chemical properties of the substrate. The mixture was irrigated to allow the plant solution to permeate the concrete pores. Commercially available organic potting soil and untreated

TABLE 7 Medium and heavy metal content of improved vegetation substrate.

Expt	Sb	Cd	Cr	As	Mn	Cu	Zn
GEMR	—	0.001	0.003	0.02	1,089.11	0.275	0.069
G91	—	0.001	0.001	0.01	1,040.74	0.292	0.056
G82	—	0.001	0.001	0.01	930.78	0.301	0.069
G73	—	0.001	0.001	0.01	880.12	0.329	0.059
G64	—	0.001	0.001	0.01	760.92	0.337	0.088
G55	—	0.001	0.001	0.01	693.53	0.380	0.097
GB3838-2002	≤0.005	≤0.005 (II)	≤0.01 (II)	≤0.05 (I)	≤0.1	≤1 (II)	≤1 (II)

Note: "-" indicates levels below the detection limit; "GEMR" represents electrolytic manganese residue with added amendments, and "G91," "G82," "G73," "G64," and "G55" represent planting substrates with amended electrolytic manganese residue and phosphogypsum at mass ratios of 9:1, 8:2, 7:3, 6:4, and 5:5, respectively.

10.3389/fenvs.2024.1539964

TABLE 8 Germination rate and germination potential of seeds under different treatments.

Sample	Tetrapanax quinquefolium			Shearling			Ryegrass		
	Germination rate (%)	Germination potential (%)	Germination index	Germination rate (%)	Germination potential (%)	Germination index	Germination rate (%)	Germination potential (%)	Germination index
E:P = 9:1	80a	20ab	4.93ab	70a	15a	3.22a	30a	10b	1.75c
E:P = 8:2	55b	15ab	3.01ab	30a	0b	0.83a	55a	45b	5.61c
E:P = 7:3	40b	25a	3.68ab	45a	5ab	2.32a	40a	20b	2.64c
E:P = 6:4	55b	15ab	3.36ab	30a	0b	1.23a	30a	15b	2.60c
E:P = 5:5	45b	0b	2.70b	20a	5ab	1.28a	35a	20b	3.45c
CK	80a	35a	5.80a	90a	10ab	3.48a	75a	40b	5.50c

Note: CK, represents distilled water.

phosphogypsum were used as blank controls. After 45 days, plant height, germination rate, and biomass were measured.

3 Results and discussion

3.1 Structural performance of vegetative eco-concrete

The strength of environmentally-friendly concrete is determined by the binder material, the aggregate, and the bonding strength between the binder and aggregate. Among these factors, the one with the lowest strength has the most significant impact on the overall strength of the eco-concrete. Experimental results for eco-concrete prepared according to the mix ratios in Table 2 are presented in Table 3. In Mix Design 3, the primary failure occurred at the bonding points between binder materials, resulting in the lowest compressive strength at 14 days. The failure in eco-concretes from Mix Designs 1 and 2 was primarily due to infiltration of the aggregate. Mix Design 1 showed a 14-day compressive strength of 3.49 MPa, significantly higher than that of Mix Designs 2 and 3.When force is applied to eco-concrete with shale aggregate, it is transmitted through the connection points between aggregates. If the aggregate has high strength and the bond area and thickness between the aggregate and binder are minimal, failure usually does not occur within the aggregate itself but at the interface between the aggregate and binder or within the hardened binder (Liang, 2010). On the other hand, if the aggregate strength is lower, the bonding between binder materials thickens, causing initial failure within the aggregate, which gradually extends into the hardened binder layer.The porosity of vegetative eco-concrete should be between 20% and 35% to meet plant growth requirements (Hu et al., 2006), and all three mixes satisfied this porosity criterion. As shown in Figure 3, the water absorption rate of eco-concrete made with various rubber-bone ratios was initially the lowest at approximately 38% within 5 min, gradually increasing to 50% after 24 h, which aids rapid water retention. This characteristic mainly results from using lightweight ceramsite aggregate, which reduces the overall mass of the eco-concrete. The absorption rate of Mix Design 1 surpassed that of Mix Designs 2 and 3 after the initial 5 min. Based on these comprehensive tests, Mix Design 1 was identified as the optimal ratio for eco-concrete. Compared to fly ash and slag-based concretes, phosphogypsum-based ecological concrete demonstrates slightly lower 14-day compressive strength (Table 4) (Rabatho et al., 2011; Araujo et al., 2004; Mun et al., 2005; Potgieter et al., 2003). However, its significantly enhanced total porosity and water retention offer distinct advantages for ecological restoration and plant growth applications. The increased porosity provides an optimal environment for plant root aeration and water absorption, while the improved water retention ensures consistent moisture availability, particularly under arid or low-rainfall conditions. Additionally, the lower permeability coefficient of phosphogypsum concrete reduces water loss, making it an essential feature for vegetation-supporting ecological concretes. Experimental results further highlight that the percentage improvements in both compressive strength and water retention validate its feasibility and underscore its potential to balance mechanical performance with ecological functionality.

TABLE 9 Plant height and biomass of ryegrass under different treatments.

No.	45 days plant height (cm)	Biomass (g/pot)	Germination rate (%)
G91	6.65 ± 0.78 c	0.46 ± 0.01 ab	75.17 ± 1.18 b
EMR	14.10 ± 0.28 a	0.85 ± 0.01 ab	80.83 ± 5.90 b
GEMR	11.85 ± 0.49 b	0.77 ± 0.04 b	73.33 ± 2.36 b
CK	15.35 ± 0.35 a	0.97 ± 0.02 a	97.50 ± 1.18 a

3.2 Analysis of nutrient composition in the planting substrate

The pH and nutrient content of the planting substrate are crucial for plant growth. As shown in Table 5, PG has a pH of 2.39, and as the amount of PG increases, the pH gradually rises, neutralizing its acidity. PG provides a rich phosphorus source, with an available phosphorus content as high as 4,295.9 mg/kg, while EMR supplies abundant nitrogen, with an alkali-hydrolyzable nitrogen content of 7,509.6 mg/kg. The alkali-hydrolyzable nitrogen content in the PG-based planting substrate is relatively low, and in combination with EMR, this nitrogen content is balanced in the substrate and decreases as PG content increases. The phosphorus content in the planting substrate increases with the addition of PG, while both substrates have relatively high potassium content. After mixing, the pH, alkali-hydrolyzable nitrogen, available phosphorus, and potassium levels in the substrate are balanced, with the nutrient elements in PG and EMR complementing each other to support plant growth.When PG is mixed with the humus components of the soil (EMR), the phosphorus (P) can be readily adsorbed and immobilized by metal ions in EMR, transforming plant-available phosphorus into an insoluble form. EMR contains high levels of Fe and Al, making it likely that phosphorus will exist in forms such as iron phosphate (Fe-P), aluminum phosphate (Al-P), or occluded phosphorus (O-P) (Lu et al., 2013). These insoluble phosphates provide a slow-release fertilizing effect that is not easily absorbed by plants but offers a sustained, long-term nutrient supply. When phosphorus in the substrate is insufficient for plant needs, plant roots release organic acids, which gradually dissolve insoluble phosphates, improving the phosphorus microenvironment around the root system and maintaining essential plant life processes (Liu et al., 2018). Therefore, the PG-modified planting substrate, rich in nitrogen, phosphorus, and potassium, can adequately meet the nutrient requirements for plant growth.

3.3 Leaching toxicity of the planting substrate

3.3.1 Toxicity leaching of planting substrate under different ratios

Although the PG-EMR composite substrate is nutrient-rich and meets the requirements for plant growth, both PG and EMR contain various heavy metals and metalloids such as As, Cd, Cr, Cu, and Sb, which have high toxicity (Liu et al., 2022; Ismaeel et al., 2023), These metals can be absorbed and accumulated by plants from the substrate, potentially adversely affecting plant growth. Therefore, conducting a toxicity leaching test on the planting substrate is essential. As shown in Table 6, the manganese (Mn) concentration in the leachate of the PG-EMR composite substrate ranged from 894.94 to 1,350.05 mg/L, exceeding the Class I emission standard of the *Integrated Wastewater Discharge Standard* (GB 8978-1996) by over 447 times. In contrast, the levels of other heavy metals were relatively low. Excessive Mn in the substrate could hinder plant growth by obstructing the uptake of essential elements such as Fe, Mg, Ca, and Mo, potentially damaging chloroplast structure in leaves and reducing photosynthetic rates, leading to oxidative damage in plants (Zhang et al., 2010). Therefore, further improvements to the planting substrate are necessary to stabilize and immobilize the excessive Mn content.

3.3.2 Acute toxicity of luminescent bacteria

Studies indicate that luminescent bacteria maintain stable luminescence within a pH range of 5.0–9.0, so no further pH adjustment is required for water samples within this range (Wang et al., 2004). In this experiment, pH was left unadjusted, and the leachate from the planting substrate was directly used for toxicity testing. Toxicity levels were classified according to the relative luminescence intensity using the Microtox acute toxicity classification method (Sang, 2004). As shown in Figure 4, the relative luminescence intensity in the EMR-mixed substrate exceeded 100%, indicating a non-toxic level; the high manganese concentration in EMR did not inhibit luminescent bacterial activity, but rather appeared to promote it. Conversely, PG had a significant inhibitory effect on luminescent bacteria, exhibiting high toxicity. As PG concentration increased, the toxicity of the sample also increased. When the PG to EMR ratio reached 1:1, the relative luminescence of the bacteria remained above 75%, indicating a low toxicity level. This suggests that the combined PG and EMR planting substrate is classified as non-toxic or minimally toxic.

A filtrate with pH >4 can be toxic to luminescent bacteria, while the pH of the PG filtrate is typically below 3, resulting in strong inhibition of luminescent bacteria. In comparison, when PG was mixed with EMR, the pH of the leachate from the experimental plant substrate stabilized between 5.0 and 9.0, reducing toxicity to the luminescent bacteria. This reduction in toxicity can be attributed, in part, to the buffering effect of EMR on PG's low pH. Additionally, certain nutrients in the mixture may have antagonistic effects on toxic substances, further lowering the filtrate's toxicity (Zhao et al., 2010). Moreover, the plant substrate, rich in nitrogen, phosphorus, potassium, and other nutrients, may stimulate bacterial activity and enhance luminescence under low-toxicity conditions, which can ultimately support plant growth.

3.4 Effect of amendments on the leaching toxicity of the planting substrate

The results of the leaching toxicity test indicated that the PG-EMR composite planting substrate contains elevated levels of certain heavy metals, particularly Mn. To stabilize and immobilize the excess heavy metals within the substrate, 2.5% straw biochar and 2.5% diatomaceous earth were added as amendments. Comparison of Tables 6, 7 shows that, except for an increase in Cu content, the concentrations of other metals decreased in the amended substrate, suggesting that the addition of amendments effectively immobilizes heavy metals in the substrate. Specifically, Mn concentration was reduced to only 79.86% of its original level, demonstrating effective stabilization.Furthermore, the heavy metal content in the amended planting substrate meets the limits set by the *Soil Environmental Quality Agricultural Land Soil Pollution Risk Control Standard (Trial)* (GB15618-2018). Overall, the amendments significantly improved the substrate quality, making it suitable for use as a planting substrate.

3.5 Germination rate and germination potential of the planting substrate at different ratios

In the germination rate and germination potential tests for substrates with various ratios, clover, Bermuda grass, and alfalfa were excluded due to a 7-day germination rate of zero, with some alfalfa seeds showing signs of decay. As shown in Table 8, the germination rates of perennial ryegrass, ryegrass, and bentgrass decrease with increasing PG content, indicating a clear inhibitory effect on seed germination. The G91 planting substrate exhibited relatively high germination rates and germination potential, suggesting that it may be suitable for further planting experiments.

3.6 Testing the vegetative performance of ecological concrete

As shown in Table 9, plants grown in the CK group with organic nutrient soil as the substrate performed well, exhibiting the highest germination rate, plant height, and biomass after 45 days. EMR significantly inhibited germination rate and plant height, with notable differences in germination rate and biomass compared to the CK group. The amendment-treated groups, GEMR and G91, did not show significant improvement and adversely affected plant growth, although the germination rate of G91 increased slightly compared to the substrate without amendments. This is primarily because $Ca(OH)_2$ in the ecological concrete effectively inhibited heavy metals in EMR during early plant growth, maintaining growth within acceptable limits. Furthermore, it was observed that an excess of polycyclic aromatic hydrocarbons (PAHs) in biochar significantly inhibited seed germination and seedling growth (Li et al., 2015). In the later stages of the experiment, all plant groups except the control exhibited signs of drying and wilting, likely due to nutrient depletion in the substrate, ongoing carbonation of the concrete, and a gradual decrease in alkalinity. Additionally, heavy metals in the substrate may have been absorbed by the plants, accumulating to a toxic level and resulting in plant toxicity.

4 Conclusion

(1) In this study, ecological concrete specimens were prepared using a composite binder of PG and EMR as the adhesive and ordinary clay ceramsite as the aggregate. With a rubber-bone ratio of 1.485, the 14-day compressive strength reached 3.49 MPa, the permeability coefficient was 1.37, and the total porosity was 24.5%, meeting the requirements for vegetative concrete. The high content of available phosphorus, alkali-hydrolyzable nitrogen, and available potassium in PG and EMR can satisfy the nutrient needs of vegetative concrete, making it possible to create a nutrient-rich planting substrate.

(2) Adding a mixed amendment of biochar and diatomaceous earth effectively stabilized heavy metals within the substrate, demonstrating a strong immobilization effect. After amendment, the manganese concentration in the leachate from the planting substrate decreased by 79.86%, indicating a successful stabilization outcome.

(3) The germination rate tests for the planting substrate indicated that bentgrass, perennial ryegrass, and Kentucky bluegrass adapted well, while alfalfa, clover, and Beruda grass showed poor adaptability, with no germination observed within 7 days.

Data availability statement

The raw data supporting the conclusions of this article will be made available by the authors, without undue reservation.

Author contributions

RL: Conceptualization, Writing–original draft. CL: Investigation, Writing–review and editing, Methodology. JD: Project administration, Writing–review and editing. CW: Methodology, Writing–review and editing. YY: Formal Analysis, Visualization, Writing–review and editing. XZ: Software, Validation, Writing–review and editing.

Funding

The author(s) declare that no financial support was received for the research, authorship, and/or publication of this article.

Conflict of interest

Authors RL, CL, JD, CW, and YY were employed by China Overseas Construction Limited.

The remaining author declares that the research was conducted in the absence of any commercial or financial relationships that could be construed as a potential conflict of interest.

Generative AI statement

The author(s) declare that no Generative AI was used in the creation of this manuscript.

Publisher's note

References

Araujo, A., Viana, P., and Peres, A. (2004). Reagents in iron ores flotation. *Miner. Eng.* 18 (2), 219–224. doi:10.1016/j.mineng.2004.08.023

Cao, B. D. (2018). Study on the influence factors of strength of phosphogypsum-based composite cementitious materia. *New Build. Mater.* 45 (03), 23–26. doi:10.3969/j.issn.1001-702X.2018.03.007

Chen, Y. F. (2021). Low alkalinity porous ecological permeable concrete based on solid waste and its preparation method. *Sichuan Cem.* (10), 7–8. doi:10.3969/j.issn.1001-702X.2018.03.007

Cui, R. Z., Bai, H. D., Gao, Y. F., and Xue, X. F. (2022). Current situation of comprehensive utilization of phosphogypsum and its development trend of 14th Five-Year Plan. *Inorg. Chem. Ind.* 54 (04), 1–4. doi:10.19964/j.issn.1006-4990.2022-0086

Du, M., Wang, J., Dong, F., Wang, Z., Yang, F., Tan, H., et al. (2022). The study on the effect of flotation purification on the performance of α-hemihydrate gypsum prepared from phosphogypsum. *Sci. Rep.* 12 (1), 95. doi:10.1038/s41598-021-04122-w

Fu, F., Qiao, H. X., Feng, Q., Li, Y. Q., and Xue, C. Z. (2023). Review of new methods for resource utilisation of electrolytic manganese residue and its application in building materials. *Constr. Build. Mater.*, 401.

Garg, M. S. a. M. (1995). Activation of gypsum anhydrite-slag mixtures. *Cem. Concr. Researc* 25, 332–338. doi:10.1016/0008-8846(95)00018-6

Hameed, M. O., Usman, F., Hayder, G., and Al-Ani, Y. (2023). Investigation of mechanical and thermal performance of nanoclay modified concrete for energy efficiency. *Ann. de Chimie - Sci. des Matériaux* 47 (4), 225–235. doi:10.18280/acsm.470405

Hu, Y. Y., Hu, C. M., Xie, L., Guo, Q. W., Wang, X., Zhang, T. P., et al. (2006). Effect of void status in eco-concrete for planting on plant G rowth. *J. South China Univ. Technol. Sci. Ed.* (12), 5–9. doi:10.3321/j.issn:1000-565X.2006.12.002

Huang, D., Zong, S. R., Ma, H., Wan, B. L., Nian, Z. W., Li, D. G., et al. (2023). Research and application progress of resource utilization technology of phosphogypsum. *Eco-industry Sci. and Phosphorus Fluor. Eng.* 38 (05), 17–22. doi:10.3969/j.issn.1007-6220.2023.05.006

Huang, X. Q., Zhao, X. R., Tang, C. L., Du, Y. J., and Chen, B. Y. (2016). Properties and leaching characteristics of cemented phosphate tailings backfill with phosphogypsum-based cementation material. *Chin. J. Environ. Eng.* 10 (10), 5957–5963. doi:10.12030/j.cjee.201601080

Huang, Y., Qian, J., Kang, X., Yu, J., Fan, Y., Dang, Y., et al. (2019). Belite-calcium sulfoaluminate cement prepared with phosphogypsum: influence of P2O5 and F on the clinker formation and cement performances. *Constr. Build. Mater.* 203, 432–442. doi:10.1016/j.conbuildmat.2019.01.112

Ismaeel, M. A., Usman, F., Hayder, G., and Al-Ani, Y. (2023). Analysis of mechanical and environmental effects of utilizing waste glass for the creation of sustainable ultra-high performance concrete. *Ann. de Chimie - Sci. des Matériaux* 47 (2), 111–123. doi:10.18280/acsm.470208

Jassam, A. Z., Usman, F., Hayder, G., and Al-Ani, Y. (2023). Investigating the mechanical and thermal properties of concrete with recycled nanoplastics for enhanced sustainability. *Ann. de Chimie - Sci. des Matériaux* 47 (5), 341–350. doi:10.18280/acsm.470508

Jin, Y. T., Yang, D., Wu, Y. H., Zhou, F., Yu, J. X., Chi, R., et al. (2024). Preparation of biofertilizer with phosphogypsum and straw: microbial community changes and plant growth effects. *J. Soil Sci. Plant Nutr.* 31, 17511–17523.

Junakova, N., and Junak, J. (2017). Sustainable use of reservoir sediment through partial application in building material. *Sustainability* 9 (5), 852. doi:10.3390/su9050852

Li, B. X., Li, L. C., Ma, Y., and Zhou, M. K. (2002). Modification of phosphogypsum using circulating fluidized bed fly ash and carbide slag for use as cement retarder. *Construc. Building. Materi.* (10), 11–13.

Li, Y., Shen, F., Guo, H., Wang, Z., Yang, G., Wang, L., et al. (2015). Phytotoxicity assessment on corn stover biochar, derived from fast pyrolysis, based on seed germination, early growth, and potential plant cell damage. *Environ. Sci. Pollut. Res. Int.* 22 (12), 9534–9543. doi:10.1007/s11356-015-4115-5

Liang, H.-H., and Li, J.-L. (2015). The influence of hydration and swelling properties of gypsum on the preparation of lightweight brick using water supply reservoir sediment. *Constr. Build. Mater.* 94, 691–700. doi:10.1016/j.conbuildmat.2015.07.111

Liang, L. M. (2010). *Preparation, porous structure and Camouflage performance of porousecological conerete*. Nanjing, China: Nanjing University of Aeronautics and Astronautics.

Liu, S., Wu, F. H., Qu, G. F., Zhao, C. Y., Chen, B. J., Yang, Y. Y., et al. (2022). Migration and transformation of heavy metals in phosphogypsum stor-age process and their ecological effect. *Asian J. Ecotoxicol.* 17 (04), 302–314. doi:10.7524/AJE.1673-5897.20210803002

Liu, X. L., Zhang, B. X., Wang, G. J., Miao, L. L., and Wu, J. J. (2018). Research progress of root exudates for Efficient Dissociation of insoluble phosphorus. *Heilongjiang Agric. Sci.* (12), 157–160. doi:10.11942/j.issn1002-2767.2018.12.0157

Lou, Y., Liu, F., Ren, J., and Zhu, J. (2020). Effects of rooting media amendments on seed germination and seedling growth of four bioenergy grass species grown on electrolytic manganese residue. *Acta Prataculturae Sin.* 29 (11), 118–128. doi:10.11686/cyxb2020005

Lu, X. C., Han, X. Z., and Zou, W. X. (2013). Advance in the efficient utilization of soil phosphorus by crops. *Soils Crops* 2 (04), 164–172. doi:10.11689/j.issn.2095-2961.2013.04.004

Ma, M. (2002). *Development and application of new bioassay methods in aquatic ecotoxicology*. Beijing, China: Graduate school of the chinese academy of sciences Ecological Environment Research Center.

M S, D., Andrzej, B., Arkadiusz, G., Raczko, J., Mordak, K., Grądziel, I., et al. (2020). Phosphogypsum and clay mineral/phosphogypsum ceramic composites as useful adsorbents for uranium uptake. *Appl. Geochem.* 123 (prepublish), 104793. doi:10.1016/j.apgeochem.2020.104793

Mun, K., Hyoung, W., Lee, C., So, S., and Soh, Y. (2005). Basic properties of non-sintering cement using phosphogypsum and waste lime as activator. *Constr. Build. Mater.* 21 (6), 1342–1350. doi:10.1016/j.conbuildmat.2005.12.022

Peng, B., Jiang, C. b., and Xiang, T. S. (2013). Experimental study on porosity of vegetation type porous concrete. *China Water Transp.* 13 (05), 281–282.

Potgieter, J., Potgieter, S., McCrindle, R., and Strydom, C. (2003). An investigation into the effect of various chemical and physical treatments of a South African phosphogypsum to render it suitable as a set retarder for cement. *Cem. Concr. Res.* 33 (8), 1223–1227. doi:10.1016/s0008-8846(03)00036-x

Rabatho, J., Tongamp, W., Kato, J., Haga, K., Takasaki, Y., and Shibayama, A. (2011). Effect of flotation reagents for upgrading and recovery of Cu and Mo from mine tailing by flotation. *Resour. Process.* 58 (1), 14–21. doi:10.4144/rpsj.58.14

Sang, L. Y. (2004). Law of silica powder influence on cement stone strength development. *Drill. Fluid and Complet. Fluid* 21, 41–43.

Said, A., Mohamad, E., Aicha, B., Kamar, M., and Midani, M. (2024b). Properties, purification, and applications of phosphogypsum: a comprehensive review towards circular economy. *Mater. Circ. Econ.* 6 (1), 9. doi:10.1007/s42824-024-00100-5

Said, A., Mohamad, E., Aicha, B., Mohamed, K., and Midani, M. (2024a). Properties, purification, and applications of phosphogypsum: a comprehensive review towards circular economy. *Mater. Circ. Econ.* 6 (1), 9. doi:10.1007/s42824-024-00100-5

Shichao, C., Fang, W., Lihua, M., and Che, J. (2023). Study on physical properties of desulfurized electrolytic manganese residue cement and properties of mortar. *Mater. Basel, Switz.* 16 (11), 4035. doi:10.3390/ma16114035

Song, F. L. (2009). *Studies on the Technology of ecological slope protection based on the material-vegetation system[D]*. Anhui, China: Anhui Agricultural University.

Wang, J., Peng, B., Chai, L., Zhang, Q., and Liu, Q. (2013). Preparation of electrolytic manganese residue–ground granulated blastfurnace slag cement. *Powder Technol.* 241, 24112–24118. doi:10.1016/j.powtec.2013.03.003

Wang, L. S., Wei, D. B., and Hu, H. Y. (2004). Optimization of luminescent bacteria toxicity test and application of toxicity reference substance. *Res. Environ. Sci.* 04, 61–62. doi:10.13198/j.res.2004.04.63.wanglsh.016

Yang, M., and Qian, J. (2011). Activation of anhydrate phosphogypsum by K2SO4 and hemihydrate gypsum. *J. Wuhan Univ. Technology-Mater. Sci. Ed.* 26 (6), 1103–1107. doi:10.1007/s11595-011-0371-5

Yang, S. Z., Song, H. T., Yang, X. Y., and Zhu, Y. Q. (2003). *Modification of phosphogypsum and its application for cement retarder*. Wuhan, China: Journal of Wuhan University of Technology, 23–25. doi:10.3321/j.issn:1671-4431.2003.01.007

Yatesh, T., Akanksha, T., and Sudipta, S. (2023). Utilization of industrial waste phosphogypsum as geomaterial: a review. *J. Hazard. Toxic, Radioact. Waste* 27 (2). doi:10.1061/jhtrbp.hzeng-1181

Yu, Y. Y. (2016). *Study on the composite cementitions material based on gypsu[D]*. Xi'an, China: Chang'an University.

Zhang, X. (2022). *Study on the preparation and Planting performance of Eco-concrete based on electrolytic manganese slag[D]*. Guiyang, China: Guizhou University.

Zhang, Y., Wang, X. P., and Li, D. X. (2011). Performance research on the gypsum based cementing material incorporating with large dosage of waste gypsum. *Bull. Chin. Ceram. Soc.* 32 (02). doi:10.16552/j.cnki.issn1001-1625.2011.02.029

Zhang, Y. X., Li, L. F., Chai, T. Y., Lin, D., and Zhang, H. M. (2010). Mechanisms of manganese toxicity and manganese tolerance in plants. *J. Integr. Plant Biol.* 45 (04), 506–520. doi:10.3969/j.issn.1674-3466.2010.04.014

Zhao, Y. Y., Hu, J. L., and Shao, L. J. (2010). Study on the influencing factors of luminescent bacteria toxicity testing. *Mod. Sci. Instrum.* No.131 (03), 75–78.

Zhou, L. N., Zhou, M. K., Zhao, Q. L., and Li, J. H. (2007). The influence of different modification methods on the performance of phosphogypsum cement setting agent. *Cement* (08), 16–18. doi:10.3969/j.issn.1002-9877.2007.08.004

frontiers | Frontiers in Environmental Science

TYPE Original Research
PUBLISHED 01 August 2025
DOI 10.3389/fenvs.2025.1602385

OPEN ACCESS

EDITED BY
Zhenming Zhang,
Guizhou University, China

REVIEWED BY
Sinem Çolak,
Bülent Ecevit University, Türkiye
Yunfei Hu,
Bozhou University, China
Ziyu Guo,
Guizhou Centre for Disease Control and Prevention, China

*CORRESPONDENCE
Bing Hao,
Bing.Hao@ynau.edu.cn
Wei Fan,
fanwei1128@aliyun.com

†These authors have contributed equally to this work

RECEIVED 29 March 2025
ACCEPTED 10 July 2025
PUBLISHED 01 August 2025

CITATION
Qian X, Luo Y, Yang H, Wang J, Zhang H, Shi H, Li Q, Song Z, Hao B and Fan W (2025) Assessment and analysis of heavy metal pollution in key production areas of *Gastrodia elata* in Yunnan, China.
Front. Environ. Sci. 13:1602385.
doi: 10.3389/fenvs.2025.1602385

Assessment and analysis of heavy metal pollution in key production areas of *Gastrodia elata* in Yunnan, China

Xixi Qian[1,2,3†], Yu Luo[4†], Honglei Yang[1,2,3], Jinghui Wang[1,2,3], Huimin Zhang[1,2,3], Huineng Shi[1,2,3], Qi Li[1,2,3], Zhanhua Song[1,2,3], Bing Hao[2,3*] and Wei Fan[1,2,3*]

[1]College of Resources and Environment, Yunnan Agricultural University, Kunming, China, [2]The Key Laboratory of Medicinal Plant Biology of Yunnan Province, Yunnan Agricultural University, Kunming, China, [3]National and Local Joint Engineering Research Center on Germplasm Innovation and Utilization of Chinese Medicinal Materials in Southwest China, Yunnan Agricultural University, Kunming, China, [4]College of Food Science and Technology, Yunnan Agricultural University, Kunming, China

Introduction: As a newly recognized medicinal and edible Chinese herbal medicine, the safety of Gastrodia elata has garnered significant attention. Yunnan Province is the main production area of G. elata in China, but there is a lack of systematic assessments of the distribution patterns of heavy metals in the soil-plant system and their associated human health risks.

Methods: This study evaluated the pollution status of five heavy metals—cadmium (Cd), arsenic (As), lead (Pb), mercury (Hg), and copper (Cu)—in the surface soil (0–20 cm) and G. elata tubers across four major planting areas: Kunming (KM), Zhaotong (ZT), Lijiang (LJ) and Tengchong (TC) in Yunnan Province. The concentrations of heavy metals in soil and G. elata tubers were determined using inductively coupled plasma mass spectrometry (ICP-MS) and atomic fluorescence spectrometry (AFS). The pollution status of heavy metals in soil was evaluated using the single pollution index (Pi), comprehensive pollution index (PN), potential ecological risk index (PERI), and enrichment factor (EF). The bioconcentration factor (BCF) was applied to assess the accumulation capacity of heavy metals in the plants, while the target hazard quotient (HQ) and total hazard index (HI) were used to evaluate the human health risks associated with heavy metals in G. elata tubers.

Results and discussion: The findings revealed that the surface soils in the sampling areas were acidic, with total nitrogen (TN), total potassium (TK), soil organic matter (SOM), and cation exchange capacity (CEC) reaching abundant levels, while total phosphorus (TP) was relatively low. The pollution levels of the five heavy metals were ranked as Hg > Cd > Cu > As > Pb, with Hg, Cd, and Cu identified as severely polluted. The potential ecological risk assessment indicated a moderate risk, with ZT showing the highest comprehensive pollution level and ecological risk. The enrichment capacity of heavy metals in soil was ranked as Hg > Cd > As > Pb > Cu, while in G. elata tubers it was Cd > Cu > Pb > As. However, there was no significant risk to human health. Correlation analysis indicated that soil Cd and Pb were significantly positively correlated with their respective heavy

metal content in G. elata ($P < 0.05/P < 0.001$). This study provides a scientific basis for controlling soil heavy metal pollution in G. elata planting areas and for assessing the safety of Chinese herbal medicines.

KEYWORDS

***Gastrodia elata*, heavy metal contamination, Yunnan Province, soil-plant system,, health risk assessment**

1 Introduction

Traditional Chinese medicine (TCM) herbs are fundamental components of ancient medical system, increasingly gaining global prominence due to their unique therapeutic effects and relatively mild side effects (Zhang et al., 2013; Ekor, 2014). In recent years, driven by a growing inclination towards natural remedies, the global market for TCM herbs has expanded significantly, with projections estimating it will surpass $150 billion by 2025 (Hu et al., 2020; Zhang L. et al., 2021). As the leading producer and consumer of TCM herbs, China plays a crucial role in the global herbal medicine industry. However, this rising demand has brought about concerns related to the quality and safety of TCM herbs, particularly regarding heavy metal contamination (Yang et al., 2021; Liu J. J. et al., 2024). Research indicates that many TCM herb species possess a pronounced capacity for heavy metal accumulation due to their unique physiological characteristics. Coupled with their relatively long cultivation cycles, this has resulted in widespread instances of heavy metal contamination, often exceeding safety standards (Wang et al., 2019; Chen et al., 2020).

Heavy metal contamination not only diminishes the medicinal value of TCM herbs but also poses potential health risks. Common heavy metal contaminants found in TCM herbs include cadmium (Cd), arsenic (As), lead (Pb), mercury (Hg), and copper (Cu), which can lead to toxic effects such as neurotoxicity, liver and kidney damage, and carcinogenicity (Harris et al., 2011; Luan et al., 2015). Analyses of herbal samples from various regions in China have shown that at least one-third contain heavy metals at levels above the limits set by U.S. dietary supplement (NSF/ANSI Standard 173) (Harris et al., 2011). A study of 131 batches of herbal samples reported exceedance rates of 16.79% for Cd and 11.45% for Pb (Luan et al., 2015), while a more extensive examination of 2,427 batches highlighted severe Cd contamination with a 20.9% exceedance rate (Fei et al., 2021). Moreover, regulatory standards for heavy metals vary globally. For example, the limits for Cd, As, Pb, and Hg in China's "Green Industry Standards for the Import and Export of Medicinal Plants and Preparations" are lower than those in the United States and the European Union (Chen et al., 2020; Fei et al., 2021). Therefore, evaluating the safety of TCM herbs based on current Chinese standards may lead to heavy metal contamination issues becoming a significant bottleneck for the external development of the TCM herbs industry.

Gastrodia elata, a perennial herbaceous plant of the Orchidaceae family, is one of the most valued TCM herbs and features a unique symbiotic relationship with medicinal fungi (Zhan et al., 2016). Its primary active components constituent—gastrodin, phenolic compounds, polysaccharides, and organic acid—endow *G. elata* with remarkable pharmacological properties, particularly in treating neurological disorders (Zhu et al., 2019). Clinical studies affirm its efficacy in managing headaches, epilepsy, and cardiovascular diseases (Zhan et al., 2016; Lu et al., 2022). Unlike many TCM herbs, *G. elata* is a heterotrophic, relying entirely on fungi such as *Armillaria* sp. for nutrient acquisition (Liu Y. et al., 2024). However, studies suggest that these fungi may also facilitate the absorption for certain heavy metals, raising concerns about potential contamination in *G. elata* (Ferrol et al., 2016; Yin et al., 2021; Goswami et al., 2023).

Yunnan Province is the main planting area of *G. elata* in China, with both its planting area and output ranking first nationwide (Wang et al., 2023). The unique geographical and climatic conditions in Yunnan create an excellent environment for *G. elata* cultivation, but they also pose potential risks of heavy metal pollution. Studies have shown that the background values of heavy metals in Yunnan's soil are generally high, with Cd, Pb, and Hg levels exceeding the national averages (Xu et al., 2024). Soil heavy metal pollution in *G. elata* planting areas displays both regional and composite characteristics, and environmental factors from different planting sites significantly influence the heavy metal content in *G. elata* (Jin et al., 2022; Chen and Deng, 2025; Huang et al., 2025). As one of the main planting regions, Zhaotong in Yunnan has been the subject of studies investigating the heavy metal content in soil and *G. elata*, but the scope of related research remains limited (Xu et al., 2018; Zhao et al., 2018). In contrast, research on emerging planting areas such as Lijiang, Kunming, and Tengchong remains relatively limited. Moreover, most existing studies have concentrated on the heavy metal content, pesticide residues, and sulfur dioxide residues in commercially available *G. elata* products (Zhang et al., 2018; Yan et al., 2021; Huang et al., 2024).

This study systematically investigated the heavy metal pollution status in the main *G. elata* planting areas of Yunnan Province. It aims to comprehensively analyze and assess the distribution characteristics of five key heavy metals in both soil and *G. elata* samples, and further identify the spatial distribution of soil heavy metals and the physicochemical properties of the soil in different *G. elata* planting regions. This research will not only provide a scientific foundation for sustainable development of Yunnan's *G. elata* industry but also offer significant theoretical and practical insights for ensuring the quality and safety of TCM herbs.

2 Materials and methods

2.1 Sample collection and processing

This study collected *G. elata* tubers and soil samples from major cultivation regions in Yunnan Province between December 2023 and January 2024 (Liu et al., 2015). The sampling locations included: Luquan County, Kunming City (KM-LQ, 16 sites); Yiliang

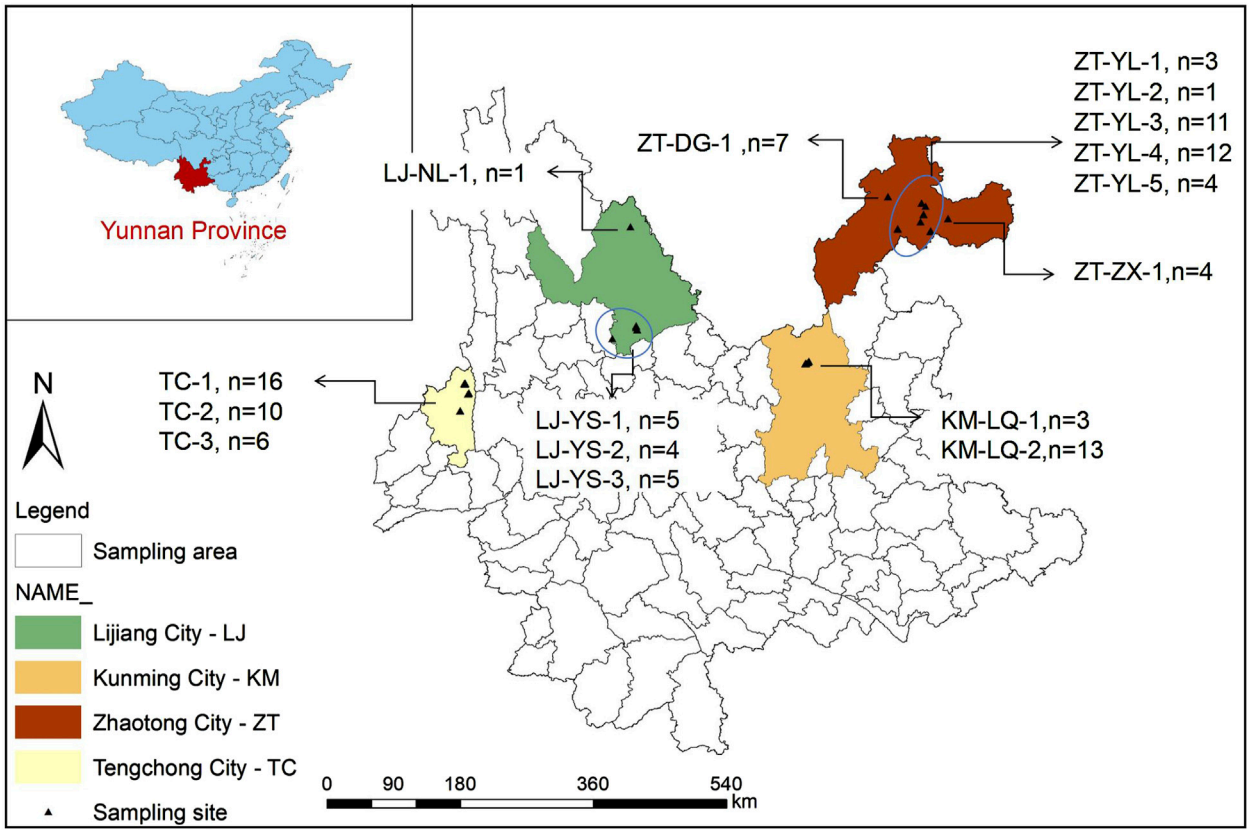

FIGURE 1
Sampling site locations in the *Gastrodia elata* cultivation area of Yunnan Province.

County (ZT-YL, 31 sites), Zhenxiong County (ZT-ZX, 4 sites), and Daguan County (ZT-DG, 7 sites) in Zhaotong City; Yongsheng County (LJ-YS, 14 sites) and Ninglang County (LJ-NL, 1 site) in Lijiang City; and Tengchong City (TC, 32 sites) (Figure 1). The sampling area encompassed latitudes N25 18′53″to N27 55′10″, longitudes E98 34′52″to E104 30′48″, and elevations ranging from 1,379.21 to 3,434.68 m (Supplementary Table S1). *G. elata* predominantly grew in environments characterized by *Cyclobalanopsis glauca*, *Pinus yunnanensis*, and *Quercus dolicholepis*, with soil types including red, brown, yellow-brown, and yellow soils (pH 4.10–6.10) (Tian et al., 2016; Zhang M. et al., 2021). To ensure the representativeness of the samples and the reliability of the data, this study employed a five-point sampling method at each site to collect surface soil (0–20 cm). The 1 kg of soil was collected from each of the five points and combined to form a single composite soil sample, resulting in a total of 105 mixed soil samples. The soil samples were air-dried indoors, and after drying, impurities such as dead branches, fallen leaves, and stones were removed. The soil was then ground using wooden tools and passed through a nylon sieve. The processed soil samples were preserved for future analysis. At each sampling site, 3 *G. elata* plants were also collected, yielding a total of 315 tuber samples, which were further grouped into 16 composite samples based on the variations in geographical names (Supplementary Table S1). The tuber samples were sequentially washed with tap water and deionized water, and excess surface moisture was removed with absorbent paper. Subsequently, the tubers were steamed in a steamer for about 10 m to ensure there was no white core. After that, the tubers were sliced and dried in a 65°C oven for 72 h until they reached a constant weight. Finally, the samples were pulverized, sieved, and stored in polyethylene self-sealing bags for subsequent analysis (Sun et al., 2016; Huang et al., 2025).

2.2 Indicator determination

2.2.1 Determination of soil physicochemical properties

Soil samples sieved through 2 mm or 0.149 mm (100-mesh) sieves were measured to determine physicochemical properties: pH, total nitrogen (TN), total phosphorus (TP), total potassium (TK), soil organic matter (SOM), and cation exchange capacity (CEC). The pH was determined using the electrode method. Soil was mixed with deionized water at a water-to-soil ratio of 1:2.5, shaken, allowed to settle, and the supernatant was analyzed with a pH meter (Xu et al., 2021). TN was determined using the semi-micro Kjeldahl method; TP was measured using the NaOH fusion-molybdenum antimony anti-spectrophotometric method; TK was assessed using the NaOH fusion-flame photometric method; SOM was analyzed using the potassium dichromate volumetric method with external heating; CEC was measured employing the 1 mol/L ammonium acetate exchange method (Lu et al., 2024).

10.3389/fenvs.2025.1602385

TABLE 1 Descriptive statistical analysis of heavy metal content in soil (mg·kg^{-1}).

Statistics	Cd	As	Pb	Hg	Cu	pH
Range	0.07~1.83	6.78~48.45	3.60~122.27	0.02~0.68	2.49~205.78	4.10~6.10
Mean ± SD	0.48 ± 0.44	18.56 ± 9.57	30.21 ± 20.81	0.23 ± 0.12	54.58 ± 59.44	4.92 ± 0.44
Median	0.33	15.72	24.77	0.23	17.49	4.92
CV	0.93	0.52	0.69	0.53	1.09	0.09
Background value (K1)	0.22	18.40	40.60	0.06	46.30	5.70
Risk screening value (K2)	0.30	40.00	70.00	1.30	50.00	pH < 5.5
Risk control value (K3)	1.50	150.00	400.00	2.00	-	pH < 5.5
K1 (Exceedance percentage/%)	55.24	33.33	21.90	86.67	34.29	2.86
K2 (Exceedance Percentage/%)	52.38	3.81	3.81	-	34.29	-
K3 (Exceedance Percentage/%)	4.76	-	-	-	-	-

Note: "-" indicates that there is no relevant data or the standard is not exceeded, K1 indicates the soil background value of the surface layer (layer A) in Yunnan, China Province (China National Environmental Monitoring Center, 1990), K2 indicates the screening value of agricultural land soil pollution risk, and K3 indicates the control value of agricultural land soil pollution risk. For details, please refer to the environmental quality risk control standard of agricultural soil pollution in China (GB15618-2018).

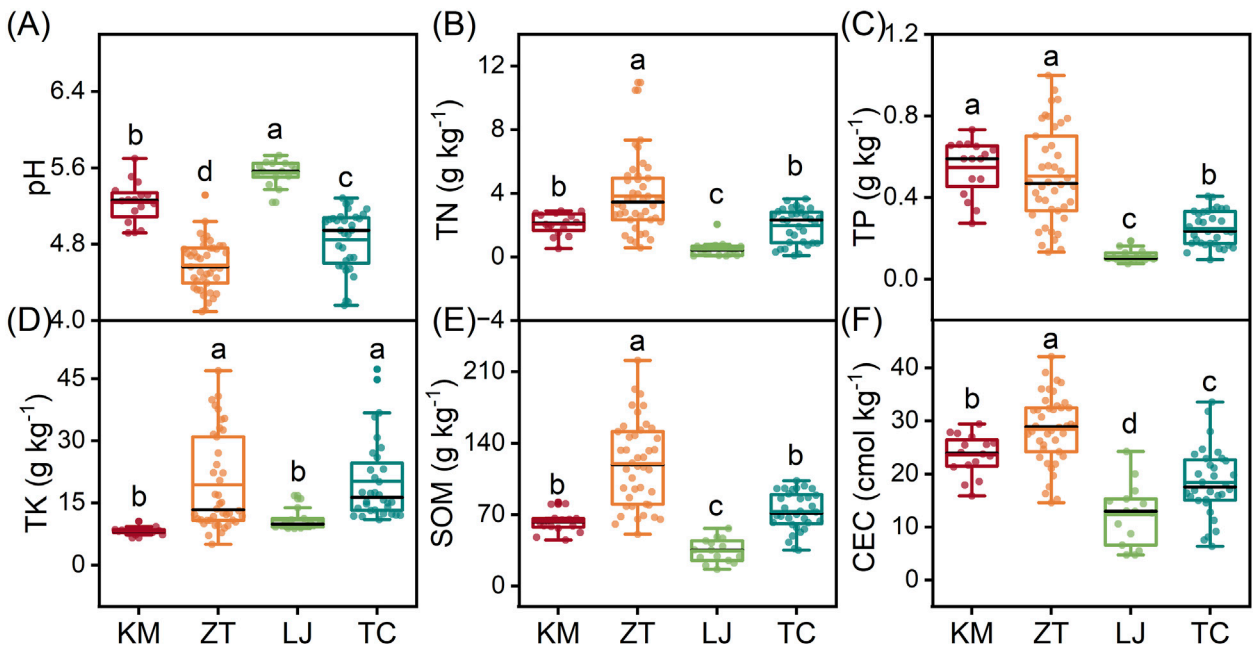

FIGURE 2
Changes in soil pH, total nitrogen (TN), total phosphorus (TP), total potassium (TK), organic matter (SOM) and cation exchange capacity (CEC) in different regions. (Note: **(A)** pH, **(B)** TN, **(C)** TP, **(D)** TK, **(E)** SOM, **(F)** CEC, there are statistical differences between different lowercase letters, $P < 0.05$, black represents the median line and the same color represents the mean line.)

2.2.2 Heavy metal content determination

Soil and plant samples that passed through a 100-mesh sieve were weighed at 0.2–1 g (accurate to 0.0001 g) using a precision balance with an accuracy of one ten-thousandth of a Gram (Mettler-Toledo ME204E). The concentrations of Cd, Pb, Cu, and Zr in the soil, as well as Cd, Pb, and Cu in the *G. elata*, were determined using an inductively coupled plasma mass spectrometer (Spectro SUPEC 7000), following the HJ1315–2023 and GB 5009.268–2016 methods, respectively. Ministry of Ecology and Environment of the People's Republic of China, 2023; Ministry of Environmental Protection of People's Republic of China, 2013; National Health and Family Planning Commission of the People's Republic of China, 2014; National Health and Family Planning Commission of the People's Republic of China, China Food and Drug Administration, 2016; National Health and Family Planning Commission of the People's Republic of China, China Food and Drug Administration, 2021. The concentrations of As and Hg in the soil were measured using an atomic fluorescence spectrometer (Jitian AFS-820), according to the HJ 680–2013 method (Lu et al., 2024). The concentrations of Hg and As in *G. elata* were also measured using an atomic fluorescence

TABLE 2 Single factor pollution index and comprehensive pollution index of soil heavy metals.

Element	Single factor pollution index (P_{iave})	Proportion of different pollution levels (%)				Comprehensive pollution index (P_{Nave})
		Unpolluted	Slightly polluted	Moderately polluted	Highly polluted	
Cd	2.16	43.81	13.33	17.14	25.71	6.08
As	1.01	65.71	27.62	6.67	-	1.99
Pb	0.74	78.10	18.10	2.86	0.95	2.19
Hg	3.78	13.33	9.52	13.33	63.81	6.57
Cu	1.18	65.71	7.62	10.48	16.19	3.25

Note: P_{iave} represents the average single-factor index of each heavy metal at the sampling points (n = 105), while P_{Nave}, denotes the average comprehensive index of each heavy metal at the same sampling points (n = 105).

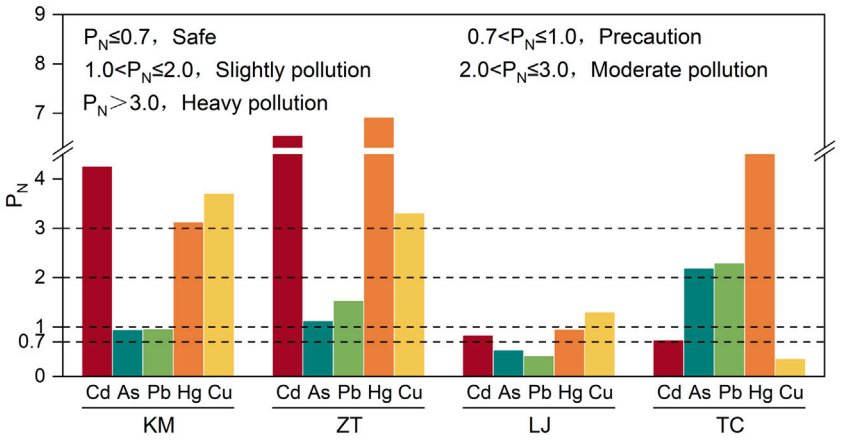

FIGURE 3
Comprehensive pollution index (P_N) of soil heavy metals in different regions.

TABLE 3 Soil potential ecological risk index.

Element	Single factor potential ecological risk index (E_r^i ave)	Potential ecological risk index (*RI*)	Proportion of ecological risk (%)				
			Low	Moderate	High	Slightly heavy	Heavy
Cd	64.81	235.88	47.67	20.95	23.81	8.57	-
As	10.09		100.00	-	-	-	-
Pb	3.72		100.00	-	-	-	-
Hg	151.37		13.33	9.52	28.57	46.67	1.90
Cu	5.89		100.00	-	-	-	-

spectrometer, following the GB 5009.11–2014 and GB 5009.17–2021 methods, respectively. The detection limits for heavy metals in the soil (Cd, As, Pb, Hg, Cu, Zr) were 0.03, 0.01, 1, 0.002, 0.7, and 2 mg/kg, respectively, while those for plant samples (Cd, As, Pb, Hg, Cu) were 0.002, 0.01, 0.02, 0.0002, and 0.05 mg/kg, with quantification limits set at four times the detection limits. For additional information related to this experiment, please refer to the supplementary materials.

2.3 Heavy metal pollution assessment

2.3.1 Single factor pollution index (P_i)

The pollution level of a specific heavy metal in soil was calculated using the formula:

$$P_i = \frac{C_i}{S_i}$$

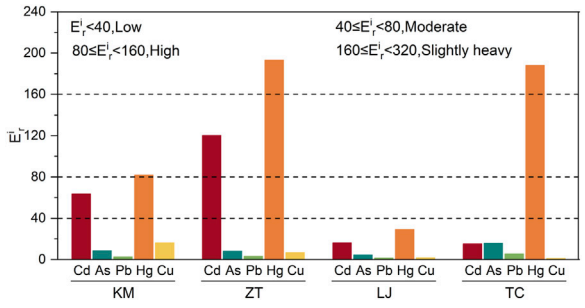

FIGURE 4
Single-factor potential ecological risk index (E_r^i) of heavy metals in soil in different regions.

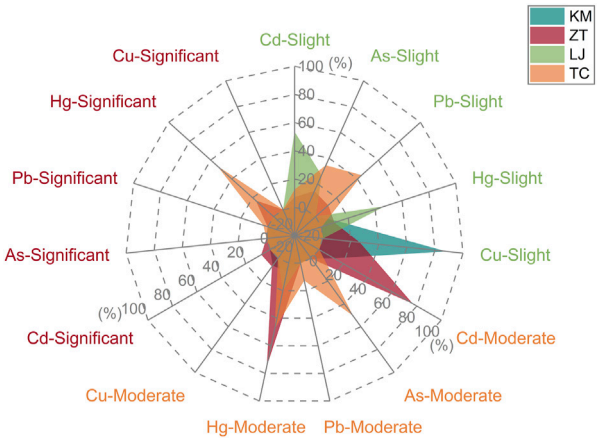

FIGURE 5
Proportion of soil heavy metal enrichment factor (EF) in different regions.

where P_i is the pollution index of heavy metal i; C_i is the measured concentration of heavy metal i (mg·kg^{-1}); and S_i is the evaluation standard value for heavy metal i (mg·kg^{-1}). The background value of surface (A horizon) soil in Yunnan Province is selected as the standard for evaluating heavy metal pollution (Table 1) (Chen et al., 2021; China National Environmental Monitoring Center, 1990).

2.3.2 Comprehensive pollution index (P_N)

The comprehensive pollution index (P_N) incroporates both the average and maximum values of single-factor pollution indices, reflecting the overall pollution level of different contaminants in the soil. The calculation formula is as follows:

$$P_N = \sqrt{\frac{P_{imax}^2 + P_{iave}^2}{2}}$$

Where P_{imax} refers to the maximum value of the pollution index among the pollutants; P_{iave} refers to the average value of the pollution index. The grading standards are shown in Supplementary Table S2 (Ruan et al., 2023).

2.3.3 Potential ecological risk index (RI)

Based on heavy metal toxicity and environmental behavior, the potential ecological risk index (RI) was employed to assess soil heavy metal pollution levels (Hakanson, 1980; Yan et al., 2024). The calculation formulas are as follows:

$$RI = \sum_i^n E_r^i$$

$$E_r^i = T_r^i \times C_r^i = T_r^i \times C_n / B_n$$

where B_n is the background value of heavy metal i, C_n is the concentration of heavy metal i in the sample, E_r^i is the single-factor potential ecological risk index, and T_r^i is the toxic response factor of the heavy metal (assigned values: Cd = 30, As = 10, Pb = 5, Hg = 40, Cu = 5).

2.3.4 Enrichment factor (EF)

The enrichment factor (EF) serves as a critical indicator for evaluating pollutant sources and tracing the origins of elemental contamination. Zirconium (Zr) was selected as the reference element for calculating enrichment factors (Kuang et al., 2020), with the formula as follows:

$$EF_i = \frac{(C_i/Zr_i)}{(B_i/Zr_n)}$$

where EF is the enrichment factor of element i in soil; C_i and Zr_n represents the concentrations of element i and the reference element Zr in the sample, respectively; B_i and Zr_n refer to the background values of element i and Zr in the soil. The background values of

TABLE 4 Soil heavy metal enrichment factor.

Element	EF_{ave}	Proportion of different enrichment levels (%)			
		Negligible	Slight	Moderate	Significant
Cd	1.70	50.48	14.29	32.38	2.86
As	1.09	64.76	20.00	15.24	-
Pb	0.80	77.14	18.10	3.81	0.95
Hg	3.74	15.24	14.29	47.62	22.86
Cu	0.73	72.38	23.81	3.81	-

Note: EF_{ave}, represents the average enrichment factor of each heavy metal at the sampling points (n = 105).

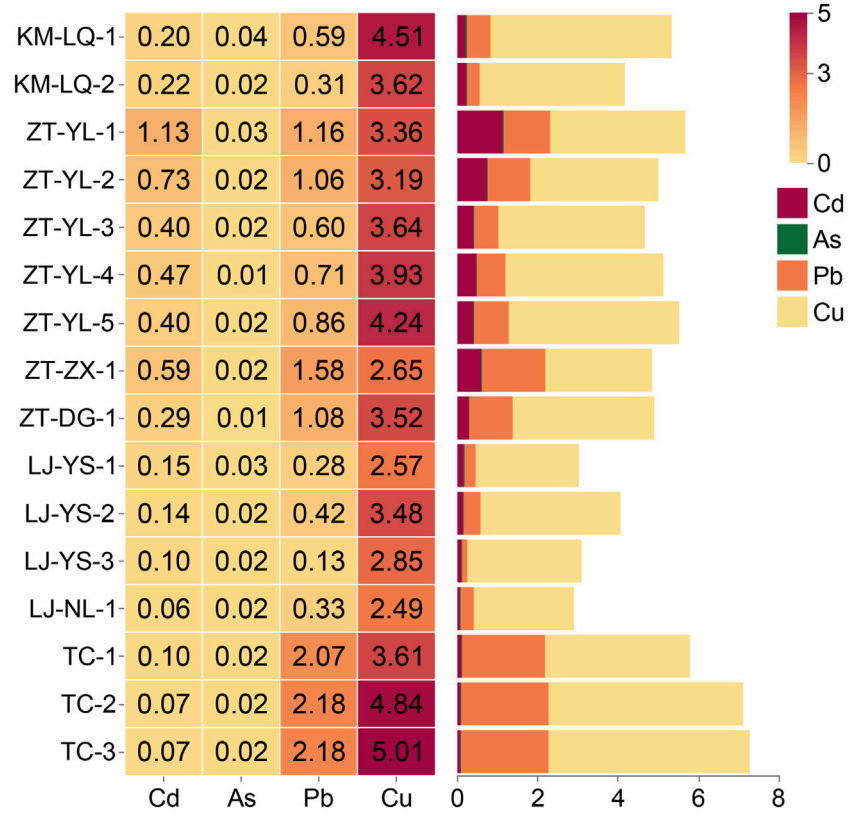

FIGURE 6
Distribution of heavy metal content of *Gastrodia elata* in different regions (mg·kg^{-1}).

TABLE 5 Descriptive statistical analysis of heavy metal content in *Gastrodia elata* tubers (mg·kg^{-1}).

Element	Range	Mean ± standard deviation	Coefficient of variation	Import and export standards (K4)	K4 (exceedance percentage/%)
Cd	0.06~1.13	0.32 ± 0.30	0.92	0.30	37.5
As	0.01~0.04	0.02 ± 0.01	0.34	2.00	-
Pb	0.13~2.18	0.97 ± 0.70	0.72	5.00	-
Hg	-	-	-	0.20	-
Cu	2.49~5.01	3.59 ± 0.77	0.21	20.00	-

Note: The mean represents the average concentration of each heavy metal at the sampling points (n = 16). K4 indicates the limit standard of heavy metals as defined in the *Green Industry Standard for Import and Export of Medicinal Plants and Preparations*. "-" denotes no relevant data or no exceedance.

surface (A layer) soils in Yunnan Province were selected as the standard for each heavy metal: Cd 0.22 mg·kg^{-1}, Pb 40.6 mg·kg^{-1}, Cu 46.3 mg·kg^{-1}, Hg 0.06 mg·kg^{-1}, As 18.4 mg·kg^{-1}, and Zr 229 mg·kg^{-1} (China National Environmental Monitoring Center, 1990; Barbieri, 2016).

2.3.5 Bioconcentration factor (BCF)

The bioconcentration factor (BCF) reflects the capacity of soil heavy metals to accumulate in plants (Tong et al., 2022). The calculation formula is as follows:

$$BCF = \frac{\text{Content of a specific heavy metal in plants}}{\text{Corresponding heavy metal content in soil}} \times 100\%$$

Based on BCF values, the uptake intensity of *G. elata* for soil heavy metals is classified into four levels: Low enrichment (0 < BCF ≤1.5), Medium enrichment (1.5 < BCF ≤4.5), and High enrichment (BCF >4.5) (Dong et al., 2023).

2.3.6 Hazard quotient (HQ) and hazard index (HI)

The hazard quotient (HQ) is commonly used to assess non-carcinogenic risks posed by pollutants. The target hazard quotient is defined as the ratio of a pollutant's exposure dose to its reference dose (RFD), determined by the following formula:

$$HQ = \frac{C \times EF \times ED \times IRD \times t}{BW \times AT \times RFD}$$

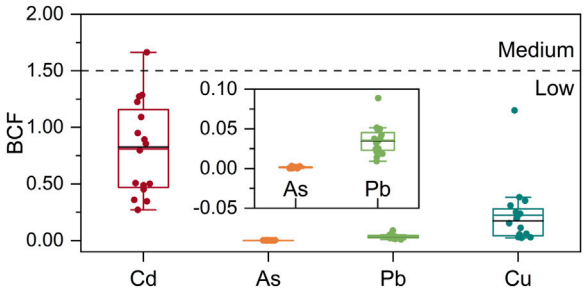

FIGURE 7
Bioconcentration factor (BCF) of *Gastrodia elata* (Note: black represents the median line and the same color represents the mean line.).

TABLE 6 Analysis of the hazard quotient and hazard index of *Gastrodia elata*.

Element	HQ	HI
Cd	2.00E-04~3.70E-03	3.13E-02
As	1.13E-04~5.75E-04	
Pb	6.16E-05~1.02E-03	
Cu	1.02E-04~2.06E-04	

Note: the calculation range of HQ, is based on the recommended usage and dosage of *Gastrodia elata* in ⟪Pharmacopoeia Standard⟫, Volume I, 2020 (10 g).

Where C (mg·kg^{-1}) represents the detected concentration of each metal in *G. elata*; *EF* is the exposure frequency (set to 90 days/year); *ED* is the exposure duration (set to 20 years); *IRD* is the ingestion rate (set to 0.01 kg·d^{-1}) based on the maximum dosage in the Chinese Pharmacopoeia (National Pharmacopoeia Committee, 2020); the transfer rate (t) of heavy metals to the medicinal plant vary: 14% for Cd, Cu, and Pb; 35% for As; and 24% for Hg. The average body weight (*BW*) is set to 60 kg, following international standards; the averaging time for non-carcinogenic toxicity (*AT*) is calculated as 70 years × 365 days; and the *RFD* values are Cu 0.04 μg·g^{-1}, As 0.0003 μg·g^{-1}, Cd 0.0005 μg·g^{-1}, Hg 0.0003 μg·g^{-1}, and Pb 0.0035 μg·g^{-1} (Luo et al., 2021).

When multiple heavy metals coexist in *G. elata*, the total target hazard index (HI) is calculated to assess the combined pollution risk:

$$HI = \Sigma HQ$$

Here, HQ represents the target hazard quotients of the five heavy metals. Higher HQ or HI values indicate greater health risks to humans, with an HI > 1 suggesting potential health risk.

2.4 Data analysis

Descriptive statistics were conducted using Excel 2010. One-way ANOVA was performed with SPSS 26.0 software to evaluate differences in soil pH, TN, TP, TK, SOM, and CEC among different regions. Prior to ANOVA, Levene's test was used to assess the homogeneity of variances across groups. For variables with significant ANOVA results, Duncan's multiple range test was applied as a *post hoc* analysis to identify which regions differed significantly in means ($P < 0.05$). Pearson correlation coefficient analysis was used to examine the relationship between soil and plant heavy metals. Data visualization was carried out using Origin 2021. The sampling point map for the *G. elata* planting area in Yunnan Province was generated with ArcGIS 10.8.

3 Results and discussion

3.1 Analysis of soil physicochemical properties

The spatial distribution of heavy metals is influenced by multiple factors, including geochemical characteristics, microbial activity, human activities, and soil physicochemical properties (Lima et al., 2024; Korkanç et al., 2024; Zhong et al., 2011). In the study area, the surface soil exhibited a pH range of 4.10~6.10, with TN, TP, TK, SOM, and CEC values spanning 0.08–10.97 g·kg^{-1}, 0.08–1.00 g·kg^{-1}, 5.05–47.33 g·kg^{-1}, 16.48–221.24 g·kg^{-1}, and 4.74–42.16 cmol·kg^{-1}, respectively (Figure 2). Among these, TN, TK, SOM, and CEC levels were found to be abundant, whereas TP was relatively low (National Soil Survey Center, 1988). Notably, the pH in ZT was significantly lower than in KM, LJ, and TC, with 97.62% of the samples exhibiting a pH below 4.5, indicating strong to extremely strong acidity (Figure 2A). Interestingly, the levels of TN, SOM, and CEC levels in ZT were significantly higher than those in other regions (Figures 2B–F). The soil in ZT predominantly consists of yellow soil, yellow-brown soil, and purple soil, among which yellow soil covers the largest area, accounting for 66.42% of ZT's total soil area. This soil type is characterized by relatively low pH and higher organic matter content compared to others (Zhaotong Municipal People's Government, 2023; Ji et al., 2023). The parent material of yellow soil originates from acidic rocks such as sandstone and shale, which release aluminum (Al^{3+}) and proton (H^{+}) during weathering, contributing to soil acidification (Hamer, 2024). At the same time, high TN levels can enhance the activity of ammonia-oxidizing bacteria, accelerating nitrification and releasing in further H^{+}, which exacerbates soil acidity (Liu et al., 2023). The average annual temperature in ZT ranges from 11°C to 21°C, coupled with annual precipitation levels between 600 and 1,230 mm (Yuan et al., 2022). Such a humidity environment accelerates the leaching of base cations (Ca^{2+}, Mg^{2+}), while promoting the accumulation of organic acids, such as humic acid, which may further contribute to soil acidification (Wen et al., 2023). It is noteworthy that this study collected soil and *G. elata* samples during winter. The average temperature in the sampling areas ranged from 8°C to 15°C, while in the ZT region it was even lower, between 2°C and 9°C. During this period, frequent light rains occurred, with precipitation from December to January ranging from 66 to 272 mm. Winter rainfall may promote the migration and diffusion of heavy metals. Additionally, freeze-thaw cycles in the ZT region may alter the soil pore structure, further affecting the adsorption and migration of heavy metals (Tang et al., 2023; Gao et al., 2024).

Importantly, the average SOM content (84.95 g·kg^{-1}) in the sampling areas was significantly higher than the cultivated soils in Yunnan Province, which averaged 9.15 ± 29.01 g·kg^{-1} (Figure 2E)

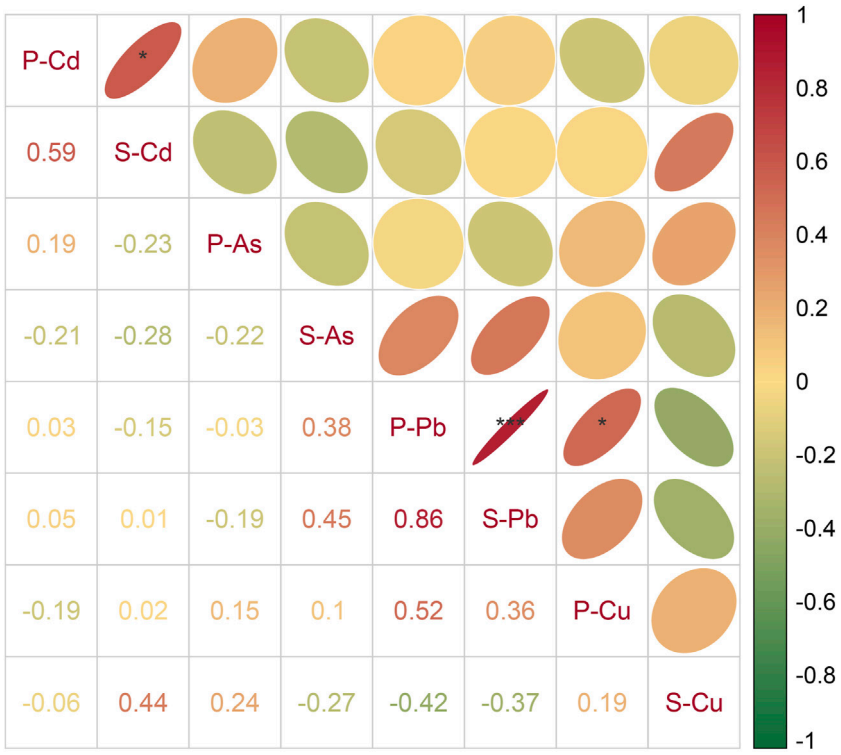

FIGURE 8
Heatmap of the correlation between heavy metals in soil and plants. (Note: S- represents heavy metals in soil and P- represents heavy metals in plants; *, ** and *** indicate significant correlation at the levels of 0.05, 0.01 and 0.001 respectively.).

(Sun et al., 2022). This difference may be attributed to organic carbon inputs from understory vegetation, litterfall, microbial activity, and tree species diversity (Adamczyk et al., 2019; Augusto and Boča, 2022; Shen et al., 2024). The highly acidic environment also inhibits microbial decomposition of organic matter, promoting SOM retention (Li et al., 2024). This phenomenon may explain why ZT exhibits the lowest pH among all sampling areas, while concurrently having the highest SOM content (Figures 2A,E).

3.2 Risk assessment of soil heavy metal pollution

3.2.1 Analysis of soil heavy metal content

As shown in Table 1, the heavy metal content in the soil of the *G. elata* planting area varied significantly. The concentrations of Cd, As, Pb, Hg, and Cu ranged from 0.07–1.83, 6.78–48.45, 3.60–122.27, 0.02–0.68, and 2.49–205.78 mg·kg^{-1}, respectively, with average concentrations of 0.48, 18.56, 30.21, 0.23, and 54.58 mg·kg^{-1}. Among the 105 sampling points, the exceedance rates of heavy metals compared to the background values of Yunnan soil followed the order of Hg > Cd > Cu > As > Pb, while the exceedance rate of Cd reached as high as 55.24%. Except for Pb, the average concentrations of the other four heavy metals exceeded their background values: 2.18 times (Cd), 1.01 times (As), 3.83 times (Cu), and 1.18 times (Hg) times the background levels, indicating potential pollution point sources in the *G. elata* planting area. Specifically, the average concentrations of Cd and Cu exceeded the soil pollution risk screening values for agricultural land by 1.6 and 1.09 times, respectively, while As, Pb, and Hg did not exceed the risk screening or control values (GB 15618–2018). Overall, the issue of Cd exceedance is particularly pronounced. Compared to previous studies, the issue of soil Cd exceeding standards in *G. elata* planting areas appears to be more severe (Jin et al., 2022).

Coefficient of variation (CV) analysis revealed that the CVs for Cd, As, Pb, Hg, and Cu were 0.93, 0.52, 0.69, 0.53, and 1.09, respectively, indicating strong variability (CV > 0.2), whereas pH exhibited weak variability (CV < 0.2) (Table 1). This suggests that the soil heavy metals in the sampling area may be influenced by varying degrees of anthropogenic interference (Chen et al., 2021; Du et al., 2024), with higher CVs for Cd and Cu indicating that their distribution is significantly impacted by human activities.

3.2.2 Analysis of heavy metal pollution index

Pollution indices, P_i and P_N, are essential for assessing soil heavy metal pollution risk. By calculating the ratio of predicted no-effect concentration to exposure concentration, the risk level of heavy metals in soil can be determined (Zhang et al., 2023). According to Table 2, the pollution levels of five heavy metals were ranked as Hg > Cd > Cu > As > Pb. Notably, the P_i values for Hg and Cd were 3.78 and 2.16, respectively, while the P_i values for the remaining heavy metals were less than 2, indicating that Hg pollution is the

most severe, followed by Cd. Specifically, the proportion of unpolluted from Hg was 13.33%, slightly polluted accounted for 9.52%, moderately polluted was 13.33%, and highly polluted was 63.81%; for Cd, the proportion of unpolluted was 43.81%, slightly polluted was 13.33%, moderately polluted was 17.14%, and highly polluted was 25.71%; both Cu and As had the same proportion of unpolluted (65.71%), but Cu had a 16.19% highly polluted, whereas As had highly polluted; the proportion of unpolluted for Pb was 78.10%, indicating a lower pollution risk. Thus, it is evident that Hg and Cd have a wider range of pollution, followed by Cu, while As and Pb have a smaller range of pollution.

From the perspective P_N value, heavy metal pollution levels were ranked as Hg > Cd > Cu > Pb > As. Among these, Hg, Cd and Cu were classified as severely polluted, Pb as moderately polluted, and As as mildly polluted. Comparative analysis of the P_N values across the four regions showed that Hg exhibited high P_N levels, ranked as ZT > TC > KM > LJ, where ZT, TC and KM reflected heavy pollution, while LJ remained at a precautionary level (Figure 3). Cd pollution levels followed, with rankings of ZT > KM > LJ > TC, where both ZT and KM also indicated heavy pollution, while LJ and TC were categorized as precautionary (Figure 3). Cu and Cd displayed similar regional pollution patterns, with both ZT and KM experiencing heavy pollution (Figure 3). Notably, the non-ferrous metal smelting industry is a primary sources of heavy metal pollution, with approximately 45.6% of smelting enterprises in China located in Jiangxi, Yunnan, Henan, Guangdong, and Hunan provinces. Research indicates that ZT and its vicinity including KM are crucial zones for non-ferrous metal smelting within Yunnan province. Cd and Hg from smelting emissions can contaminate soil through atmospheric deposition (Han et al., 2023; Shao et al., 2013). Moreover, Cu from tailings in the ZT lead-zinc mining area is dispersed via runoff, increasing mobilization in acidic soils (Yu et al., 2025), contributing to elevated levels of Cd and Cu contamination.

3.2.3 Potential ecological risk assessment of heavy metals

RI is an important tool for quantitatively assessing the ecological risks of toxic metals in soil and sediments (Wang et al., 2024). As shown in Table 3, the RI values of the five heavy metals ranged from 150 to 300, indicating a moderate potential ecological risk. The values of E_r^i follwed the order of Hg > Cd > As > Cu > Pb, with Hg recording an E_r^i of 151.37, where the proportion of heavy risk reached 46.67%. Cd had an E_r^i of 64.81, indicating a slight heavy risk (8.57%), while As, Pb, and Cu exhibited low risk levels. To reduce the influence of sampling point differences, E_r^i values of the five heavy metals were calculated across the four regions. Results showed that Hg risk was particularly pronounced in the order of ZT > TC > KM > LJ, with ZT and TC reaching slightly heavy risk, while KM was categorized as high risk. The risk for Cd ranked second to Hg, in the order of ZT > KM > LJ > TC, with ZT reaching high risk levels; low risk was observed for As, Pb, and Cu across the four regions (Figure 4). Notably, the toxicity coefficient of Hg (40) is significantly higher than that of other elements (e.g., Cd = 30), meaning that even low concentrations can significantly elevate the RI value (Hakanson, 1980). Thus, the pollution level and potential ecological risk of Cd in ZT warrant heightened attention.

3.2.4 Heavy metal enrichment factor analysis

The EF for the five heavy metals in the soil were as follows: Cd 0.24–6.90, As 0.17–4.75, Pb 0.06–6.47, Hg 0.28–12.95, and Cu 0.05–3.55, with EF levels ranked as Hg > Cd > As > Pb > Cu (Table 4). Among these, the proportion deemed negligible for Cd, As, Pb, and Cu was the highest (50.48%–72.38%), while moderate enrichment for Hg accounted for the largest proportion (47.62%). A comparison of EF levels across the four regions revealed notable Cd and Hg enrichment in ZT, with significant Hg and As enrichment in TC (Figure 5). The study suggests that Hg enrichment in TC may be linked to transboundary pollutants, such as emissions from coal combustion carried by the South Asian monsoon (Tripathee et al., 2019). ZT, located in the Pb-Zn polymetallic mining belt of Sichuan, Yunnan, and Guizhou, has a high baseline value of native Cd, further exacerbated by smelting emissions (Li et al., 2013). Additionally, the high SOM in ZT can adsorb Hg^{2+} through functional groups, such as carboxyl and phenolic hydroxyl, preventing vertical migration and resulting in surface enrichment (Li et al., 2012).

3.3 Heavy metal evaluation of *Gastrodia elata*

3.3.1 Analysis of heavy metal content

In the sampled *G. elata* tubers, except for Hg, which was not detected, the content ranges of Cd, As, Pb, and Cu were found to be 0.06–1.13, 0.01–0.04, 0.13–2.18, and 2.49–5.01 $mg{\cdot}kg^{-1}$, respectively, with average contents of 0.32, 0.02, 0.97, and 3.59 $mg{\cdot}kg^{-1}$ (Figure 6). It is worth noting that, compared to the study by Lv et al. (2016), this research found relatively high levels of Cd and Pb in the ZT area, whereas As and Cu concentrations were relatively low. According to the "Green Industry Standards for the Import and Export of Medicinal Plants and Preparations," the exceedance rate of Cd in *G. elata* tubers was 37.5%, while As, Pb, and Cu levels did not exceed the limits (Table 5). According to the same standards, Jin et al. (2022) investigated the planting areas of *G. elata* in Yunnan (region not specified) and found that the soil exhibited slight Cd pollution, with a Cd exceedance rate of 3.1% in tubers. Our study showed that the median Cd content in tubers from the ZT area was 2.3, 3.9, and 6.6 times higher than that in the KM, LJ, and TC regions, respectively (Figure 6). ZT is primarily involved in building materials, chemical manufacturing, lignite chemical production, and mineral processing, boasting the largest coal and sulfur reserves in the province and the top three non-ferrous metal bases in Yunnan, as well as possesses the second-largest lignite field in southern China (Pang et al., 2022; Wang et al., 2022; Shao et al., 2024). These factors are likely contributed to the elevated levels of Cd pollution observed.

3.3.2 Heavy metal enrichment capacity

Previous studies highlight that ZT has the highest enrichment coefficient for Cd in the edible parts of crops among 11 cities in Yunnan Province (Dong et al., 2022). Analysis of the heavy metal enrichment capacity in *G. elata* tubers revealed that these tubers exhibit the strongest capacity for Cd, with an average enrichment coefficient of 0.8100, while As exhibited the weakest, with an average enrichment coefficient of 0.0015. Except for non-detectable Hg, the average enrichment coefficients for heavy metals in *G. elata* tubers

followed the order: Cd > Cu > Pb > As (Figure 7). Notably, despite the relatively high soil concentrations of Hg and Cu where *G. elata* is cultivated (Table 2), excessive accumulation of these metals in the tubers was not observed. Conversely, the accumulation of Cd in *G. elata* appears more influenced by total Cd content. One explanation is that acidic soils (pH < 5.5) enhance Cd availability by facilitating its desorption from soil colloids, thereby promoting absorbed by plants (Li et al., 2021). In contrast, Hg^{2+} tends to form stable complexes with SOM, such as Hg-SOM, which limits its bioavailability (Xu et al., 2014). Moreover, *G. elata* is a mycoheterotrophic plant reliant on *Armillaria* spp. for nutrient absorption (Liu J. J. et al., 2024). Fungal hyphae can absorb and accumulate Cd (Vinichuk et al., 2019), selectively enriching Cd^{2+} through membrane transport proteins (e.g., ZIP family) and transferring it to *G. elata* tubers via the hyphal network. In contrast, Hg and Cu may be excluded or sequestered within vacuoles by the hyphae, thus limiting their transfer to the host plant (Long et al., 2025).

3.3.3 Health risk assessment of heavy metals in humans

Using a health risk assessment model, the HQ and HI values for heavy metal intake through *G. elata* tubers consumed by residents near the sampling points were calculated. The results indicated that the HQ and HI values for Cd, As, Pb, and Cu were all below 1 (Table 6). According to the National Center for Food Safety Risk Assessment's publication, "Opinions on Managing 9 Substances as Both Food and Traditional Medicinal Materials," the recommended daily intake of *G. elata* is ≤ 3 g (not suitable for pregnant women, breastfeeding women, or infants) (Zhao et al., 2018). This indicates that the risk of heavy metal contamination in *G. elata* is within acceptable limits. Although current health risks from heavy metals in *G. elata* are low, further research is needed on the long-term accumulation of heavy metals in the human body and their potential health effects.

3.4 Soil and plant correlation analysis

Certain elements may exhibit synergistic or antagonistic effects, with variations in soil heavy metal content significantly influencing their accumulation in plants (Gong et al., 2024). Correlation analysis revealed an extremely significant positive correlation of Pb ($P < 0.001$, $R^2 = 0.86$) and a significant correlation of Cd ($P < 0.05$, $R^2 = 0.56$) between soil and *G. elata* (Figure 8). Cd^{2+} and Pb^{2+} compete for ion channels in plant roots (such as Ca^{2+} channels) due to their similar charge; however, in acidic soils, the bioavailable forms of Cd are more readily absorbed by plants, resulting in a significantly higher Cd accumulation coefficient compared to Pb (Figure 7) (Kanwal et al., 2024). Conversely, As and Cu levels in both *G. elata* and the soil did not exhibit significant correlation (Figure 8). In the soil, As primarily exists in the forms such as As^{5+} or As^{3+}, with its absorption by plants highly dependent on its redox state and adsorption by rhizosphere iron oxides (Chen et al., 2022). Cu tends to forms stable complexes with SOM, particularly in soils rich in high organic matter (Bradl, 2004).

4 Conclusion

In Yunnan Province, the degree of soil heavy metal pollution in the main *G. elata* planting areas follows the order: Hg > Cd > Cu > As > Pb, with a P_N values ranging from 1 to 7, indicating slight to heavy pollution and a moderate potential ecological risk. The EF for the five heavy metals are ranked as Hg > Cd > As > Pb > Cu, with EF indices between 0 and 4, suggesting no enrichment to moderate enrichment. Regionally, the P_N and P_i values for soil Hg and Cd are highest in the ZT area, indicating a more serious pollution risk compared to the KM, LJ and TC areas. The exceedance rate of Cd in *G. elata* is 37.5%, while other heavy metals remain within standard limits and do not pose a health risk. The accumulation ability of *G. elata* for Cd shows a significant positive correlation with soil Cd, but there is no accumulation of Hg. When selecting areas for *G. elata* cultivation, special attention should be given to soil levels of Hg, Cd, and Cu, and monitoring and control of Cd pollution in the ZT area should be strengthened.

Data availability statement

The original contributions presented in the study are included in the article/Supplementary Material, further inquiries can be directed to the corresponding authors.

Author contributions

XQ: Writing – review and editing, Methodology, Writing – original draft, Visualization, Data curation. YL: Methodology, Data curation, Visualization, Writing – review and editing, Writing – original draft. HY: Methodology, Writing – review and editing, Data curation. JW: Methodology, Writing – review and editing, Data curation. HZ: Data curation, Methodology, Writing – review and editing. HS: Methodology, Writing – review and editing, Data curation. QL: Writing – review and editing. ZS: Writing – review and editing. BH: Writing – review and editing, Supervision, Writing – original draft. WF: Supervision, Writing – original draft, Writing – review and editing.

Funding

The author(s) declare that financial support was received for the research and/or publication of this article. This work was supported by the National Key Research and Development Program Project Supported by the Scientific Research Fund of Yunnan Education Department (2022YFD1601810).

Conflict of interest

The authors declare that the research was conducted in the absence of any commercial or financial relationships that could be construed as a potential conflict of interest.

Generative AI statement

The author(s) declare that no Generative AI was used in the creation of this manuscript.

Publisher's note

All claims expressed in this article are solely those of the authors and do not necessarily represent those of their affiliated organizations, or those of the publisher, the editors and the reviewers. Any product that may be evaluated in this article, or claim that may be made by its manufacturer, is not guaranteed or endorsed by the publisher.

Supplementary material

The Supplementary Material for this article can be found online at: https://www.frontiersin.org/articles/10.3389/fenvs.2025.1602385/full#supplementary-material

References

Adamczyk, B., Sietiö, O. M., Straková, P., Prommer, J., Wild, B., Hagner, M., et al. (2019). Plant roots increase both decomposition and stable organic matter formation in boreal forest soil. *Nat. Commun.* 10 (1), 3982. doi:10.1038/s41467-019-11993-1

Augusto, L., and Boča, A. (2022). Tree functional traits, forest biomass, and tree species diversity interact with site properties to drive forest soil carbon. *Nat. Commun.* 13 (1), 1097. doi:10.1038/s41467-022-28748-0

Barbieri, M. (2016). The importance of enrichment factor (EF) and geoaccumulation index (igeo) to evaluate the soil contamination. *J. Geol. Geophys.* 5 (1), 1–4. doi:10.4172/2381-8719.1000237

Bradl, H. B. (2004). Adsorption of heavy metal ions on soils and soils constituents. *J. Colloid. Interface Sci.* 277, 1–18. doi:10.1016/j.jcis.2004.04.005

Chen, G. G., Du, Y. H., Fang, L. P., Wang, X. Q., Liu, C. P., Yu, H. Y., et al. (2022). Distinct arsenic uptake feature in rice reveals the importance of N fertilization strategies. *Sci. Total Environ.* 854, 158801. doi:10.1016/j.scitotenv.2022.158801

Chen, W. D., Zhu, K., Cai, Y. K., Wang, Y. L., and Liu, Y. P. (2021). Distribution and ecological risk assessment of arsenic and some trace elements in soil of different land use types, tianba town, China. *Environ. Technol. Innov.* 24, 102041. doi:10.1016/j.eti.2021.102041

Chen, Y., and Deng, Z. H. (2025). Heavy metal pollution in *Gastrodia elata* planting soil and remediation strategies. *Agric. Technol.* 45 (9), 6–11. doi:10.19754/j.nyyjs.20250515002

Chen, Y. W., Zou, J. Y., Sun, H., Qin, J. H., and Yang, J. Y. (2020). Metals in traditional chinese medicinal materials (TCMM): a systematic review. *Ecotoxicol. Environ. Saf.* 207, 111311. doi:10.1016/j.ecoenv.2020.111311

China National Environmental Monitoring Center (1990). *Background value of soil elements in China*. Beijing: China Environmental Science Press.

Dong, C. Y., Zhang, M., Zhang, H., Yang, H. C., Li, J. Q., Tan, F. M., et al. (2022). Heavy metal characteristics and comprehensive quality index evaluation of soil-crop system in 11 cities of Yunnan province, China. *J. Geosci. Environ. Prot.* 10, 257–272. doi:10.4236/gep.2022.104016

Dong, H. Z., Gao, Z. J., Liu, J. T., and Jiang, B. (2023). Study on the accumulation of heavy metals in different soil-crop systems and ecological risk assessment: a case study of jiao river basin. *Agronomy* 13 (9), 2238. doi:10.3390/agronomy13092238

Du, H. M., Lu, X. W., and Han, X. F. (2024). Determination of priority control factors for risk management of heavy metal(loid)s in park dust in mianyang city. *Sci. Rep.* 14 (1), 27440. doi:10.1038/s41598-024-79157-w

Ekor, M. (2014). The growing use of herbal medicines: issues relating to adverse reactions and challenges in monitoring safety. *Front. Pharmacol.* 4, 177. doi:10.3389/fphar.2013.00177

Fei, Y. Q., Xiao, L., Wang, B., Zhu, H. L., and Nie, J. (2021). Residue analysis and risk assessment of heavy metals and harmful elements in 37 plant medicinal materials. *Chin. J. Pharm. Anal.* 41 (6), 1000–1008. doi:10.16155/j.0254-1793.2021.06.09

Ferrol, N., Tamayo, E., and Vargas, P. (2016). The heavy metal paradox in arbuscular mycorrhizas: from mechanisms to biotechnological applications. *J. Exp. Bot.* 67 (22), 6253–6265. doi:10.1093/jxb/erw403

Gao, W. Y., Xiang, C., Wu, C., Li, X., Zhang, W., Tang, L., et al. (2024). Unveiling heavy metal(loid) contamination and migration at an abandoned smelting site: integrated geophysical and hydrological analyse. *Chem. Eng. J.* 500, 156853. doi:10.1016/j.cej.2024.156853

Gong, Y. F., Ren, W., Li, F. P., Jiang, Y. C., and Zhang, Z. M. (2024). The role of soil elemental forms in the soil-plant migration system: an example of heavy metals in epimedium production areas. *Environ. Technol. Innov.* 36, 103800. doi:10.1016/j.eti.2024.103800

Goswami, V., Deepika, S., Diwakar, S., and Kothamasi, D. (2023). Arbuscular mycorrhizas amplify the risk of heavy metal transfer to human food chain from fly ash ameliorated agricultural soils. *Environ. Pollut.* 329, 121733. doi:10.1016/j.envpol.2023.121733

Hakanson, L. (1980). An ecological risk index for aquatic pollution control: a sedimentological approach. *Water Res.* 14 (8), 975–1001. doi:10.1016/0043-1354(80)90143-8

Hamer, M. (2024). Assessing the resilience of soils to acidification on different time scales. *Environ. Anal. Eco Stud.* 11 (5), 000772. doi:10.31031/EAES.2024.11.000772

Han, X. Y., Guo, J. Y., Shi, J. W., Li, D. S., Wang, Y. M., Ning, P., et al. (2023). Characterization and health risk of heavy metals in PM2.5 from road fugitive dust in five cities of Yunnan province. *Environ. Sci.* 44 (6), 3463–3474. doi:10.13227/j.hjkx.202207173

Harris, E. S., Cao, S. G., Littlefield, B. A., Craycroft, J. A., Scholten, R., Kaptchuk, T., et al. (2011). Heavy metal and pesticide content in commonly prescribed individual raw Chinese herbal medicines. *Sci. Total Environ.* 409 (20), 4297–4305. doi:10.1016/j.scitotenv.2011.07.032

Hu, Y. B., Zeng, H. L., Huang, J. H., Jiang, L., Chen, J., and Zeng, Q. H. (2020). Traditional Asian herbs in skin whitening: the current development and limitations. *Front. Pharmacol.* 11, 982. doi:10.3389/fphar.2020.00982

Huang, W. J., Liang, Y. F., Tang, D., Zhang, Q., L, D. D., and Wang, Q. Y. (2025). Influence of introduction and cultivation on the content of active ingredients and elements in *Gastrodia elata*. *Sci. Technol. Food Industry* 46 (07), 283–290. doi:10.13386/j.issn1002-0306.2024110405

Huang, X. L., Tan, C. R., Zhu, D. W., Y, L. J., and Zheng, R. (2024). Analysis of exogenous pollutants of *Gastrodia elata* and Ganoderma lucidum. *Chem. Reagents* 46 (03), 73–80. doi:10.13822/j.nki.hxsj.2023.075000001006

Ji, C., Huang, J., Li, J., Zhang, X., Yang, G., Ma, Y., et al. (2023). Deciphering the impacts of chromium contamination on soil bacterial communities: a comparative analysis across various soil types. *J. Environ. Manage.* 348, 119335. doi:10.1016/j.jenvman.2023.119335

Jin, Z. Q., Shang, B. P., Zhang, G. X., Cui, X. M., Guo, L. P., Du, P., et al. (2022). Safety evaluation of three Yunnan medicinal materials, *Gastrodia elata, Polygonatum sibiricum* and maca, and heavy metals in their planting soil. *China Mod. Chin. Med.* 24 (8), 1525–1530. doi:10.13313/j.issn.1673-4890.20210617003

Kanwal, F., Riaz, A., Ali, S., and Zhang, G. (2024). NRAMPs and manganese: magic keys to reduce cadmium toxicity and accumulation in plants. *Sci. Total Environ.* 921, 171005. doi:10.1016/j.scitotenv.2024.171005

Korkanç, S. Y., Korkanç, M., and Amiri, A. F. (2024). Effects of land use/cover change on heavy metal distribution of soils in wetlands and ecological risk assessment. *Sci. Total Environ.* 923, 171603. doi:10.1016/j.scitotenv.2024.171603

Kuang, H. F., Hu, C. H., Wu, G. L., and Chen, M. (2020). Combination of PCA and PMF to apportion the sources of heavy metals in surface sediments from Lake poyang during the wet season. *J. Lake Sci.* 32 (4), 964–976. doi:10.18307/2020.0406

Li, J. Y., Cheng, H., Liang, X. M., Chen, Y. L., Wu, S. W., and Hu, C. X. (2024). Research progress on acidified soil improvement and carbon fixation. *Acta Ecol. Sin.* 44 (17), 7871–7884. doi:10.20103/j.stxb.202312252817

Li, P., Feng, X., Qiu, G., Shang, L., and Wang, S. (2012). Mercury pollution in wuchuan Mercury mining area, Guizhou, Southwestern China: the impacts from large scale and artisanal Mercury mining. *Environ. Int.* 42, 59–66. doi:10.1016/j.envint.2011.04.008

Li, Z. M., Liang, Y., Hu, H. W., Shaheen, S. M., Zhong, H., Tack, F. G., et al. (2021). Speciation, transportation, and pathways of cadmium in soil-rice systems: a review on the environmental implications and remediation approaches for food safety. *Environ. Int.* 156, 106749. doi:10.1016/j.envint.2021.106749

Li, Z. Y., Ma, Z. W., Kuijp, T., Yuan, Z. W., and Huang, L. (2013). A review of soil heavy metal pollution from mines in China: pollution and health risk assessment. *Sci. Total Environ.* 468-469, 843–853. doi:10.1016/j.scitotenv.2013.08.090

Lima, L. H. V., da Silva, F. B. V., da Silva, Y. J. A. B., de Lima Veloso, V., de Sousa, M. G. F., de Souza Junior, V. S., et al. (2024). Integrating environmental, ecological and

human health risk assessments for heavy metals in tropical ultramafic soils. *Sci. Total Environ.* 957, 177343. doi:10.1016/j.scitotenv.2024.177343

Liu, J. J., Yang, X. Q., Li, Z. Y., Miao, J. Y., Li, S. B., Zhang, W. P., et al. (2024a). The role of symbiotic fungi in the life cycle of *Gastrodia elata* blume (orchidaceae): a comprehensive review. *Front. Plant Sci.* 14, 1309038. doi:10.3389/fpls.2023.1309038

Liu, X. Y., Zhang, G. X., Tian, M. H., Zhang, C. F., Yu, X. L., Guo, Y. G., et al. (2015). Determination and comparison of *gastrodin* content between different grades of zhaotong Black *Gastrodia elata* and *Gastrodia elata* from other places. *Chin. Mod. Chin. Med.* 17 (1), 35–38. doi:10.13313/j.issn.1673-4890.2015.1.009

Liu, Y., Fu, K. Z., Leng, A. J., Zhang, L., and Qu, J. L. (2024b). Spotlight on the accumulation of heavy metals in Traditional Chinese medicines: a holistic view of pollution status, removal strategies and prospect. *Sci. Total Environ.* 953, 176025. doi:10.1016/j.scitotenv.2024.176025

Liu, Z. X., Wang, Z. T., Zhao, D. Q., Wu, G., Ling, J., Zhou, S. L., et al. (2023). Effects of soil warming and straw returning on soil nutrients and extracellular enzyme activities. *Acta Ecol. Sin.* 43 (23), 9867–9876. doi:10.20103/j.stxb.202211193352

Long, X. N., Zhang, X. K., Wu, Y., You, X. X., Tang, S. S., Zheng, T. X., et al. (2025). Research progress on the mechanism of arbuscular mycorrhizal fungi improving the resistance of medicinal plants to cadmium stress. *Chin. Herb. Med.* 56 (4), 1477–1488. doi:10.7501/j.issn.0253-2670.2025.04.034

Lu, C. C., Qu, S. H., Zhong, Z. F., Luo, H., Lei, S. S., Zhong, H. J., et al. (2022). The effects of bioactive components from the rhizome of *Gastrodia elata* blume (tianma) on the characteristics of Parkinson's disease. *Front. Pharmacol.* 13, 963327. doi:10.3389/fphar.2022.963327

Lu, J., Gao, L., and Wang, H. Y. (2024). Contamination characteristics of heavy metals and enrichment capacity of native plants in soils around typical coal mining areas in Gansu, China. *Sci. Rep.* 14 (1), 29983–14. doi:10.1038/s41598-024-81740-0

Luan, S., Zhao, Y. C., Han, C. H., and Dou, J. (2015). Determination and analysis of residuals of lead and cadmium in 77 kinds of Chinese herbal medicines. *China Pharm.* 26 (12), 1678–1681. doi:10.6039/j.issn.1001-0408.2015.12.33

Luo, L., Wang, B., Jiang, J. W., Fitzgerald, M., Huang, Q., Yu, Z., et al. (2021). Heavy metal contaminations in herbal medicines: determination, comprehensive risk assessments, and solutions. *Front. Pharmacol.* 11, 595335. doi:10.3389/fphar.2020.595335

Lv, Z. X., Xiang, P. Y., Chen, J., and Tang, Y. (2016). Determination of lead, cadmium, arsenic, Mercury and copper in 14 batches of cultivated *Gastrodia elata*. *China Pharm.* 25 (11), 65–68.

Ministry of Ecology and Environment of the People's Republic of China (2023). Soil and sediment-Determination of 19 total metal elements-inductively coupled plasma mass spectrometry: HJ 1315—2023.

Ministry of Environmental Protection of People's Republic of China (PRC) (2013). Soil and sedimen-Determination of Mercury,arsenic,selenium,bismuth,antimony-Microwave Dissolution/atomic fluorescence spectrometry: HJ 680—2013.

National Health and Family Planning Commission of the People's Republic of China, China Food and Drug Administration (CFDA) (2016). *Determination of multi-elements in food by national standard for food safety: GB 5009*, 268–2016.

National Health and Family Planning Commission of the People's Republic of China (2014). "Determination of total arsenic and inorganic arsenic," in *Food as national standard for food safety: GB 5009*, 11–2014.

National Health and Family Planning Commission of the People's Republic of China, China Food and Drug Administration (CFDA) (2021). *Determination of total mercury and organic mercury in food: GB 5009*, 17–2021.

National Pharmacopoeia Committee (2020). *People's Republic of China (PRC) pharmacopoeia: part one*. Beijing: China Medical Science and Technology Press.

National Soil Survey Center (1988). *Soils in China*. Beijing: China Agriculture Press.

Pang, X. C., Han, X. Y., Shi, J. W., Bao, Y. Z., Ning, P., Zhang, C. N., et al. (2022). Pollution characteristics and health risk of heavy metals in fugitive dust around zhaotong city. *Huan Jing Ke Xue* 43 (1), 180–188. doi:10.13227/j.hjkx.202106018

Ruan, X. L., Ge, S. J., Jiao, Z. Q., Zhan, W. H., and Wang, Y. Y. (2023). Bioaccumulation and risk assessment of potential toxic elements in the soil-vegetable system as influenced by historical wastewater irrigation. *Agric. Water Manag.* 279, 108197. doi:10.1016/j.agwat.2023.108197

Shao, F. L., Li, K. N., Ouyang, D., Zhou, J. W., Luo, Y. T., and Zhang, H. B. (2024). Sources apportionments of heavy metal(loid)s in the farmland soils close to industrial parks: integrated application of positive matrix factorization (PMF) and cadmium isotopic fractionation. *Sci. Total Environ.* 924, 171598. doi:10.1016/j.scitotenv.2024.171598

Shao, X., Cheng, H. G., Li, Q., and Lin, C. (2013). Anthropogenic atmospheric emissions of cadmium in China. *Atmos. Environ.* 79, 155–160. doi:10.1016/j.atmosenv.2013.05.055

Shen, K. H., Li, L., Wei, S. G., Liu, J. R., and Zhao, Y. (2024). A network meta-analysis on responses of forest soil carbon concentration to interventions. *Ecol. Process.* 13 (1), 41. doi:10.1186/s13717-024-00513-9

Sun, J., Zhu, D., Lu, Y., Chen, P. C., Xiong, K., and Lan, Y. Y. (2016). Residue analysis of heavy metals and harmful elements in soil and *Gastrodia elata* in *Gastrodia elata* planting base. *Chin. J. Exp. Tradit. Med. Formulae* 22 (12), 32–36. doi:10.13422/j.cnki.syfjx.2016120032

Sun, T., Tong, W. J., Chang, N. J., Deng, A. X., Lin, Z. L., Feng, X. B., et al. (2022). Estimation of soil organic carbon stock and its controlling factors in cropland of Yunnan province, China. *J. Integr. Agric.* 21 (5), 1475–1487. doi:10.1016/S2095-3119(21)63620-1

Tang, L., Liu, J., Zeng, J. Q., Luo, X. H., Ke, W. S., Li, C. X., et al. (2023). Anthropogenic processes drive heterogeneous distributions of toxic elements in shallow groundwater around a smelting site. *J. Hazard. Mat.* 453, 131377. doi:10.1016/j.jhazmat.2023.131377

Tian, M. H., Wang, J. J., Zhang, G. X., Dai, K., Liu, X. Y., Zhang, C. F., et al. (2016). Characteristics and evaluation of soil fertility in different producing areas of *Gastrodia elata* in zhaotong, Yunnan. *J. Southwest. Agric.* 29 (11), 2653–2659. doi:10.16213/j.cnki.scjas.2016.11.026

Tong, S. M., Yang, L. S., Gong, H. Q., Wang, L., Li, H. R., Yu, J. P., et al. (2022). Bioaccumulation characteristics, transfer model of heavy metals in soil-crop system and health assessment in Plateau region, China. *Ecotoxicol. Environ. Saf.* 241, 113733. doi:10.1016/j.ecoenv.2022.113733

Tripathee, L., Guo, J., Kang, S., Paudyal, R., Huang, J., Sharma, C. M., et al. (2019). Spatial and temporal distribution of total Mercury in atmospheric wet precipitation at four sites from the nepal-himalayas. *Sci. Total Environ.* 655, 1207–1217. doi:10.1016/j.scitotenv.2018.11.338

Vinichuk, M. M., Skyba, G. V., Yelnikova, T. O., and Mandro, Y. N. (2019). Bioaccumulation of selected metals and non-metals in mycelium and fruit bodies of ectomycorrhizal fungi. *Visnyk Kharkiv Univ. Ser. Ecol.* 20, 23–31. doi:10.26565/1992-4259-2019-20-02

Wang, N., Liu, Z., Sun, Y., Lu, N., and Luo, Y. (2024). Analysis of soil fertility and toxic metal characteristics in open-pit mining areas in northern Shaanxi. *Sci. Rep.* 14 (1), 2273. doi:10.1038/s41598-024-52886-8

Wang, N., Luo, Y. H., Liu, Z., and Sun, Y. Y. (2022). Spatial distribution characteristics and evaluation of soil pollution in coal mine areas in loess Plateau of northern Shaanxi. *Sci. Rep.* 12 (1), 16440. doi:10.1038/s41598-022-20865-6

Wang, Y. H., Xu, J., Yuan, Q. S., Guo, L. P., Xiao, C. H., Yang, C. G., et al. (2023). Effect of symbiotic fungi-Armillaria gallica on the yield of *Gastrodia elata* bl. And insight into the response of soil microbial community. *Front. Microbiol.* 14, 1233555. doi:10.3389/fmicb.2023.1233555

Wang, Z. Z., Wang, H. B., Wang, H. J., Li, Q. C., and Li, Y. (2019). Heavy metal pollution and potential health risks of commercially available Chinese herbal medicines. *Sci. Total Environ.* 653, 748–757. doi:10.1016/j.scitotenv.2018.10.388

Wen, H. T., Dong, Q. Y., Wang, P., Song, C., Yang, Z. J., Zhao, Y. Y., et al. (2023). Spatial variation characteristics and influencing factors of soil pH value at the northern foot of tongbai Mountain. *Chin. J. Soil Sci.* 54 (2), 295–305. doi:10.19336/j.cnki.trtb.2022022401

Xu, J. J., Ceng, J., Dong, W. J., Chen, J. L., Hu, Y. D., Xu, Y. Y., et al. (2018). Difference analysis of heavy metal elements in *Gastrodia elata* planting soil in zhaotong area, Yunnan province. *soil Sci.* 6 (4), 115–124. doi:10.12677/hjss.2018.200181888876

Xu, L., Guan, J. Y., Ba, Y., Chen, W. Z., Huang, J. Z., Cheng, Y. X., et al. (2024). Spatial distribution pattern and driving mechanism of heavy metal elements in soils of middle-alpine hilly region, Yunnan province. *Geol. China* 51 (1), 304–326. doi:10.12029/gc20230427003

Xu, W. M., Wu, F. Y., Wang, H. J., Zhao, L. Y., Liu, X., Xiang, P., et al. (2021). Key soil parameters affecting the survival of *Panax notoginseng* under continuous cropping. *Sci. Rep.* 11 (1), 5656. doi:10.1038/s41598-021-85171-z

Xu, Z. Y., Bravo, A. G., Lagerkvist, A., Bertilsson, S., Sjöblom, R., and Kumpiene, J. (2014). Sources and remediation techniques for Mercury contaminated soil. *Environ. Int.* 74, 42–53. doi:10.1016/j.envint.2014.09.007

Yan, H., Chen, J., and Du, J. M. (2024). Heavy metal contamination and ecological risk assessment of soil around quandian coal mine, Henan Province of China. *Appl. Ecol. Environ. Res.* 22 (3), 2367–2376. doi:10.15666/aeer/2203_23672376

Yan, H. Y., Gong, W. L., Liu, Y., Zhou, T., Guo, L. P., Peng, H. S., et al. (2021). Analysis and evaluation of mineral elements in *Gastrodia elata* from different habitats and specifications. *Chin. J. Exp. Tradit. Med. Formulae* 27 (12), 147–156. doi:10.13422/j.cnki.syfjx.20210719

Yang, C. M., Chien, M. Y., Chao, P. C., Huang, C. M., and Chen, C. H. (2021). Investigation of toxic heavy metals content and estimation of potential health risks in Chinese herbal medicine. *J. Hazard. Mat.* 412, 125142. doi:10.1016/j.jhazmat.2021.125142

Yin, Z., Zhang, Y., Hu, N., Shi, Y., Li, T., and Zhao, Z. (2021). Differential responses of 23 maize cultivar seedlings to an arbuscular mycorrhizal fungus when grown in a metal-polluted soil. *Sci. Total Environ.* 789, 148015. doi:10.1016/j.scitotenv.2021.148015

Yu, Q., Gao, B., and Zhang, X. (2025). Agricultural wastes improve soil quality and enhance the phytoremediation efficiency of economic crops for heavy metal-contaminated soils in mining areas. *Environ. Geochem. Health.* 47, 65. doi:10.1007/s10653-025-02381-4

Yuan, Y., Wen, Q., Zhao, X., Liu, S., Zhu, K., and Hu, B. (2022). Identifying grassland distribution in a mountainous region in southwest China using multi-source remote sensing images. *Remote Sens.* 14 (6), 1472. doi:10.3390/rs14061472

Zhan, H. D., Zhou, H. Y., Sui, Y. P., Du, X. L., Wang, W. H., Dai, L., et al. (2016). The rhizome of *Gastrodia elata* Blume–An ethnopharmacological review. *J. Ethnopharmacol.* 189, 361–385. doi:10.1016/j.jep.2016.06.057

Zhang, A., Sun, H., and Wang, X. (2013). Recent advances in natural products from plants for treatment of liver diseases. *Eur. J. Med. Chem.* 63, 570–577. doi:10.1016/j.ejmech.2012.12.062

Zhang, J., Liu, Z., Tian, B., Li, J., Luo, J., Wang, X., et al. (2023). Assessment of soil heavy metal pollution in provinces of China based on different soil types: from normalization to soil quality criteria and ecological risk assessment. *J. Hazard. Mat.* 441, 129891. doi:10.1016/j.jhazmat.2022.129891

Zhang, L., Zhang, N. M., Zhang, Y. J., Deng, H., and Yang, H. Y. (2021a). Spatial distribution of selenium content in cultivated soil in Yunnan and its influencing factors. *Soil* 53 (3), 578–584. doi:10.13758/j.cnki.tr.2021.03.018

Zhang, M., Wang, C., Zhang, R., Chen, Y., Zhang, C., Heidi, H., et al. (2021b). Comparison of the guidelines on good agricultural and collection practices in herbal medicine of the european union, China, the WHO, and the United States of America. *Pharmacol. Res.* 167, 105533. doi:10.1016/j.phrs.2021.105533

Zhang, Y. L., Song, D., and Zheng, X. W. (2018). Determination of heavy metals and harmful elements in *Gastrodia elata* from different habitats by ICP-MS. *Electromech. Inf.* (14), 44–47. doi:10.19514/j.cnki.cn32-1628/tm.2018.14.009

Zhao, X. H., Xu, Y., Lin, J., and Xu, D. X. (2018). Evaluation and analysis of various metal elements in fresh *Gastrodia elata* in xiaocaoba. *J. Food Saf. Qual. Insp.* 9 (22), 5987–5992. doi:10.3969/j.issn.2095-0381.2018.22.032

Zhaotong Municipal People's Government (2023). *Bulletin of zhaotong municipal people's government*. Zhaotong: Zhaotong Municipal People's Government Office.

Zhong, X. L., Zhou, S. L., Zhu, Q., and Zhao, Q. G. (2011). Fraction distribution and bioavailability of soil heavy metals in the yangtze river Delta—A case study of kunshan city in Jiangsu Province, China. *J. Hazard. Mat.* 198, 13–21. doi:10.1016/j.jhazmat.2011.10.003

Zhu, H., Liu, C., Hou, J., Long, H., Wang, B., Guo, D. A., et al. (2019). *Gastrodia elata* blume polysaccharides: a review of their acquisition, analysis, modification, and pharmacological activities. *Molecules* 24 (13), 2436. doi:10.3390/molecules24132436

frontiers | Frontiers in Environmental Science

TYPE Systematic Review
PUBLISHED 29 August 2025
DOI 10.3389/fenvs.2025.1623566

OPEN ACCESS

EDITED BY
Nsikak U. Benson,
Topfaith University, Nigeria

REVIEWED BY
Jin Qian,
Northwestern Polytechnical University, China
V N Meena Devi,
Noorul Islam University, India

*CORRESPONDENCE
Yaoguang Guo,
ygguo@sspu.edu.cn
Quanfa Zhou,
zhouquanfa@163.com

RECEIVED 06 May 2025
ACCEPTED 11 August 2025
PUBLISHED 29 August 2025

CITATION
Chen Q, Zhu X, Guo Y and Zhou Q (2025) Research progress of micro-nano-bubbles in environmental remediation field.
Front. Environ. Sci. 13:1623566.
doi: 10.3389/fenvs.2025.1623566

Research progress of micro-nano-bubbles in environmental remediation field

Qin Chen, Xinjie Zhu, Yaoguang Guo* and Quanfa Zhou*

Shanghai Collaborative Innovation Centre for WEEE Recycling, School of Resources and Environmental Engineering, Shanghai Polytechnic University, Shanghai, China

Introduction: MNBs (MNBs), relying on its special chemical and physical properties, such as high surface potential, long stability and free radical generation capacity, have shown broad application prospects in environmental remediation.

Methods: Based on 508 related papers in the Web of Science database, this paper conducts a scientific knowledge mapping analysis using VOSviewer and CiteSpace software to reveal the research situation and trends. Researches show that MNB technology demonstrates remarkable effects in water pollution control (industrial wastewater, surface water, and groundwater) and soil pollution remediation.

Results and Discussion: For instance, ozone MNBs can increase the removal rate of plastic pollutants in industrial wastewater to 94.18% and enhance the degradation efficiency of polycyclic aromatic hydrocarbons through interfacial reactions. In soil remediation, their synergistic effect with surfactants can improve the petroleum pollutants' removal efficiency. From the perspective of research hotspots, the coupling of MNBs with advanced oxidation technologies (such as Fenton, plasma, and photocatalysis) has become the mainstream direction, significantly enhancing the degradation efficiency of pollutants through interfacial effects and radical generation mechanisms. The author collaboration network indicates that Chinese scholars have made outstanding contributions. The team led by Hu Liming from Tsinghua University has achieved fruitful results in groundwater remediation using ozone MNBs. However, the international cooperation network still needs to be strengthened. In terms of institutional collaboration, the Chinese Academy of Sciences (CAS) leads in both the volume of publications and academic influence, with its research covering multiple application areas such as semiconductor cleaning and membrane treatment. Keyword co-occurrence analysis divides the research topics into three major categories: degradation mechanisms, ozone MNB technology, and multi-technology coupling applications. Among them, "free radicals", "mass transfer", and "photocatalysis" are the core keywords. Although MNB technology has achieved phased progress, its long-term stability in complex environments, large-scale application costs, and cross-disciplinary collaborative mechanisms still need in-depth exploration.

KEYWORDS

MNBs, environmental remediation, ozone oxidation, photocatalysis, free radicals, multi-technology coupling

1 Introduction

With the acceleration of global urbanization and industrialization, environmental pollution issue is becoming increasingly severe, posing a serious threat to ecosystems and human health (Hoang et al., 2022; Wei et al., 2021). Among various pollution issues, water and soil pollution stand out prominently, making the search for efficient pollution control technologies an urgent matter. MNB technology, with its unique chemical and physical characteristics, has shown great environmental remediation potential and has become a research hotspot in recent years (Xiao et al., 2025; Haris et al., 2020; Xia et al., 2018; Xiao et al., 2019).

MNBs are bubbles with diameters at the micrometer and nanometer ranges. Compared with traditional macroscopic bubbles, they possess numerous superior characteristics, such as a high internal pressure, a large specific surface area, a longer residence time in liquids, and a high surface Zeta potential (Azuma et al., 2019; John et al., 2022; Loh et al., 2021; Temesgen et al., 2017). The large specific surface area of MNBs significantly increases the gas-liquid interface area, greatly enhancing various mass transfer efficiencies and rates (Xiao et al., 2022). Additionally, the surface of MNBs carries a charge, forming a double electric layer structure with a high interface potential. This property enables them to adsorb pollutants and promote their oxidative decomposition. Moreover, MNBs exhibit excellent stability in solutions and can persist for long periods due to their slow rising speed and charged surface. Some studies have shown that the existence time of oxygen MNBs (180–350 nm) can exceed 5 days, with the longest reaching 60 days (Zhou et al., 2021a), nitrogen MNBs (200–300 nm) can remain stable for a month (Ulatowski et al., 2019), and the existence time of air nano bubbles exceeds 3 months (Michailidi et al., 2020). When MNBs dissolve under pressure, they generate free radicals with strong oxidation capabilities, effectively degrading many refractory organic pollutants and enhancing the removal effect of pollutants (Li et al., 2009).

In the field of environmental remediation, MNB technology demonstrates broad application potential. In water pollution control, whether it is industrial wastewater, surface water, or groundwater pollution, this technology can play a significant role. For industrial wastewater, MNB ozonation can significantly increase the oxidation rate of ozone and effectively degrade organic pollutants (Kim et al., 2022; Zhang et al., 2018), with a removal rate of plastic reaching 94.18% (Masry et al., 2021). In surface water purification, MNBs can perform multiple functions such as aeration mass transfer, air flotation, advanced oxidation, and sterilization and disinfection, effectively removing suspended degrading organic and solids pollutants from water (Wang et al., 2024a). For groundwater pollution, MNBs can carry oxidants into the aquifer to achieve *in-situ* remediation (Chen and Chang, 2022; Shen et al., 2024).

In soil pollution remediation, MNBs also have significant application value. They can serve as carriers to transport oxygen and nutrients into the soil, enhancing the degradation ability of microorganisms towards organic pollutants (Kwon et al., 2020; Pa et al., 2009). Additionally, MNBs can improve the treatment effect on petroleum-contaminated soil and oil sludge by synergistically acting with surfactants, increasing the removal efficiency of petroleum pollutants (Chen et al., 2018; Ji et al., 2018; Sun et al., 2020a).

In summary, MNB technology holds broad application prospects in environmental remediation, but further in-depth research and improvement are still needed. This study utilized software like CiteSpace and VOSviewer to conduct a comprehensive analysis of relevant literature and create a scientific knowledge graph, including source journals, keywords, hotspots, publication trends, research frontiers, author contributions and collaborations, *etc.* The analysis identified and tracked the research frontiers and hotspots in this field, identified scientific hotspots, research topics and their dynamic evolution, and paid attention to existing and emerging research topics and trends. By understanding the current research hotspots and challenges in the technology, it is expected to promote its large-scale practical application and provide effective technical support for solving global environmental pollution problems.

2 Data sources and research methods

2.1 Data source

Web of Science is a globally renowned comprehensive academic information resource database, covering numerous disciplines. The literature it includes has high academic influence and wide representativeness, effectively reflecting the cutting-edge trends and development directions of international academic research. This article conducts a bibliometric analysis using Web of Science as the data source. In the advanced search interface of Web of Science, the search conditions are set as: the subject contains “Micro nano bubble”, “nano bubble”, and “micro bubble”, and on the basis of the above search results, further search for literature with the full text containing “degradation”. The search mode is set to exact match, and the search time range is from the establishment of the database to 1 April 2025. After the search, a total of 509 articles related to the management of hazardous waste in small and micro enterprises were obtained. After duplicate removal using Note Express software, 508 articles were finally obtained for subsequent in-depth analysis. The search scope is set as “subject” (TS): TS = [“Micro nano bubble” or “nano bubble” or “micro bubble” AND TS = (“degradation”)]. The specific screening items are shown in Table 1, excluding irrelevant research topics and directions such as “endocrinology and metabolism” and “agriculture”, while Table 1 presents the final data results.

2.2 Research methods

Compared with traditional bibliometric methods, visualization methods can more intuitively present citation information of literature and its inherent hierarchical structure, facilitating in-depth exploration of interaction relationships in complex networks. This paper, by means of the scientific knowledge mapping method, uses CiteSpace and VOSviewer software to conduct trend analysis of publications, research institutions, scholars, and keyword co-occurrence analysis based on the obtained 508 related literature data, and draw corresponding knowledge maps, thereby comprehensively and intuitively presenting the research situation in this field.

TABLE 1 Article selection situation and outputs.

Filter condition	Language	Document types	Time interval
	English	Article and review	No requirement—2025.04.01

Result	Papers	Countries	Institutions	Journals	Author
	508	211	5012	442	9213

TABLE 2 Top 20 authors in the field of MNBs.

Authors	Volume of publications	Citations	Country
Hu Liming	**10**	245	China
Fan Wei	8	214	China
Ma Xing	7	297	China
Wang Yong	5	279	China
Li Jia	5	87	China
Zheng Chan	5	86	China
Pumera Martin	4	**362**	Czech Republic
Wang Joseph	4	347	The United States
Sun Hongqi	4	183	China
Wang Shaobin	4	183	China
Moholkar Vijyanand s	4	176	The United States
Huo Mingxin	4	158	China
Zuo Min	4	46	China
Wang Sheng	4	32	China
Duan Yalong	4	28	China
Yu Jiang	4	28	China
Lan Ziwei	4	17	China
Xu Dandan	3	208	China
Villa Katherine	3	208	Czech Republic
Yuan Hao	3	167	China

The bolded parts of the numbers indicate the authors with the highest number of published articles or the highest number of citations for their articles.

3 Basic article information architecture

3.1 Author information

Authors and their collaborations within a certain research field are key factors in promoting academic progress and spreading knowledge. Bibliometric analysis can identify authors who have contributed to a specific research field and their collaboration patterns. Table 2 shows the top 20 authors who have published the most papers in photocatalytic oxidation of volatile organic compounds (VOCs). There are 16 authors from China, demonstrating China's outstanding contributions to this field. Hu Liming from Tsinghua University has published the most papers, with a total of 10. His most influential paper studied the characteristics of ozone MNBs, including their bubble number, size distribution, and zeta potential. The experiment investigated the ozone MNBs' mass transfer rate. They used ozone MNBs to deal with water contaminated with organic matter, which showed significant purification efficiency. They also conducted the column tests to research the efficiency of ozone MNBs in the remediation of groundwater contaminated with organic matter. Field monitoring was carried out on a site contaminated with trichloroethylene (TCE). The results indicated that ozone MNBs could significantly enhance the remediation efficiency and are an innovative *in-situ* remediation technology of groundwater contaminated with organic matter (Hu and Xia, 2018). His team mainly focuses on the ozone MNB technology application in groundwater pollution treatment, confirming the groundwater pH influence and salinity on the treatment capacity of the technology (Xia and Hu, 2019; Li et al., 2013). They believe that ozone MNBs have great oxidation capacity and low secondary

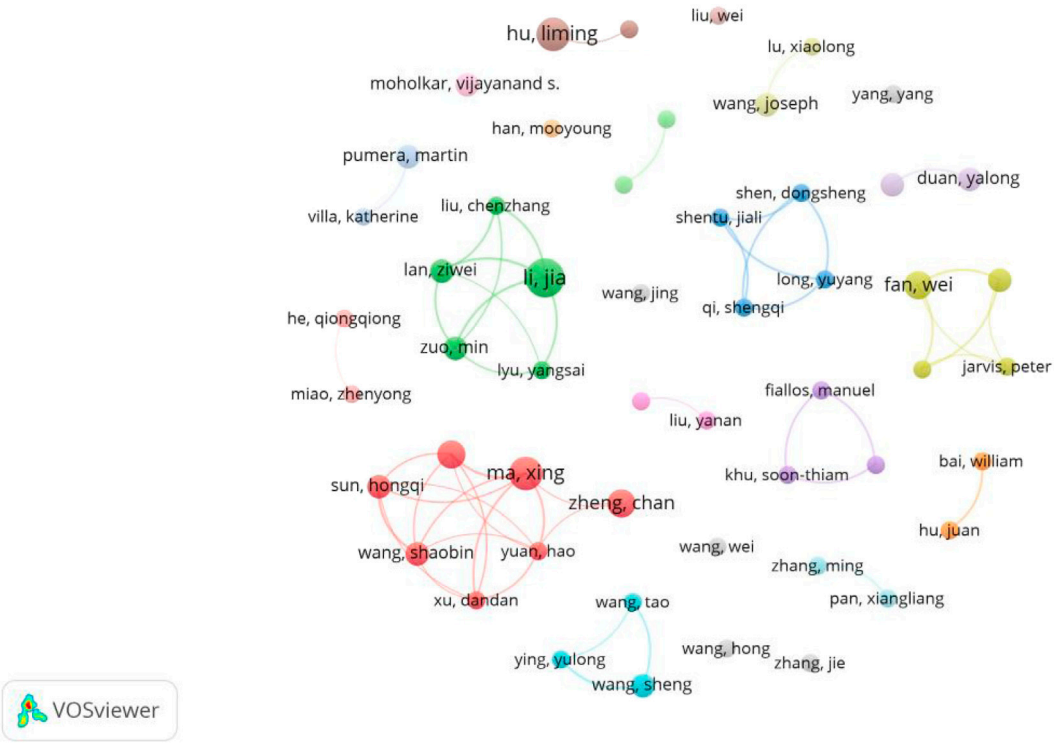

FIGURE 1
Network of author collaboration.

pollution (Cao et al., 2023), and possess the ability to transport and dissolve in porous media (Li et al., 2014), making it a promising *in-situ* remediation technology of groundwater contaminated with organic matter. Fan Wei from Jiangnan University ranks second with eight papers. The representative research direction of this author with the second-highest influence integrates MNB and photocatalytic technology. They found that the MNBs' interfacial photoelectric effect was also proved to be beneficial for pollutant degradation. MNBs guided strong light scattering, increasing 54.8% of the light path length in the photocatalytic medium at 700 nm and strengthening the photocatalyst light adsorption (Fan et al., 2021; Fan et al., 2019).

The author collaboration distribution map can well reflect the cooperation and joint research in environmental industrial pollution treatment using MNB technology (Figure 1). Each node's size in the figure represents the paper number published by the author (the larger node means that the author has published more papers), while the connecting lines represent the authors' collaboration. Figure 1 shows the degree of author collaboration, with several closely collaborating author groups emerging, including the teams of Ma Xing and Zheng Chan, as well as Li Jia and Lan Ziwei. Unlike the author with the highest volume of publications, their main research direction is nanomotors (Ma et al., 2016; Ye et al., 2021; Yang et al., 2023a). The closeness of the connections between different authors is shown in the figure, meaning that the international cooperation intensity in this field still needs to be strengthened. Analyzing the collaboration level among researchers is important because such collaboration not only helps to collect expertise from different disciplines, promoting innovation and progress, but also improves the reliability, quality and efficiency of research through peer review, knowledge transfer and resource sharing, *etc.* Moreover, collaboration can promote the scientific research internationalization, help solve complicated interdisciplinary problems, and accelerate the transformation of research outcomes into practical applications, especially in the fields of pollution control and environmental protection.

3.2 Information graphic of the issuing institution

Research institution analysis provides information on the most influential and productive research institutions in a certain research field, which could make scholars well understand the current situation and field trends, and guide how to solve important problems and promote innovation. Figure 2 shows the knowledge domain of collaborative organizations using the software VOSviewer. Every circular node represents an organization, and the circle size indicates the published paper number. Inter-institutional collaboration is represented by a line between two nodes, with the thickness of the line indicating the degree of collaboration. The CAS occupies the highest ranking and has published the most papers in Table 3, which has a critical academic influence. In its latest research, it reviewed the benefits of MNB in the cleaning process, then analyzed in depth the factors affecting its cleaning effect and the possible mechanisms involved. Additionally, it summarized the production and application of MNB in various cleaning scenarios and elaborated on its applications in semiconductor cleaning (Takahashi et al., 2015), membrane cleaning (Lee et al., 2015) and metal cleaning (Ulatowski

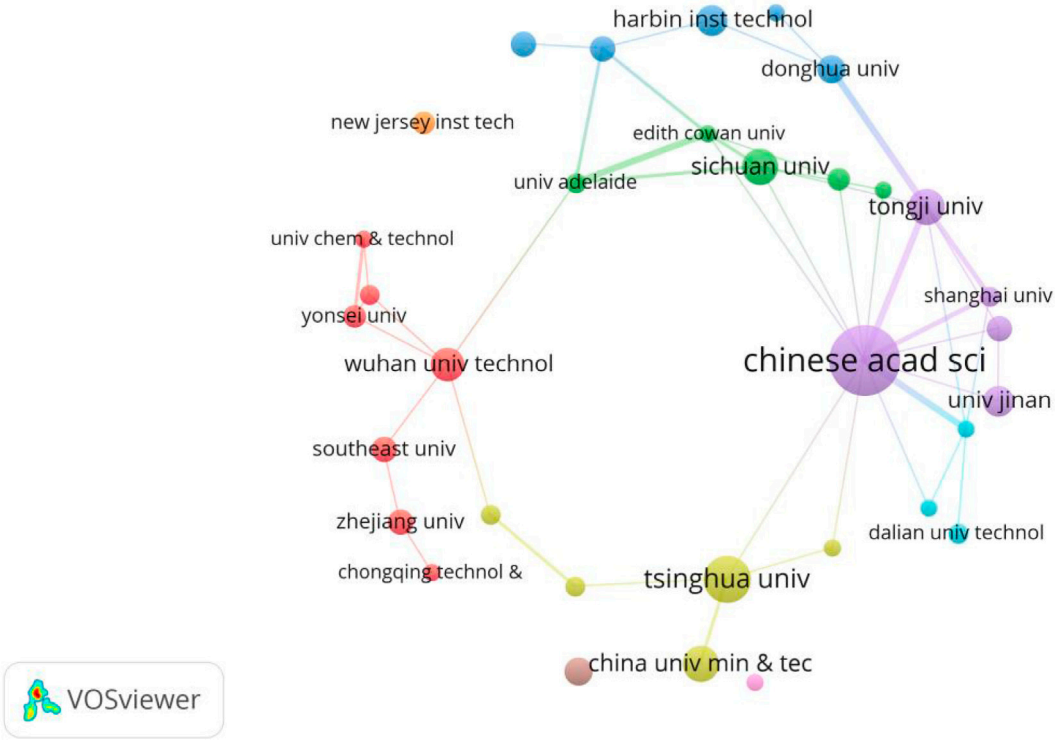

FIGURE 2
Institutional collaboration mapping.

et al., 2024). In its latest research, it was found that the MNB technology enhanced the vacuum ultraviolet degradation rate by improving the mixing and mass transfer within the solution, optimizing the light performance in the solution, and increasing the dissolved oxygen level (El Aswar et al., 2025). Moreover, as shown in Figure 2, the CAS, Shanghai University, and Tongji University have relatively close cooperative relationships. Their works mainly focus on the application of MNB technology in treating polycyclic aromatic hydrocarbon pollution in groundwater, where the technology can enhance the surfactants transfer and thus improving the degradation capacity (Dai et al., 2023; Han et al., 2025).

3.3 Journal information

Journals in a research field help researchers understand the main academic resources and knowledge dissemination channels. The h-index is a hybrid quantitative indicator which could be used to evaluate the academic output quantity and quality. It was proposed by George Hirsch, a physicist at the University of California, San Diego, in 2005. As it can be seen in Table 4, the analysis of the journals has identified the top ten publications with the highest citation counts in the field of MNB technology for environmental pollution degradation. Chemical Engineering Journal is the journal with the highest number of articles published in this field, with 21 articles, and it is also the publication with the highest citation count, indicating its importance in the field. Next are Separation and Purification Technology and Ultrasonics Sonochemistry, which have published 18 and 13 articles respectively. Additionally, although ACS Nano has only published seven research papers on MNBs, its citation count ranks second, suggesting that this publication is highly trusted by readers in the field and the articles published in it have significant influence within the field.

The different colored areas in the Figure 3 represent the different research preferences of various publications on the article's research direction. The publications in the red area led by Ultrasonics Sonochemistry mainly focus on the generation mechanism and methods of MNBs. Ultrasonics Sonochemistry mainly uses ultrasound to generate MNBs for water pollution treatment, with two main approaches: activating intermediate substances [such as quantum dots (Entezari and Ghows, 2011), nanomaterials (Bao et al., 2023), *etc.*] to enhance their oxidation capacity and enhancing the generation of free radicals through sonochemistry (Pétrier et al., 2010), to strengthen the effect of wastewater treatment. The publications in the yellow area led by Separation and purification technology mainly focus on the technology of using MNBs to clean dirt. This journal mainly studies the use of MNB technology to clean filter membranes, solve the problem of membrane fouling, thereby improving the stability of the membrane and enhancing the degradation capacity of water treatment (Duan et al., 2025; Duan et al., 2022; Mo et al., 2024). The publications in the green area led by Acs nano mainly focus on the R&D of water treatment materials and equipment. This journal mainly studies the nanoscale micro-motors application in water pollution treatment (Villa et al., 2018; Zhang et al., 2024; Soler et al., 2013). The publications in the blue area led by Chemical engineering journal have a relatively comprehensive research direction, covering various aspects of MNB technology.

TABLE 3 Top 20 organizations in the field of MNBs.

Organization	Volume of publications	Citations	Country
Chinese Acad Sci	19	649	China
Tsinghua Univ	14	328	China
China Univ Min and Technol	12	195	China
Sichuan Univ	11	132	China
Wuhan Univ Technol	9	305	China
Harbin Inst Technol	9	262	China
UnivJinan	9	121	China
Seoul Natl Univ	9	187	Republic of Korea
Harbin Inst Technol Shenzhen	7	309	China
Tianjin Univ	7	66	China
Zhejiang Univ	7	285	China
Beijing Univ Chem Technol	7	192	China
Univ Adelaide	6	402	Australia
Chongqing Technol and Business Univ	6	72	China
Xi'an Jiao Tong Univ	5	221	China
Univ Calif San Diego	5	390	The United States
Northeast Normal Univ	5	214	China
Edith Cowan Univ	4	183	Australia
Jiangsu Univ	4	116	China
Nanjing Tech Univ	4	162	China

TABLE 4 Top 10 most co-cited papers in the field of MNBs.

Source journal	Volume of publications	Citations	IF①	CPP②
Chemical Engineering Journal	21	896	13.4	43
ACS Nano	7	834	15.8	120
Ultrasonics Sonochemistry	13	585	8.7	45
Separation and Purification Technology	18	516	8.1	29
Journal of Hazardous Materials	9	476	12.2	53
Water Research	12	311	11.4	26
ACS Applied Materials and Interfaces	6	278	8.3	47
Nano Energy	4	269	16.8	68
Chemosphere	7	264	8.8	38
Small	4	250	13.3	63

① 2024 impact factor; ② Citations per paper (the number of citations per paper on average).

4 The development of MNB technology

4.1 Trend of annual publications

By conducting a statistical analysis of the published paper number from 1995 to 2025, the status, maturity and development trend of MNB technology research achievements can be clearly shown. Figure 4 presents the research result distribution on MNB technology in environmental treatment based on the time series. From 1995 to 2007, less than five articles on MNB technology were published each year. From 2008 to 2017, this field showed a overall slow growth trend, and the annual publication volume in this field

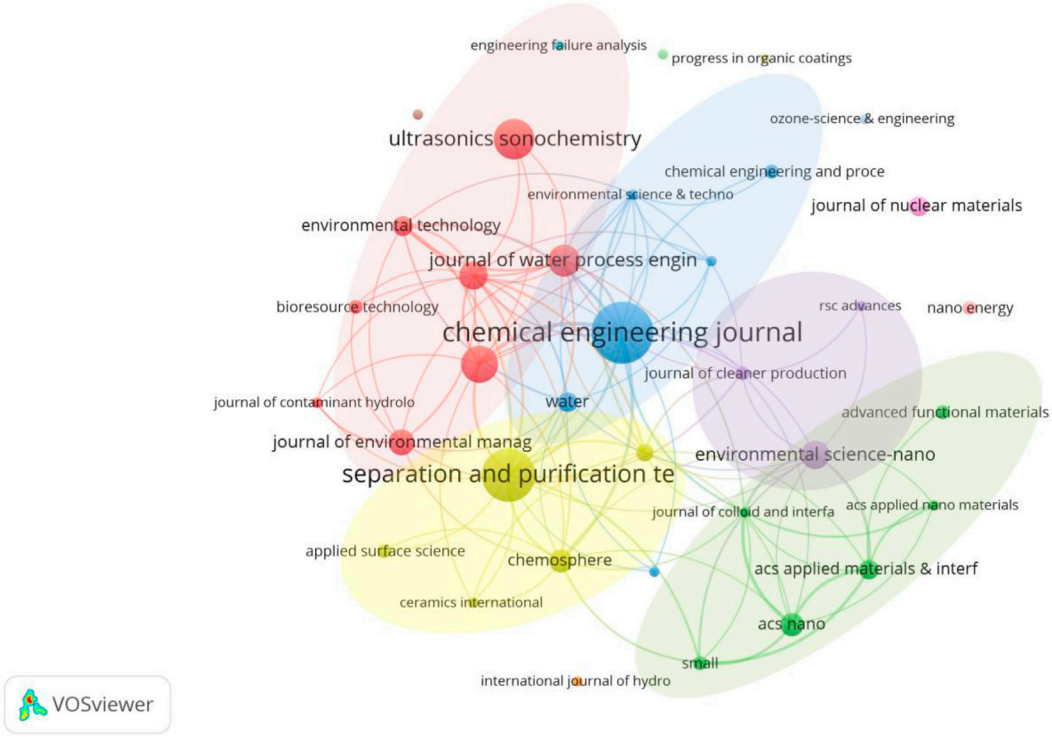

FIGURE 3
Graphic representation of the knowledge domains of journal co-citations in the field.

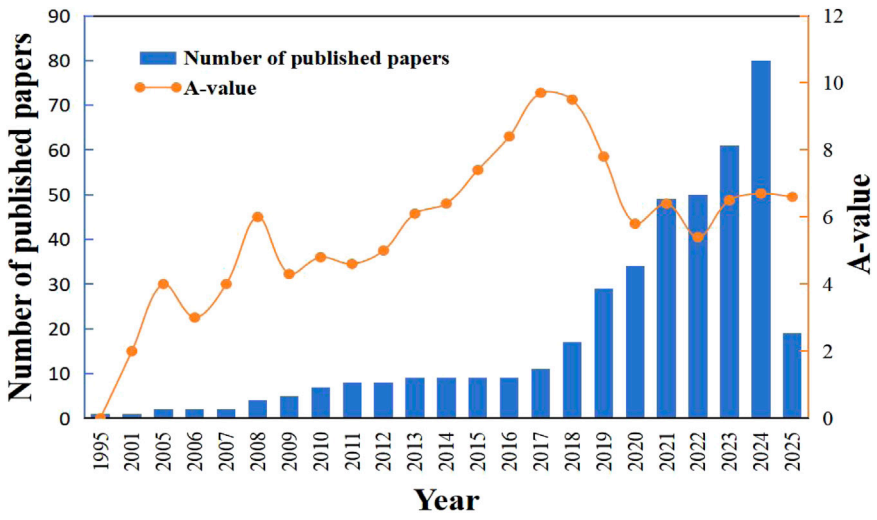

FIGURE 4
Annual and cumulative volume of publications.

exceeded 10 for the first time in 2017. After that, research related to MNB technology gradually became a hot topic, which is inseparable from the pollution control and environmental protection policies of many countries as well as major technological breakthroughs. From 2017 to 2024, the published paper number increased significantly, with an annual publication volume of over 50 for five consecutive years, and the publication volume reached 80 in 2024. As of 2025, 508 papers have been published in VOCs photocatalytic oxidation research. The continuous increase in the number of papers in this field indicates that researchers have paid more attention to the application of MNB technology in environmental pollution degradation.

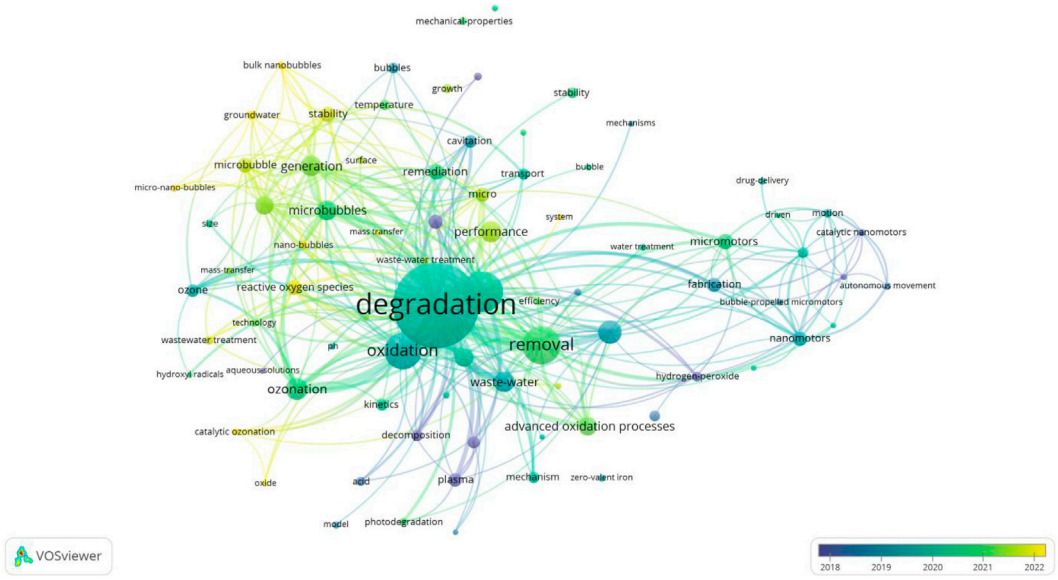

FIGURE 5
Research technology trends over the years.

4.2 Research technology trends over the years

Based on the timeline (Figure 5), the development process of MNB technology has been sorted out, covering its key progress from the theoretical assumption to the exploration of applications in multiple fields such as water treatment and disinfection, demonstrating the continuous expansion of its application boundaries and the deepening of research. In the theoretical assumption stage, Parker et al. first hypothesized the MNBs existence in 1994, laying the theoretical foundation for subsequent related research and opening the door to the study of this special type of bubble (Parker et al., 1994). During the early application exploration period of MNB technology (1999–2007), Ishida et al. imaged bulk MNBs using atomic force microscopy (AFM), providing a direct understanding of the physical morphology of MNBs (Ishida et al., 2000). Chu et al. reported the application of ozone MNBs in dye removal and water disinfection, expanding the application ideas of MNBs in water treatment (Chu et al., 2007).

From 2009 to 2018, it was the development period of MNB technology. Tasaki et al. studied the degradation effect of MNBs under ultraviolet (UV) irradiation on methyl orange, exploring the water treatment technology of light-MNB synergy (Utaka et al., 2009). In 2011, the first review on the application of MNB technology in water treatment was conducted, systematically summarizing the application achievements and prospects of this technology in water treatment at that time. In 2016, Agarwal et al. reviewed the history of MNBs, retrospectively summarizing its development trajectory from a more macroscopic perspective (Agarwal et al., 2016).

As shown in the figure, it is the time distribution map of key words related to MNB technology. During the explosive period after 2018, due to its excellent mass transfer ability and the ability to produce active oxidative species, MNB technology was coupled with different environmental pollution degradation technologies and applied in multiple fields. There were studies on the degradation of aniline using non-thermal plasma/MNBs, further enriching the technical means of MNBs in the treatment of refractory organic pollutants. In 2019, Fenton/MNBs were used for dye separation and microplasma bubbles for inactivating microorganisms, exploring new directions for the combination of MNBs with other technologies. MNBs were used to enhance the degradation of oxytetracycline under visible light, broadening the application scope of MNBs in the field of photocatalytic degradation. In 2021, it was found that MNBs could promote the photocatalytic disinfection of microbial spores, and the stability of oxygen-containing MNBs in fresh water was confirmed, providing new evidence for their application in the disinfection field. In 2022, the exploration of ultraviolet C (UV-C)/hydrogen peroxide (H_2O_2)/MNBs as a new disinfection technology further explored the potential of MNBs in disinfection technology innovation.

From 2023 to 2025, the development of MNB technology has been rapid, and research has delved deeper. The focus of research on the applicability of MNB technology has mainly been on exploring the coupling effect of MNBs with other technologies. In previous studies, it was found that MNBs can effectively enhance gas mass transfer and the production of active species. Scholars have thus focused on the coupling effect between MNBs and various oxidants, using the strong oxidation effect of MNBs to activate different oxidants (such as persulfate, ferrous ions, and nano zero-valent iron) and treat complex pollutants in different media, continuously expanding the application scope of MNB technology. Jing et al. utilized MNBs to enhance the immobilized Chlorella technology. Thanks to the excellent mass

TABLE 5 Research on MNB technology in various application scenarios over the past 2 years.

Types of MNBs	Coupling technology	Target pollutants	Treatment effect	The main active species	References
Air	Advanced oxidation; Thermal-activated persulfate	Rhodamine B	Removal rate: 94.53%	·OH, SO_4^-	Yang et al. (2023b)
Air	Advanced oxidation; Fe(II) and persulfate	Atrazine and its membrane fouling	Effectively reduce by 72%	·OH, SO_4^-,$^1O_2$	Zhang et al. (2025)
Air	Advanced oxidation; Ferrous oxalate complex	4,4′-Sulfonyldiphenol (BPS)	The removal efficiency of BPS is increased by approximately 35%		Li et al. (2025a)
Air	Advanced oxidation; Persulfate	Printing and dyeing wastewater	The water quality meets the discharge standards		Yang et al. (2023c)
Air	Advanced oxidation; Sodium hypochlorite	Norfloxacin	The water quality meets the discharge standards		Li et al. (2024)
Air	Advanced oxidation; Cobalt-iron catalyst and persulfate	Tetracycline	The degradation efficiency is 95.63%	·OH, SO_4^-,$^1O_2$	Ye et al. (2025)
Air	Vacuum ultraviolet photocatalysis	Sulfamethazine	The degradation rate increased by two times after the addition of MNBs	·OH	El Aswar et al. (2025)
Air	photocatalysis; AC/TiO2	Indigo carmine, reactive black 5 and methylene blue	The degradation rates were 69.09%, 60.06% and 55.19% respectively		Boonwan et al. (2024)
Ozone	Advanced oxidation	Sulfadiazine	The reaction rate constant is 5.5 times that of conventional oxidation technology	·OH, $\cdot O_2^-$	Liu et al. (2025)
Ozone	Advanced oxidation; H_2O_2	Ibuprofen	Except for an efficiency of 94.75%	·OH	Li et al. (2025b)
Ozone	Advanced oxidation	2-Methylisoborneol and geosmin	Within 15 min, 94.38% of 2-MIB and 95.45% of GSM were removed	$\cdot O_2^-$	Ren et al. (2025)
Ozone	Advanced oxidation	Tetracycline	Degradation efficiency: 85%	Reactive oxygen species (ROS)	Zhao et al. (2024b)
Ozone	Micro-nano cavitation technology	Gaseous acetate ester	155.544 mg/m^3 degraded within 21.961 min	High temperature and high pressure caused by cavitation collapse	Wang et al. (2024b)

transfer capacity of MNBs, the biomass of Chlorella increased by 2.48 times, significantly improving the removal efficiency of ofloxacin (Jing et al., 2025). Chi et al. studied the degradation of tetracycline, a commonly used antibiotic in wastewater, using a system based on zero-valent nano-iron assisted by MNBs. MNBs can serve as an ideal carrier for zero-valent nano-iron. When they burst, they generate shock waves and highly reactive substances (such as •OH), which can significantly enhance the degradation efficiency (Chi et al., 2024). Table 5 presents a portion of the relevant research on MNB technology in various application scenarios over the past 2 years.

Meanwhile, due to the mature development of ozone MNB technology, in recent studies, scholars no longer confine their research to the laboratory and have conducted many practical application studies, mainly exploring the influence of factors such as air intake rate, air intake volume, and pollutant concentration (Hu et al., 2023; Zhao et al., 2024a). Ponce-Robles et al. actively promoted the practical application of MNB technology. By adjusting the size of ozone MNBs, the air intake volume, and the air intake rate, they conducted experiments in large-scale pharmaceutical wastewater. They replaced the traditional tertiary sewage treatment equipment with ozone MNB technology, which enhanced the treatment capacity and reduced costs (Ponce-Robles et al., 2023).

5 Analysis of hotspots in MNB technology

5.1 Keyword clustering analysis

In the keyword spectrum diagram, VOSviewer has classified the keywords. Co-occurrence analysis of keywords helps to understand the basic themes and concepts in the literature or dataset. It assists researchers in positioning their research, decision-making, and collaboration to achieve a more comprehensive understanding of the challenges and opportunities in a specific field or topic. As shown in Figure 6, the keywords in the MNB field are divided into five categories. The three main categories are the red area led by “degradation”, which mainly focuses on the application of MNB technology to assist other different treatment technologies, such as non-thermal plasma bubbles, advanced oxidation, photocatalysis, *etc.*, and ultimately focuses on the degradation effect of pollutants. The second category is the pink area, mainly summarizing the development of ozone MNB technology. The combination of ozone and MNB technology is the most developed technology. Between these two areas is the purple area, mainly summarizing the core keywords of MNB technology, “oxides” and “reactive oxygen species”. Next, we will further analyze the three key categories.

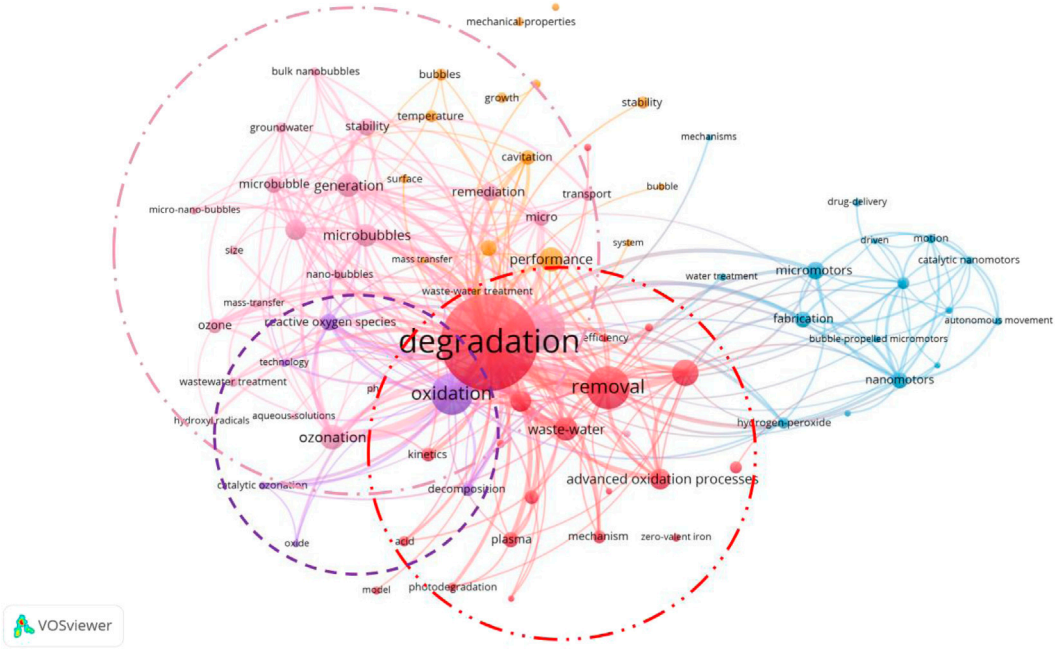

FIGURE 6
Keyword clustering information analysis chart.

5.2 The principle of MNB technology

First, let's discuss the purple area section (Figure 6), which outlines the core principle of MNB technology. Now, two representative views explains the generation of reactive oxygen species (ROS) during MNB oxidation: one is the view of interface ion accumulation during the MNB contraction process (Takahashi et al., 2007a; Yang et al., 2023d). As MNBs contract, the surface Zeta potential increases with the increase in the contraction rate, which is inversely proportional to the bubble size. This indicates that the surface charge migration rate is insufficient to counteract the increase in the MNB contraction rate, leading to the accumulation of charges at the gas-liquid interface and the formation of a high chemical potential (Takahashi et al., 2015). According to this theory, under a wide range of pH conditions, MNBs carry a negative charge. Therefore, during the bubble contraction process, OH^- is more easily adsorbed onto the bubble surface than H^+, resulting in an interface environment with high ion concentration and a double-layer structure (Takahashi et al., 2007b). When ozone gas diffuses and dissolves into the liquid phase within MNBs, the high concentration of OH^- at the interface triggers the ozone self-decomposition chain reaction, leading to the generation of ·OH (Cheng et al., 2018; Khuntia et al., 2012; Cheng et al., 2019). This theory is applicable to ozone MNBs. Since ozone itself is a highly reactive oxidizing species, when ozone gas diffuses and dissolves into the liquid phase within MBs, the high concentration of OH^- at the interface triggers the ozone self-decomposition chain reaction, leading to the generation of •OH (Cheng et al., 2018; Khuntia et al., 2012; Cheng et al., 2019). During the accumulation of air and oxygen MNBs at the bubble interface, the reaction between oxygen and OH^- is slow and inefficient, and thus cannot generate a large amount of reactive oxygen free radicals. Zhao et al. revealed the main free radicals produced and the pathways of ozone generating free radicals (Equations 1–4) when using ozone MNB technology to treat tetracycline wastewater, verifying the working mechanism of ozone MNBs (Zhao et al., 2024b).

$$2O_3 \rightarrow 1O_2 + 2O_2 \quad (1)$$

$$O_3 + OH^{2-} \rightarrow \cdot OH + \cdot O_2^- + O_2 \quad (2)$$

$$O_3\cdot^- \rightarrow O\cdot^- + O_2 \quad (3)$$

$$O\cdot^- + H_2O \rightarrow \cdot OH + OH^- \quad (4)$$

The other view is the adiabatic compression during the MNB collapse process (Shi et al., 2021; Yasui et al., 2016; Zhou et al., 2020). As MNBs contract, the reduction in volume increases the internal gas pressure. Before reaching the critical collapse state, MNBs typically withstand an internal pressure of 0.83–1.65 MPa, which is over 50 times the atmospheric pressure (Yasui et al., 2019). At this point, ozone molecules remain in a dense state, colliding more frequently in a smaller space, resulting in a higher energy state. Simultaneously, the MNB wall contraction speed reaches 90 m/s, raising the critical temperature inside the bubble to 3,000 K and the temperature of the liquid near the bubble to 360 K. Although these extreme conditions of high temperature and pressure only last for approximately 19 picoseconds, a quasi-adiabatic compression effect is formed at the MNB interface, which is sufficient to trigger the thermal decomposition of gas molecules, thereby leading to the generation of free radicals. The applicability of this theory is not only limited to ozone MNBs, but also applies to MNBs composed of oxygen and air. Although the free radical yield of oxygen is far less than that of ozone, with the support of adiabatic compression theory, it can be coupled with different types of other technologies (such as advanced oxidation, photocatalysis, *etc.*) to

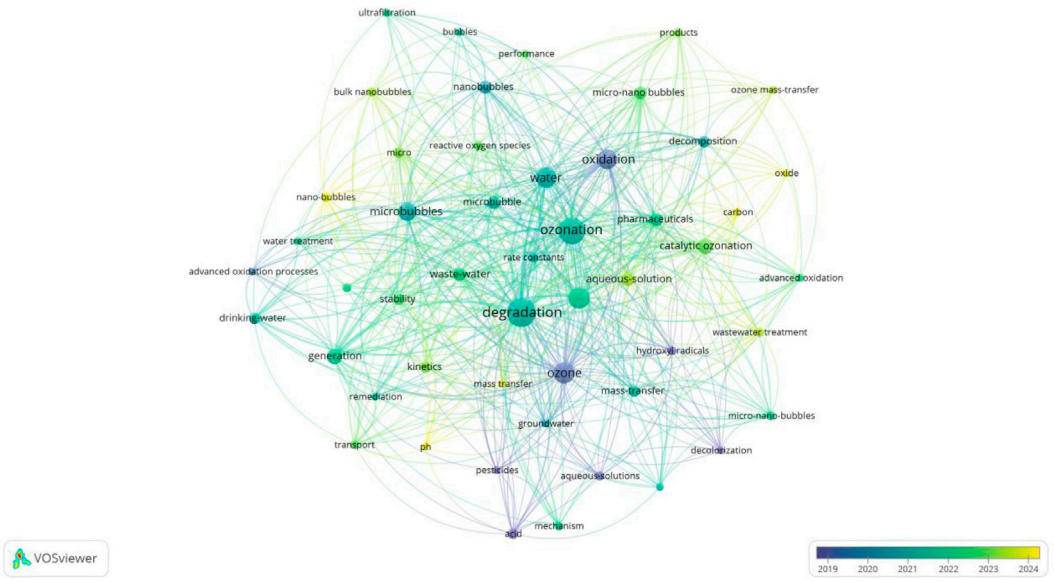

FIGURE 7
The application of MNB technology in ozone oxidation technology.

enhance the oxidation capacity and assist other water treatment technologies. Considering the cost, oxygen MNBs are cheaper than ozone MNBs and more suitable for coupling with other technologies. Li et al. found in the experiment of using divalent iron to catalyze the treatment of 4,4′-sulfonyl diphenol (BPS) that the degradation efficiency of pollutants increased by 35% after the addition of MNBs for co-treatment (Li et al., 2025a). El Aswad et al. utilized MNBs to assist in the ultraviolet photocatalytic degradation of sulfamethazine in water, doubling the degradation efficiency (El Aswar et al., 2025). During the treatment process, the presence of hydroxyl radicals was detected using pCBA, CCl_4, and MDE probe compounds to identify •OH, $•O_2^-$, and $^1O_2$ respectively. The discovery of hydroxyl radicals indicates that the energy and free radicals generated during the collapse of MNBs are conducive to the oxidative degradation of water pollution. This inexpensive and simple bubble technology is expected to become an auxiliary means to enhance existing environmental pollution treatment technologies and engineering.

5.3 Ozone MNB technology

5.3.1 The principle of ozone MNB technology

The pink area (Figure 6) mainly focuses on the research of ozone MNB technology. By adding ozone as a search term and connecting it with "and" in the search formula, the keyword distribution map as shown in Figure 7 is obtained. The appearance of "Oxide" in the figure indicates that ozone is a strong oxidant with a high oxidation-reduction potential of 2.07 V, which can rapidly oxidize various organic and inorganic pollutants and convert them into harmless or low-harm substances. However, in traditional ozone water treatment technology, due to the low solubility of ozone in water and its easy decomposition, its utilization rate is not high (≤10 mg L^{-1}) and it is only suitable for water treatment under neutral pH and room temperature conditions (Khan and Carroll, 2020; Levanov et al., 2017). Therefore, a higher O_3 addition amount greatly increases the cost of gas preparation. The emergence of MNBs technology provides a new way to improve the utilization efficiency of ozone. Keywords such as "Mass transfer", "Stay time", and "ROS" imply the advantages of ozone MNBs. After ozone is integrated into the MNB system, the special properties of MNBs can effectively improve the dissolution and dispersion state of ozone in water, extend its residence time in water, significantly increase the contact probability and reaction efficiency between ozone and pollutants, and thereby enhance the removal ability of pollutants. The high stability in aqueous solutions and efficient mass transfer coefficient can overcome the problems of low solubility, short half-life, and low mass transfer coefficient of conventional O_3 (Deng et al., 2021; Seridou and Kalogerakis, 2021). The ozone oxidation assisted by MNBs includes three main steps: (i) generating O_3 by sequentially guiding gaseous oxygen through a traditional ozone generator and an MNBs generator to produce MNBs; (ii) transferring O_3 from MNBs to water molecules; (iii) using dissolved O_3 to target pollutants and generate ROS.

5.3.2 Control factors of ozone MNB technology

The characteristics of ozone microbubbles (MBs), such as small size and long residence time, can promote the decomposition of ozone and gas-liquid mass transfer, thereby enhancing the removal effect of refractory organic compounds. Therefore, any parameters that affect the characteristics of MBs, such as bubble size, stability, mass transfer efficiency, and interfacial environment, will indirectly affect the treatment efficiency.

First, within a certain temperature range, the influence of temperature on the removal rate of pollutants is not significant. In the experiments of phenol and TOC removal, the temperature change has a negligible effect on the degradation rate, as the positive

and negative effects cancel each other out (Cheng et al., 2021; Mohite and Garg, 2017). Rising temperature will reduce the solubility of ozone in water, accelerate the escape of ozone, and lower the gas-liquid mass transfer rate. At the same time, it will decrease the mechanical strength of the bubble walls of MBs, making them more prone to rupture and accelerating the release of ozone. The temperature increase will significantly enhance the ozone oxidation rate (in line with the Van't Hoff equation, for every 10 °C increase in temperature, the reaction rate approximately doubles). Therefore, the optimal temperature should be determined based on the actual situation.

The influence of gas-liquid ratio on MNBs shows a phased pattern. Increasing the gas-liquid ratio enhances the air flow rate and the number of MBs, strengthens gas-liquid mass transfer, raises the dissolved ozone concentration, accelerates the oxidation process, and significantly boosts the degradation rate in the PhOH degradation experiment. When the gas flow rate exceeds the critical point, the increase in degradation rate and mass transfer efficiency slows down as the mass transfer flux has exceeded the reaction demand. Excessively high gas-liquid ratios may also lead to an increase in bubble size and a decrease in specific surface area, which in turn reduces mass transfer efficiency. The ozone MBs process can enhance mass transfer efficiency through small bubbles and long residence time at a low gas-liquid ratio. Therefore, in practical applications, the gas-liquid ratio and bubble size need to be optimized to maximize the effect.

Surface tension mainly affects the size and stability of MBs. The lower the surface tension of the solution, the easier it is to generate small-diameter MBs. The average diameter of MBs generated by sodium dodecyl sulfate (SDS) with a surface tension of 29.5 mN/m is 13.3 μm, which is significantly smaller than that in high surface tension systems, and small bubbles are usually beneficial for mass transfer (Melich et al., 2019). Surfactants can slow down the contraction, coalescence and rupture of bubbles, prolong the lifespan of MBs and enhance the stability of the interface, but they may reduce the mass transfer rate at the gas-liquid interface.

Finally, pH significantly alters the removal efficiency by influencing ozone decomposition, free radical generation, and the ionization state of organic compounds. A high pH promotes the self-decomposition of ozone and accelerates the generation of ·OH radicals, thereby enhancing the degradation rate of refractory organic compounds. The degradation rate constant of PhOH at pH 11 is 2.7 times that at pH 3 (Lim et al., 2022).

5.3.3 The application of ozone MNB technology

Ozone MNB technology has unique advantages in water treatment, being capable of removing organic pollutants in water and inhibiting the growth of microorganisms, ensuring the chemical and biological safety of drinking water. This technology oxidizes organic pollutants through the generation of ·OH, converting them into harmless substances, while also destroying the cell structure of microorganisms to achieve disinfection and sterilization. Compared with traditional drinking water treatment technologies, ozone MNB technology is green and clean, does not cause secondary pollution, and meets the strict requirements of drinking water treatment, providing a reliable technical means for ensuring drinking water safety. Studies have found that ozone MNB technology shows significant advantages in treating antibiotic wastewater. At an ozone concentration of 8 mg/L, it can completely degrade 100 mg/L of tetracycline within 20 min (Koundle et al., 2024). The degradation process not only relies on the direct oxidation effect of ozone but also benefits from the large amount of hydroxyl radicals (·OH) generated when MNBs burst. ·OH has extremely strong oxidation ability and can rapidly oxidize tetracycline molecules, converting them into harmless substances. In the treatment of wastewater containing aromatic hydrocarbons, ozone MNB technology also performs well. According to research, compared with ordinary ozonated water, ozone MNB water increases the oxidation rate of aromatic hydrocarbons such as toluene, ethylbenzene, o-xylene, and p-xylene by 13.6%–22.6% (Shen et al., 2023). This is mainly because the interface effect of MNBs promotes the contact between aromatic hydrocarbons and ·OH, making the oxidation reaction easier to proceed. Studies have shown that ozone MNB technology can effectively penetrate low-permeability aquifers and oxidize and degrade organic pollutants in them (Shen et al., 2024). In the remediation of low-permeability aquifers contaminated by toluene, the removal rate of toluene is significantly improved by injecting encapsulated ozone MNB water (EOMBW).

Ozone MNB technology can also be applied to the treatment of organic petroleum pollution in soil. The micro-nano bubble oxidation process features short duration, low cost and high efficiency. It can enhance the effectiveness of surfactants and additives, providing a practical solution for the efficient remediation of petroleum pollution. MNBs can increase the negative zeta potential on the surface of soil particles, thereby enhancing the electrostatic repulsion between oil droplets and soil particles and weakening their adsorption, making it easier for oil droplets to detach from the soil surface. MNBs (such as 1 μm bubbles) can withstand extremely high pressure (about 390 kPa, four times the atmospheric pressure), and their collapse will generate intense pressure waves and micro-jets. This local impact force can directly act on the surface of soil particles such as sand grains, physically stripping off the adhered oil films or oil droplets. The small size characteristics of MNBs (large specific surface area and long residence time in the liquid phase) can significantly increase the collision probability with oil droplets and enhance the adhesion between particles and bubbles, enabling more oil droplets to be carried by bubbles and detached from the soil matrix. Finally, MNBs can capture dispersed oil stains and carry them to the soil surface or treatment system through buoyancy, facilitating subsequent separation and removal. Huang et al. utilized the saponin and cyclodextrin + MNBs enhanced system to degrade diesel in soil. The enhancement of MNBs increased the sand erosion diesel removal rate by more than 20% (Huang et al., 2021). Sun et al. utilized ozone MNB technology to degrade TPH in petroleum waste sludge, achieving a removal rate of 71.7%–79.5% (Sun et al., 2020b).

5.3.4 The application of ozone MNB technology

Ozone micro-nano bubble (MBs) technology has demonstrated high efficiency in oxidation and environmental friendliness in wastewater treatment, but it still has significant shortcomings. Technically, the generation devices of MBs are difficult to achieve uniform and controllable bubble sizes, making it hard to clearly distinguish the characteristics and degradation patterns of MBs of

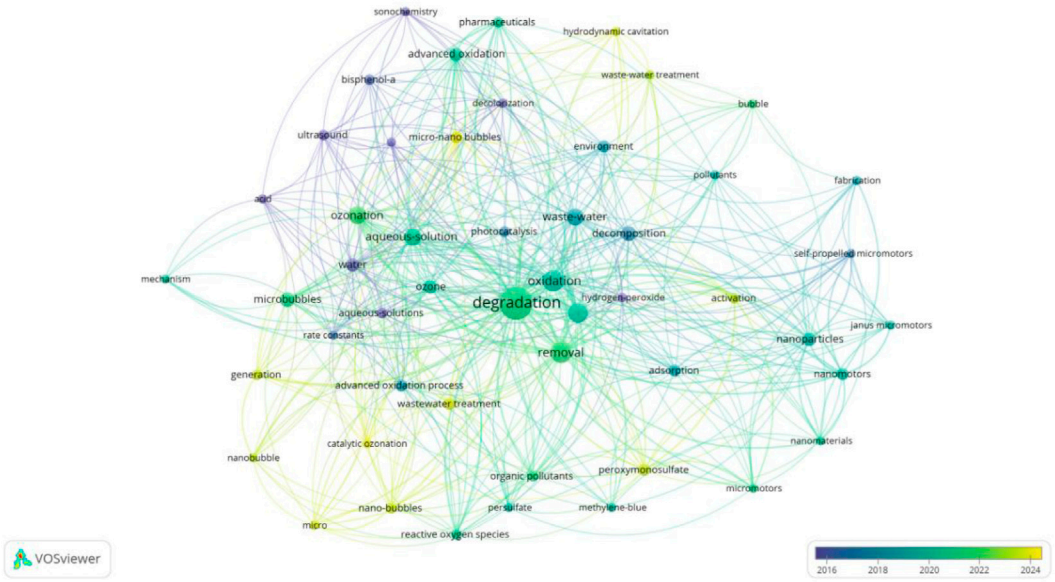

FIGURE 8
Application of MNB coupled Fenton oxidation technology.

different sizes, which restricts the research on the mechanism. The correlation between the dynamic characteristics of MBs (such as residence time, contraction and expansion) and the oxidation effect has not been systematically analyzed, and there are theoretical disputes about the generation pathways and core mechanisms of reactive oxygen species (ROS) (such as the hypotheses of interface ion accumulation and adiabatic compression). In terms of application, most existing studies are limited to laboratory or pilot-scale, lacking long-term operation data in actual scenarios, making it difficult to deal with complex conditions such as water quality fluctuations; economic feasibility analysis is insufficient, and the quantitative assessment of the full life cycle cost, including equipment maintenance and energy consumption, is lacking, which limits large-scale promotion.

In future research, it is first necessary to optimize the generation device to achieve precise control of bubble size, and combine ERT, CFD and other technologies to analyze the dynamic characteristics of MBs of different sizes. Secondly, the degradation mechanism should be verified, the action path of ROS clarified, and a structure-activity relationship model constructed. Finally, a full life cycle cost analysis should be carried out to enhance economic sustainability and promote large-scale field trials to verify the technical stability. With the resolution of these issues, ozone MNB technology is expected to become a core technology for advanced wastewater treatment and the removal of refractory pollutants, providing important support for environmental resource protection.

5.4 The application of MNB technology

The red area of the keyword spectrum (Figure 6) mainly focuses on the application of MNB technology in combination with various other technologies. It summarizes the excellent auxiliary degradation ability of MNBs. The functionalization of MNBs, their ability to generate reactive oxygen species (ROS), and their light scattering effect also contribute to assisting oxidation degradation reactions. Specifically, for instance, in the Fenton reaction, a Fe(II) catalytic layer can be constructed on the surface of MNBs, which not only adsorbs pollutants but also promotes the Fenton reaction *in situ* while adsorbing pollutants (Zhang et al., 2022a), thereby enhancing the oxidation reaction rate (Yi et al., 2023). Additionally, during the interface contraction process of MNBs, ROS can also be generated at the interface, directly leading to the degradation of pollutants (Wu et al., 2019). Moreover, the light scattering effect at the interface of MNBs can effectively extend the effective path length of light, thereby improving the photocatalytic efficiency (Fan et al., 2021). These indicate that the application of MNBs plays a crucial role in enhancing oxidation performance.

5.4.1 Fenton oxidation

Adding "Fenton" as a search term in the search formula and connecting it with "and", the keyword distribution map as shown in Figure 8 is obtained. The Fenton oxidation process generates non-selective degradation of organic pollutants. Under acidic conditions, H_2O_2 is activated by the single-electron transfer of Fe(II) to form ·OH, while Fe(III) is reduced to Fe(II) by H_2O_2, ensuring the regeneration of Fe ions and the continuous progress of the Fenton reaction (Huang et al., 2019). However, the limited active sites restrict the generation of reactive oxygen species (ROS) (Chen et al., 2023), and the short lifetime of ·OH reduces the degradation efficiency (Zhang et al., 2023). The keywords such as "Specific surface area" and "Interface reaction" in the figure imply that MNBs may enhance the Fenton oxidation process due to their huge specific surface area and dynamic interface reactions (Zhang et al., 2022b). The Fenton process assisted by MNBs has been proven to be effective in the removal of organic pollutants.

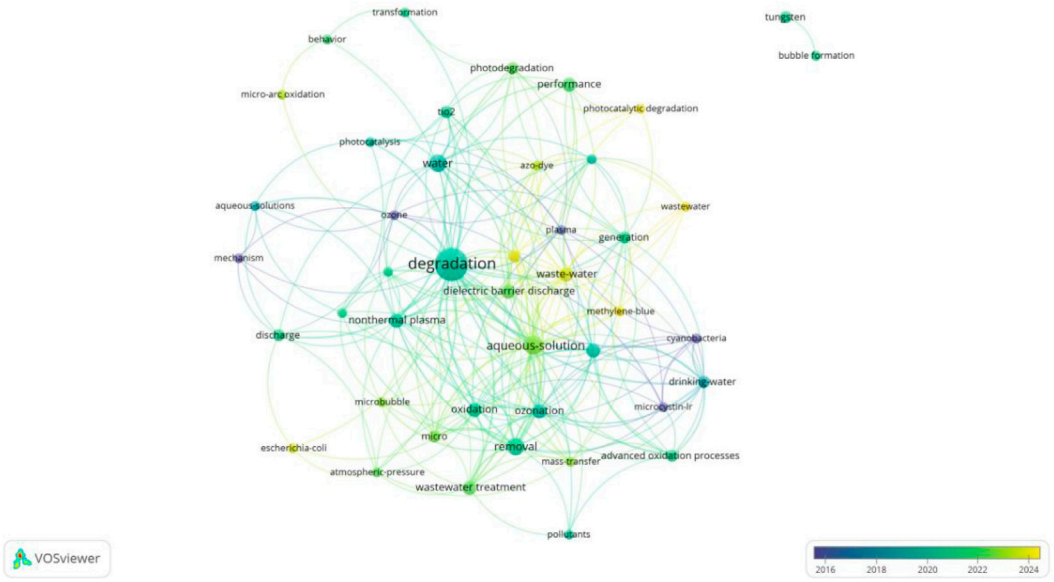

FIGURE 9
The application of MNB coupled plasma technology.

5.4.2 Plasma technology

Adding "plasma" as a search term in the search formula and connecting it with "and", the keyword distribution map as shown in Figure 9 is obtained. "Advanced oxidation" indicates that plasma technology, as one of the AOPs, can effectively degrade organic pollutants in water by generating active species with strong oxidation capacity, such as hydroxyl radicals (·OH), ozone (O_3), superoxide anions (O_2^-), *etc.* Plasma is a partially or fully ionized gas composed of electrons, free radicals, ions, and neutral substances, which can be generated through various discharges (Jiang et al., 2014; Rao et al., 2023). Plasma bubble technology combines the advantages of plasma and bubbles, bringing new breakthroughs to water pollution control. The key term "Dielectric barrier discharge" (DBD) is the most common driving method for generating non-thermal plasma (NTP), which is typically used in water treatment (Zhou et al., 2021b). Traditional plasma water treatment technologies, such as surface discharge and submerged discharge, have problems such as low transfer efficiency of active species and short contact time with pollutants (Zhang et al., 2021a). However, plasma bubble technology encapsulates the active species generated by plasma within bubbles, using the bubbles as carriers to extend the residence time of active species in the solution and increase the gas-liquid interface area, thereby significantly improving the degradation efficiency of pollutants (Zhang et al., 2022a). The highly reactive substances inside can be continuously released into the water and interact with pollutants through the annihilation of bubbles. The MNB-assisted method avoids the early consumption of ROS, thereby enhancing the removal efficiency of pollutants and reducing energy consumption. In the MNB-assisted plasma oxidation process, for plasma MNBs at room temperature, the bubbles must be larger than 30 μm to remain stable (Liu et al., 2018). After the formation of plasma MNBs, the presence of liquid films inside or between the MNBs under the influence of the streamer generated by the plasma can produce micro-discharge effects, thereby increasing the production of plasma reactive species (Chen et al., 2017).

Liu et al. constructed a plasma-microbubble system (BE-plasma), which demonstrated a strong synergistic effect in treating wastewater contaminated with diclofenac (DCF) (Liu et al., 1999). Under optimized process parameters, the degradation efficiency of DCF reached 90.9% within 45 min, far exceeding the treatment efficiency of using plasma or microbubbles alone. In the treatment of antibiotic pollution, Zhou et al. utilized non-thermal plasma bubbles to degrade cefixime antibiotics (Zhang et al., 2021b). The study found that this technology had a significant degradation effect on cefixime, with an energy yield of 1.5 g/kWh in a micro-porous reactor after 30 min of plasma treatment, and ·OH radicals played a key role in the degradation process.

In terms of gas pollution control, although related research is relatively scarce, plasma bubble technology also shows certain potential. In the treatment of VOCs, plasma bubble technology can degrade VOCs molecules into harmless small molecules through the reaction of active species generated. The principle is that high-energy electrons, free radicals, and other active species produced during the plasma discharge can break the chemical bonds in VOCs molecules, causing oxidation and decomposition reactions. Compared with traditional gas treatment technologies, plasma bubble technology has the advantages of mild reaction conditions and no need for catalysts, and is expected to become an efficient method for gas pollution control.

5.4.3 Photocatalytic technology

Photocatalytic technology is an advanced oxidation technology based on semiconductor materials. When semiconductor catalysts (such as "TiO_2", "heterojunctions", *etc.*) are exposed to light with energy greater than their band

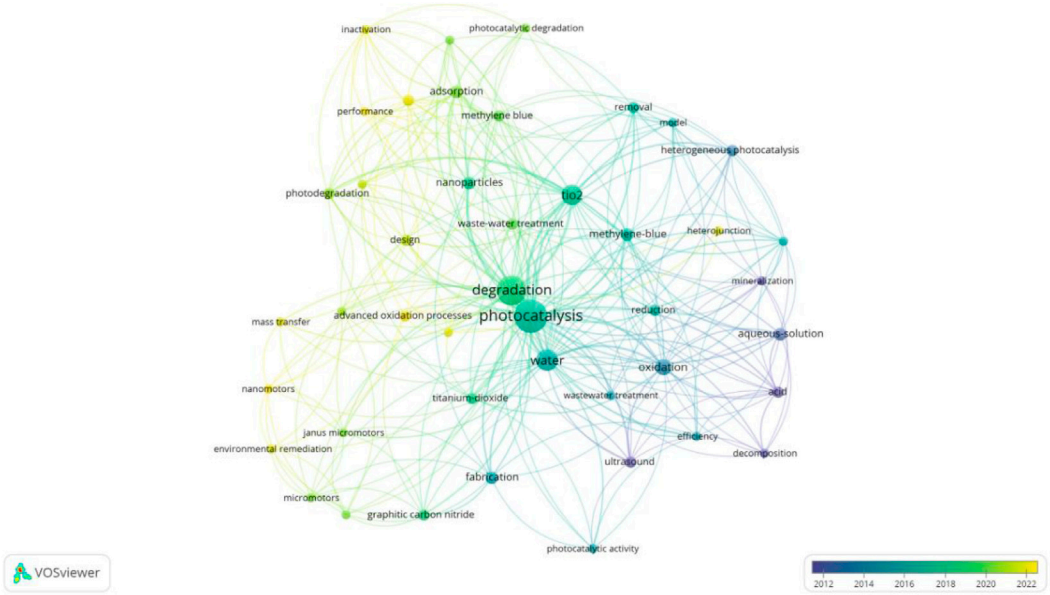

FIGURE 10
The application of MNB coupled photocatalytic technology.

gap energy, electrons are excited from the valence band to the conduction band, leaving holes in the valence band, thereby generating electron-hole pairs with strong oxidation capacity (Fu et al., 2019). These electron-hole pairs can react with substances such as water and oxygen adsorbed on the catalyst surface, generating ROS such as hydroxyl radicals (·OH), superoxide anions, *etc.*) (Liu et al., 2020; Weng et al., 2019). These reactive oxygen species have extremely high redox potentials and can oxidize and decompose various organic pollutants into harmless small molecules such as CO_2 and H_2O, achieving the degradation and mineralization of pollutants. However, photocatalytic technology still faces some challenges in practical applications. For example, photogenerated carriers (electrons and holes) are prone to recombination, reducing their efficiency in participating in photocatalytic reactions; the adsorption capacity of photocatalysts for pollutants is limited, and their dispersion in the reaction system is poor, affecting the rate and effect of photocatalytic reactions (Hao et al., 2021).

Coupling photocatalytic technology with MNB technology can achieve complementary advantages. The key to the combined application of photocatalytic technology and micro-nano bubble technology is demonstrated in Figure 10. On the one hand, MNBs can provide abundant oxygen for photocatalytic reactions, promote the separation of photogenerated carriers, and reduce the recombination of electron-hole pairs, thereby improving the efficiency of photocatalytic reactions (Agarwal et al., 2011; Dong et al., 2022). On the other hand, the reactive species generated by photocatalysis can synergize with the reactive species produced by the rupture of MNBs to enhance the oxidation and degradation of pollutants. Additionally, the presence of MNBs can improve the dispersion of photocatalysts in the solution, increase the contact opportunities between photocatalysts and pollutants, and further enhance the degradation effect.

In water pollution control, this coupled technology has shown significant advantages. Studies have shown that this technology has high efficiency in degrading various organic pollutants, such as dyes, antibiotics, and pesticides. When treating wastewater containing methylene blue, the photocatalytic and MNB coupled system can achieve efficient decolorization and mineralization of methylene blue in a relatively short time (Yang et al., 2022). MNBs not only increase the dissolved oxygen content in the system, promoting the progress of photocatalytic reactions, but also directly participate in the degradation of pollutants through the reactive species produced by their own rupture. At the same time, the reactive oxygen species generated by photocatalysis can also synergize with MNBs to improve the degradation efficiency (Selihin and Tay, 2022). In the treatment of wastewater containing bacteria, this coupled technology has a good inactivation effect on microorganisms. By destroying the cell structure of bacteria through various reactive oxygen species, they lose their activity, thereby achieving disinfection and purification of water bodies (Fan et al., 2021).

In the field of air pollution control, the coupled technology of photocatalysis and MNBs also has potential application value. For the degradation of VOCs, MNBs can carry oxygen and other oxidants, increasing the contact opportunities between VOCs and oxidants. Under light conditions, photocatalytic reactions generate a large number of reactive species, oxidizing and decomposing VOCs into harmless substances.

5.4.4 The advantages and prospects of the combined application of MNB technology

At present, the combination of MBs with various environmental treatment technologies is the most suitable development direction for MNB technology. The standalone MNB technology cannot generate sufficient active free radicals to degrade most pollutants

in the environment. Although the ozone MNB technology is relatively mature, due to the uncertainty of control factors such as bubble existence form, stability, and size, as well as the lack of large-scale experimental data for complex polluted environments, the single MNB technology cannot be put into practical large-scale use yet. However, as an auxiliary technology coupled with other mature environmental treatment technologies, it benefits from its excellent free radical generation capacity and mass transfer efficiency, providing a better oxidation environment and enhancing the efficiency of other treatment technologies in degrading pollutants. It is a relatively practical auxiliary treatment technology. Especially, the combination of MBs with various advanced oxidation methods or photocatalytic methods has attracted increasing attention. This technology overcomes the limitations of ozone mass transfer utilization, effectively improving the oxidation efficiency of ozone. The presence of MBs keeps the catalyst particles in a dynamic dispersed state, effectively increasing the contact frequency between the catalyst and refractory organic compounds, significantly enhancing the mineralization efficiency of refractory organic compounds, and achieving efficient wastewater treatment.

6 Conclusion

MNB technology, with its unique physicochemical properties (such as large specific surface area, high surface Zeta potential, long stability and strong ability to generate oxidative free radicals), has demonstrated significant advantages in water pollution control (industrial wastewater, surface water, groundwater) and soil pollution remediation, and has become a research hotspot in the environmental field. By coupling with technologies such as ozone oxidation, photocatalysis, Fenton reaction and plasma technology, its pollutant degradation efficiency is significantly enhanced. For instance, the removal rate of plastic pollutants in industrial wastewater by ozone MNBs reaches 94.18%, and when combined with photocatalysis, it can increase the light absorption efficiency at a 700 nm light path by 54.8%.

China holds a dominant position in research in this field. Institutions such as Tsinghua University and the CAS have achieved remarkable results in applications such as groundwater remediation with ozone MNBs and semiconductor cleaning. However, the international cooperation network still needs to be strengthened. Keyword clustering analysis indicates that “degradation”, “ozone MNBs”, “free radicals”, and “photocatalysis” are the core research themes, and the coupling mechanism of technologies and interface reaction theory are the current exploration focuses.

However, the long-term stability of MNB technology in complex environments, the energy consumption and cost issues in large-scale applications, as well as the cross-disciplinary collaborative mechanisms (such as the interaction between microorganisms and bubbles) still require further research. In the future, efforts should be focused on technological optimization and adaptation to actual scenarios to promote its transformation from laboratory research to industrial applications, providing efficient solutions for global environmental pollution control.

Data availability statement

The original contributions presented in the study are included in the article/supplementary material, further inquiries can be directed to the corresponding author.

Author contributions

QC: Formal Analysis, Writing – original draft, Conceptualization, Investigation, Data curation. XZ: Formal Analysis, Writing – original draft, Methodology, Data curation. YG: Project administration, Validation, Supervision, Writing – review and editing, Funding acquisition. QZ: Funding acquisition, Writing – review and editing, Project administration.

Funding

The author(s) declare that no financial support was received for the research and/or publication of this article.

Acknowledgments

The present work was financially supported by Natural Science Foundation of China (52270129), Oriental Talent Youth Program, Shanghai Shuguang Program (23SG52), and Guizhou Provincial Key Technology R&D Program [QKHZC(2024)153]. Guo also thanks the financial support of Science and Technology Development Fund of Pudong New Area (PKJ2022-C07), and Scientific Research Fund Project of Shanghai Polytechnic University (A10GY25G004-02).

Conflict of interest

The authors declare that the research was conducted in the absence of any commercial or financial relationships that could be construed as a potential conflict of interest.

Generative AI statement

The author(s) declare that no Generative AI was used in the creation of this manuscript.

Any alternative text (alt text) provided alongside figures in this article has been generated by Frontiers with the support of artificial intelligence and reasonable efforts have been made to ensure accuracy, including review by the authors wherever possible. If you identify any issues, please contact us.

Publisher's note

References

Agarwal, A., Ng, W. J., and Liu, Y. (2011). Principle and applications of microbubble and nanobubble technology for water treatment. *Chemosphere* 84, 1175–1180. doi:10.1016/j.chemosphere.2011.05.054

Agarwal, M., Dikshit, P. K., Bhasarkar, J. B., Borah, A. J., and Moholkar, V. S. (2016). Physical insight into ultrasound-assisted biodesulfurization using free and immobilized cells of Rhodococcus rhodochrous MTCC 3552. *Chem. Eng. J.* 295, 254–267. doi:10.1016/j.cej.2016.03.042

Azuma, T., Otomo, K., Kunitou, M., Shimizu, M., Hosomaru, K., Mikata, S., et al. (2019). Removal of pharmaceuticals in water by introduction of ozonated microbubbles. *Sep. Purif. Technol.* 212, 483–489. doi:10.1016/j.seppur.2018.11.059

Bao, J. F., Guo, S. S., Fan, D. D., Cheng, J. L., Zhang, Y., and Pang, X. (2023). Sonoactivated nanomaterials: a potent armament for wastewater treatment. *Ultrason. Sonochemistry* 99, 106569. doi:10.1016/j.ultsonch.2023.106569

Boonwan, C., Rojviroon, T., Rojviroon, O., Rajendran, R., Paramasivam, S., Chinnasamy, R., et al. (2024). Micro-nano bubbles in action: AC/TiO_2 2 hybrid photocatalysts for efficient organic pollutant degradation and antibacterial activity. *Biocatal. Agric. Biotechnol.* 61, 103400. doi:10.1016/j.bcab.2024.103400

Cao, Y. Z., Hu, L. M., Jing, S., Wang, M. J., Wu, Z. X., Ji, L. J., et al. (2023). "Field Test Study of organics-contaminated groundwater In-Situ remediation by ozone micro-nano-bubbles," in *Proceedings of the 14th congress of the international-association-for-engineering-geology-and-the-environment (IAEG)* (Chengdu: PEOPLES R CHINA), 709–719.

Chen, Y. C., and Chang, J. E. (2022). Removal of chlorine-contaminated groundwater by two-stage ozonation and biostimulation methods. *J. Environ. Manag.* 317, 115417. doi:10.1016/j.jenvman.2022.115417

Chen, C., Li, F. Y., Chen, H. L., and Kong, M. G. (2017). Aqueous reactive species induced by a PCB surface micro-discharge air plasma device: a quantitative study. *J. Phys. D-Applied Phys.* 50, 445208. doi:10.1088/1361-6463/aa8be9

Chen, T. F., Yavuz, B. M., Delgado, A. G., Montoya, G., Van Winkle, D., Zuo, Y., et al. (2018). Impacts of moisture content during ozonation of soils containing residual petroleum. *J. Hazard. Mater.* 344, 1101–1108. doi:10.1016/j.jhazmat.2017.11.060

Chen, C., Wang, Y. Y., Huang, Y. J., Hua, J., Qu, W., Xia, D. H., et al. (2023). Overlooked self-catalytic mechanism in phenolic moiety-mediated Fenton-like system: formation of Fe(III) hydroperoxide complex and co-treatment of refractory pollutants. *Appl. Catal. B-Environment Energy* 321, 122062. doi:10.1016/j.apcatb.2022.122062

Cheng, W., Quan, X. J., Li, R. H., Wu, J., and Zhao, Q. H. (2018). Ozonation of phenol-containing wastewater using O3/Ca(OH)2 system in a micro bubble gas-liquid reactor. *Ozone-Science and Eng.* 40, 173–182. doi:10.1080/01919512.2017.1399791

Cheng, W., Jiang, L., Quan, X. J., Cheng, C., Huang, X. X., Cheng, Z. L., et al. (2019). Ozonation process intensification of p-nitrophenol by in situ separation of hydroxyl radical scavengers and microbubbles. *Water Sci. Technol.* 80, 25–36. doi:10.2166/wst.2019.227

Cheng, C., Huang, X. X., Cheng, W., Quan, X. J., Cheng, Z. L., Jiang, L., et al. (2021). Ozonation of biologically-treated municipal solid waste leachate using an integrated process of O3/Ca(OH)2 and microbubble reactor. *Environ. Technol.* 42, 2402–2412. doi:10.1080/09593330.2019.1703143

Chi, C. B., Huo, B. Q., Liang, Z. D., Hu, C. X., Sun, Q. Y., and Zhou, S. F. (2024). Study on tetracycline degradation in wastewater based on zero-valent nano iron assisted micro-nano bubbles. *Alexandria Eng. J.* 86, 577–583. doi:10.1016/j.aej.2023.12.004

Chu, L. B., Xing, X. H., Yu, A. F., Zhou, Y. N., Sun, X. L., and Jurcik, B. (2007). Enhanced ozonation of simulated dyestuff wastewater by microbubbles. *Chemosphere* 68, 1854–1860. doi:10.1016/j.chemosphere.2007.03.014

Dai, C. M., Han, Y. M., Zhang, Y. L., Duan, Y. P., Tong, W. K., Liu, S. G., et al. (2023). Cyclic solubilization and release of polycyclic aromatic hydrocarbons (PAHs) using gemini photosensitive surfactant combined with micro-nano bubbles: a promising enhancement technology for groundwater remediation. *Sep. Purif. Technol.* 309, 123042. doi:10.1016/j.seppur.2022.123042

Deng, S. H., Jothinathan, L., Cai, Q. Q., Li, R., Wu, M. Y., Ong, S. L., et al. (2021). FeOx@GAC catalyzed microbubble ozonation coupled with biological process for industrial phenolic wastewater treatment: catalytic performance, biological process screening and microbial characteristics. *Water Res.* 190, 116687. doi:10.1016/j.watres.2020.116687

Dong, G. H., Chen, B., Liu, B., Hounjet, L. J., Cao, Y. Q., Stoyanov, S. R., et al. (2022). Advanced oxidation processes in microreactors for water and wastewater treatment: development, challenges, and opportunities. *Water Res.* 211, 118047. doi:10.1016/j.watres.2022.118047

Duan, Y. L., Yu, J., Zhang, R. X., Han, P. F., Ren, P., Liu, M., et al. (2022). Integrated MnO2 nanosheet ultrafiltration ceramic membrane with micro-nano bubbles for catalytic treatment of dye wastewater. *Sep. Purif. Technol.* 300, 121786. doi:10.1016/j.seppur.2022.121786

Duan, Y. L., Zhao, D., Liu, Z. Y., and Yu, J. (2025). Hydrogen peroxide enhancing the process of MnO2-modified ceramic membrane catalyzing micro-nano bubble. *Sep. Purif. Technol.* 353, 128320. doi:10.1016/j.seppur.2024.128320

El Aswar, E. I., Li, M. K., Huang, Y. Y., Sun, Z., Li, W. T., and Qiang, Z. M. (2025). Enhanced vacuum ultraviolet/ultraviolet process for advanced water treatment by using air micro/nano bubbles. *J. Hazard. Mater.* 489, 137602. doi:10.1016/j.jhazmat.2025.137602

Entezari, M. H., and Ghows, N. (2011). Micro-emulsion under ultrasound facilitates the fast synthesis of quantum dots of CdS at low temperature. *Ultrason. Sonochemistry* 18, 127–134. doi:10.1016/j.ultsonch.2010.04.001

Fan, W., Zhou, Z., Wang, W. T., Huo, M. X., Zhang, L. L., Zhu, S. Y., et al. (2019). Environmentally friendly approach for advanced treatment of municipal secondary effluent by integration of micro-nano bubbles and photocatalysis. *J. Clean. Prod.* 237, 117828. doi:10.1016/j.jclepro.2019.117828

Fan, W., Cui, J. Y., Li, Q., Huo, Y., Xiao, D., Yang, X., et al. (2021). Bactericidal efficiency and photochemical mechanisms of micro/nano bubble-enhanced visible light photocatalytic water disinfection. *Water Res.* 203, 117531. doi:10.1016/j.watres.2021.117531

Fu, Y. S., Li, J., and Li, J. G. (2019). Metal/semiconductor nanocomposites for photocatalysis: fundamentals, structures, applications and properties. *Nanomaterials* 9, 359. doi:10.3390/nano9030359

Han, Y. M., Dai, C. M., Li, J. X., Li, Z., Zhang, Y. L., Hon, L. K., et al. (2025). Reversible surfactant combined with micro-nano bubbles and peroxymonosulfate: a method for cyclic remediation of PAHs contaminated soil and groundwater. *Sep. Purif. Technol.* 354, 129491. doi:10.1016/j.seppur.2024.129491

Hao, L., Huang, H. W., Zhang, Y. H., and Ma, T. Y. (2021). Oxygen vacant semiconductor photocatalysts. *Adv. Funct. Mater.* 31, 2100919. doi:10.1002/adfm.202100919

Haris, S., Qiu, X. B., Klammler, H., and Mohamed, M. M. A. (2020). The use of micro-nano bubbles in groundwater remediation: a comprehensive review. *Groundw. Sustain. Dev.* 11, 100463. doi:10.1016/j.gsd.2020.100463

Hoang, S. A., Bolan, N., Madhubashani, A. M. P., Vithanage, M., Perera, V., Wijesekara, H., et al. (2022). Treatment processes to eliminate potential environmental hazards and restore agronomic value of sewage sludge: a review. *Environ. Pollut.* 293, 118564. doi:10.1016/j.envpol.2021.118564

Hu, L. M., and Xia, Z. R. (2018). Application of ozone micro-nano-bubbles to groundwater remediation. *J. Hazard. Mater.* 342, 446–453. doi:10.1016/j.jhazmat.2017.08.030

Hu, L. L., Chen, B. Y., and Ma, J. (2023). Micro-/nano-bubbles ozonation for effective industrial wastewater remediation: from lab to pilot-scale application. *J. Environ. Chem. Eng.* 11, 110807. doi:10.1016/j.jece.2023.110807

Huang, X. P., Chen, Y., Walter, E., Zong, M. R., Wang, Y., Zhang, X., et al. (2019). Facet-specific photocatalytic degradation of organics by heterogeneous fenton chemistry on hematite nanoparticles. *Environ. Sci. and Technol.* 53, 10197–10207. doi:10.1021/acs.est.9b02946

Huang, Z. L., Chen, Q. Y., Yao, Y., Chen, Z., and Zhou, J. (2021). Micro-bubbles enhanced removal of diesel oil from the contaminated soil in washing/flushing with surfactant and additives. *J. Environ. Manag.* 290, 112570. doi:10.1016/j.jenvman.2021.112570

Ishida, N., Inoue, T., Miyahara, M., and Higashitani, K. (2000). Nano bubbles on a hydrophobic surface in water observed by tapping-mode atomic force microscopy. *Langmuir* 16, 6377–6380. doi:10.1021/la000219r

Ji, H. D., Gong, Y. Y., Duan, J., Zhao, D. Y., and Liu, W. (2018). Degradation of petroleum hydrocarbons in seawater by simulated surface-level atmospheric ozone: reaction kinetics and effect of oil dispersant. *Mar. Pollut. Bull.* 135, 427–440. doi:10.1016/j.marpolbul.2018.07.047

Jiang, B., Zheng, J. T., Qiu, S., Wu, M. B., Zhang, Q. H., Yan, Z. F., et al. (2014). Review on electrical discharge plasma technology for wastewater remediation. *Chem. Eng. J.* 236, 348–368. doi:10.1016/j.cej.2013.09.090

Jing, M. Y., Zhang, J. P., Li, G. J., Zhang, D., Liu, F. J., and Yang, S. K. (2025). Micro-nano bubbles enhanced immobilized Chlorella vulgaris to remove ofloxacin from groundwater. *J. Contam. Hydrology* 268, 104458. doi:10.1016/j.jconhyd.2024.104458

John, A., Brookes, A., Carra, I., Jefferson, B., and Jarvis, P. (2022). Microbubbles and their application to ozonation in water treatment: a critical review exploring their benefit and future application. *Crit. Rev. Environ. Sci. Technol.* 52, 1561–1603. doi:10.1080/10643389.2020.1860406

Khan, N. A., and Carroll, K. C. (2020). Natural attenuation method for contaminant remediation reagent delivery assessment for in situ chemical oxidation using aqueous ozone. *Chemosphere* 247, 125848. doi:10.1016/j.chemosphere.2020.125848

Khuntia, S., Majumder, S. K., and Ghosh, P. (2012). Microbubble-aided water and wastewater purification: a review. *Rev. Chem. Eng.* 28, 191–221. doi:10.1515/revce-2012-0007

Kim, S. Y., Park, J. W., Noh, J. H., Bae, Y. H., and Maeng, S. K. (2022). Potential organic matter management for industrial wastewater guidelines using advanced dissolved organic matter characterization tools. *J. Water Process Eng.* 46, 102604. doi:10.1016/j.jwpe.2022.102604

Koundle, P., Nirmalkar, N., Momotko, M., Makowiec, S., and Boczkaj, G. (2024). Tetracycline degradation for wastewater treatment based on ozone nanobubbles advanced oxidation processes (AOPs) - focus on nanobubbles formation, degradation kinetics, mechanism and effects of water composition. *Chem. Eng. J.* 501, 156236. doi:10.1016/j.cej.2024.156236

Kwon, H., Mohamed, M. M., Annable, M. D., and Kim, H. (2020). Remediation of NAPL-contaminated porous media using micro-nano ozone bubbles: bench-scale experiments. *J. Contam. Hydrology* 228, 103563. doi:10.1016/j.jconhyd.2019.103563

Lee, E. J., Kim, Y. H., Kim, H. S., and Jang, A. (2015). Influence of microbubble in physical cleaning of MF membrane process for wastewater reuse. *Environ. Sci. Pollut. Res.* 22, 8451–8459. doi:10.1007/s11356-014-3928-y

Levanov, A. V., Isaikina, O. Y., Gasanova, R. B., and Lunin, V. V. (2017). Coefficient of ozone mass transfer during its interaction with an aqueous solution of formic acid in a bubble column reactor. *Russ. J. Phys. Chem. A* 91, 1427–1431. doi:10.1134/s0036024417080167

Li, P., Takahashi, M., and Chiba, K. (2009). Degradation of phenol by the collapse of microbubbles. *Chemosphere* 75, 1371–1375. doi:10.1016/j.chemosphere.2009.03.031

Li, H. Z., Hu, L. M., and Xia, Z. R. (2013). Impact of groundwater salinity on bioremediation enhanced by micro-nano bubbles. *Materials* 6, 3676–3687. doi:10.3390/ma6093676

Li, H. Z., Hu, L. M., Song, D. J., and Al-Tabbaa, A. (2014). Subsurface transport behavior of micro-nano bubbles and potential applications for groundwater remediation. *Int. J. Environ. Res. Public Health* 11, 473–486. doi:10.3390/ijerph110100473

Li, G. J., Cheng, Y., Jing, M. Y., Zhang, D., Ma, Y. F., and Yang, S. K. (2024). Degradation of norfloxacin by the synergistic effect of micro-nano bubbles and sodium hypochlorite: kinetics, influencing factors and pathways. *Environ. Science-Processes and Impacts* 26, 2189–2202. doi:10.1039/d4em00490f

Li, P., Huang, X. J., Yang, Q., Xia, H. Z., Li, C. B., Zhang, Z. Q., et al. (2025a). Micro-nano bubbles enhanced degradation of emerging contaminants by ferrous-oxalate complexes: synergistic interaction between oxidation and coagulation. *Front. Environ. Sci. and Eng.* 19, 66. doi:10.1007/s11783-025-1986-7

Li, L. N., Fang, L. L., Shen, J. M., Wang, B. Y., Yuan, L., and Guo, Y. Q. (2025b). Removal of ibuprofen via the O_3/H_2O_2 oxidation system: performance, degradation mechanism, and toxicity evaluation. *Water* 17, 1414. doi:10.3390/w17101414

Lim, S., Shi, J. L., von Gunten, U., and McCurry, D. L. (2022). Ozonation of organic compounds in water and wastewater: a critical review. *Water Res.* 213, 118053. doi:10.1016/j.watres.2022.118053

Liu, J., Lam, Y. L., Chan, Y. C., Zhou, Y., and Yao, J. (1999). Fabrication of high-performance dispersion compensating fiber by plasma chemical vapor deposition. *Fiber Integr. Opt.* 18, 63–67. doi:10.1080/014680399244703

Liu, Y. A., Zhang, H., Sun, J. H., Liu, J. X., Shen, X., Zhan, J. X., et al. (2018). Degradation of aniline in aqueous solution using non-thermal plasma generated in microbubbles. *Chem. Eng. J.* 345, 679–687. doi:10.1016/j.cej.2018.01.057

Liu, B. S., Wu, H., and Parkin, I. P. (2020). New insights into the fundamental principle of semiconductor photocatalysis. *Acs Omega* 5, 14847–14856. doi:10.1021/acsomega.0c02145

Liu, S. T., Yang, J. W., Zhang, Y. L., Wu, T. L., and Chen, C. M. (2025). High-efficiency degradation mechanism of sulfadiazine by ozone micro-nano bubbles: the effect of gas flow rate. *Sep. Purif. Technol.* 376, 134140. doi:10.1016/j.seppur.2025.134140

Loh, W. H., Cai, Q. Q., Li, R., Jothinathan, L., Lee, B. C. Y., Ng, O. H., et al. (2021). Reverse osmosis concentrate treatment by microbubble ozonation-biological activated carbon process: organics removal performance and environmental impact assessment. *Sci. Total Environ.* 798, 149289. doi:10.1016/j.scitotenv.2021.149289

Ma, X., Jang, S., Popescu, M. N., Uspal, W. E., Miguel-López, A., Hahn, K., et al. (2016). Reversed janus micro/nanomotors with internal chemical engine. *Acs Nano* 10, 8751–8759. doi:10.1021/acsnano.6b04358

Masry, M., Rossignol, S., Roussel, B. T., Bourgogne, D., Bussi, P. O., R'Mili, B., et al. (2021). Experimental evidence of plastic particles transfer at the water-air interface through bubble bursting. *Environ. Pollut.* 280, 116949. doi:10.1016/j.envpol.2021.116949

Melich, R., Valour, J. P., Urbaniak, S., Padilla, F., and Charcosset, C. (2019). Preparation and characterization of perfluorocarbon microbubbles using Shirasu Porous Glass (SPG) membranes. *Colloids Surfaces a-Physicochemical Eng. Aspects* 560, 233–243. doi:10.1016/j.colsurfa.2018.09.058

Michailidi, E. D., Bomis, G., Varoutoglou, A., Kyzas, G. Z., Mitrikas, G., Mitropoulos, A. C., et al. (2020). Bulk nanobubbles: production and investigation of their formation/stability mechanism. *J. Colloid Interface Sci.* 564, 371–380. doi:10.1016/j.jcis.2019.12.093

Mo, J. C., Lin, T., Liu, W., Zhang, Z. B., and Yan, Y. (2024). Cleaning efficiency and mechanism of ozone micro-nano-bubbles on ceramic membrane fouling. *Sep. Purif. Technol.* 331, 125698. doi:10.1016/j.seppur.2023.125698

Mohite, R. G., and Garg, A. (2017). Performance of heterogeneous catalytic wet oxidation for the removal of phenolic compounds: catalyst characterization and effect of pH, temperature, metal leaching and non-oxidative hydrothermal reaction. *J. Environ. Chem. Eng.* 5, 468–478. doi:10.1016/j.jece.2016.12.024

Park, J. Y., Choi, Y. J., Moon, S., Shin, D. Y., and Nam, K. (2009). Microbubble suspension as a carrier of oxygen and acclimated bacteria for phenanthrene biodegradation. *J. Hazard. Mater.* 163, 761–767. doi:10.1016/j.jhazmat.2008.07.024

Parker, J. L., Claesson, P. M., and Attard, P. (1994). Bubbles, cavities, and the long-ranged attraction between hydrophobic surfaces. *J. Phys. Chem.* 98, 8468–8480. doi:10.1021/j100085a029

Pétrier, C., Torres-Palma, R., Combet, E., Sarantakos, G., Baup, S., and Pulgarin, C. (2010). Enhanced sonochemical degradation of bisphenol-A by bicarbonate ions. *Ultrason. Sonochemistry* 17, 111–115. doi:10.1016/j.ultsonch.2009.05.010

Ponce-Robles, L., Pagán-Muñoz, A., Lara-Guillén, A. J., Masdemont-Hernández, B., Munuera-Pérez, T., Nortes-Tortosa, P. A., et al. (2023). Full-scale O_3/Micro-Nano bubbles system based advanced oxidation as alternative tertiary treatment in WWTP effluents. *Catalysts* 13, 188. doi:10.3390/catal13010188

Rao, N., Chu, X., Hadinoto, K., Angelina, A., Zhou, R., Zhang, T., et al. (2023). Algal cell inactivation and damage *via* cold plasma-activated bubbles: mechanistic insights and process benefits. *Chem. Eng. J.* 454, 140304. doi:10.1016/j.cej.2022.140304

Ren, Y. H., Wang, Y. L., Wang, X. L., Liu, B. Z., He, G. L., Gong, Y. L., et al. (2025). The degradation of 2-methylisobornyl alcohol and geosmin through a micro-nano bubble-activated ozone process: the dual mechanism of enhanced degradation efficiency. *Environ. Science-Water Res. and Technol.* 11, 1177–1185. doi:10.1039/d4ew00944d

Selihin, N. M., and Tay, M. G. (2022). A review on future wastewater treatment technologies: micro-nanobubbles, hybrid electro-Fenton processes, photocatalytic fuel cells, and microbial fuel cells. *Water Sci. Technol.* 85, 319–341. doi:10.2166/wst.2021.618

Seridou, P., and Kalogerakis, N. (2021). Disinfection applications of ozone micro- and nanobubbles. *Environ. Science-Nano* 8, 3493–3510. doi:10.1039/d1en00700a

Shen, D. S., Xie, Z. M., Shentu, J., Long, Y. Y., Lu, L., Li, L. L., et al. (2023). Enhanced oxidation of aromatic hydrocarbons by ozone micro-nano bubble water: mechanism and influencing factors. *J. Environ. Chem. Eng.* 11, 110281. doi:10.1016/j.jece.2023.110281

Shen, D. S., Li, L. L., Luo, J., Jia, J., Tang, L., Long, Y. Y., et al. (2024). Enhanced removal of toluene in heterogeneous aquifers through injecting encapsulated ozone micro-nano bubble water. *J. Hazard. Mater.* 468, 133810. doi:10.1016/j.jhazmat.2024.133810

Shi, X. N., Xue, S., Marhaba, T., and Zhang, W. (2021). Probing internal pressures and long-term stability of nanobubbles in water. *Langmuir* 37, 2514–2522. doi:10.1021/acs.langmuir.0c03574

Soler, L., Magdanz, V., Fomin, V. M., Sanchez, S., and Schmidt, O. G. (2013). Self-propelled micromotors for cleaning polluted water. *ACS Nano* 7, 9611–9620. doi:10.1021/nn405075d

Sun, Z. Y., Chen, X. L., Yang, K. Y., Zhua, N. W., and Lou, Z. Y. (2020a). The progressive steps for TPH stripping and the decomposition of oil refinery sludge using microbubble ozonation. *Sci. Total Environ.* 712, 135631. doi:10.1016/j.scitotenv.2019.135631

Sun, Z. Y., Xia, F. J., Lou, Z. Y., Chen, X. L., Zhu, N. W., Yuan, H. P., et al. (2020b). Innovative process for total petroleum hydrocarbons reduction on oil refinery sludge through microbubble ozonation. *J. Clean. Prod.* 256, 120337. doi:10.1016/j.jclepro.2020.120337

Takahashi, M., Chiba, K., and Li, P. (2007a). Free-radical generation from collapsing microbubbles in the absence of a dynamic stimulus. *J. Phys. Chem. B* 111, 1343–1347. doi:10.1021/jp0669254

Takahashi, M., Chiba, K., and Li, P. (2007b). Formation of hydroxyl radicals by collapsing ozone microbubbles under strongly acidic conditions. *J. Phys. Chem. B* 111, 11443–11446. doi:10.1021/jp074727m

Takahashi, M., Horibe, H., Matsuura, K., and Tatera, K. (2015). Effect of microbubbles on ozonized water for photoresist removal. *J. Photopolym. Sci. Technol.* 28, 293–298. doi:10.2494/photopolymer.28.293

Temesgen, T., Bui, T. T., Han, M., Kim, T. I., and Park, H. (2017). Micro and nanobubble technologies as a new horizon for water-treatment techniques: a review. *Adv. Colloid Interface Sci.* 246, 40–51. doi:10.1016/j.cis.2017.06.011

Ulatowski, K., Sobieszuk, P., Mróz, A., and Ciach, T. (2019). Stability of nanobubbles generated in water using porous membrane system. *Chem. Eng. Processing-Process Intensif.* 136, 62–71. doi:10.1016/j.cep.2018.12.010

Ulatowski, K., Szczygielski, P., and Sobieszuk, P. (2024). Impact of water purity and oxygen content in gas phase on effectiveness of surface cleaning with microbubbles. *Materials* 17, 6046. doi:10.3390/ma17246046

Utaka, Y., Okuda, S., and Tasaki, Y. (2009). Configuration of the micro-layer and characteristics of heat transfer in a narrow gap mini/micro-channel boiling system. *Int. J. Heat Mass Transf.* 52, 2205–2214. doi:10.1016/j.ijheatmasstransfer.2008.11.020

Villa, K., Palenzuela, C. L. M., Sofer, Z., Matejková, S., and Pumera, M. (2018). Metal-free visible-light photoactivated C3N4 bubble-propelled tubular micromotors with inherent fluorescence and On/Off capabilities. *Acs Nano* 12, 12482–12491. doi:10.1021/acsnano.8b06914

Wang, B. G., Wang, L. J., Cen, W. X., Lyu, T., Jarvis, P., Zhang, Y., et al. (2024a). Exploring a chemical input free advanced oxidation process based on nanobubble technology to treat organic micropollutants. *Environ. Pollut.* 340, 122877. doi:10.1016/j.envpol.2023.122877

Wang, Y. L., Wei, J. J., Hu, J., Guo, Z. M., and Bai, W. L. (2024b). Research on the kinetics and degradation pathways of gaseous acetic acid ester organics. *Environ. Technol.* 45, 2721–2734. doi:10.1080/09593330.2023.2185819

Wei, Z. H., Le, Q. V., Peng, W. X., Yang, Y. F., Yang, H., Gu, H. P., et al. (2021). A review on phytoremediation of contaminants in air, water and soil. *J. Hazard. Mater.* 403, 123658. doi:10.1016/j.jhazmat.2020.123658

Weng, B., Qi, M. Y., Han, C., Tang, Z. R., and Xu, Y. J. (2019). Photocorrosion inhibition of semiconductor-based photocatalysts: basic principle, current development, and future perspective. *Acs Catal.* 9, 4642–4687. doi:10.1021/acscatal.9b00313

Wu, C., Li, P., Xia, S. J., Wang, S., Wang, Y., Hu, J., et al. (2019). The role of interface in microbubble ozonation of aromatic compounds. *Chemosphere* 220, 1067–1074. doi:10.1016/j.chemosphere.2018.12.174

Xia, Z. R., and Hu, L. M. (2019). Treatment of organics contaminated wastewater by ozone micro-nano-bubbles. *Water* 11, 55. doi:10.3390/w11010055

Xia, Z. R., Hu, L. M., Kusaba, S., and Song, D. J. (2018). "Remediation of TCE contaminated site by ozone micro-nano-bubbles," in *Proceedings of the 8th international Congress on environmental geotechnics (ICEG)* (Hangzhou: PEOPLES R CHINA), 796–803.

Xiao, Z. G., Bin Aftab, T., and Li, D. X. (2019). Applications of micro-nano bubble technology in environmental pollution control. *Micro and Nano Lett.* 14, 782–787. doi:10.1049/mnl.2018.5710

Xiao, W., Zhang, H., Wang, X. H., Wang, B., Long, T., Deng, S., et al. (2022). Interaction mechanisms and application of Ozone micro/nanobubbles and nanoparticles: a review and perspective. *Nanomaterials* 12, 1958. doi:10.3390/nano12121958

Xiao, Y. T., Liu, H. L., Sun, C. X., Wang, D. Z., Li, L. H., Shao, L., et al. (2025). Research progress of micro-nano bubbles in environmental remediation: mechanisms, preparation methods, and applications. *J. Environ. Manag.* 375, 124387. doi:10.1016/j.jenvman.2025.124387

Yang, C. Y., Xue, Z. W., Yin, H., Lu, K., and Liu, W. (2022). Aqueous foam loaded TiO2 nano-catalysts for promoting photodegradation of methylene blue. *J. Nanoparticle Res.* 24, 59. doi:10.1007/s11051-022-05441-3

Yang, X. D., Li, J., Song, R., Zhao, B., Tang, J. M., Kong, L. A., et al. (2023a). Highly reproducible van der Waals integration of two-dimensional electronics on the wafer scale. *Nat. Nanotechnol.* 18, 471–478. doi:10.1038/s41565-023-01342-1

Yang, Y., Yao, X., Wu, S. H., Wang, X., Feng, L., Feng, X. D., et al. (2023b). Enhanced treatment of azo dyes in wastewater using heat-activated persulfate with micro-nano bubble aeration. *Chem. Eng. Res. and Des.* 197, 24–37. doi:10.1016/j.cherd.2023.07.013

Yang, Y., Wang, X., Wu, S. H., Yao, X., Feng, L., Feng, X. D., et al. (2023c). Insight into the application of micro-nano bubbles combined with heat-activated persulfate oxidation for removing dissolved organic matter from printing and dying wastewater. *J. Water Process Eng.* 56, 104463. doi:10.1016/j.jwpe.2023.104463

Yang, X. L., Chen, L., Oshita, S., Fan, W. H., and Liu, S. (2023d). Mechanism for enhancing the ozonation process of Micro- and nanobubbles: bubble behavior and interface reaction. *Acs Es&T Water* 3, 3835–3847. doi:10.1021/acsestwater.3c00031

Yasui, K., Tuziuti, T., and Kanematsu, W. (2016). Extreme conditions in a dissolving air nanobubble. *Phys. Rev. E* 94, 013106. doi:10.1103/PhysRevE.94.013106

Yasui, K., Tuziuti, T., and Kanematsu, W. (2019). High temperature and pressure inside a dissolving oxygen nanobubble. *Ultrason. Sonochemistry* 55, 308–312. doi:10.1016/j.ultsonch.2019.01.013

Ye, H., Wang, Y., Xu, D. D., Liu, X. J., Liu, S. M., and Ma, X. (2021). Design and fabrication of micro/nano-motors for environmental and sensing applications. *Appl. Mater. Today* 23, 101007. doi:10.1016/j.apmt.2021.101007

Ye, J., Ling, Z. X., Li, C., Dai, M. Y., Chen, Q., Gu, Y. L., et al. (2025). Micro-nanobubble-assisted tetracycline degradation by biochar-supported FeCo-metal-organic framework derivatives/persulfate system. *Colloids Surfaces a-Physicochemical Eng. Aspects* 718, 136911. doi:10.1016/j.colsurfa.2025.136911

Yi, H., Almatrafi, E., Ma, D. S., Huo, X. Q., Qin, L., Li, L., et al. (2023). Spatial confinement: a green pathway to promote the oxidation processes for organic pollutants removal from water. *Water Res.* 233, 119719. doi:10.1016/j.watres.2023.119719

Zhang, J., Huang, G. Q., Liu, C., Zhang, R. N., Chen, X. X., and Zhang, L. (2018). Synergistic effect of microbubbles and activated carbon on the ozonation treatment of synthetic dyeing wastewater. *Sep. Purif. Technol.* 201, 10–18. doi:10.1016/j.seppur.2018.02.003

Zhang, H., Li, P., Zhang, A., Sun, Z. Y., Liu, J. X., Héroux, P., et al. (2021a). Enhancing interface reactions by introducing microbubbles into a plasma treatment process for efficient decomposition of PFOA. *Environ. Sci. and Technol.* 55, 16067–16077. doi:10.1021/acs.est.1c01724

Zhang, T. Q., Zhou, R. W., Wang, P. Y., Mai-Prochnow, A., McConchie, R., Li, W. S., et al. (2021b). Degradation of cefixime antibiotic in water by atmospheric plasma bubbles: performance, degradation pathways and toxicity evaluation. *Chem. Eng. J.* 421, 127730. doi:10.1016/j.cej.2020.127730

Zhang, M., Liu, J. Y., Tang, L. F., Hu, N., Zhang, D. Y., and Pan, X. L. (2022a). Fenton micro-reactor on a bubble: a novel microbubble-triggered simultaneous capture and catalytic oxidation strategy for recalcitrant organic pollutant removal. *Sci. Total Environ.* 835, 155556. doi:10.1016/j.scitotenv.2022.155556

Zhang, Y., Fan, W. H., Li, X. M., Wang, W. X., and Liu, S. (2022b). Enhanced removal of free radicals by aqueous hydrogen nanobubbles and their role in oxidative stress. *Environ. Sci. and Technol.* 56, 15096–15107. doi:10.1021/acs.est.2c03707

Zhang, M., Yu, B. L., Fang, Q. K., Liu, J. Y., Xia, Q. Y., Ye, K., et al. (2023). Microbiome recognition of virulence-factor-governed interfacial mechanisms in antibiotic resistance and pathogenicity removal by functionalized microbubbles. *Water Res.* 242, 120224. doi:10.1016/j.watres.2023.120224

Zhang, J. H., Fang, Y. M., Lin, J. W., Du, W. X., Feng, Z. Y., Lin, Y., et al. (2024). Generalized and scalable synthesis of manganese dioxide-based tubular micromotors for heavy metal ion removal. *Acs Nano* 18, 29248–29260. doi:10.1021/acsnano.4c11716

Zhang, B., Chen, Q. H., Tang, H. L., Qi, R. Q., and Shi, W. X. (2025). Micro-nano bubbles enhance the Fe(II)/persulfate process for ultrafiltration membrane fouling control: performance and mechanisms. *J. Membr. Sci.* 733, 124371. doi:10.1016/j.memsci.2025.124371

Zhao, M. Y., Cui, H. N., Wang, C., and Song, Q. J. (2024a). Development of a 10-litre pilot scale micro-nano bubble (MNB)-enhanced photocatalytic system for wastewater treatment. *Environ. Technol.* 45, 6200–6209. doi:10.1080/09593330.2024.2328660

Zhao, K., Padervand, M., Ren, H. T., Jia, T. T., Guo, Q. Q., Yang, L. P., et al. (2024b). Enhancing tetracycline removal efficiency through Ozone micro-nano bubbles: environmental implication and degradation pathway. *Acs Es&T Eng.* 4, 1860–1870. doi:10.1021/acsestengg.4c00102

Zhou, L. M., Wang, X. Y., Shin, H. J., Wang, J., Tai, R. Z., Zhang, X. H., et al. (2020). Ultrahigh density of gas molecules confined in surface nanobubbles in ambient water. *J. Am. Chem. Soc.* 142, 5583–5593. doi:10.1021/jacs.9b11303

Zhou, Y. L., Han, Z. Y., He, C. L., Feng, Q., Wang, K. T., Wang, Y. B., et al. (2021a). Long-term stability of different kinds of gas nanobubbles in deionized and salt water. *Materials* 14, 1808. doi:10.3390/ma14071808

Zhou, R. W., Zhang, T. Q., Zhou, R. S., Wang, S., Mei, D. H., Mai-Prochnow, A., et al. (2021b). Sustainable plasma-catalytic bubbles for hydrogen peroxide synthesis. *Green Chem.* 23, 2977–2985. doi:10.1039/d1gc00198a

frontiers | Frontiers in Environmental Science

TYPE Original Research
PUBLISHED 10 September 2025
DOI 10.3389/fenvs.2025.1646864

OPEN ACCESS

EDITED BY
Yaoguang Guo,
Shanghai Polytechnic University, China

REVIEWED BY
Na Liu,
Suzhou University, China
Baoyi Lv,
Shanghai Maritime University, China

*CORRESPONDENCE
Delin Qi,
delinqi@126.com
Zhe Ma,
mazhe@isl.ac.cn

RECEIVED 14 June 2025
ACCEPTED 18 August 2025
PUBLISHED 10 September 2025

CITATION
Lu X, Wang Q, Wang Z, Ma Y, Shi Z, Qi D and Ma Z (2025) Pollutant distribution characteristics and microbial response mechanisms in surface and deep brines of the Qaidam Basin.
Front. Environ. Sci. 13:1646864.
doi: 10.3389/fenvs.2025.1646864

Pollutant distribution characteristics and microbial response mechanisms in surface and deep brines of the Qaidam Basin

Xiaohang Lu[1], Qiugui Wang[2], Zhendong Wang[3], Ying Ma[3], Zhen Shi[3], Delin Qi[1]* and Zhe Ma[4]*

[1]State Key Laboratory of Plateau Ecology and Agriculture, Qinghai University, Xining, China, [2]Key Laboratory for Water Quality and Conservation of the Pearl River Delta, Ministry of Education; School of Environmental Science and Engineering, Guangzhou University, Guangzhou, China, [3]Qinghai Geological Survey, Xining, China, [4]Key Laboratory of Green and High-end Utilization of Salt Lake Resources, Qinghai Institute of Salt Lakes, Chinese Academy of Sciences, Xining, China

This research investigates the distinctions between surface and deep brines in the Salt Lake region of the Qaidam Basin, with an emphasis on their physicochemical properties, organic matter content, heavy metal concentrations, organic pollutants, and microbial community structures. Both surface and deep brine samples were subjected to analysis for total and dissolved organic carbon, heavy metals (specifically Mn, Pb, and Cd), and pollutants, including phthalate esters (PAEs), halogenated compounds, and sulfides. The microbial communities were characterized through high-throughput sequencing, and redundancy analysis (RDA) coupled with correlation heatmaps was employed to evaluate the relationships between pollutants and microbial communities. The findings revealed that surface brines contained higher levels of organic matter, whereas deep brines exhibited significantly elevated concentrations of heavy metals and pollutants. The microbial community composition also varied, with Proteobacteria being predominant in deep brines and Firmicutes in surface brines, along with notable shifts at the genus level. Statistical analyses identified pollutants, particularly Pb, Cd, PAEs, halogenated compounds, and sulfides, as major determinants of microbial community variation. The findings indicate that the accumulation of pollutants in deep brines significantly impacts microbial community structures and ecological functions. Integrating microbial response data into environmental risk assessments is crucial for the sustainable development of deep brine resources in the Qaidam Basin.

KEYWORDS

deep brine, heavy metal pollution, organic pollutants, microbial community structure, extreme environment

1 Introduction

Human activities are significantly impacting the ecological stability of natural hypersaline environments, particularly in arid and semi-arid regions. The intensification of salt mining, petroleum extraction, and industrial brine discharge has led to the increased introduction of various pollutants, both organic and inorganic, into surface brine systems (Corsellis et al., 2016; Sayed et al., 2021). These pollutants tend to accumulate in closed or

semi-closed water bodies (Rojo-Nieto et al., 2011; Wang et al., 2016), disrupting indigenous microbial communities and impairing critical ecological functions such as biogeochemical cycling and pollutant degradation (Bai et al., 2017). While pollution in freshwater and marine systems has garnered considerable attention in recent years (Huang et al., 2025; Mossotto et al., 2025), the mechanisms by which microorganisms in hypersaline ecosystems respond to pollution remain largely underexplored.

Hypersaline environments, characterized by extreme salinity, elevated osmotic pressure, and limited nutrient availability, support uniquely adapted halophilic microbial communities, comprising a diverse array of bacteria and archaea (Menéndez-Serra et al., 2020; Santini et al., 2022). These microorganisms are integral to ecosystem stability, exhibiting distinctive metabolic capabilities, that significantly contribute to the biogeochemical cycling of carbon, nitrogen, sulfur, and other essential elements (Wang and Bao, 2022; Feng et al., 2023). However, the introduction of exogenous stressors including not only organic compounds but also heavy metals such as Mn, Cd, Co and Cu can profoundly disrupt these microbial networks. Heavy metals are known to exert toxic effects on cellular processes, inhibit microbial growth and enzymatic activity, and induce alterations in community structure and functional potential (Lichter et al., 2006; Cristiano et al., 2021). Their accumulation in brine environments, particularly in regions lacking historical baseline data, complicates ecological risk assessments.

The Qaidam Basin, located in the northern Qinghai-Tibet Plateau, exemplifies a typical arid inland basin characterized by extensive distributions of salt lakes and deep brine systems (Zheng et al., 2016). This area serves as an exemplary natural setting for examining the effects of environmental pollution on hypersaline ecosystems. Its unique geological and climatic conditions give rise to two contrasting brine environments: geochemically stable deep gravel-layer brine (Bai et al., 2024; Fan et al., 2024), which remains isolated from surface influence, and surface brines that are directly impacted by anthropogenic disturbances. Due to high evaporation and poor hydrological exchange, surface brines are particularly susceptible to the accumulation of both organic and inorganic pollutants, including heavy metals and persistent organic compounds (Minella et al., 2013). Recent surveys have revealed that organic contaminants originating from industrial activities and transportation have permeated both surface and, to a lesser extent, deep brine systems (Besser and Hamed, 2019; Wang et al., 2023), thereby providing a natural "deep–surface" comparative framework for studying pollution and microbial ecological responses.

While previous research has investigated microbial diversity in salt lakes (Oren et al., 2009; Tazi et al., 2014), comprehensive comparisons of microbial community structures between surface and deep brines, particularly concerning environmental pollution, remain scarce. It remains uncertain whether deep brines preserve their indigenous microbial assemblages or have been altered by anthropogenic pollutants. Moreover, the impact of various pollutants—especially heavy metals and organic compounds—on the composition and diversity of microbial communities in hypersaline environments is not well understood. Understanding these relationships is essential for evaluating ecological risks and predicting microbial responses in extreme environments under escalating environmental pressures.

In this study, we conducted an investigation on three representative brine samples from the Qaidam Basin, comprising two deep gravel-layer brines and one surface brine. Employing 16S rRNA high-throughput sequencing, gas chromatography-mass spectrometry (GC-MS) for organic pollutant profiling, and inductively coupled plasma mass spectrometry (ICP-MS) for trace metal analysis, our objectives were to: 1) compare the microbial community composition between surface and deep brines; 2) analyze the distribution patterns of heavy metals and organic pollutants across different brine environments; and 3) explore potential microbial responses to complex pollution stress. The outcomes of this study are anticipated to provide significant insights into pollutant–microbe interactions within deep and surface hypersaline systems, thereby contributing to future environmental monitoring and pollution risk assessments in extreme saline environments.

2 Materials and methods

2.1 Hydrogeological conditions

The study area is situated in the northwestern region of the Qaidam Basin. The predominant stratigraphic units exposed in this region are the Upper Pleistocene deposits of the Quaternary System. The lithological composition primarily consists of gray to gray-white gravel and sand, with an approximate thickness of 3 m. The groundwater within this study area is part of the Mahai Basin, a subsidiary basin of the Qaidam Basin. The groundwater in the Mahai Basin is primarily sourced from atmospheric precipitation and the melting of ice and snow in the mid to high-altitude mountainous regions of the northern and eastern Qilian Mountains. It is subsequently depleted through lake water discharge and surface evaporation. The groundwater dynamics are influenced and regulated by a multitude of factors, including geological structures, landforms, lithofacies, climate, and hydrological conditions. The hilly regions serve as natural barriers to groundwater flow, while the extensive unconsolidated deposits in the piedmont alluvial fans and lacustrine plains to the east and north provide substantial capacity for groundwater storage.

The deep brine examined in this research is characterized as fracture pore water within clastic rock formations. The aquifer's lithology comprises Neogene and Paleogene sandstone, silt-fine sandstone, as well as Cretaceous and Jurassic sandstone. This highly mineralized brine frequently coexists with oil and natural gas deposits. The burial depth of the water-bearing rock formations typically ranges from 300 to 2018 m. The chemical composition of the deep brine in the study area is predominantly of the chloride type, exhibiting moderate mineralization.

2.2 Sampling locations

This study selected two deep brine samples and one surface brine sample as research subjects, based on variations in water types and spatial distribution. These samples are designated as B1, B2, and C1 (Figure 1). B1 and B2 are deep brine samples situated within the same tectonic unit in the western region of the Qaidam Basin, north of Dezong Mahai Lake. In contrast, C1 is a surface brine sample

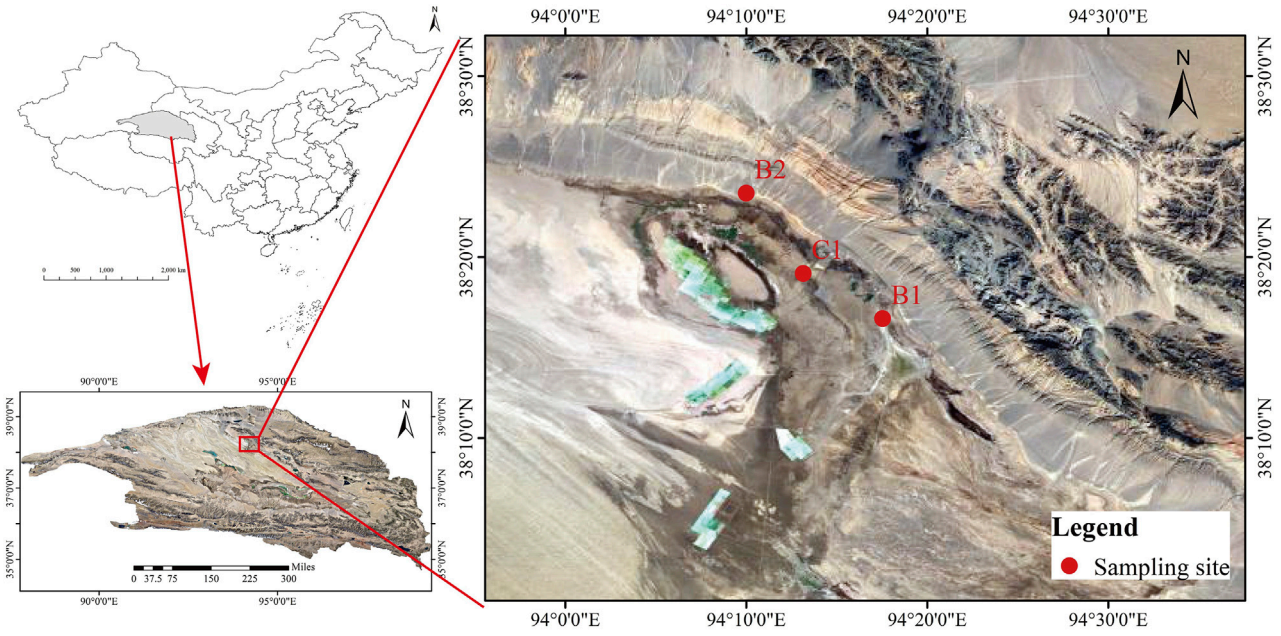

FIGURE 1
Schematic diagram of sampling point locations.

collected from the Mahai Mining Area. The sampling depths of B1 and B2 are 1092.45 m and 1122.32 m, respectively, and the horizontal distance is approximately 16 km. Despite their similar burial depths and essentially identical tectonic backgrounds, the distinct geographical locations of B1 and B2 reflect differences in spatial distribution within the deep brine system, thereby facilitating the understanding of lateral variation characteristics in this system. C1 is situated between B1 and B2 and primarily derives from DeZong Mahai Lake, representing a typical surface brine environment. The origins of the deep brines in B1 and B2 are preliminarily attributed to mountain-front leaching, which percolates underground to form these deposits.

2.3 Sample collection, transportation, and storage

In August 2024, water sampling was conducted at three locations: B1 (deep brine), B2 (deep brine), and C1 (surface brine). Five samples were collected at each sampling point, with each sample being 1L, totaling 15 samples. At each location, three samples were collected using sterile water sampling bags for 16sRNA detection, and two samples were collected using PVC bottles (rinsed three times with the water sample before collection) for heavy metal detection and GC-MS. The samples were stored at 4 °C, transported to the laboratory, and immediately subjected to microbial testing and routine ion analysis.

2.4 Heavy metal analysis

Samples were digested with $HClO_4$, HNO_3, HF, and HCl, diluted with dilute HCl, and analyzed by ICP-OES (Agilent 5110, Malaysia). For elevated Bi/Hg/Mo/Ag/W concentrations, appropriate dilutions were prepared prior to ICP-MS analysis. After correcting for spectral interferences, final results were obtained. All samples were measured in triplicate, with precision (relative deviation, RD) and accuracy (relative error, RE) controlled to <10%.

2.5 Physicochemical analysis of brines

All samples were diluted to salinity <2 g/L prior to analysis. Carbonate/bicarbonate, chloride, and magnesium were quantified by volumetric titration, while potassium, sodium, calcium, and sulfate were measured using ICP-OES (Agilent 5900, United States). Triplicate measurements yielded relative standard deviations (RSD) < 5% for all analytes.

2.6 GC-TOF-MS analysis

5 mL sample and 10 μL internal standard were added into a 20 mL Agilent headspace bottle, then placed on the sampling tray and analyzed by gas chromatograph coupled with a time-of-flight mass spectrometer (GC-TOF-MS).

GC-TOF-MS analysis was performed using an Agilent 7890B gas chromatograph coupled with a time-of-flight mass spectrometry system (Pegasus BT, Leco). A DB-WAX (30 m × 0.25 mm × 0.25 um)capillary column was used for separation. Helium was used as the carrier gas at a constant flow rate of 1.0 mL/min. The temperature of injection was set to 245 °C. The source temperature was 220 °C. The initial temperature was kept at 40 °C for 3 min, then raised to 105 °C at a rate of 6 °C min^{-1}, then raised to 180 °C at a rate of 4 °C min^{-1}, then raised to 245 °C at a rate of 10 °C min^{-1} and kept for 5 min at 300 °C. The energy was 70 eV in electron impact mode.

The mass spectrometry data were acquired in full-scan mode with the m/z range of 35–450 at a rate of 15 spectra per second. To assess the stability and reproducibility of the instrumental analysis, quality control (QC) samples were prepared by pooling aliquots from all individual samples and were analyzed alongside the experimental samples.

2.7 16s RNA sequencing

Firstly, the samples from the three sterile water sampling bags were filtered using a vacuum pump with a 0.22-micron organic filter membrane. After filtration, the filter membrane was placed into a cryotube and stored at −80 °C, then sent for analysis. This part of the process was completed by Zhongke New Life Co., Ltd. Then, Total genome DNA from samples were extracted using Mag-bind soil DNA kit (Omega), and tests the purity and concentration of DNA. For microbial analysis, each sample was subjected to six technical replicates to ensure the accuracy and reliability of the results. According to the selection of sequencing region, the selected V3-V4 variable region was amplified by PCR using specific primers with Barcode and high-fidelity DNA polymerase. PCR products were detected by 2% agarose gel electrophoresis, and the target fragments were cut and recovered by Quant-iT PicoGreen dsDNA Assay Kit. Referring to the preliminary quantitative results of electrophoresis, the PCR amplification recovered products were detected and quantified with the Microplate reader (BioTek, FLx800) fluorescence quantitative system, and the corresponding proportions were mixed according to the sequencing requirements of each sample. The library was constructed using TruSeq Nano DNA LT Library Prep Kit from Illumina. The constructed library is inspected by Agilent Bioanalyzer 2100 and Promega Quanti Fluor. After the library is qualified, it is sequenced.

2.8 Data analysis

Raw sequencing data were in FASTQ format. Paired-end reads were then preprocessed using cutadapt software to detect and cut off the adapter. After trimming, paired-end reads were filtering low quality sequences, denoised, merged and detect and cut off the chimera reads using DADA2 with the default parameters of QIIME2. At last, the software output the representative reads and the ASV abundance table. The representative read of each ASV was selected using QIIME 2 package. Representative sequence reads were taxonomically annotated using the SILVA database (version 138, 16S/18S rDNA) through the classify-sklearn classifier with default parameters. Alpha and beta diversity indices were calculated using QIIME2. Alpha diversity assesses microbial richness and diversity within individual samples, while beta diversity compares microbial community composition between samples.

Due to the limited environmental monitoring infrastructure and lack of reliable baseline pollution data in the study area, the screening criteria for organic pollutants detected by GC-MS were established with reference to the U.S. EPA's Integrated Risk Information System (IRIS) database and the National Institute of Standards and Technology (NIST). The correlations between dominant microorganisms and hydrochemical factors were analyzed using SPSS software (IBM SPSS Statistics 23) and represented the results through a correlation heat map. The Mantel test and redundancy analysis (RDA) were performed using R software (v 4.5.0) to determine the response relationships between microbial community diversity and hydrochemical factors.

3 Results

3.1 Physicochemical properties of brine samples

In order to gain insight into the variability of organic matter and its sources in surface and deep brines, this study examined the characteristics of the distribution of Total Organic Carbon (TOC), Dissolved Organic Carbon (DOC), Total Nitrogen (TN), pH, and Total dissolved solids (TDS) of different samples (Table 1).

The results revealed that although B1 and B2 were collected at similar depths and within the same structural unit, they exhibited substantial differences in organic matter content. Specifically, B1 contained significantly higher organic matter (11.33%) than B2 (7.26%), whereas B2 demonstrated elevated dissolved organic carbon levels (3.63%) compared to B1 (2.19%). As shown in the table, the pH values of both surface and deep brines exhibit minimal variation, maintaining a neutral range of 6.8–6.9. According to the groundwater quality standard (GB/T 14848-2017), deep brine should be classified as a Class V water body and should not be used as a source of domestic drinking water. And TDS levels exceed the standard, possibly due to hydrogeological influences. Based on TDS classification, both surface and deep brine are categorized as brine. The TDS in surface water exceed those in deep brine, a phenomenon closely linked to evaporation processes occurring within the mining area.

Additionally, the organic matter content in surface brine is two to three times higher than that in deep brine, while the total nitrogen content remains relatively consistent between the two. The surface brine has the highest DOC concentration of 18.64 mg/L, which is 6–9 times higher than that of deep brine.

3.2 Pollutant distribution characteristics

3.2.1 Heavy metal pollutant distribution characteristics

According to the groundwater quality standard (GB/T14848-2017), analysis of Figures 2a–c reveals that both surface and deep brines are contaminated with heavy metals to varying extents. Currently, three primary heavy metal pollutants have been identified: Mn, Cd and Pb. Notably, while the concentrations of most heavy metals in deep brines exhibit minimal variation, the Mn concentration in sample B2 (average 9.70 mg/L) is significantly higher than in sample B1 (average 3.00 mg/L). Furthermore, deep brine generally exhibits higher concentrations of heavy metals compared to surface brine. Specifically, Mn concentrations in surface brine range from 0.48 to 0.52 mg/L, whereas in deep brine, they range from 2.84 to 10.10 mg/L. The Mn concentration in deep brine significantly exceeds the background value, reaching levels 2 to 7 times higher. Additionally, the

TABLE 1 Physical and chemical properties of different samples.

Sample	TOC (mg/L)	DOC (mg/L)	TN (mg/L)	pH	TDS (mg/L)	C/N
B1	11.33	2.19	11.043	6.9	2.23×10^5	1.03
B2	7.262	3.63	11.147	6.8	2.49×10^5	0.65
C1	22.193	18.64	13.062	6.9	4.98×10^5	1.70

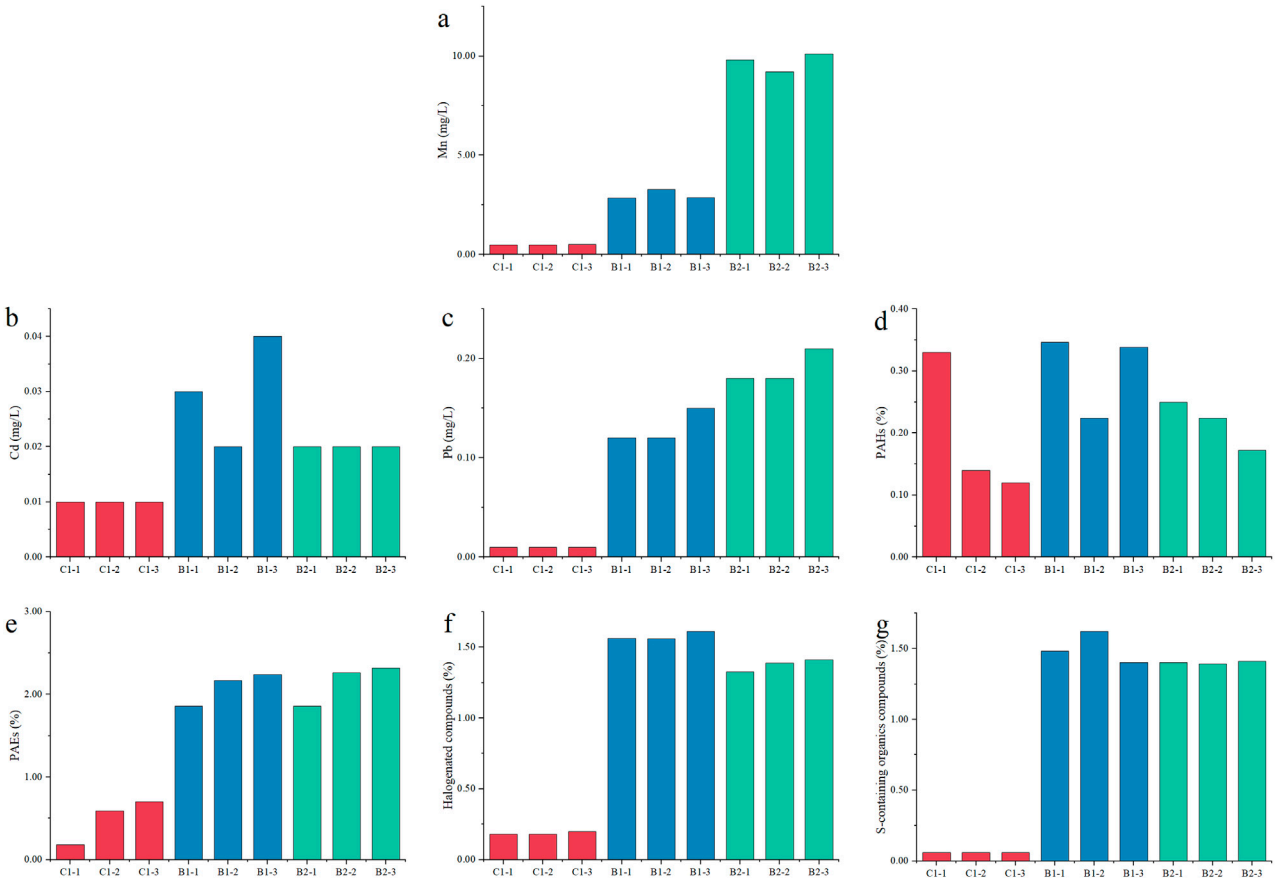

FIGURE 2
Contents of organic pollutants and heavy metal pollutants in deep brine and surface brine. **(a)**: Mn content, **(b)**: Cd content, **(c)**: Pb content, **(d)**: PAHs content, **(e)**: PAEs content, **(f)**: Halogenated compounds content, **(g)**: S-containing organics compounds content.

concentrations of Cd (0.02–0.04 mg/L) and Pb (0.12–0.18 mg/L) in deep brine are slightly elevated compared to those in surface brine (0.01–0.03 mg/L for Cd and 0.01 mg/L for Pb).

3.2.2 Volatile organic pollutant distribution characteristics

Utilizing the databases from the National Institute of Standards and Technology (NIST) and U.S. EPA Integrated Risk Information System (IRIS), we classified anthropogenic contaminants in both deep and surface brines into four categories: polycyclic aromatic hydrocarbons (PAHs), phthalate esters (PAEs), halogenated hydrocarbons, and sulfur-containing compounds. In deep brines, we identified five PAH species, compared to four in surface brines, three PAEs, compared to four, four halogenated hydrocarbons, compared to seven, and one sulfur-containing compound, compared to three (Supplementary Table S1). Although surface brines exhibited a greater diversity of organic pollutants, with a total of 15 species compared to 13 in deep brines, the concentrations of contaminants were consistently higher in deep brines (Figures 2d–g).

3.3 Microbial diversity and community structure

The Alpha diversity index values of the microbial communities in surface and deep brines are summarized in Supplementary Table S2. The coverage values of each sample were greater than 99%, indicating that most microorganisms could be explained by the applied sequencing depth. The ACE and Chao1 indexes used to estimate the total number of microbial species ranged from 319.32 to

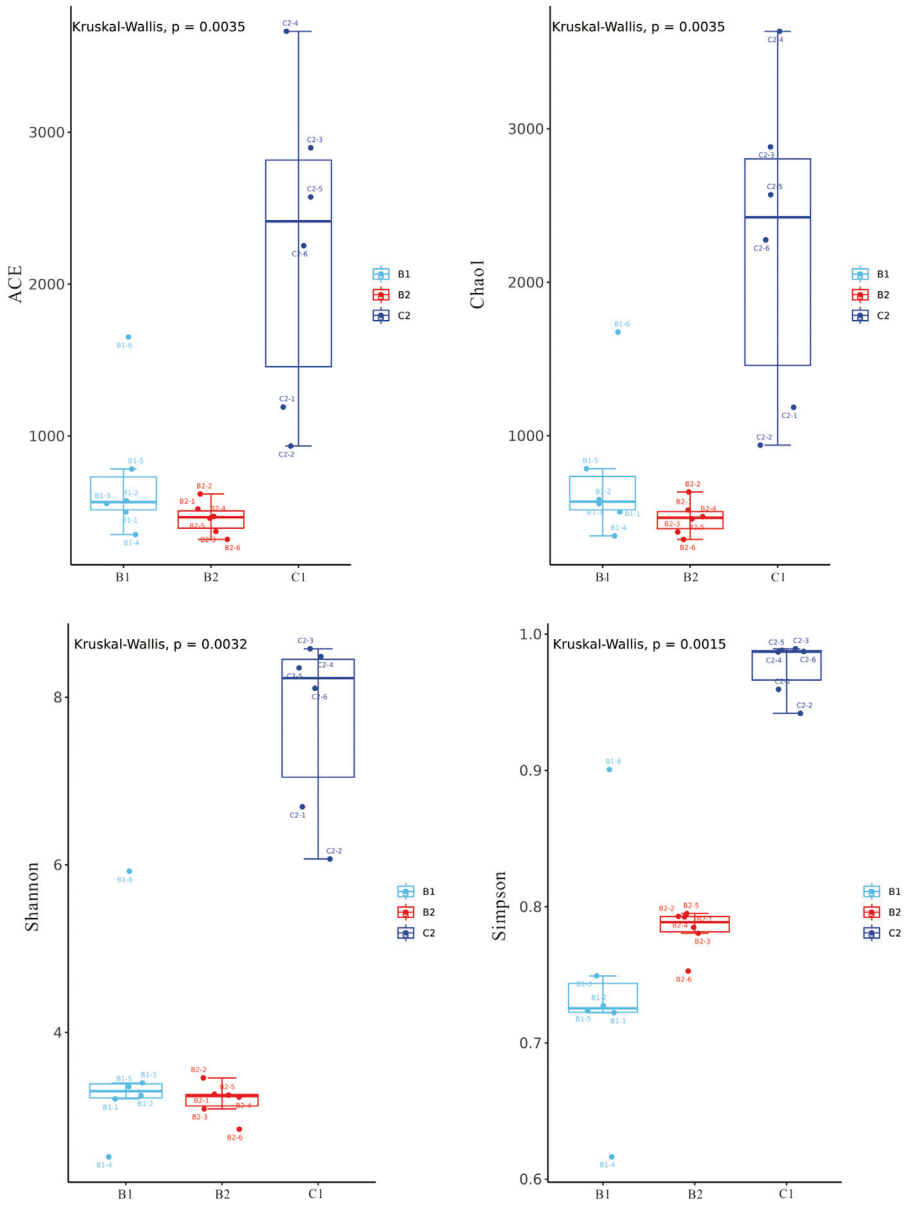

FIGURE 3
Analysis on the difference of α diversity index between deep brine and surface brine.

1651.56 and 324.25 to 1675.12 in deep brines, and from 933.92 to 3665.13 and 938.73 to 2882.30 in surface brine, respectively. The Shannon and Simpson indexes, used to estimate microbial diversity in samples, ranged from 2.52 to 5.92 and 0.62 to 0.96 in deep brines, and from 6.69 to 8.58 and 0.94 to 0.99 in surface brine (Figure 3).

The composition of microbial communities exhibited significant differences between surface and deep brines. At the phylum level, four phyla were predominant (>1%) in deep brines (Figure 4a). Among these dominant phyla, *Proteobacteria* and *Halanaerobiaeota* collectively constituted over 80%. In surface brines, four phyla were also dominant, with *Proteobacteria* and *Firmicutes* account for 74% (Figure 4a). To further elucidate the differences in microbial communities between surface and deep brines, the microbial composition was analyzed at the genus level (Figure 4b). At this level, it was observed that common genera varied considerably among samples, including those from deep brines. In sample B1, four genera were dominant (>1%), namely, including *Halovibrio*, *f_Halomonadaceae|g_uncultured*, *Halanaerobaculum* and *Halanaerobacter*, with *Halovibrio* and *Halanaerobaculum* together comprising 73% of the total. In sample B2, three genera were dominant (>1%), including *f_Halomonadaceae|g_uncultured*, *Halanaerobium* and *Paraliobacillus*, with *f_Halomonadaceae|g_uncultured* and *Halanaerobium* together accounting for 77% of the total. In sample C1, only two genera were dominant (>1%), namely, *f_uncultured|g_uncultured* and *Thiohalorhabdus*, and these two dominant genera together account for 74%.

The Venn diagram presented in Figure 4c delineates the distribution of microorganisms across various samples. In the deep

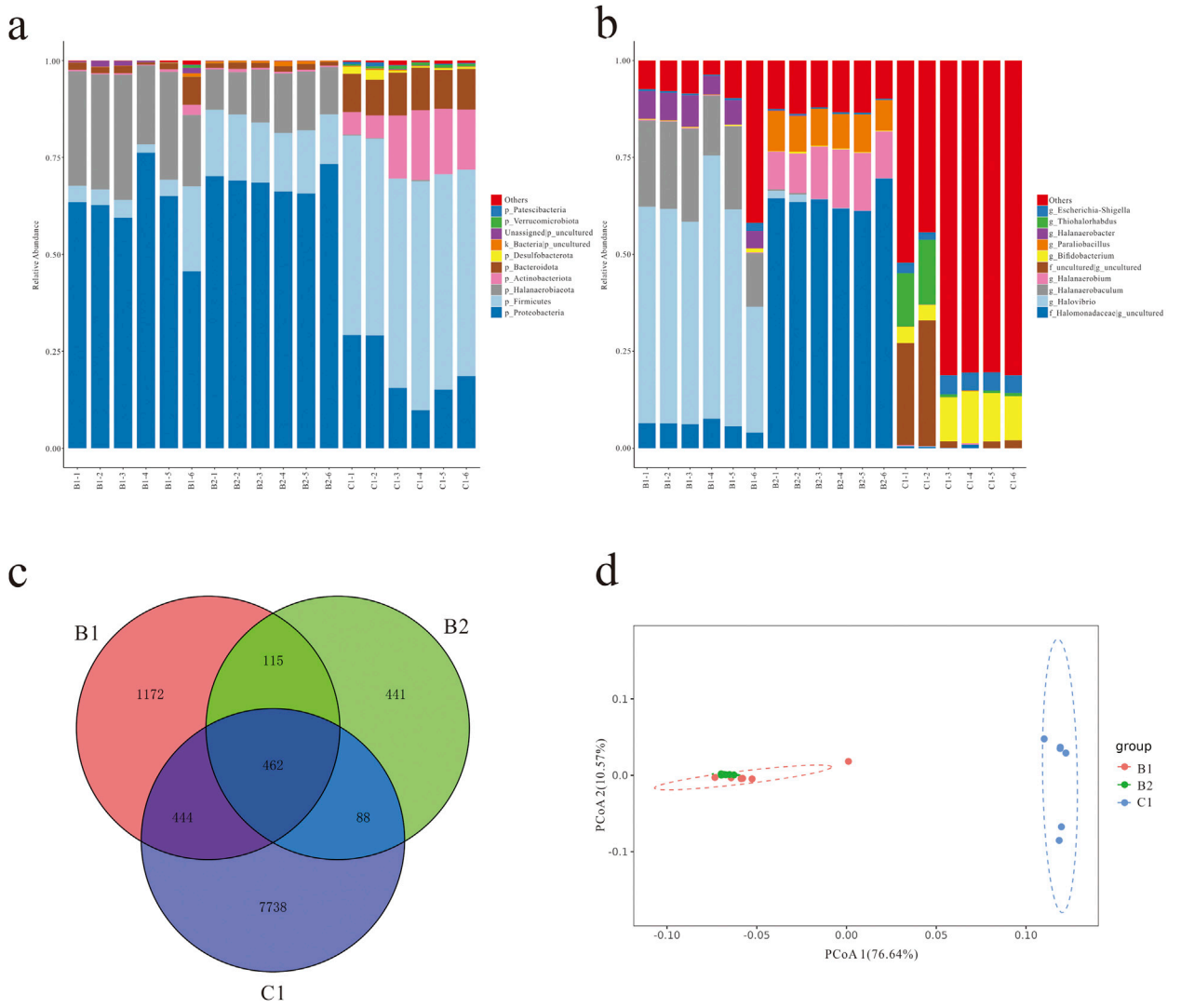

FIGURE 4
Distribution of microbial community structure in brine: **(a,b)** present the composition of the brine microbial community at the phylum and genus levels respectively, **(c)**: shows the Venn diagram of the OTU sample distribution, **(d)**: shows the PCoA analysis of the brine sample.

brine environment, sample B1 exhibits 1,172 unique Operational Taxonomic Units (OTUs), while sample B2 contains 441 unique OTUs. The surface brine sample harbors the highest number of unique OTUs, totaling of 7,738. Among the three samples, B1 and B2 share 115 OTUs, B2 and C1 share 88 OTUs, B1 and C1 share 444 OTUs, and all three samples collectively share 462 OTUs. These findings indicate significant differences in the structural composition of microbial communities between surface and deep brine environments. As depicted in the Principal Coordinate Analysis (PCoA) correlation analysis in Figure 4d, the principal components PC1 and PC2 account for 76.64% and 10.57% of the variance in microbial community composition, respectively. The PCoA results reveal that the microbial community structures within deep brine samples are similar and form distinct clusters, yet they differ markedly from those in surface brine samples.

Figure 5 illustrates the microbial taxa with LDA scores exceeding 2, indicating significant intergroup differences, alongside their phylogenetic clades. The blue nodes denote surface brine, which contains 311 significantly differentiated species primarily from the phyla *Firmicutes*, *Actinobacteriota*, and *Bacteroidota*. In contrast, the green and red nodes represent deep brine layers B2 and B1, which harbor 31 and 16 distinct microbial taxa, respectively, predominantly from the phyla *Proteobacteria* and *Halanaerobiaeota*. The results demonstrate substantially higher abundance of differential microbial communities in surface brine compared to the deep layers (311 vs. 31/16), likely due to the more open environmental conditions of the surface brine. Further investigation is necessary to explore potential correlations with environmental factors.

3.4 Relationship among microbial community structure, pollutants and environmental factors

Through a detailed analysis of the correlations among pollutants, environmental factors, and microbial communities, a

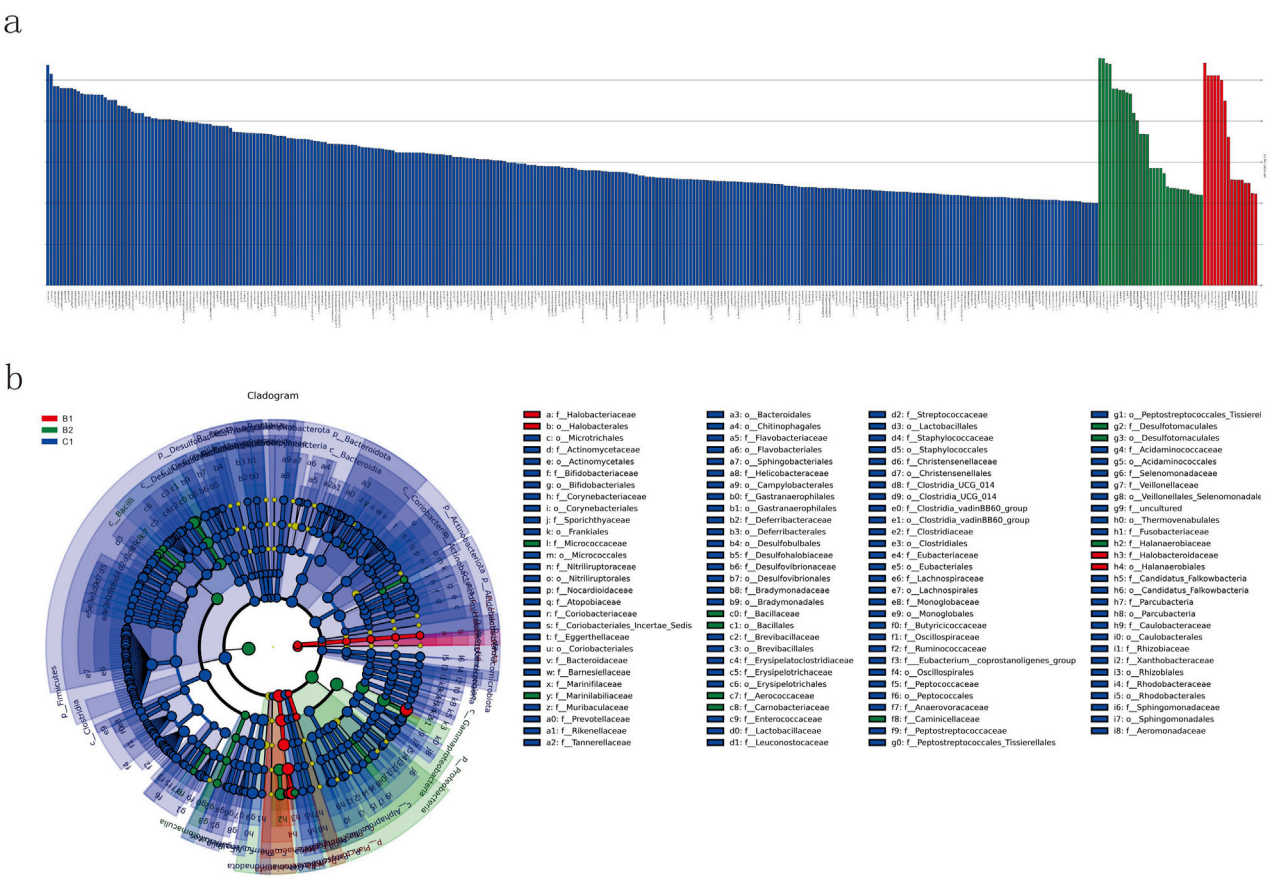

FIGURE 5
The potential biomarker was defined by LEfSe. **(a)** shows a histogram of linear discriminant analysis (LDA) scores for features rich in differences between groups. The log LDA score threshold for discriminant features is set to 2.0, **(b)** shows a cladistic plot representing significant differences in classification between deep and surface brine formations.

correlation heatmap was constructed (Figure 6), elucidating the intricate interactions between water chemistry, pollutants, and microbial composition. The findings indicated that, with the exception of PAHs and Mn, all other pollutants exerted a significant influence on the five dominant microbial groups in the brine. Although most water chemistry parameters did not exhibit strong correlations with PAHs and Mn, TC and TOC were notable exceptions, showing certain degrees of association. Specifically, Pb showed strong positive correlations with TN, TOC, TC, sulfate (SO_4^{2-}), magnesium (Mg^{2+}), TDS, and DOC. Cd was strongly correlated with TDS and potassium (K^+). PAEs exhibited significant correlations with DOC, TDS, K^+, Mg^{2+}, SO_4^{2-}, TC, and TOC. Halogenated compounds were closely related to DOC, TDS, K^+, Mg^{2+}, SO_4^{2-}, TC, TOC, and TN. Sulfides showed strong correlations with DOC, Ca^{2+}, Mg^{2+}, SO_4^{2-}, TC, TOC, and TN. Overall, the majority of pollutants were strongly associated with organic matter in the brine. Furthermore, significant correlations were identified among water chemistry parameters, as well as between water chemistry and pollutants. Consequently, further research is warranted to investigate the interactions among microbial community structure, water chemistry, and pollutants. This will enhance our understanding of the effects of pollutants on microbial composition and ecological functions.

This study conducted Redundancy Analysis (RDA) and Principal Component Analysis (PCA) to evaluate the impact of pollutants and hydrochemical factors on the microbial community structure in both deep and surface brine environments. The RDA findings demonstrated that the first two axes, RDA1 and RDA2, accounted for 70.23% and 25.41% of the variation in the native microbial community structure within high-salinity water bodies affected by organic and heavy metal pollution (Figure 7). Collectively, the influence of 20 variables explained 95.64% of the observed variation in microbial community composition. Notably, both organic and heavy metal pollutants significantly influenced the variation in microbial communities in deep brine. Importantly, both organic and heavy metal pollutants were found to significantly affect the variation in microbial communities in deep brine. Specifically, the presence of Cd, Pb, PAEs, halogenated compounds, and sulfur-containing organics exhibited strong correlations with the distribution of dominant deep-brine genera such as *Halanaerobaculum*, *Halanaerobacter*, and *Halovibrio*, as indicated by the RDA analysis. These genera exhibited distinct directional associations with the previously mentioned pollutants along the primary RDA axis (RDA1, 70.23%), indicating that fluctuations in pollutant concentrations are intricately connected to the structuring of microbial communities in hypersaline subsurface environments.

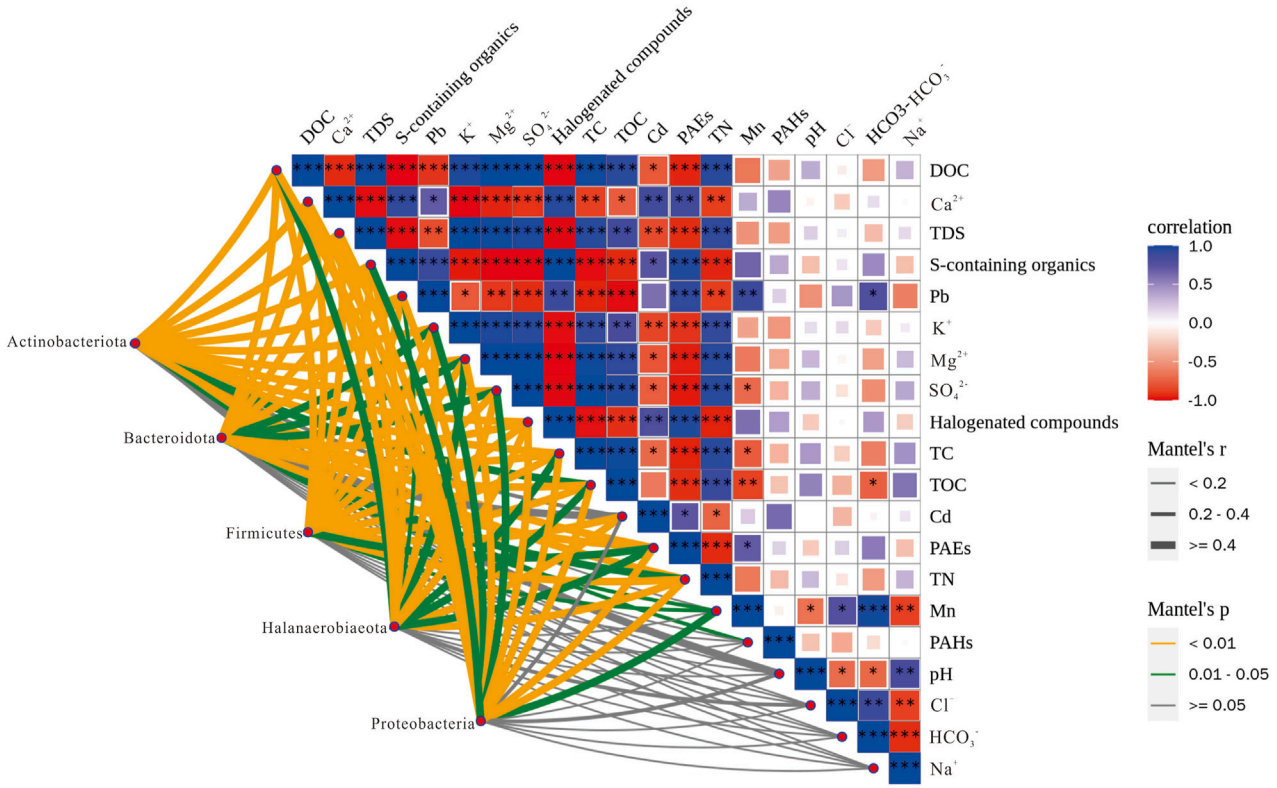

FIGURE 6
The correlation heat map depicting the relationships between different hydrochemical factors, as well as between hydrochemical factors and dominant phylum in deep brines and surface brine of the study area (All variables were normalized using Z-score transformation to enable direct comparison across different units and magnitudes).

4 Discussion

4.1 Composition and sources of organic matter in brine

Dissolved organic matter (DOM) is prevalent in high-salinity waters (Xu and Guo, 2017) and plays a crucial role in influencing nutrient cycling (Mopper et al., 1991), pH buffering capacity (Carter et al., 2012), and the solubility, toxicity, and bioavailability of metals and organic pollutants (Worms et al., 2019). In this study, we found that the TDS, TC, TOC, and DOC in surface brine were elevated compared to those in deep brine, although the total nitrogen content did not exhibit a substantial difference. Previous research has demonstrated that increasing salinity in lakes correlates with an increase in TDS, and the average molecular weight of DOM in brine tends to be larger with a higher degree of oxidation (Xu et al., 2020). Moreover, surface brine is more exposed to external influences compared to deep brine, potentially leading to greater impacts from external organic matter, such as atmospheric precipitation. Based on the analysis of the carbon-to-nitrogen (C/N) ratio, both surface and deep brines demonstrated C/N values below 2. This ratio indicates that the organic matter in these environments predominantly originates from algae (Khan et al., 2015), with a higher concentration of algae present in surface water relative to deep brine. Studies have demonstrated that microbial communities in brine, especially halophilic bacteria, are capable of efficiently utilizing organic nitrogen (Wang and Cui, 2024) and consuming organic carbon (Bonfá et al., 2013; Bonaglia et al., 2020), thereby significantly reducing the C/N ratio. This efficient utilization of organic nitrogen by microbes generally leads to an imbalance between organic carbon and nitrogen, further decreasing the C/N ratio.

Despite B1 and B2 being sampled from comparable depths within the same tectonic unit, their organic matter compositions exhibit notable differences. Specifically, B1 is characterized by a higher total organic carbon (TOC) content of 11.33%, whereas B2 contains a greater proportion of dissolved organic carbon (DOC) at 3.63%. This pattern implies that the organic matter in B2 may have undergone more extensive microbial degradation, leading to an increased presence of soluble organic fractions (Servais et al., 2020), while B1 retains a larger amount of particulate or recalcitrant organic components. This divergence is likely attributable to localized microenvironmental variations between the two boreholes. For example, increased ionic strength could lead to organic matter salting-out effects, thereby promoting the formation of colloids and particulate matter (Tóth et al., 2005). These findings underscore the existence of significant spatial heterogeneity in organic carbon composition and reactivity, even within the same deep brine system. Conversely, while microbial activity predominantly influences brine, external pollutants, notably anthropogenic contamination, may also directly contribute to organic nitrogen inputs (Valiente et al., 2022), potentially

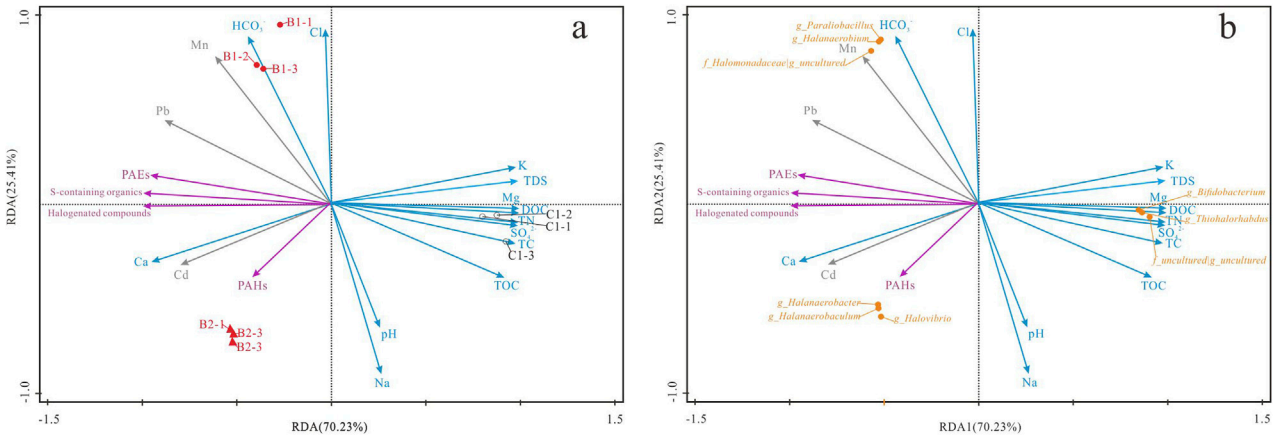

FIGURE 7
The response relationship between indigenous microflora and hydrochemical factors in deep brines and surface brine. **(a)** displays the RDA diagram, highlighting the correlation between samples and hydrochemical factors, **(b)** show cases the RDA diagram, revealing the correlation between dominant genera and hydrochemical factors in groundwater.

accounting for the exceptionally low C/N ratio observed. Thus, although microbial activity remains the principal factor, the impact of external organic nitrogen should be taken into account to offer a more comprehensive understanding of the variations in C/N ratios within brine.

4.2 Mechanisms and accumulation of heavy metals

In both surface and deep brines, we identified three heavy metals with significantly elevated concentrations: Mn, Cd, and Pb. Manganese (Mn) is recognized for its potential to induce a range of neurotoxic symptoms in clinical contexts, with chronic or acute exposure potentially resulting in severe outcomes, including cognitive and psychiatric symptoms, Parkinson's disease, motor dysfunction, and other neurodegenerative disorders (Das et al., 2015). Mn is widely distributed in geological formations, particularly with in aquifer sediments, and can leach into groundwater, thereby constituting a common chemical component (Wu et al., 2019). In natural environments, the predominant mechanism facilitating the release and migration of Mn from aquifer sediments to groundwater is its redox dissolution (Moon et al., 2020). Although Mn in groundwater primarily originates from natural sources (Zhai et al., 2019), research has also indicated that its concentration may be influenced by anthropogenic activities (Li et al., 2020). Previous research has demonstrated a positive correlation between Mn concentrations in groundwater and organic matter content (Liu et al., 2020). Additionally, the presence of organic pollutants has been shown to facilitate the release of Mn from sediments into the water (Liu et al., 2019; Zhai et al., 2021). Contrary to these findings, the present study observed that despite lower organic matter content in deep brines compared to surface brines, Mn concentrations were significantly elevated, exceeding typical industrial heavy metal pollution levels in groundwater (0.663 mg/L) as reported by Adeyemi and Ojekunle (2021). Furthermore, our data indicate substantially higher Mn concentrations in site B2 relative to site B1, which may be associated with increased levels of DOC. This suggests that DOC could potentially enhance Mn mobility through microbially-mediated and chemical reduction processes (Jiann et al., 2013).

Simultaneously, we propose the hypothesis that sediments within deep aquifers may exhibit elevated concentrations of Mn. Additionally, the relatively isolated geographical environment of deep brines may contribute to the accumulation of heavy metals to a certain degree (Stamatis et al., 2019). Pb and Cd, recognized as prevalent heavy metal contaminants, are ubiquitously found in soils (Zhou et al., 2019), rivers (Nasrabadi, 2015), and lakes (Şener et al., 2023), thereby posing substantial threats to both environmental integrity and human health. Studies have shown that Pb and Cd in soils not only affect plant growth but also presents potential health risks to animals and humans through bioaccumulation in the food chain (Chrysochoou and Dermatas, 2015). In rivers and lakes, Pb and Cd pollution predominantly arises from anthropogenic activities (Niu et al., 2021), including wastewater discharge and fertilizer application (Fei et al., 2020). In recent years, Pb and Cd contamination has also been found in high salinity environments, such as salt springs (Rezaei et al., 2019), salt lakes (Baati et al., 2022), and sediments (Rezaei et al., 2021), with primary sources attributed to industrial wastewater from factories, oilfields, and the deposition of industrial particles. This study found that the concentrations of Pb and Cd in deep brines were comparable to those found in freshwater lakes with values of 0.111 mg/L and 0.135 mg/L, respectively (Muneer et al., 2022). However, these concentrations were significantly elevated compared to those in surface brines, thereby reinforcing the hypothesis that closed environments facilitate the accumulation of heavy metals.

4.3 Types and possible sources of organic pollutants

In this study, organic pollutants characterized by their persistence and bioaccumulative properties, were identified in both surface and deep brine samples. Four major classes were

detected: PAHs, PAEs, halogenated compounds, and S-containing organics. PAHs, which consist of multiple fused aromatic rings, are well-documented for their carcinogenic potential and environmental persistence (McCarrick et al., 2019). Research indicates shown that low-molecular-weight PAHs exhibit greater water solubility, whereas high-molecular-weight PAHs are more prone to accumulation in suspended solids and sediments (Rabodonirina et al., 2015). In lakes and rivers, PAHs predominantly originate from the combustion of fossil fuels or biomass (e.g., shrubs or forests) (Wei et al., 2015), as well as from petroleum contamination (Bandowe et al., 2014). Conversely, in saline lakes, atmospheric deposition regarded as the principal source of PAHs (Idowu et al., 2020). The present study found that the PAH concentrations in surface and deep brines were comparable, measuring 0.26% and 0.20%, respectively. In light of the absence of vegetation and oil fields within the study area, it is inferred that atmospheric deposition constitutes the primary source of PAHs in surface brine. This observation further substantiates the hypothesis that deep brine originates from the infiltration of snowmelt into subsurface strata, resulting in the formation of highly mineralized brine under closed conditions (Hongpu et al., 2022). PAEs, extensively utilized as plasticizers, are frequently detected in aquatic environments and sediments. Elevated concentrations of PAEs have been reported in lakes and rivers situated near industrial zones (Gong et al., 2024). In our study, the presence of PAEs in brine is likely attributable to wastewater discharge from mining activities. The elevated levels of PAEs detected in deep brine suggest their accumulation within the confined subsurface environment over time. Halogenated hydrocarbons in saline lakes predominantly originate from biological halogenation processes, which are intensified by elevated sodium chloride concentrations (Timms, 2009).

Previous research has indicated that concentrations of halogenated hydrocarbons are elevated in neutral to alkaline saline lakes compared to acidic ones (Ruecker et al., 2015). Additionally, halophilic microorganisms and enzyme-mediated reactions are pivotal in the formation of halogens within hypersaline environments (Rhew et al., 2000). In this study, deep brine exhibited a significantly higher content of halogenated compounds (1.48%) than surface brine (0.19%), despite comparable NaCl concentrations. This suggests that microbial communities associated with halogenation processes may be considerably more abundant in deep brine. S-containing organic compounds have garnered significant attention due to their implications in atmospheric chemistry and global climate regulation (Andreae and Crutzen, 1997). In freshwater lakes, sulfide formation is generally linked to microbial activity (Hu et al., 2007) and the metabolism of sulfur-containing amino acids (Caron and Kramer, 1994). Conversely, in saline lakes, sulfide formation is more closely related to microbial degradation and sulfate reduction processes (Fritz and Bachofen, 2000; Torfstein et al., 2005).

Furthermore, salinity alterations resulting from anthropogenic activities may influence microbial community functions, thereby impacting sulfide production (Mr et al., 2017). In our study area, the deep brine, although currently undeveloped, exhibited a higher concentration of S-containing organic compounds compared to the surface brine. This suggests a greater prevalence of sulfate-reducing bacteria in the deep brine. Microbial community analysis corroborated this finding, revealing that the relative abundance of *Proteobacteria* in deep brine was more than three times greater than in surface brine, while the abundance of *Halanaerobiaeota* was over 200 times higher. Previous research has identified Proteobacteria as major sulfate-reducing species in high-salinity environments (Santos et al., 2020). Additionally, Boidi et al. (2022) reported that sulfate-reducing functional groups within the microbial mats of Laguna Negra's high-salinity environments are predominantly composed of *Halanaerobiaeota*, underscoring the significant role of sulfate reduction in deep brine.

4.4 Differences in microbial community structure and the effects of pollutants on microorganisms

As shown in Figure 4A, the microbial community in deep brine was predominantly composed of the phylum *Proteobacteria*, whereas *Firmicutes* emerged as the most abundant phylum in surface brine. Within the *Proteobacteria*, both *α-Proteobacteria* and *γ-Proteobacteria* are extensively acknowledged as pivotal microbial groups involved in the degradation of organic pollutants (Moxley and Schmidt, 2012; Cui et al., 2014; Moghadam et al., 2014). *Firmicutes*, frequently associated with petroleum degradation, flourish in eutrophic environments and plays an important role in carbon and nitrogen cycling (Hellal et al., 2021; Fang et al., 2023). In addition to Proteobacteria, the deep brine also exhibited relatively high proportions of *Firmicutes* (6.84%–15.65%) and *Halanacrobiacota* (12.95%–26.35%). Conversely, surface brine demonstrated higher relative abundances of *Actinobacteriota* (13.06%) and *Bacteroidota* (10.26%). These dominant microbial phyla have been documented in hypersaline environments and are known for their capabilities in degrading organic pollutants and heavy metals (Ye et al., 2016; Alvarez et al., 2017; Liu et al., 2023).

At the genus level (Figure 4B), several taxa exhibited high relative abundances within the brine samples, including *f_Halomonadaceae|g_uncultured*, *Halovibrio*, *Halanaerobaculum*, *Halanaerobium*, Bifidobacterium, *Paraliobacillus*, and *Thiohalorhabdus*. Notably, substantial differences were observed among the microbial communities at the genus level across samples B1, B2, and C1. Specifically, *Halovibrio* was predominant in B1, *f_Halomonadaceae|g_unculture*d was the most prevalent in B2, while Bifidobacterium was the dominant genus in C1. These observations indicate significant differences in the indigenous microbial composition between deep and surface brine, potentially attributable to variations in hydrogeological conditions, physicochemical properties, pollutant concentrations, and organic matter composition. Importantly, despite the high salinity conditions, the majority of the dominant genera identified possess known capabilities for degrading heavy metals and organic contaminants (Ottoson, 2009; Mohammadipanah et al., 2015; Cui et al., 2019; Boltyanskaya et al., 2023). Figure 4C illustrates the unique and shared OTUs between deep brine and surface brine samples. The deep brine contained the highest number of unique OTUs, totaling 7,738, indicating significantly greater microbial diversity compared to surface brine.

Additionally, PCoA demonstrated a distinct separation between the microbial communities of surface and deep brine, with a high degree of similarity observed between samples B1 and B2. Remarkably, RDA indicated that pollutants exerted a more pronounced influence on the microbial communities in deep brine compared to those in surface brine. The structure of local microbial communities was significantly shaped by most organic pollutants and heavy metals. Interestingly, PAHs exhibited a relatively minor impact on the microbial community, potentially due to their limited bioavailability in brine systems (Lindgren et al., 2014). Nonetheless, considering that the ecological effects of PAHs can vary substantially across different environmental contexts (Picariello et al., 2020), it is crucial to further investigate the conditions under which PAHs might influence microbial community dynamics in brine systems. In contrast to the long-exposed surface brine, deep brine exists in a more isolated environment. However, under high-salinity conditions, organic pollutants and heavy metals tend to accumulate and persist more readily in deep brine, exerting stronger impacts on subterranean microbial ecosystems. Consequently, greater emphasis must be placed on these factors when evaluating the future exploitation and utilization of deep brine resources.

5 Conclusion

This study conducted a systematic comparison of the surface and deep brines from the Qaidam Basin, focusing on their physicochemical properties, organic matter composition, distributions of heavy metals and organic pollutants, and microbial community structures. The results revealed that surface brine exhibited significantly higher contents of TC, TOC, and DOC, whereas deep brine showed elevated levels of Mn, Pb, and Cd. This suggests that closed subsurface environments are conducive to the accumulation of heavy metals. Furthermore, the low C/N ratios in both brine types imply a predominantly microbial origin of organic matter, potentially supplemented by exogenous organic nitrogen.

Among the pollutants identified, PAHs, PAEs, halogenated compounds, and S-containing organics were more concentrated in deep brines. This enrichment suggests that their sources are likely related to atmospheric deposition, biogenic halogenation, industrial activities, and wastewater discharge from mining operations. Microbial community analysis showed that *Proteobacteria* predominated in deep brines, whereas *Firmicutes* were more prevalent in surface brines. Variations at the genus level, OTU distributions, and PCoA results confirmed significant microbial divergence between the two environments. Furthermore, RDA and correlation heatmaps indicated that pollutants such as Cd, Pb, PAEs, halogenated compounds, and sulfides exerted substantial influences on microbial community structures, with more pronounced pollutant-driven effects observed in deep brines.

In summary, the enclosed and hypersaline environments of deep brines not only promote the accumulation and preservation of heavy metals and organic pollutants but also substantially influence the structuring of microbial communities. These findings highlight that microbial responses not only mirror the ecological stress induced by pollutants but also play a pivotal role in shaping ecological risks. Consequently, these factors should be meticulously considered in the development of future strategies for deep brine resource exploitation and pollution management.

Data availability statement

The original contributions presented in the study are included in the article/Supplementary Material, further inquiries can be directed to the corresponding authors.

Author contributions

XL: Resources, Funding acquisition, Conceptualization, Validation, Project administration, Visualization, Writing – review and editing, Methodology, Formal Analysis, Writing – original draft. QW: Software, Writing – original draft. ZW: Formal Analysis, Writing – original draft. YM: Writing – original draft, Resources, Data curation. ZS: Writing – original draft, Investigation. DQ: Project administration, Writing – original draft, Writing – review and editing, Supervision, Validation. ZM: Writing – original draft, Project administration, Validation, Conceptualization, Writing – review and editing.

Funding

The author(s) declare that financial support was received for the research and/or publication of this article. This research was funded by the Key Research and Development and Transformation Program Project of the Qinghai Provincial Department of Science and Technology (2024-QY-207).

Acknowledgments

The authors are thankful to the support of Qinghai University for the use of laboratory facilities.

Conflict of interest

The authors declare that the research was conducted in the absence of any commercial or financial relationships that could be construed as a potential conflict of interest.

Generative AI statement

The author(s) declare that no Generative AI was used in the creation of this manuscript.

Any alternative text (alt text) provided alongside figures in this article has been generated by Frontiers with the support of artificial intelligence and reasonable efforts have been made to ensure

accuracy, including review by the authors wherever possible. If you identify any issues, please contact us.

Publisher's note

All claims expressed in this article are solely those of the authors and do not necessarily represent those of their affiliated organizations, or those of the publisher, the editors and the reviewers. Any product that may be evaluated in this article, or claim that may be made by its manufacturer, is not guaranteed or endorsed by the publisher.

Supplementary material

The Supplementary Material for this article can be found online at: https://www.frontiersin.org/articles/10.3389/fenvs.2025.1646864/full#supplementary-material

References

Adeyemi, A. A., and Ojekunle, Z. O. (2021). Concentrations and health risk assessment of industrial heavy metals pollution in groundwater in Ogun state, Nigeria. *Sci. Afr.* 11, e00666. doi:10.1016/j.sciaf.2020.e00666

Alvarez, A., Saez, J. M., Davila Costa, J. S., Colin, V. L., Fuentes, M. S., Cuozzo, S. A., et al. (2017). Actinobacteria: current research and perspectives for bioremediation of pesticides and heavy metals. *Chemosphere* 166, 41–62. doi:10.1016/j.chemosphere.2016.09.070

Andreae, M. O., and Crutzen, P. J. (1997). Atmospheric Aerosols: biogeochemical sources and role in atmospheric chemistry. *Science* 276, 1052–1058. doi:10.1126/science.276.5315.1052

Baati, H., Bahloul, M., Amdouni, R., and Azri, C. (2022). Behavior assessment of moderately halophilic bacteria in brines highly enriched with heavy metals: Sfax solar saltern (Tunisia), A case study. *Geomicrobiol. J.* 39, 341–351. doi:10.1080/01490451.2021.2008548

Bai, Y., Huo, Y., Liao, K., and Qu, J. (2017). Influence of microbial community diversity and function on pollutant removal in ecological wastewater treatment. *Appl. Microbiol. Biotechnol.* 101, 7293–7302. doi:10.1007/s00253-017-8464-5

Bai, H., Pan, T., Han, G., Fan, Q., Miao, Q., and Bu, H. (2024). Hydrochemical characteristics and genesis of sand–gravel brine deposits in the Mahai Basin of the northern Qinghai–Tibetan plateau. *Water* 16, 3562. doi:10.3390/w16243562

Bandowe, B. A. M., Lueso, M. G., and Wilcke, W. (2014). Oxygenated polycyclic aromatic hydrocarbons and azaarenes in urban soils: a comparison of a tropical city (Bangkok) with two temperate cities (Bratislava and Gothenburg). *Chemosphere* 107, 407–414. doi:10.1016/j.chemosphere.2014.01.017

Besser, H., and Hamed, Y. (2019). Causes and risk evaluation of oil and brine contamination in the Lower Cretaceous Continental Intercalaire aquifer in the Kebili region of southern Tunisia using chemical fingerprinting techniques. *Environ. Pollut.* 253, 412–423. doi:10.1016/j.envpol.2019.07.020

Boidi, F. J., Mlewski, E. C., Fernández, G. C., Flores, M. R., Gérard, E., Farías, M. E., et al. (2022). Community Vertical composition of the Laguna Negra hypersaline microbial mat, Puna region (Argentinean Andes). *Biology* 11, 831. doi:10.3390/biology11060831

Boltyanskaya, Y., Zhilina, T., Grouzdev, D., Detkova, E., Pimenov, N., and Kevbrin, V. (2023). Halanaerobium polyolivorans sp. nov.—a Novel halophilic Alkalitolerant bacterium capable of Polyol degradation: Physiological properties and genomic insights. *Microorganisms* 11, 2325. doi:10.3390/microorganisms11092325

Bonaglia, S., Broman, E., Brindefalk, B., Hedlund, E., Hjorth, T., Rolff, C., et al. (2020). Activated carbon stimulates microbial diversity and PAH biodegradation under anaerobic conditions in oil-polluted sediments. *Chemosphere* 248, 126023. doi:10.1016/j.chemosphere.2020.126023

Bonfá, M. R. L., Grossman, M. J., Piubeli, F., Mellado, E., and Durrant, L. R. (2013). Phenol degradation by halophilic bacteria isolated from hypersaline environments. *Biodegradation* 24, 699–709. doi:10.1007/s10532-012-9617-y

Caron, F., and Kramer, J. R. (1994). Formation of volatile sulfides in freshwater environments. *Sci. Total Environ.* 153, 177–194. doi:10.1016/0048-9697(94)90197-X

Carter, H. T., Tipping, E., Koprivnjak, J.-F., Miller, M. P., Cookson, B., and Hamilton-Taylor, J. (2012). Freshwater DOM quantity and quality from a two-component model of UV absorbance. *Water Res.* 46, 4532–4542. doi:10.1016/j.watres.2012.05.021

Chrysochoou, M., and Dermatas, D. (2015). Editorial. *J. Hazard Mater* 281, 1. doi:10.1016/j.jhazmat.2014.10.006

Corsellis, Y. Y., Krasovec, M. M., Sylvi, L. L., Cuny, P. P., and Militon, C. C. (2016). Oil removal and effects of spilled oil on active microbial communities in close to salt-saturation brines. *Extremophiles* 20, 235–250. doi:10.1007/s00792-016-0818-x

Cristiano, W., Giacoma, C., Carere, M., and Mancini, L. (2021). Chemical pollution as a driver of biodiversity loss and potential deterioration of ecosystem services in Eastern Africa: a critical review. *South Afr. J. Sci.* 117. doi:10.17159/sajs.2021/9541

Cui, Z., Xu, G., Gao, W., Li, Q., Yang, B., Yang, G., et al. (2014). Isolation and characterization of *Cycloclasticus* strains from Yellow Sea sediments and biodegradation of pyrene and fluoranthene by their syntrophic association with *Marinobacter* strains. *Int. Biodeterior. and Biodegrad.* 91, 45–51. doi:10.1016/j.ibiod.2014.03.005

Cui, Y.-X., Biswal, B. K., Guo, G., Deng, Y.-F., Huang, H., Chen, G.-H., et al. (2019). Biological nitrogen removal from wastewater using sulphur-driven autotrophic denitrification. *Appl. Microbiol. Biotechnol.* 103, 6023–6039. doi:10.1007/s00253-019-09935-4

Das, A. P., Ghosh, S., Mohanty, S., and Sukla, L. B. (2015). "Advances in Manganese pollution and its bioremediation," in *Environmental microbial Biotechnology*. Editors L. B. Sukla, N. Pradhan, S. Panda, and B. K. Mishra (Cham: Springer International Publishing), 313–328. doi:10.1007/978-3-319-19018-1_16

Fan, Q., Han, G., Chen, T., Pang, T., Bai, H., Liu, J., et al. (2024). Inheritance recharge of subsurface brine constrains on formation of K-bearing sand-gravel brine in the alluvial fan zone of mountain-basin system on the Qinghai-Tibetan Plateau. *J. Hydrology* 645, 132029. doi:10.1016/j.jhydrol.2024.132029

Fang, T., Wang, T., Zhao, M., Bai, L., Deng, Y., and Ruan, W. (2023). Food waste digestate composting enhancement by sodium polyacrylate addition: effects on nitrogen transformation processes and bacterial community dynamics. *J. Environ. Manag.* 325, 116531. doi:10.1016/j.jenvman.2022.116531

Fei, X., Lou, Z., Xiao, R., Ren, Z., and Lv, X. (2020). Contamination assessment and source apportionment of heavy metals in agricultural soil through the synthesis of PMF and GeogDetector models. *Sci. Total Environ.* 747, 141293. doi:10.1016/j.scitotenv.2020.141293

Feng, L., Zhang, Z., Yang, G., Wu, G., Yang, Q., and Chen, Q. (2023). Microbial communities and sediment nitrogen cycle in a coastal eutrophic lake with salinity and nutrients shifted by seawater intrusion. *Environ. Res.* 225, 115590. doi:10.1016/j.envres.2023.115590

Fritz, M., and Bachofen, R. (2000). Volatile organic sulfur compounds in a Meromictic Alpine lake. *Acta hydrochimica hydrobiologica* 28, 185–192. doi:10.1002/1521-401x(20004)28:4<185::aid-aheh185>3.0.co;2-v

Gong, X., Xiong, L., Xing, J., Deng, Y., Qihui, S., Sun, J., et al. (2024). Implications on freshwater lake-river ecosystem protection suggested by organic micropollutant (OMP) priority list. *J. Hazard Mater* 461, 132580. doi:10.1016/j.jhazmat.2023.132580

Hellal, J., Joulian, C., Urien, C., Ferreira, S., Denonfoux, J., Hermon, L., et al. (2021). Chlorinated ethene biodegradation and associated bacterial taxa in multi-polluted groundwater: insights from biomolecular markers and stable isotope analysis. *Sci. Total Environ.* 763, 142950. doi:10.1016/j.scitotenv.2020.142950

Hongpu, L., Xianhua, H., Mianping, Z., Fu, F., Xixi, L., and Shuli, W. (2022). Metallogenic model and prospecting direction of Pleistocene gravel brine Potassium deposit in western Qaidam Basin. *J. Lake Sci.* 34, 1–13. doi:10.18307/2022.0327

Hu, H., Mylon, S. E., and Benoit, G. (2007). Volatile organic sulfur compounds in a stratified lake. *Chemosphere* 67, 911–919. doi:10.1016/j.chemosphere.2006.11.012

Huang, Y., Li, F., Wang, C., Teng, Y., Sun, R., Tang, J., et al. (2025). Predictive framework for species Sensitivity distribution Curves of emerging contaminants: a comparative study in marine and freshwater environments. *Environ. Sci. and Technol.* 59, 8016–8026. doi:10.1021/acs.est.4c12654

Idowu, O., Carbery, M., O'Connor, W., and Thavamani, P. (2020). Speciation and source apportionment of polycyclic aromatic compounds (PACs) in sediments of the largest salt water lake of Australia. *Chemosphere* 246, 125779. doi:10.1016/j.chemosphere.2019.125779

Jiann, K.-T., Santschi, P. H., and Presley, B. J. (2013). Relationships between geochemical parameters (pH, DOC, SPM, EDTA concentrations) and trace metal (Cd, Co, Cu, Fe, Mn, Ni, Pb, Zn) concentrations in river waters of Texas (USA). *Aquat. Geochem* 19, 173–193. doi:10.1007/s10498-013-9187-6

Khan, N. S., Vane, C. H., Horton, B. P., Hillier, C., Riding, J. B., and Kendrick, C. P. (2015). The application of δ13C, TOC and C/N geochemistry to reconstruct Holocene relative sea levels and paleoenvironments in the Thames Estuary, UK. *J. Quat. Sci.* 30, 417–433. doi:10.1002/jqs.2784

Li, Q., Zhang, H., Guo, S., Fu, K., Liao, L., Xu, Y., et al. (2020). Groundwater pollution source apportionment using principal component analysis in a multiple land-use area in

southwestern China. *Environ. Sci. Pollut. Res.* 27, 9000–9011. doi:10.1007/s11356-019-06126-6

Lichter, J., Caron, H., Pasakarnis, T. S., Rodgers, S. L., Squiers, T. S., and Todd, C. S. (2006). The ecological Collapse and partial Recovery of a freshwater Tidal ecosystem. *nena* 13, 153–178. doi:10.1656/1092-6194(2006)13[153:tecapr]2.0.co;2

Lindgren, J. F., Hassellöv, I.-M., and Dahllöf, I. (2014). PAH effects on meio- and microbial benthic communities strongly depend on bioavailability. *Aquat. Toxicol.* 146, 230–238. doi:10.1016/j.aquatox.2013.11.013

Liu, S., Liu, H., Wang, Z., Cui, Y., Chen, R., Peng, Z., et al. (2019). Benzene promotes microbial Fe(III) reduction and flavins secretion. *Geochimica Cosmochimica Acta* 264, 92–104. doi:10.1016/j.gca.2019.08.013

Liu, W., Wang, Y., Li, J., Qian, K., and Xie, X. (2020). Indices of the dual roles of OM as electron donor and complexing compound involved in as and Fe mobilization in aquifer systems of the Datong Basin. *Environ. Pollut.* 262, 114305. doi:10.1016/j.envpol.2020.114305

Liu, Y.-H., Mohamad, O. A. A., Gao, L., Xie, Y.-G., Abdugheni, R., Huang, Y., et al. (2023). Sediment prokaryotic microbial community and potential biogeochemical cycle from saline lakes shaped by habitat. *Microbiol. Res.* 270, 127342. doi:10.1016/j.micres.2023.127342

McCarrick, S., Cunha, V., Zapletal, O., Vondráček, J., and Dreij, K. (2019). *In vitro* and *in vivo* genotoxicity of oxygenated polycyclic aromatic hydrocarbons. *Environ. Pollut.* 246, 678–687. doi:10.1016/j.envpol.2018.12.092

Menéndez-Serra, M., Ontiveros, V. J., Triadó-Margarit, X., Alonso, D., and Casamayor, E. O. (2020). Dynamics and ecological distributions of the Archaea microbiome from inland saline lakes (Monegros Desert, Spain). *FEMS Microbiol. Ecol.* 96, fiaa019. doi:10.1093/femsec/fiaa019

Minella, M., Maurino, V., Minero, C., and Vione, D. (2013). Modelling photochemical transformation of emerging organic pollutants in surface waters: effect of water level fluctuations following outflow or evaporation, relevant to arid and semi-arid environments. *Int. J. Environ. Anal. Chem.* 93, 1698–1717. doi:10.1080/03067319.2013.803284

Moghadam, S., Mohsen, E., Gholamhossein, A., Khazaei, N., and Karbasi, N. (2014). Statistical Optimization of Crude oil biodegradation by Marinobacter sp. isolated from Qeshm Island, Iran. *Iran. J. Biotechnol.* 12, 35–41. doi:10.5812/ijb.15392

Mohammadipanah, F., Hamedi, J., and Dehhaghi, M. (2015). "Halophilic bacteria: Potentials and applications in Biotechnology," in *Halophiles: Biodiversity and Sustainable exploitation*. Editors D. K. Maheshwari and M. Saraf (Cham: Springer International Publishing), 277–321. doi:10.1007/978-3-319-14595-2_11

Moon, J.-W., Paradis, C. J., Joyner, D. C., Von Netzer, F., Majumder, E. L., Dixon, E. R., et al. (2020). Characterization of subsurface media from locations up- and down-gradient of a uranium-contaminated aquifer. *Chemosphere* 255, 126951. doi:10.1016/j.chemosphere.2020.126951

Mopper, K., Zhou, X., Kieber, R. J., Kieber, D. J., Sikorski, R. J., and Jones, R. D. (1991). Photochemical degradation of dissolved organic carbon and its impact on the oceanic carbon cycle. *Nature* 353, 60–62. doi:10.1038/353060a0

Mossotto, C., Anselmi, S., Trevisan, S., Provenza, F., Maganza, A., Gabetti, A., et al. (2025). Assessing the toxicity of gadolinium in freshwater and marine ecosystems: effects across trophic levels. *Environ. Toxicol. Pharmacol.* 115, 104673. doi:10.1016/j.etap.2025.104673

Moxley, K., and Schmidt, S. (2012). Isolation of a phenol-utilizing marine bacterium from Durban Harbour (South Africa) and its preliminary characterization as Marinobacter sp. KM2. *Water Sci. Technol.* 65, 932–939. doi:10.2166/wst.2012.940

Mr, L., C, A., N, F., G, S., J, A., E, A., et al. (2017). Microbialite response to an anthropogenic salinity gradient in Great Salt Lake, Utah. *Geobiology* 15, 131–145. doi:10.1111/gbi.12201

Muneer, J., AlObaid, A., Ullah, R., Rehman, K. U., and Erinle, K. O. (2022). Appraisal of toxic metals in water, bottom sediments and fish of fresh water lake. *J. King Saud Univ. - Sci.* 34, 101685. doi:10.1016/j.jksus.2021.101685

Nasrabadi, T. (2015). An indexapproach tometallic pollution in riverwaters. *Int. J. Environ. Res.* 9, 385–394.

Niu, Y., Chen, F., Li, Y., and Ren, B. (2021). Trends and sources of heavy metal pollution in global river and lake sediments from 1970 to 2018. *Rev. Environ. Contam. Toxicol.* 257, 1–35. doi:10.1007/398_2020_59

Oren, A., Baxter, B., and Weimer, B. (2009). Microbial communities in salt lakes: phylogenetic diversity, metabolic diversity, and *in situ* activities. *Nat. Resour. Environ. Issues* 15. Available online at: https://digitalcommons.usu.edu/nrei/vol15/iss1/51.

Ottoson, J. R. (2009). Bifidobacterial survival in surface water and implications for microbial source tracking. *Can. J. Microbiol.* 55, 642–647. doi:10.1139/W09-007

Picariello, E., Baldantoni, D., and De Nicola, F. (2020). Acute effects of PAH contamination on microbial community of different forest soils. *Environ. Pollut.* 262, 114378. doi:10.1016/j.envpol.2020.114378

Rabodonirina, S., Net, S., Ouddane, B., Merhaby, D., Dumoulin, D., Popescu, T., et al. (2015). Distribution of persistent organic pollutants (PAHs, Me-PAHs, PCBs) in dissolved, particulate and sedimentary phases in freshwater systems. *Environ. Pollut.* 206, 38–48. doi:10.1016/j.envpol.2015.06.023

Rezaei, M., Zarasvandi, A., Heidari, M., and Azhdari, A. (2019). Geochemistry of heavy metals in brine springs of Khouzestan province: Tracing of pollution potential of water resources and Persian Gulf. *J. Mar. Sci. Technol.* 18, 75–87. doi:10.22113/jmst.2019.166210.2249

Rezaei, M., Zarasvandi, A., Azdari, A., Mousavi, S. S., Heidari, M., and Azizi, N. (2021). Assessment of geological source and geochemical dispersion of heavy metals in the sediments of brine springs in Khouzestan Province. *Adv. Appl. Geol.* 11, 349–364. doi:10.22055/aag.2020.35770.2182

Rhew, R. C., Miller, B. R., and Weiss, R. F. (2000). Natural methyl bromide and methyl chloride emissions from coastal salt marshes. *Nature* 403, 292–295. doi:10.1038/35002043

Rojo-Nieto, E., Garrido-Pérez, C., Anfuso-Melfi, G., Lopez-Aguayo, F., Sales-Marquez, D., and Perales-Vargas-Machuca, J. A. (2011). The zoning of semi-enclosed bodies of water according to the sediment pollution: the Bay of Algeciras as a case example. *Estuaries Coasts* 34, 1129–1139. doi:10.1007/s12237-011-9389-3

Ruecker, A., Weigold, P., Behrens, S., Jochmann, M., Barajas, X. L. O., and Kappler, A. (2015). Halogenated hydrocarbon formation in a moderately acidic salt lake in Western Australia – role of abiotic and biotic processes. *Environ. Chem.* 12, 406–414. doi:10.1071/EN14202

Santini, T. C., Gramenz, L., Southam, G., and Zammit, C. (2022). Microbial community structure is most strongly associated with geographical distance and pH in Salt Lake sediments. *Front. Microbiol.* 13, 920056. doi:10.3389/fmicb.2022.920056

Santos, J. C. dos, Lopes, D. R. G., Da Silva, J. D., De Oliveira, M. D., Dias, R. S., Lima, H. S., et al. (2020). Diversity of sulfate-reducing prokaryotes in petroleum production water and oil samples. *Int. Biodeterior. and Biodegrad.* 151, 104966. doi:10.1016/j.ibiod.2020.104966

Sayed, K., Baloo, L., and Sharma, N. K. (2021). Bioremediation of total petroleum hydrocarbons (TPH) by Bioaugmentation and Biostimulation in water with Floating oil Spill Containment Booms as Bioreactor basin. *Int. J. Environ. Res. Public Health* 18, 2226. doi:10.3390/ijerph18052226

Şener, E., Şener, Ş., and Bulut, C. (2023). Assessment of heavy metal pollution and quality in lake water and sediment by various index methods and GIS: a case study in Beyşehir Lake, Turkey. *Mar. Pollut. Bull.* 192, 115101. doi:10.1016/j.marpolbul.2023.115101

Servais, S., Kominoski, J. S., Coronado-Molina, C., Bauman, L., Davis, S. E., Gaiser, E. E., et al. (2020). Effects of Saltwater Pulses on soil microbial enzymes and organic matter Breakdown in freshwater and Brackish coastal Wetlands. *Estuaries Coasts* 43, 814–830. doi:10.1007/s12237-020-00708-1

Stamatis, N., Kamidis, N., Pigada, P., Sylaios, G., and Koutrakis, E. (2019). Quality Indicators and possible ecological risks of heavy metals in the sediments of three semi-closed east Mediterranean Gulfs. *Toxics* 7, 30. doi:10.3390/toxics7020030

Tazi, L., Breakwell, D. P., Harker, A. R., and Crandall, K. A. (2014). Life in extreme environments: microbial diversity in Great Salt Lake, Utah. *Extremophiles* 18, 525–535. doi:10.1007/s00792-014-0637-x

Timms, B. (2009). Study of the saline lakes of the Esperance Hinterland, Western Australia, with special reference to the roles of acidity and episodicity. *Nat. Resour. Environ. Issues* 15. Available online at: https://digitalcommons.usu.edu/nrei/vol15/iss1/44.

Torfstein, A., Gavrieli, I., and Stein, M. (2005). The sources and evolution of sulfur in the hypersaline Lake Lisan (paleo-Dead Sea). *Earth Planet. Sci. Lett.* 236, 61–77. doi:10.1016/j.epsl.2005.04.026

Tóth, J., Kardos-Fodor, A., and Halász-Péterfi, S. (2005). The formation of fine particles by salting-out precipitation. *Chem. Eng. Process. Process Intensif.* 44, 193–200. doi:10.1016/j.cep.2004.02.013

Valiente, N., Jirsa, F., and Gómez-Alday, J. J. (2022). Saline lakes as barriers against pollution: a multidisciplinary overview. *Limnetica* 41, 281–303. doi:10.23818/limn.41.17

Wang, Y., and Bao, G. (2022). Diversity of prokaryotic microorganisms in alkaline saline soil of the Qarhan Salt Lake area in the Qinghai–Tibet plateau. *Sci. Rep.* 12, 3365. doi:10.1038/s41598-022-07311-3

Wang, L., and Cui, Y.-W. (2024). Mutualistic symbiosis of fungi and nitrogen-fixing bacteria in halophilic aerobic granular sludge treating nitrogen-deficient hypersaline organic wastewater. *Bioresour. Technol.* 394, 130183. doi:10.1016/j.biortech.2023.130183

Wang, L., Lim, C. K., Dang, H., Hanson, T. E., and Klotz, M. G. (2016). D1FHS, the type Strain of the Ammonia-Oxidizing bacterium Nitrosococcus wardiae spec. Nov.: enrichment, isolation, phylogenetic, and growth Physiological characterization. *Front. Microbiol.* 7, 512. doi:10.3389/fmicb.2016.00512

Wang, X., Ren, L., Long, T., Geng, C., and Tian, X. (2023). Migration and remediation of organic liquid pollutants in porous soils and sedimentary rocks: a review. *Environ. Chem. Lett.* 21, 479–496. doi:10.1007/s10311-022-01506-w

Wei, C., Han, Y., Bandowe, B. A. M., Cao, J., Huang, R.-J., Ni, H., et al. (2015). Occurrence, gas/particle partitioning and carcinogenic risk of polycyclic aromatic hydrocarbons and their oxygen and nitrogen containing derivatives in Xi'an, central China. *Sci. Total Environ.* 505, 814–822. doi:10.1016/j.scitotenv.2014.10.054

Worms, I. A. M., Chmiel, H. E., Traber, J., Tofield-Pasche, N., and Slaveykova, V. I. (2019). Dissolved organic matter and associated trace metal dynamics from river to lake, under ice-Covered and ice-Free conditions. *Environ. Sci. Technol.* 53, 14134–14143. doi:10.1021/acs.est.9b02184

Wu, B., Amelung, W., Xing, Y., Bol, R., and Berns, A. E. (2019). Iron cycling and isotope fractionation in terrestrial ecosystems. *Earth-Science Rev.* 190, 323–352. doi:10.1016/j.earscirev.2018.12.012

Xu, H., and Guo, L. (2017). Molecular size-dependent abundance and composition of dissolved organic matter in river, lake and sea waters. *Water Res.* 117, 115–126. doi:10.1016/j.watres.2017.04.006

Xu, W., Gao, Q., He, C., Shi, Q., Hou, Z.-Q., and Zhao, H.-Z. (2020). Using ESI FT-ICR MS to characterize dissolved organic matter in salt lakes with different salinity. *Environ. Sci. Technol.* 54, 12929–12937. doi:10.1021/acs.est.0c01681

Ye, T., Cai, H., Liu, X., and Jiang, H.-L. (2016). Dominance of Oscillospira and Bacteroides in the bacterial community associated with the degradation of high-concentration dimethyl sulfide under iron-reducing condition. *Ann. Microbiol.* 66, 1199–1206. doi:10.1007/s13213-016-1207-5

Zhai, Y., Zheng, F., Zhao, X., Xia, X., and Teng, Y. (2019). Identification of hydrochemical genesis and screening of typical groundwater pollutants impacting human health: a case study in Northeast China. *Environ. Pollut.* 252, 1202–1215. doi:10.1016/j.envpol.2019.05.158

Zhai, Y., Han, Y., Xia, X., Li, X., Lu, H., Teng, Y., et al. (2021). Anthropogenic organic pollutants in groundwater increase releases of Fe and Mn from aquifer sediments: impacts of pollution degree, mineral content, and pH. *Water* 13, 1920. doi:10.3390/w13141920

Zheng, M., Zhang, Y., Liu, X., Qi, W., Kong, F., Nie, Z., et al. (2016). Progress and Prospects of Salt Lake research in China. *Acta Geol. Sin. - Engl. Ed.* 90, 1195–1235. doi:10.1111/1755-6724.12767

Zhou, S., Hursthouse, A., and Chen, T. (2019). Pollution characteristics of Sb, as, Hg, Pb, Cd, and Zn in soils from different zones of Xikuangshan Antimony mine. *J. Anal. Methods Chem.* 2019, 1–9. doi:10.1155/2019/2754385

Frontiers in Environmental Science

Explores the anthropogenic impact on our natural world

An innovative journal that advances knowledge of the natural world and its intersections with human society. It supports the formulation of policies that lead to a more inhabitable and sustainable world.

Discover the latest Research Topics

See more →

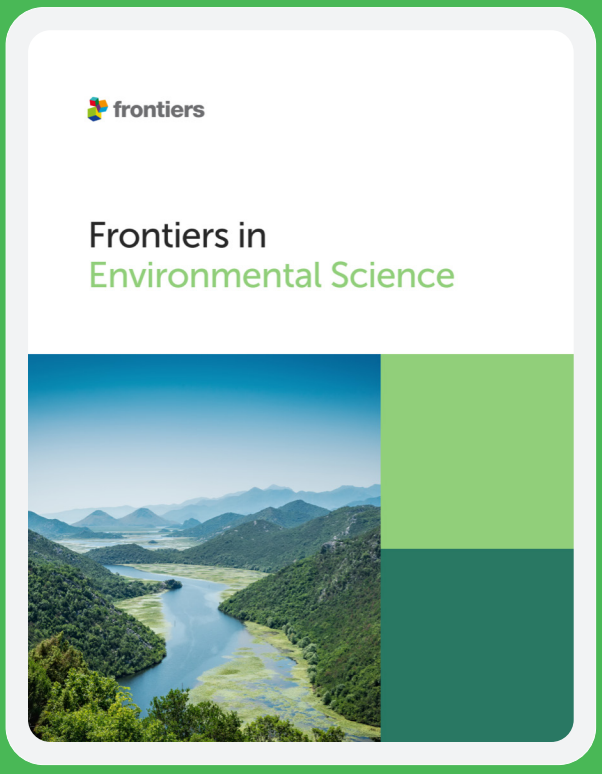

Frontiers

Avenue du Tribunal-Fédéral 34
1005 Lausanne, Switzerland
frontiersin.org

Contact us

+41 (0)21 510 17 00
frontiersin.org/about/contact